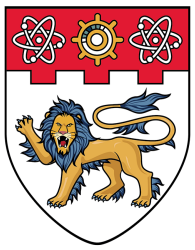

NANYANG TECHNOLOGICAL UNIVERSITY
SINGAPORE

ANALYTICS IN SUPPORT OF REGIONAL SCALE RISK REDUCTION

MARICAR L. RABONZA

Asian School of the Environment
College of Science

A thesis submitted to the Nanyang Technological University in partial fulfilment of the requirement for the degree of Doctor of Philosophy

2023

Candidate Statement of Originality

I hereby certify that the work embodied in this thesis is the result of original research, is free of plagiarised materials, and has not been submitted for a higher degree to any other University or Institution. I confirm that the investigations were conducted in accord with the ethics policies and integrity standards of Nanyang Technological University and that the research data are presented honestly and without prejudice.

January 17, 2023

Date

Maricar L. Rabonza

Supervisor declaration

I have reviewed the content and presentation style of this thesis and declare it is of sufficient quality and grammatical clarity to be examined. To the best of my knowledge, it is free of plagiarism and the research and writing are those of the candidate except as acknowledged in the Author Attribution Statement. To the best of my knowledge, the investigations were conducted in accord with the ethics policies and integrity standards of Nanyang Technological University and that the research data are presented honestly and without prejudice.

January 17, 2023

Date

Asst. Prof. David Lallemant

Authorship Attribution Statement

This thesis contains material from the following 5 papers where I was the first author.

- 1 published journal article
- 1 published contributing article to the United Nations Office for Disaster Risk Reduction (UNDRR) Global Assessment Report (GAR) on Disaster Risk Reduction 2022
- 1 journal article under review
- 2 conference papers (peer-reviewed by 2 or more reviewers)

Chapter 2:

Chapter 2 is a journal article under review:

Rabonza M.L., Nguyen M., Biass S., Jenkins S., Taisne B., Lallemant D., (2023) Inversion and forward estimation with process-based models: an investigation into cost functions, uncertainty-based weights and model-data fusion. *Environmental Modelling Software*, Under review.

The contributions of the co-authors are as follows:

- I lead the writing, research, and analysis.
- I designed the study with Michele Nguyen and David Lallemant.
- Sebastien Biass provided guidance in conducting tephra inversion modelling.
- All authors discussed the results and commented on the manuscript.

Chapter 3:

Chapter 3 is a peer-reviewed conference paper published as follows.

Rabonza, M.L. and Lallemant, D. (2019). Accounting for time and state-dependent vulnerability of structural systems. *In Proceedings of the 13th International*

Conference on Applications of Statistics and Probability in Civil Engineering (ICASP13) Sep 2019. pp. 2298-2305. https://doi.org/10.22725/ICASP13.465

The contributions of the co-authors are as follows:

- I wrote the paper, collected the data, and performed the analysis.
- I designed the study with David Lallemant.
- David Lallemant commented on the manuscript.

Chapter 4:

Chapter 4 is a journal article published as:

Rabonza M.L., Lin Y.C. and Lallemant D. (2022) Learning From Success, Not Catastrophe: Using Counterfactual Analysis to Highlight Successful Disaster Risk Reduction Interventions. *Front. Earth Sci.* 10:847196. doi: 10.3389/feart.2022.847196

The contributions of the co-authors are as follows:

- I lead the writing, research, and analysis.
- Yolanda Lin and David Lallemant provided feedback that shaped the analysis.
- David Lallemant conceived of the idea of celebrating successes in disaster risk reduction using counterfactual analysis.
- All authors contributed to the conceptualisation and design of the study.

Appendix B

Appendix B.1 is a peer-reviewed conference paper, which is cited in Chapter 3.

Rabonza, M.L. and Lallemant, D. (2018). A time-dependent model for seismic risk reduction policy analysis. Accepted in the *17th U.S.-Japan-New Zealand Workshop on the Improvement of Structural Engineering and Resilience Nov 2018. https://hdl.handle.net/10356/164235*

- I wrote the paper, collected the data, and performed the analysis.
- I designed the study with David Lallemant.
- David Lallemant commented on the manuscript.

Appendix C

Appendix C.2 is a paper published as a Contributing Paper to the Global Assessment Report (GAR) on Disaster Risk Reduction 2022 by the United Nations Office for Disaster Risk Reduction (UNDRR). The paper is cited in the Introduction and Chapter 4.

Rabonza, M.L., Lallemant, D., Lin, Y. C., Tadepalli, S., Wagenaar, D., Nguyen, M., Choong, J., Liu, C. J. N., Sarica, G. M., Widawati, B. A. M., Balbi, M., Khan, F., Loos, S. & Lim, T. N. (2022). Shedding light on avoided disasters : measuring the invisible benefits of disaster risk management using probabilistic counterfactual analysis. *A contributing paper to the United Nations Office for Disaster Risk Reduction (UNDRR) Global Assessment Report 2022*. https://www.undrr.org/publication/shedding-light-avoided-disasters-measuring-invisible-benefits-disaster-risk-reduction

- I lead the writing, analysis design, and conceptualisation of the invisibilities in mitigation successes with David Lallemant.
- I designed the use of counterfactual analysis to address the invisibilities in risk reduction success with Yolanda Lin and David Lallemant.
- I produced the schematic figure for the types of invisibilities.
- For the risk perception section, Sanjana Tadepalli and Feroz Khan provided additional references, and assisted with editing.
- For the risk analysis framework section, Mariano Balbi and Yolanda Lin provided feedback on the writing.
- For the Nepal case study, I performed the analysis. Yolanda Lin and Sabine Loos provided feedback on the writing.
- For the India case study, Dennis Wagenaar and Bernadeti Ausie Miranda Widawati collected data and performed the analysis. Celine Liu contributed to the writing of the case study.
- For both case studies, Jeanette Choong produced the maps, and Michele Nguyen produced the visualisations of fatalities in the results.
- Michele Nguyen and Gizem Mestav Sarica assisted in collecting examples of disaster risk management (DRM) measures for which counterfactual analysis can be applied.
- Tian Ning Lim contributed to the writing about other metrics of success in DRM activities.
- All authors discussed the results and commented on the manuscript.

We the undersigned agree with the above stated "proportion of work undertaken" for each of the above published (or submitted) peer-reviewed manuscripts contributing to the thesis:

Signed:

Maricar L. Rabonza
Student
Asian School of the Environment
Nanyang Technological University
Date: January 17, 2023

Asst. Prof. David Lallemant
Supervisor
Asian School of the Environment
Nanyang Technological University
Date: January 17, 2023

Assoc Prof. Benoit Taisne
Associate Chair (Research)
Asian School of the Environment
Nanyang Technological University
Date: January 18, 2023

Acknowledgements

This dissertation is supported mainly by Singapore's National Research Foundation (NRF) under the NRF-NRFF2018-06 award, the Ministry of Education (MOE), and Nanyang Technological University (NTU) as a Research Centre of Excellence. I also acknowledge the additional support and scholarship funding from the Earth Observatory of Singapore (EOS). I describe individual project contributions in a dedicated Authorship Attribution Statement. Project-specific acknowledgements and funding are included at the end of each chapter.

This PhD journey would not have been possible without the support of countless people around the world. I have been privileged to work in the most supportive, fun, and intellectually vibrant environment. Here, I briefly describe those who have assisted me professionally and emotionally.

To my adviser, David Lallemant, thank you for being a constant source of support and positive energy since day one of my PhD. My research process has been extremely rewarding because of the freedom, unwavering guidance, and enthusiasm that you provided. I learned from you how to become a more effective, reflective, and intentional researcher. I am confident to say that you have helped me build the most amazing PhD. You have my deep gratitude.

I want to thank my esteemed thesis advisory committee members, Susanna Jenkins and Janice Teresa Ser Huay Lee, who have been a limitless source of wisdom and generosity over the last few years. Thank you to Susanna for the opportunity to collaborate with the volcano group in the Asian School of the environment, which lead to a tremendous learning experience. The learning curve for me have been steep, but you made sure I got the support I needed on the volcanology aspects, leading to one of the most rewarding research work I've done in the PhD - thank you. I am grateful to Janice for generously giving me advice on technical and non-technical aspects of being a researcher in the field. I learned how to write my first policy paper from your teaching, which made me realise new ways of thinking about success in risk reduction. Special thanks to Benoit Taisne who is generous with his time to join my thesis committee meetings while making sure he asks the tough (but super helpful) questions. Susanna, Janice, and Benoit, your patient, careful mentorship and engagement with my ideas has always made my commitment stronger and my work better.

I am thankful to the incredible training by some of the most exceptional faculty and instructors. Beyond those previously mentioned, I express my thanks to Emma Hill, Sang-Ho Yun, Adam Switzer, Patrick Martin, Pavel Adamek, Karen Lythgoe, Lujia Feng, and Eric Lindsey. To the editors and reviewers of my published work, I express my utmost appreciation for the thoughtfulness, care and professionalism you've put into the peer-review process. Thank you for the time spent suggesting improvements, engaging with, and reviewing my research, Gemma Cremen, Carmine Galasso, Gabriele Fiorentino, JC Gaillard, and Martin Joe.

I have worked, been mentored, and developed friendships with very brilliant researchers and professors. Yolanda Lin, the first few years of my PhD has been transformative for me as a researcher, and I want to express my gratitude to you for being a core part of it. You have been a personal inspiration in terms of the standards of work ethics that you demonstrate, and I am so appreciative of your support as a colleague and as a friend. Michele Nguyen, thank you for the generous support as I bridge boundaries and scientific methods in my research. I am grateful of your thoughtfulness, careful attention to detail, and insightful mentorship. Sebastien Biasse, my research on tephra inversion is much better because of your generosity in sharing your expertise. I highly appreciate your words of enthusiasm towards my ideas, as well as the patience and effort to explain the concepts of volcanic eruption parameters. Gizem Mestav Sarica, thank you for our friendship and how we continued to support one another in our work on urban growth models and beyond our academic career. Poul Grashoff, thank you for training me to use the Java Spatial Model (urban growth model) and spending hours to compile the results so that we can explore its potential for zoning policies. Daniel Vaulot, working alongside with you to teach the Data Science class has been a delightful and important learning experience for me in terms of effective teaching.

My labmates in the Disaster Analytics for Society Lab (DASL) deserve a shoutout. I'm grateful to have been part of a community that develops tools and analysis in the field of natural hazards in a way that's respectful and mindful of the implications to society. Yolanda, Feroz, Tian Ning, Sanjana, Michele, Gizem, Sabine, Mariano, Dennis, Neel, Alina, Jeanette, Celine, Pouria, Sonali, and Marcus, you all have made my PhD experience fun and intellectually engaging. Thank you as well for being amazing colleagues for our work on the Global Assessment Report paper and modelling for Typhoon Goni impacts. Those are some intense crunch times. Alina, thank you for the thorough review of my thesis Introduction. I am grateful to you, Jeanette, and Dennis for reviewing Chapter 1 given my one-day notice.

I am thankful for the chance to be connected to amazing people and researchers who provided me data and logistical resources for my research. Thank you for being thoughtful and clear in the formats and meaning of the data you provided: Nama Budhathoki (Kathmandu Living Labs), Shengji Wei, Meng Chen (Earth Observatory of Singapore), George Williams, Jasna Budhathoki, and Victoria Stevens. Christina Tee Siew Khiaw and Nuraishah Binte Kasmadi, you are rockstars in terms of the administrative support that you provide. Edwin Tan, your instructions and support have been invaluable in my use of the Komodo cluster for tephra inversion.

I have also been lucky enough to be connected and have fruitful discussions with experts passionate in methods for dynamic risk. Their work has inspired my thinking

on the topic, and broaden my knowledge on the implications and capabilities of dynamic risk modelling. Thank you to Rashmin Gunasekera, Anirudh Rao, James Daniell, Antonios Pomonis, Graeme Riddell, Gizem Sarica, and Hedwig van Delden.

It is pure enjoyment to host visiting scholars in NTU. I am thankful for the opportunity to personally interact (even though brief) with scholars whose work I found most insightful: David Wald, Brian McAdoo, JC Gaillard, Carlos Molina-Hutt, Dale Dominey-Howes, Gordon Woo, Guillermo Franco, and Olivia Jensen.

Probably one of the most unexpected yet impactful experience in my PhD is contributing to the design and launch of the Averted Disaster Award (ADA). My utmost thanks to support of the Understanding Risk Community, Global Facility for Disaster Reduction and Recovery (GFDRR), and the World Bank Group for its launch in Singapore and award ceremony in Brazil. Thank you for funding my trip to Brazil so that we can announce the first ever winners of the Averted Disaster Award (fun!). Thank you to Francis Ghesquiere for his support and enthusiasm, which made the idea start to materialise. I'm very lucky to have worked with the amazing ADA team: Carrie Levine, James Martin Ennis, Alan Dinca, Pablo Suarez, Kara Devonna Siahann, and of course David Lallemant. Thank you for the immense and intricate work it took to build such a prestigious award. Witnessing how an idea that I worked on in the PhD produced a systematic global recognition of effective risk reduction makes me the happiest.

Much of the work I presented in this thesis are technical, but what isn't shown are the countless social media posts, blog posts, newsletters, and interviews that helped share the concepts of my work to the general audience. For this I had much help, in which I am truly grateful. Thank you for providing your media, risk communication, and/or photography expertise so that I can share the counterfactual analysis work to the public effectively: Lauriane Chardot, Mark Zuckerman, Beh Lih Yi, Nick Paul, and Jared Ng.

I have found amazing community from my time in Singapore, as well as during my month-long stay in Chiang Mai, Thailand. Special shoutout to Gina Sarkawi and Anushka Rege, for being the most amazing housemates, and who are always the first people I know I can count on in Singapore. I will always remember my PhD journey with a smile because of the goofy, intellectually-stimulating, and sometimes shocking experiences that we shared together. To my friends in Singapore - Wardah, Joanne, Tian Ning, Gizem, Sanjana, Hanna, Harris, Amit, Lesley, Jessica Cho - I have so much gratitude for your warmth and kindness. Because of the Chiang Mai Field Lab, I think the number of friends I have easily increased by 30+. Specifically, I'd like to thank Ashrika Sharma, Karen Barns, Pamela Cajilig, Giuseppe Molinario, Kei Franklin, Perrine Hamel, and Robert Soden for keeping the friendly connections since then. To my lovely friends in Manila: Audrei and Rich Ybañez, Gel, Julisa, and *"103"* buddies, thank you for being there for me and the consistent friendship.

I want to thank my family for providing the resources that have allowed me to pursue this path. *Salamat po, mommy, daddy, ate, kuya bibi, at kuya manong*. I think my brother, Rian, would have been proud, had he lived to see this day. Mom, Nenita L. Rabonza, I may be the first PhD in our whole extended family, but you know, you are still the most intelligent and most resilient person I know. Thank you for making sure that you're taking best care of yourself and dad, so that I never have to worry, and have the mindspace to take on my endeavors. This wouldn't be possible without you. Dad,

Manuel Rabonza, thank you for always providing me the wisest advice I need most at every moment. You taught me the value of routine, hardwork, and calmness (amidst chaos). You and mom are my rock. Cherry Rabonza, my *ate* (sister), you have always been a source of warmth and safety in my life. The house we bought and renovated together in the last few years has been an exciting project that always inspired me to work harder.

And Inah, thank you for believing in me even when I hadn't yet. The pandemic has been a harsh time for me, being away with people I love most, but you kept me sharp, kept me sane, and made sure these pages are written. Every paper I wrote, you've transformed to the most exciting stories over countless dinners with family and friends. The safety of your love kept me going. Thank you.

In 2013, just six months after I started working on analytics of natural hazards, I witnessed first-hand the devastation of Typhoon Haiyan in the Philippines. I dedicate this dissertation to those who have survived such disaster events and others who work tirelessly to minimise the impacts from future disasters.

Contents

Abstract

Disaster risk analysis quantifies potential damages and losses using accurate hazard, exposure, and vulnerability information. Risk reduction managers rely on disaster risk analysis to make informed decisions towards promoting greater resilience. However, current approaches lack key features for proactive decision-making, such as accounting for uncertainty in hazard modeling, time-dependent processes affecting vulnerability, and highlighting successes and benefits of risk reduction.

This dissertation makes three main contributions to the field of regional disaster risk analysis. First, I develop a framework for calibrating hazard parameters (inversion) and estimating the response of a hazard system (forward estimation) using limited and uncertain spatial data. This addresses gaps in current inversion-forward estimation approaches, which includes not accounting for varying uncertainties and spatial distribution in data, as well as the assumptions of the cost function. As a test case, I implement the framework on a tephra dispersion model using thickness observations of varying uncertainty to reconstruct past volcanic eruption characteristics and associated tephra fallout. Results show consistent improvements in model predictive performance for both inversion and forward models.

Secondly, I develop a computational framework for modeling time-dependent physical vulnerability in regional risk analysis. This study addresses a gap in regional earthquake risk analysis by accounting for processes that increase vulnerability (e.g. structural deterioration) and policies that mitigate it (e.g. regional-scale structural retrofit). The method provides a flexible tool for decision-makers to investigate the outcomes of various mitigation decisions.

Finally, I propose a counterfactual probabilistic risk analysis framework to quantify and highlight the benefits of effective disaster risk reduction interventions. This approach addresses a key challenge in risk management: that successful mitigations can go unnoticed (often because they are successful), making it difficult to incentivise proactive risk reduction decisions. Through counterfactual analysis (i.e. imagining the 'what-if' scenarios in disaster risk), the thesis shows how to calculate the probabilistic benefits of interventions, highlighting and celebrating their success.

Keywords: probabilistic risk analysis; spatio-temporal processes; counterfactual analysis; model calibration; earthquake risk; tephra fall hazard; school earthquake safety

List of Figures

List of Tables

Chapter 1

Introduction

1.1 Motivation and Background

The world's population is projected to increase by nearly 2 billion in the next 30 years, of which 70% will live in cities (United Nations, 2022). This growth is like adding an entire New York City to the planet every month (UN Environment, 2017). In the face of increasing intensity and occurrence of hazards due to climate change (e.g. Stewart and Deng (2015); Yang and Frangopol (2020); IPCC (2022)), urbanisation trends towards hazardous areas (e.g. McGranahan et al. (2007); Small and Nicholls (2003)), and rapid population growth, it is urgent to incorporate disaster risk reduction. This image of a riskier future may be bleak, but this presents a critical window of opportunity for the field of disaster risk management to tailor how and where to build this massive amount of new infrastructure that will lock us into a resilient trajectory for the next century.

Many cities already have an existing insurmountable risk, thus it is more practical to focus on mitigating future risk rather than existing risk. If we take Kathmandu, Nepal as an example, very little can be done to reduce the risk of the existing hundreds of thousands seismically-vulnerable buildings exposed to the region's high-seismic hazard. Displacement of a large amount of people to safer zones or rapid and massive-scale retrofitting are both impractical and infeasible. Thus, the best possible actions to reduce risk involve prioritising the management of future risk, and placing attention to critical infrastructure, which is something Nepal has started to do for schools (Dixit et al., 2014).

To guide such long-term proactive decisions for risk reduction, governments, international organisations, and the insurance industry rely on disaster risk analysis.

For these actors, risk analysis serves as a powerful decision-making tool as it can quantify the likely damages, deaths, and losses from a potential hazard event, and highlight which risk reduction measures are most effective to reduce impact. By knowing and understanding the future impact of their policies, they can influence the distribution and quality of the future built environment in a way that is resilient.

The core procedure in disaster risk analysis is the convolution of hazard, exposure, and vulnerability, characterised in probabilistic terms. Thus, key to reliable disaster risk analysis is taking the best available representation of hazard, exposure, and vulnerability equipped with the best state-of-art methods that understand risk-sensitive forward planning.

It is encouraging that the past few decades have seen the development of state-of-art tools that help quantify risk from natural hazards (e.g. Tralli et al. (2005); Liel et al. (2009); Yun et al. (2015); Loos et al. (2020)). Earthquake risk assessments, for instance, has greatly advanced in terms of predicting the probability of collapse of a building due to an earthquake in order to design mitigation strategies for a risk level acceptable for society (e.g. Krawinkler and Miranda (2004); Liel et al. (2006); Liel (2008); Liel and Deierlein (2012)). Yet despite the progress in our understanding of natural hazards and their impact, our current analysis tools fall short in their usability for decision makers who had to manage rapidly evolving and innovating cities.

This PhD dissertation puts attention to three (3) broad issues that are currently under-emphasised in the development and implementation of current state-of-art analytics in risk and hazard quantification: (1) under-utilisation of advancements in hazard modelling using uncertain data, (2) lack of dynamic risk tools, and (3) lack of focus and ways to recognise successes from risk reduction measures. The first two issues were alluded in Galasso et al. (2021)'s editorial that listed eleven (11) issues in current tools for decision support in risk reduction research and practice. The third issue was mentioned in Lallemant (2015)'s concluding dissertation reflections about accountability of decision makers and the power of disaster risk models to enable recognition for sound decisions in risk. This dissertation does not cover other issues mentioned in Galasso et al. (2021), which include under-emphasis on social vulnerability, multi-hazard interaction, non-asset-based risk metrics, and involvement of users and local stakeholders. The purpose of this PhD dissertation is to develop new frameworks to shift the paradigm of current state-of-art analytics in risk and hazard quantification to better support decision-makers as they conduct risk-sensitive forward planning of the tremendous urban growth of the next few decades.

This chapter first defines key definitions in disaster risk analysis (Section 1.1.1) and presents three research gaps (1.1.2). Three research questions that result from these gaps

(presented in Section 1.2) are each addressed in the main body of the thesis (Chapters 2, 3, and 4). Section 1.3 briefly summarises key contributions and an overview of the dissertation structure.

1.1.1 Definition of hazard, exposure, and vulnerability

Disasters are "social in nature" — they stem not solely from the hazard, but from the interactions of the physical, built, and social environments (Mileti, 1999; Peek and Guikema, 2021). In turn, disaster risk can be broadly defined as the likelihood of future undesired consequences produced from potentially damaging events such as natural hazards as they interact with our built-natural-social environments.

In this section, I define the core components in the quantification of disaster risk: hazard, exposure, and vulnerability. The convolution of these components can produce an estimate of the extent of a disaster, which can be characterised as loss of life, physical asset damage, and social, political and economic disruptions for a specific period of time (Smith, 2005; Moore, 1958). The quantification of disaster risk through the use of models and frameworks is critical in understanding potential disaster impacts for the design and evaluation of risk management strategies. Based on the terminology of United Nations General Assembly (2016), hazard, exposure, and vulnerability can be defined as follows.

- **Hazard** is defined as the likelihood of experiencing a certain intensity of potentially damaging event (e.g. earthquake, volcanic eruption, storm, etc.) at a certain location. The characteristics of hazards are typically identified by historical or user-defined scenario, probabilistic hazard assessment, and other methods that describe the hazard's location, intensity/magnitude, probability, and frequency.

- **Exposure** refers to the situation of built-natural-social environments located in zones affected by the hazard. Exposure may include people, infrastructure, housing, production capacities and socio-economic elements. Characterisation of exposure can be in terms of number of people, types of assets for the area, cost/value of the asset, and period of time of interest.

- **Vulnerability** refers to the susceptibility of the exposure to sustain impact or harm for a given hazard intensity. Vulnerability can be expressed as fragility or vulnerability functions that relate the expected level of damage or social cost (e.g. fatalities, displaced people) with the intensity of hazard, according to a specific exposure characteristic. The level of vulnerability can be influenced by

physical, social, economic and environmental processes. Cultural and institutional factors have also been known to influence vulnerability such as poor design and construction of buildings, lack of awareness and risk communication, poverty levels and education, and disregard for responsible governance.

Some disaster risk frameworks include *capacity* as an additional component to describe risk, where capacity is defined as the attributes, abilities, and resources available within a society to manage and reduce disaster risks and improve resilience United Nations General Assembly (2016). Frameworks accounting for capacity are typically used for qualitative and index-based applications to analyse risk. As this dissertation focuses on quantitative frameworks to analyse risk, elements pertaining to capacity is not accounted for in the research.

In equation form, the impact resulting from a realised disaster event can be characterised in terms of its relevant risk parameters:

$$I_{realised} = f\left(\theta_H, \theta_E, \theta_V\right), \tag{1.1}$$

where θ_H are the hazard parameters (e.g. magnitude or intensity of the hazard occurrence), θ_E are the exposure parameters (e.g. location of buildings and number of people exposed), and θ_V are the vulnerability parameters (e.g. structural building characteristics, social vulnerability, etc.).

In most cases, a disaster event is considered as deterministic, assuming that all parameters $\theta_H, \theta_E, \theta_V$ are known and fixed. However, in some cases, some parameters are considered as fixed and others as unknown with known probability distributions, such as frequency-magnitude curves of earthquake occurrence. In such a scenario, the probability of each impact occurrence is linked to the probability of the unknown parameters. In practice, this type of calculation does not have an analytical solution and must be determined through simulation methods, such as Monte-Carlo simulation.

The case studies in this dissertation are limited to hazards caused by earthquake events and explosive volcanic eruptions. Specifically, the hazards of interest include ground shaking during an earthquake and tephra fallout (fragments of rock ejected into the air by an erupting volcano that has the potential to form widespread deposits). Exposure elements in this thesis are buildings and people/occupants of the buildings exposed to the hazard.

The scope of this study is limited to the definition of vulnerability in the physical context only. Non-physical forms of vulnerability from damage caused by natural hazards such as social-vulnerability are not within the scope of this PhD dissertation. Thus, mentions of *vulnerability* throughout the text is interchangeable with *physical vulnerability*. Under this definition, examples of drivers that can increase physical

vulnerability include deterioration processes such as corrosion, fatigue, creep, and hazard-induced damage. On the other hand, drivers that can decrease physical vulnerability are measures that adapt the infrastructure to future conditions such as retrofitting, maintenance, and building replacement and other strengthening interventions,

1.1.2 Current approach and challenges

This PhD dissertation addresses three challenges in analytics and support of regional scale risk reduction described below. *Regional scale* refers to the level of data aggregation on spatial scales, instead of a specific geographic area or region. For instance, instead of analysing data at a building-level (which many risk analysis methods are developed for), this work focuses on grouping point data into larger spatial units or regions for analysis.

The first two challenges focus on the *analytics* aspect. These refer to challenges in the methodological features of our current risk analysis tools that limit their usability for decision makers amidst risk-sensitive forward planning for rapidly evolving regions. The third challenge focuses mostly on the *support* aspect for decision-making in regional scale risk reduction. They refer to social-related factors that encourage and incentivise policy makers to promote greater resilience.

Research gap 1

Hazard modelling rarely accounts for spatial characteristics and uncertainty in data

Modelling hazards phenomena often rely on the use of process-based models, which help represent the physical processes in the hazard. Two of the most useful applications of process-based models in hazard modelling are *calibration/inversion* and *forward estimation*. In inversion, hazard parameters that are often difficult or impossible to measure directly are estimated in such a way that they best represent the observed data. Common examples include estimation of earthquake rupture characteristics from seismic station records and calibration of volcanic eruption source parameters based on tephra deposit measurements (e.g. Li et al. (2022); Georgoudas et al. (2007); Connor and Connor (2006)). In forward estimation, the calibrated hazard parameters are then used to estimate the response of the hazard system. For example, ground motion intensity can be estimated for a given earthquake rupture parameters (Worden et al., 2010; Wang et al., 2022). The accumulated tephra over a region can be estimated given eruption and wind parameters (Hurst and Turner, 1999; Folch et al.,

2009).

As hazard models consider more complex processes, and as multiple data sources are increasingly becoming more available (e.g. ground sensors, crowd-sourcing, and remote sensing), current inversion and forward estimation frameworks underemphasise the importance of particular characteristics in the data that they rely on (e.g. spatial properties, distribution, and uncertainty (Willcox et al., 2021). Not accounting for these characteristics in the data may result to significant bias in the model outputs, and influencing their predictive performance in an extent that is currently under-explored.

In Chapter 2, these issues are explored in the context of modelling tephra fallout from explosive volcanic eruptions. The spatial and uncertainty characteristics in both the model calibration (inversion) phase and forward estimation phase are studied to improve the estimated parameters and model outputs. Given that tephra measurements are often collected in batches by different fieldwork teams at different durations since the eruptive event, there is value in accounting for uncertainty variations and spatial properties in the data. Measurements that are most reliable and contain the least uncertainty are mostly those taken from a well-preserved deposit, i.e. those taken soon after an eruption has ended in areas with little deposit reworking by wind and surface runoff processes (Pyle, 2016; Blong et al., 2017). The study addresses the current lack of conventional approaches in tephra fall modelling to consider differential uncertainties, and spatial nature in data for both calibration and forward estimation settings.

Research gap 2

Current risk analysis underemphasise time-dependent change in vulnerability and the multiple regional scale factors driving the change

There has been a recent shift in the field of disaster resilience towards a more dynamic and future-focused lens (e.g. Cremen et al. (2021); Galasso et al. (2021); Hemmati et al. (2020); Sanderson et al. (2022)). However, recent methods focus on time-dependent hazards and exposure, with a lack of emphasis on time-dependent vulnerability. In a literature review by Newman et al. (2017) of more than 100 risk analysis methods for decision making, risk analysis tools with a long-term perspective (30+ years) account for future risk only in terms of changing hazards (i.e. changing climate) and exposure (i.e. urban footprint expansion). This is supported by many recent studies that focus on combining urban change modelling and hazard consequence to calculate regional risk (Deierlein and Zsarnóczay, 2021; Mesta et al., 2022; Williams et al., 2022; Calderón and Silva, 2021; Cremen et al., 2022; Hemmati et al., 2021; Sarica et al., 2020; Haer et al., 2020)

The field of earthquake risk analysis has been leading the field in terms of

accounting for time-dependent vulnerability in risk analysis. Single-building applications for time-dependent vulnerability are in the context of seismic aftershock damage, deterioration, corrosion, and climate change adaptation. Examples of studies that assessed *increasing* vulnerability in terms of damage accumulation to buildings due to an earthquake aftershock sequence include Raghunandan et al. (2015); Aljawhari et al. (2021); Gentile and Galasso (2021); Papadopoulos et al. (2021). Research on environment-induced deterioration (e.g. corrosion) as it changes the physical vulnerability of the built environment has also been advancing in recent years to cover different components of buildings and bridges (Kashani et al., 2019; Amaya-Gómez et al., 2019; Guo et al., 2019; Zanini et al., 2020; Rao et al., 2017; Zamanian et al., 2020) and to account future weather conditions (Bastidas-Arteaga and Stewart, 2015, 2016; Wang et al., 2012; Stewart et al., 2012; El Hassan et al., 2010; Yang and Frangopol, 2019; Sevieri and Galasso, 2021). Studies have also assessed *decreasing vulnerability* as achieved by adaptation measures to infrastructure to future conditions. Many of such studies are motivated by climate adaptation strategies to reduce vulnerability against wind and flood-induced damage (e.g. Stewart et al. (2014); Dong and Frangopol (2017); Li and Stewart (2011); Qin and Stewart (2020); Ward et al. (2017)).

Regional-scale applications to assess earthquake risk demonstrate vulnerability changes driven by structural enhancements such as retrofit or better building code design. One example is Lallemant et al. (2017)'s study that uses a time-dependent vulnerability framework to provide projections of building collapse for a neighborhood-scale in Kathmandu Valley, Nepal. (Lallemant et al., 2017)'s work considered incremental building expansion as the driver of changing vulnerability (Amoako and Frimpong Boamah, 2017; Ferguson and Smets, 2010).

Given that the field of earthquake risk assessment has the most progress on developing methods for accounting for time-dependent vulnerability compared to other geophysical risk studies, Chapter 3 focuses on applications for earthquake risk. Based on the studies mentioned, applications on dynamic vulnerability focus only on one driver of changing vulnerability for each application at a time. Currently, there is still no conventional framework to simultaneously model multiple drivers that may increase and/or decrease physical vulnerability of exposed structures. As regions may experience these multiple drivers at the same time, accounting for them is critical to properly understand hazard-related risk over the lifespan of the built environment. Chapter 3 explores this research gap.

Research gap 3

Successes in risk reduction measures are often invisible, resulting to lack of incentives to proactive decision-making.

Disaster risk reduction efforts try to ensure that losses from disaster are avoided (i.e. 'nothing happens'). However, this poses a dilemma for recognising and incentivising successful risk interventions since they are made invisible by the very nature of their success. As a result, there is often a lack of incentives for decision makers to commit and invest in disaster risk reduction.

One situation where effective risk reduction is made invisible occurs when success has not been realised because the hazard impact has not occurred. If the benefits of risk reduction actions manifest primarily as reduced impact when a hazard event occurs, these benefits may only be realised far in the future — particularly for rare and extreme events. Hence relying on the realisation (also known as outcome bias) of a disaster to evaluate mitigation efforts ignores the significant time delay between the investment in risk reduction and the hazard. As with many actions to mitigate climate change, disaster risk reduction interventions require immediate sacrifice for seemingly uncertain benefits at a much later time (Weber, 2006). This time delay means that risk mitigation successes are rendered invisible until the eventual realisation of a hazard; excepting situations when mitigation measures also introduce co-benefits, in which risk reduction investment not only mitigates risk but also fosters economic growth or other societal welfare (Tanner et al., 2015).

Another situation where success in risk reduction becomes invisible is when a large hazard event occurs with disastrous impacts to society. In midst of the loss of life and negative societal and economic impacts from the disaster, both news and research tend to focus on the catastrophe. For this situations, it is very rare that a past mitigation intervention is revisited for analysis to assess how effective it was. This invisibility of mitigation successes amidst catastrophe is exacerbated by the perception that disasters are rare, overwhelming "acts of god" for which it is impossible to prepare (Gaillard, 2019).

The field of social psychology provides further insight into why disaster risk reduction evaluation is often so challenging based on the concepts of risk perception. Research has shown that people's emotional responses to events are influenced by their perception of "what might have been" (Medvec et al., 1995; Roese and Olson, 2014). A disaster event is a break from normalcy that triggers imaginations of alternative realities or *counterfactuals*: What if the disaster had never happened? What if it had hit a neighbouring town instead? In the aftermath of negative experiences, these counterfactuals are usually in an "upward" direction, where one imagines a better

outcome than the realised outcome (Blix et al., 2016), e.g. thinking about the ways in which a past car accident could have been avoided. Perceiving the benefits of mitigation, however, often requires comparing reality to a worse outcome or “downward counterfactual", which is not a natural cognitive process, e.g. imagining how a past car accident could have been worse.

Driven by these challenges related to risk perception and outcome bias, four types of situations arise wherein successful disaster risk reduction interventions are made invisible. Each of these situations can be visualised with a simple graphic using stilt houses as the mitigation and flooding as the hazard shown in Figure 1.1.

1. **Success made invisible in the midst of broader disaster:** Successful mitigation may result in fewer losses after a disaster, but this success is obscured amid the catastrophe and losses that were still incurred.

2. **Success made invisible by nature of the success:** A hazard becomes a disaster on account of the impacts it has on society. If mitigation efforts are so successful that there are no perceivable impacts, both the potential disaster and the successful mitigation are made invisible.

3. **Success made invisible due to yet unrealised benefits:** On account of the large time delay between the mitigation intervention and its benefits being realised, mitigation efforts could be seen as unsuccessful or unnecessary until a hazard event occurs.

4. **Success made invisible by the randomness of the specific outcome:** hazards are stochastic processes, hence any single occurrence is only one of several possibilities that could have occurred. Recognising that the parameters of the event that actually occurred could easily have been different, successes can be made invisible if the hazard randomly does not strain mitigation measures, e.g. a near-miss.

Investing in disaster mitigation is essential, particularly with the rising frequency of disasters due to climate change (IPCC, 2022). However, doing so in the light of the time delay between taking action and seeing benefits, as well as the invisibility of successful risk reduction, means that decisions to invest in mitigation require remarkable political will. Without recognition and reward for these efforts, interventions may be perceived as ineffective or unnecessary, with potentially disastrous consequences. Thus, highlighting the invisible benefits of successful risk reduction is critical, as celebrating past successes can help sustain and amplify ongoing efforts, and provide positive examples to learn

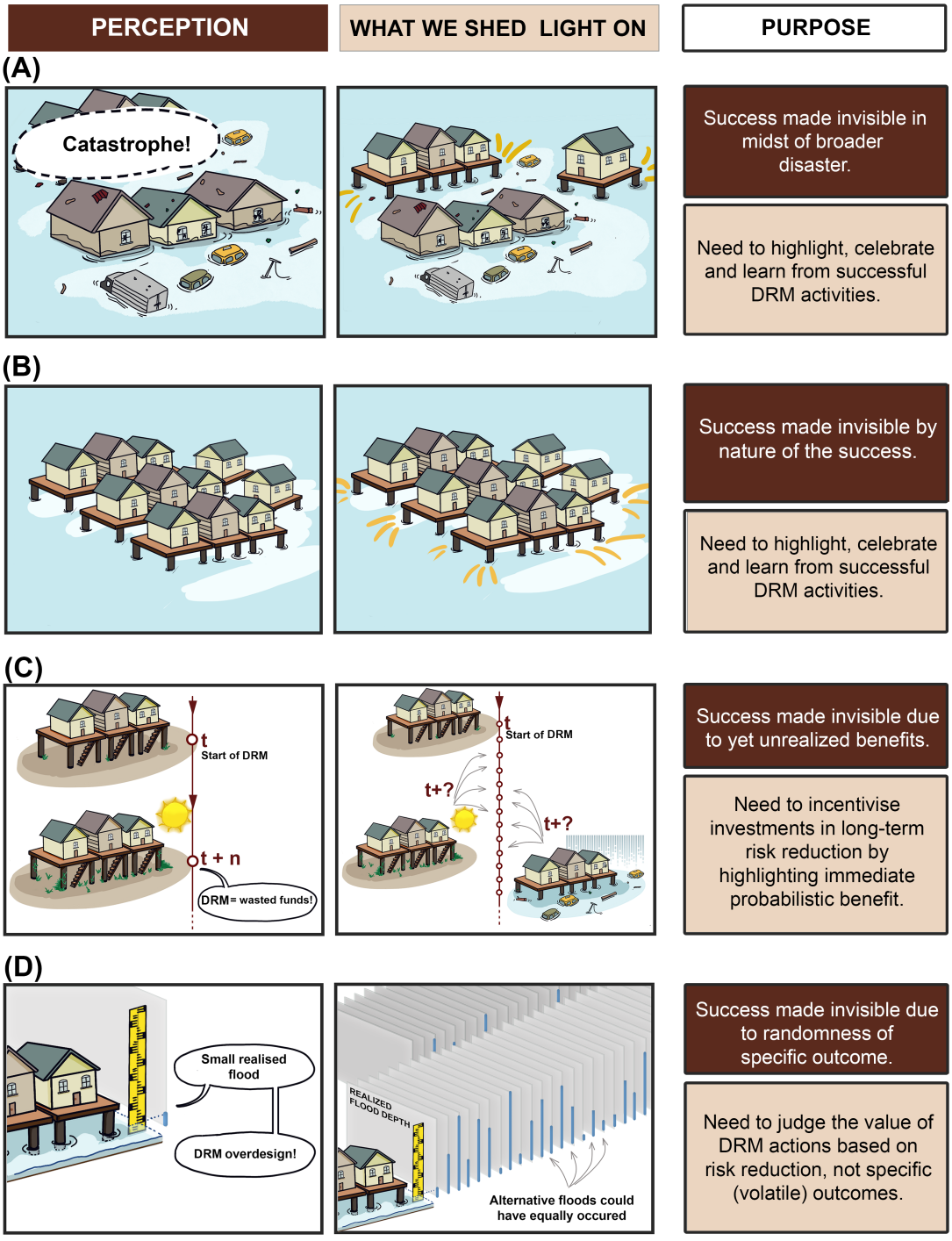

Figure 1.1: A schematic of invisibilities in mitigation successes using stilt houses as the mitigation and flooding as the hazard. This figure was developed and presented in published report for the 2022 Global Assessment Report, which I lead (Rabonza and Lallemant et al., 2022). Chapter 4 aims to address the first and the third invisibility described in this figure: (a) success invisible in midst of broader disaster, and (b) success made invisible due to yet unrealised benefits.

from, rather than focusing only on negative events that often dominate the news and research (e.g. Leach et al., 2012; Scott, 1998).

How then can policymakers be incentivised to make better risk-informed decisions when they are not credited for pro-active actions nor accountable for the consequences of doing nothing? There is a pressing need to develop better frameworks to judge the successes of disaster risk reduction interventions, both to recognise and celebrate good decisions as well as to create incentives for further investment in mitigation.

Chapter 4 addresses this research gap in the context of earthquake risk modelling. Specifically, the chapter covers analytics that address two out of the four situations of invisibility in disaster risk reduction: success made invisible in the midst of broader disaster, and success made invisible due to yet unrealised benefits (represented in Figures 1.1A and 1.1C).

1.2 Research questions

The main focus of this dissertation is to push the boundaries of risk analysis so that they can better support decision-making in risk reduction. This aim considers that current state-of-art frameworks would provide more value for decision-makers in risk reduction when they (1) consider spatial and uncertainty characteristics in the data, (2) account for the dynamic changes in the built environment, (3) provide incentives or credit to implement proactive risk reduction measures.

The specific research questions of the dissertation are:

1. How can we make the most of limited and uncertain spatial data in inversion and forward estimation with process-based hazard models?

2. How do we account for time-dependent physical vulnerability in regional scale seismic risk analysis?

3. How do we highlight the success of risk reduction programs implemented in the past and the benefits they will provide in the future using risk analytics?

1.3 Summary of contributions and structure

The body of this dissertation is a collection of three papers, corresponding to Chapters 2 through 4. Chapters 2 and 3 introduce improved risk *analytics* that enable risk-sensitive forward planning in regions where the built environment is rapidly evolving. Chapter 4 focuses on the *support* aspect for decision-making in regional scale risk reduction. The

chapters address the research questions in the context of earthquake and volcano hazards. Each chapter is autonomous with its own introduction and conclusion. References for all chapters are compiled at the end.

Contributions of the research project are summarised briefly below, and described in detail in each chapter. Their significance is discussed in the concluding chapter. The contributions all fit together to contribute to the vision of the PhD research: to provide evidence and tools for promoting greater resilience.

Chapter 2: Inversion and forward estimation with process-based hazard models: an investigation into cost functions, uncertainty-based weights and model-data fusion

Chapter 2 investigates methods that account for spatial-dependence and uncertainty in hazard modelling using limited and uncertain spatial data. Using an example of reconstructing past volcanic eruption characteristics and associated tephra fallout from different sets of field observation, I demonstrate the importance of making the best use of data-related uncertainty and spatial information in inversion and forward estimation. I present strategies for: (1) the selection of appropriate cost functions for inversion / calibration of a hazard model, accounting for their behaviour and the implied distribution of residuals, (2) the treatment of differential uncertainty when combining multiple data, and (3) the leveraging of both model and data when estimating the spatial distribution of output. These are demonstrated using data from the tephra fallout of the 2014 eruption of Kelud volcano in Java, Indonesia, and the Tephra2 model (a state-of-art approach in modelling the tephra fall accumulation around the regional vicinity of a volcano after an explosive eruption). This study makes use of methods in tephra fall hazard modelling, spatial statistics, goodness-of-fit tests, and calibration of models. Chapter 2's specific contributions include:

a) Proposed a two-step approach to evaluate the choice of cost function for inversion/calibration problems using process-based models.

b) Demonstrated that the impact of the choice of cost function in inversion is significant. This is the first study to place attention and investigate these impacts for tephra fall inversion.

c) The study added three more alternative cost functions to the default Tephra2 code, and identified one that is best-suited for the case study.

d) Extended the Tephra2 inversion algorithm to account for varying uncertainty across different data points, rather than treating each data point equally in the

optimisation.

e) Developed a model-data fusion approach based on spatial statistics methods that combines the forward model output and the data to improve estimates of the spatial distribution of tephra fall load.

f) Extended the model-data fusion methodology to also account for different levels of uncertainty associated with different sets of data.

g) Produced not only a map of tephra distribution, but also a map of uncertainties associated to the modelled tephra load in a forward estimation.

Chapter 3: Regional scale risk analysis accounting for time-dependent vulnerability

Chapter 3 presents a flexible framework to account for time-dependence in physical vulnerability for seismic risk analysis. Processes that increase vulnerability and policies that mitigate increase in vulnerability are modeled using time-homogenous Markov chains. The various state change processes are integrated within the risk analysis framework in closed form expressions. A hypothetical building stock with fragility curves derived from literature are utilised to demonstrate the framework. Multiple applications are demonstrated: (1) quantifying risk of structurally deteriorating buildings and the risk reduction impact of maintenance, (2) urban-scale seismic retrofitting policies based on various retrofit rates, and (3) impact of varying rates of building replacement to higher design grade, and an application wherein several drivers of changing vulnerability were implemented in the analysis. Chapter 3's specific contributions are:

a) Extended the Performance-Based Earthquake Engineering (PBEE) methodology (Krawinkler and Miranda, 2004) framework (the state-of-art engineering approach to assess impact from earthquake damage) to incorporate time-dependent vulnerability driven by deterioration and multiple regional scale policies.

b) Proposed to integrate a Markov chain approach with the risk analysis framework to model future regional-scale seismic risk driven by time-dependent vulnerability.

c) Demonstrate through case studies the influence of time-dependent vulnerability on a single deteriorating building, and to a neighborhood with buildings experiencing deterioration, retrofitting, and building replacements over time.

d) Introduced a proof of concept and flexible tool for decision-makers to investigate the consequences of various seismic mitigation decisions (that influence physical vulnerability) to future seismic risk.

Chapter 4: Learning from successes, not catastrophe: Using counterfactual analysis to highlight successful disaster risk reduction intervention

In Chapter 4, a framework is proposed for incentivising risk-informed measures by estimating the benefits of an intervention in a past earthquake, and for a hazard that has not yet occurred. The approach uses counterfactual modelling of a past hazard event with consequences made worse (i.e. downward counterfactual) by the absence of the mitigation intervention. Using a school building database for Kathmandu Valley, Nepal, two applications are presented: (1) the quantification of lives saved during the 2015 Gorkha earthquake as a result of the retrofitting of schools in Kathmandu Valley since 1999, (2) the quantification of the annual expected lives saved if the pilot retrofitting program was extended to all school buildings in Kathmandu Valley based on a probabilistic seismic hazard model. The analyses highlights the success of the seismic retrofitting program for schools in Nepal during the Gorkha earthquake, and the benefits of scaling up the program. Chapter 4's specific contributions are:

a) Introduced conceptual situations where successful disaster risk management interventions are made invisible with discussion derived from risk perception and social psychology.

b) Proposed a framework to quantify and highlight the benefits of effective disaster risk reduction interventions for two situations where they go unnoticed: amidst disaster, and when benefits are not yet realised by a hazard occurrence.

c) Introduced a new domain of application for counterfactual analysis in disaster research: highlighting the positives in disaster mitigation. Previous applications focus on identifying worse disaster outcomes for the purpose of insurance, preparedness, or future mitigation.

d) Pioneered a systematic approach to create incentives for good decision-making in risk reduction through quantification of probabilistic lives saved.

e) Compiled a list of other potential applications of the proposed framework beyond earthquake risk reduction and retrofitting program for schools.

Chapter 5 concludes the dissertation by summarising and synthesising the contributions of the research. The limitations and future recommendations for research are also presented.

Every chapter is introduced with three to four bullet points that serve as my "elevator pitch" for the chapter. They capture key methods and results presented in the chapter, but don't necessarily include all ideas, concepts or conclusions. Notational convention may not be strictly consistent across chapters, since notation was chosen for each paper rather than for the entire dissertation. Appendices for each chapter are compiled and organised at the end of the dissertation. This dissertation is a non-exhaustive representation of the work and research that I have conducted at Nanyang Technological University in the past 4.5 years.

Chapter 2

Inversion and forward estimation with process-based hazard models: an investigation into cost functions, uncertainty-based weights and model-data fusion

---

This chapter is a published journal article (as of June 17, 2023). Appendix A pertains to the Supplementary Material submitted with the paper.

Rabonza M.L., Nguyen M., Biasse S., Jenkins S., Taisne B., Lallemant D., (2023) Inversion and forward estimation with process-based models: an investigation into cost functions, uncertainty-based weights and model-data fusion. *Environmental Modelling Software* https://doi.org/10.1016/j.envsoft.2023.105750.

Chapter highlights

- *I propose a two-step approach to evaluate the choice of cost function in inversion.*
- *I demonstrate a calibration approach that weighs observations in the cost function based on data uncertainty.*
- *I present an improvement to spatial estimation that combines the forward model output and data.*
- *I demonstrate the methods using a tephra fallout model.*

2.1 Abstract

Process-based models for inversion and forward estimation have supported our understanding of earth, environment, and hazards processes. These methods are often applied on spatial data without accounting for their spatial nature and uncertainty. Using an example of reconstructing past volcanic eruption characteristics and associated tephra fallout from different sets of field observation, we demonstrate the importance of making the best use of data-related uncertainty and spatial information in inversion and forward estimation. We present strategies for: (1) the selection of appropriate cost functions accounting for their behaviour and implied distribution of residuals, (2) the treatment of differential uncertainty when combining multiple data, and (3) the leveraging of both model and data when estimating the spatial distribution of output. Results show that a data-informed choice of cost function and accounting for uncertainty and spatial characteristics of data leads to consistent improvements in model predictive performance for both inversion and forward models.

2.2 Introduction

Process-based models are important tools used to represent physical phenomena and processes in natural hazards analysis. In the *inversion or calibration setting*, they are used to estimate parameters that cannot be directly measured, through calibration to the observed response of the hazard system. Examples include estimating floodplain characteristics based on observations of past floods, estimating earthquake rupture characteristics based on recordings from seismic stations, or estimating volcanic eruption source parameters based on measurements of the deposited tephra (ejected particles of all sizes) across the impacted region (Li et al., 2022; Georgoudas et al., 2007; Connor and Connor, 2006). In the *forward estimation setting*, process-based models are used to estimate the *response* of the hazard system based on calibrated or assumed parameters. Examples include flood simulation using a calibrated inundation model (Uhlenbrook et al., 2004), estimating ground-motion intensity for a given earthquake magnitude and location (Worden et al., 2018; Wang et al., 2022), or estimating tephra accumulation given eruption and wind parameters (Hurst and Turner, 1999; Folch et al., 2009). Such applications of inversion and forward estimation frameworks merge the imperfect knowledge derived from data with that of process-based models in a way that utilises the reinforcing characteristics of both models and data.

As attention turns to such learning-from-data problems, recent advancements in

optimisation and uncertainty quantification underline the issue of treating inversion-forward estimation problems with a black-box perspective that ignores the characteristics of both models and data (Hollós et al., 2022; Cabaneros and Hughes, 2022; Biegler et al., 2011; Isaac et al., 2015; Oden et al., 2010). Despite advancements in data collection technologies (e.g., remote sensing) and the growing complexity of process-based models, inversion-forward estimation frameworks often overlook important data characteristics, such as distribution, uncertainty, and spatial properties (Willcox et al., 2021). Thus, there is a need to be strategic about how the inversion-forward estimation framework uses limited and uncertain data.

In this paper, we study this issue using the example of reconstructing past volcanic eruption characteristics and associated tephra fallout from observations across the impacted area. The application follows a typical inversion-forward estimation workflow shown in Figure 2.1. The inversion and forward estimation workflows can be conducted sequentially, as visualized in Figure 2.1, or separately. In the inversion/calibration setting, tephra fallout models are used to estimate eruption source parameters (ESPs, e.g. tephra mass, total grain size distribution, plume height, and plume profile) and empirical parameters (e.g. fall–time threshold, diffusion coefficient) from observations of tephra characteristics such as deposit thickness and grain size, typically collected through field surveys in the impacted area. As in any inversion process, an automated search routine finds the parameters of a model in such a way that the modelled response best approximates the observed data. The search routine optimises a *cost function* (also known as loss function or objective function), which calculates the agreement between the model estimates of tephra deposits and the observations. This process can estimate eruption parameters for past events, which is an important input for estimating the potential size and intensity of future eruptions, and their associated consequences (Newhall and Self, 1982; Carey and Sparks, 1986; Pieri and Baloga, 1986; Armienti et al., 1988; Scarpati et al., 1993; Mastin et al., 2009; Stohl et al., 2011; Pouget et al., 2013; Madankan et al., 2014; Bear-Crozier et al., 2020). In the forward estimation setting, tephra fallout models can map the distribution of tephra accumulation. The map can serve multiple purposes, including estimating eruption impacts on communities (Le Pennec et al., 2012; Wardman et al., 2012; Magill et al., 2013; Biass et al., 2017), assessing the vulnerability of buildings to tephra loading (Williams et al., 2020; Hayes et al., 2019; Spence et al., 2005), or quantifying risk to agriculture (Gómez-Romero et al., 2006; Ayris and Delmelle, 2012; Thompson et al., 2017).

Given the importance and broad applicability of process-based models, this study focuses not on the models themselves, but on how they are calibrated with limited and

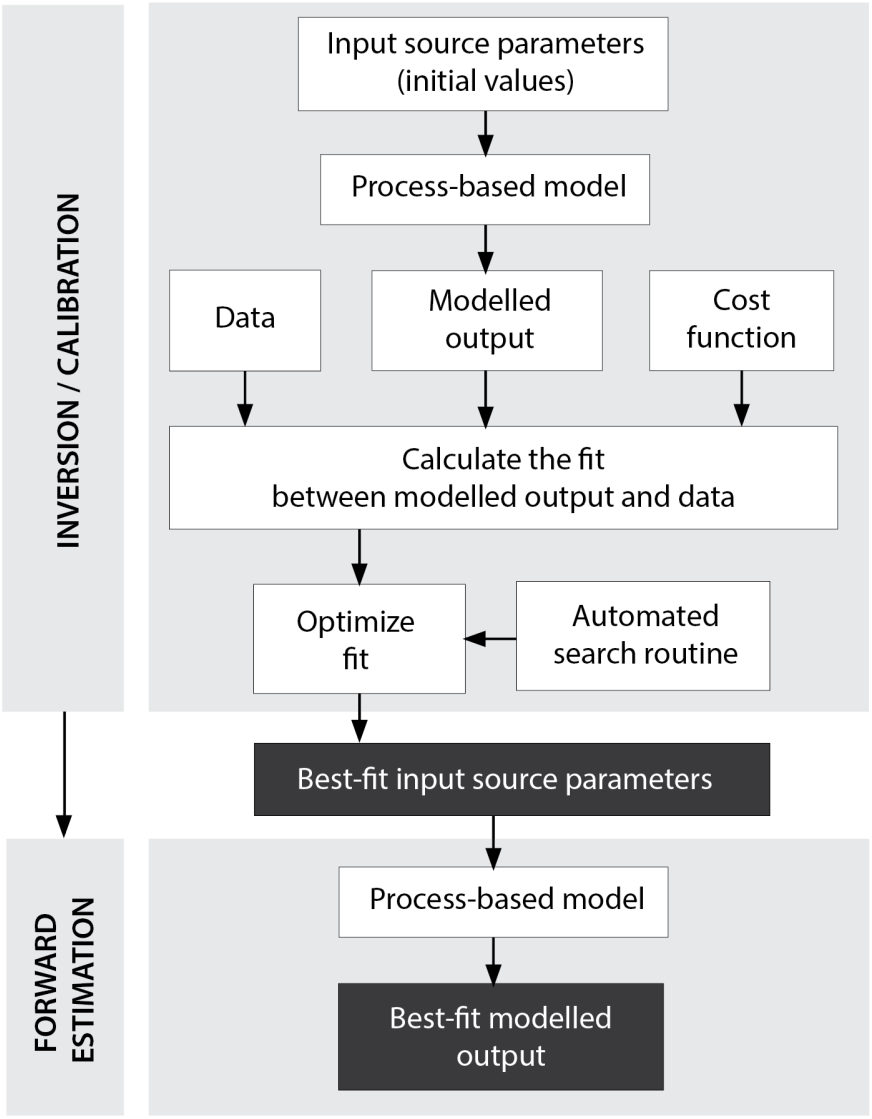

Figure 2.1: Schematic of a typical inversion-forward estimation workflow using a process-based model. The purpose of the inversion is to estimate the best-fit input source parameters (e.g. erupted mass, plume height), while the purpose of forward estimation is to obtain best-fit modelled outputs (e.g. a map of the tephra thickness). The inversion and estimation workflows can be conducted sequentially, as visualised here, or conducted separately/independently. The outputs of the inversion and estimation are shown as black boxes.

uncertain data and how they can best utilise such data in both inversion/calibration and forward estimation settings. We explore these through the study of tephra fallout from the 2014 eruption of Kelud volcano and the use of the *Tephra2* model of Bonadonna et al. (2005) as the process-based model. The inversion workflow follows Connor and Connor (2006)'s algorithm. The study does not make any particular claim or conclusions about the characteristics of the Kelud eruption or the accuracy of the *Tephra2*, both of which have been extensively studied by others (Maeno et al., 2019; Caudron et al., 2015; Hargie et al., 2019; Suzuki and Iguchi, 2019; Connor et al., 2011; Connor and Connor, 2006). Instead, this study focuses on methodological contributions into:

1. The choice of cost functions in the calibration process: What is the impact of this choice? What are the implied assumptions linked with this choice?

2. Making use of multiple data sources with varying uncertainty: How can we benefit from all data while still accounting for varying uncertainty?

3. Combining model estimates and data in the forward-model spatial estimate: How can we make use of both model results and observed data to estimate and map tephra accumulation? How do we account for varying uncertainty of the data in this estimation?

We believe that the recommendations can benefit researchers interested in improving their estimates when conducting inversion and estimation of spatially-distributed data. The approach to select the cost function, treat uncertain data, and generate spatial estimates can also be applied to other earth and environmental models. The paper proceeds as follows. Section 2 explains the current state of the art and limitations of interest in using process-based models for inversion-forward estimation of tephra fallout. Section 3 introduces our test case: modelling the tephra fallout from the 2014 eruption of the Kelud volcano using *Tephra2*. The Methods section (Section 4) illustrate the proposed improvements for model calibration and spatial estimation. We provide a combined Results and Discussion in Section 5 and the conclusions in Section 6.

2.3 Current approach and limitations

Tephra2 is an accessible and popular process-based model for inversion (Connor and Connor, 2006) and estimation of tephra fallout used in many volcanology studies (e.g. Volentik et al., 2010; Costa et al., 2012; Bonadonna and Costa, 2013; Mannen, 2014; Bonadonna et al., 2015; Connor et al., 2019; Constantinescu et al., 2021; Williams et al.,

2020). It solves the advection-diffusion equation analytically using wind and eruptive inputs, providing tephra deposit mass accumulation and grain-size distribution.

2.3.1 Choice of cost function

In the current version of the *Tephra2* inversion code, three possible cost functions are available to define the goodness of agreement or the model fit:

$$Mean\ square\ error\ (MSE) = \frac{1}{n}\sum_{i=1}^{n}(y_i - x_i)^2, \tag{2.1}$$

$$Chi\ square\ error = \frac{1}{n}\sum_{i=1}^{n}(y_i - x_i)^2/x_i, \tag{2.2}$$

$$Tokyo\ log\ error = \sum_{i=1}^{n}\left(log\frac{y_i}{x_i}\right)^2, \quad where \quad log\frac{y_i}{x_i} = 0,\ if\frac{y_i}{x_i} \leq 0 \tag{2.3}$$

where y_i is the modelled output, x_i is the observation, and n is the total number of data points.

The Tephra2 inversion algorithm, as introduced in the paper by Connor and Connor (2006), utilised the chi-square cost function. In their work, Connor and Connor (2006) highlighted that this cost function provides equal treatment to measurements of both thin and thick deposits during optimisation. There are no additional instances in the tephra modeling literature where the selection of the cost function is discussed beyond this study (Volentik et al., 2010; Costa et al., 2012; Bonadonna and Costa, 2013; Mannen, 2014; Bonadonna et al., 2015; Connor et al., 2019; Constantinescu et al., 2021; Scollo et al., 2008; Fontijn et al., 2012).

Outside the field of tephra fallout modelling, multiple studies have brought attention to the fact that different measures of model performance (implied in the choice of cost-function) may satisfy different desirable characteristics (Chen et al., 2017; Makridakis, 1993; Armstrong and Fildes, 1995). Certain cost functions penalize different magnitudes and directions of forecast error differently (Walther and Moore, 2005). An underestimation may not have the same penalty as an overestimation (Morley et al., 2018). Some characteristics may also be relevant for pragmatic purposes such as their interpretability. Such considerations help in narrowing down desirable cost functions applicable to an application.

Beyond the cost functions' characteristics, the takeaway from these studies is that no metric is inherently better for all applications. Importantly, choosing a cost function implies making an assumption on the type of distribution of the residuals (where residuals are the difference between the modeled output and the observations) (Engle,

1993). Hence, in its correct application based on the assumed residual distribution, a cost function is optimal. For instance, Hodson (2022) presented a theoretical justification that root mean square error is optimal for normal (Gaussian) residuals while mean absolute error (MAE) is optimal for Laplacian residuals. In Section 2.5.2, we implement this knowledge of the cost functions' characteristics and inherent assumptions on the residuals to demonstrate how an optimal cost function may be selected for a test case. We investigate the extent that the cost function affects the resulting estimates of tephra fallout and the associated residuals.

2.3.2 Treatment of varying uncertainty in data

For the same deposit, several factors may contribute to varying uncertainty between data points depending on how, when and where measurements are collected (Engwell et al., 2013; Bonadonna et al., 2015). According to Engwell et al. (2013), there are two types of uncertainties in tephra thickness, both of which are rarely quantified or reported in field studies and literature. Uncertainty can be due to natural variation, which is related to the physical processes of deposition, preservation, and remobilisation. The second type is observational uncertainty, or those uncertainties related to differing measurement techniques. Measurements that are most reliable and contain the least uncertainty are those taken from a well-preserved deposit, i.e. those taken soon after an eruption has ended in areas with little deposit reworking (Pyle, 2016; Blong et al., 2017). However, such conditions are often difficult to meet even for recent eruptions, and impossible when studying older eruptions. Large portions of tephra deposits may also be inaccessible while they are still well-preserved (Walker and Croasdale, 1971). Field campaigns conducted at a significantly later time after the eruption might acquire measurements subjected to post-eruption processes (e.g., compaction, soil formation, bioturbation, and remobilisation (Engwell et al., 2013)) or local weather conditions (e.g., rain or wind (Hayes et al., 2002; Wilson et al., 2011; Arnalds et al., 2013; Blong et al., 2017; Oishi et al., 2018; Dominguez et al., 2020)). Given limited data, it is advantageous to leverage all available data. However, it becomes increasingly important to appropriately address uncertainty when integrating multiple data sources with differing levels of uncertainty.

The current *Tephra2* inversion algorithm treats all data equally, potentially leading to biased tephra load estimates if relative differences in uncertainty between datasets are ignored. To address this issue, we propose a calibration approach in Section 2.5.3 that accounts for the reliability of the data by weighing the observations in the cost function. Our analysis demonstrates the importance of considering uncertainties in fitting the model to the data. However, note that our approach does not aim to

determine the optimal weights for the measurements, and we do not quantify the absolute uncertainties in the data.

2.3.3 Making use of model and data

The best-fit modelled output from the forward estimation may diverge from observations in a spatially structured way due to model approximations, unaccounted processes, and uncertainties inherent in any model. While these model-data disagreements may not cause issues for applications such as tephra volume estimation when spatial aggregates are used, they affect forward forecast or prediction performance when spatially explicit estimates are the focus and the process-based models are unable to capture the spatial complexity one might observe in the field. Hence, if the goal of the forward estimation is to obtain the spatial predictions that best agree with observations, the process-based model alone may not serve as the best tool.

Assimilation techniques can be used to combine the model output with observations and improve the quality of the model estimates. For example, studies on volcanic ash concentration forecasting apply ensemble methods such as Ensemble Kalman filters to provide optimal estimates of the spatial distribution of ash dispersal in the atmosphere (e.g. Osores et al., 2020; Pardini et al., 2020). Such assimilation methods are *online* in the sense that they actively interact with the model over a time period of interest. Observations of tephra deposits are temporally too sparse to conduct an online assimilation. Thus, we assimilate the model with observations using statistical interpolation to estimate the time-averaged state of the system from post-eruption surveys. Several statistical interpolation techniques have been used for assimilation in the geoscience and environmental literature. These include regression techniques (Horalek et al., 2005), Kalman filtering (Denby et al., 2008), and kriging methods (Thompson et al., 2014; Blond et al., 2003; Kassteele et al., 2006). Studies have shown that kriging is the most effective spatial interpolation approach (Johnston et al., 2001; Horálek et al., 2006).

In Section 2.5.4, we apply residual kriging to combine the model output and data. The proposed spatial estimation method, here we call model-data fusion, harnesses both the process-based model and the spatial structure of the data to improve the estimated spatial distribution of tephra load. In addition to treating the tephra fallout data as spatial and accounting for their spatial characteristics, the estimation method considers observations as imperfect versions of the true process, with uncertainties always associated with them. In line with the varying data uncertainties mentioned in Section 2.3.2, we investigate two variations of the estimation method. One approach weighs all the data points equally, while the other accounts for the relative uncertainty

between different groups of data.

2.4 Test case: 2014 Kelud eruption

2.4.1 Eruption characteristics

The 2014 eruption of Kelud volcano, located in East Java, Indonesia was selected as a test case for this study. The explosive activity started at 22:50 local time on 13 February 2014 and lasted for over four hours (Global Volcanism Program, 2014). The eruptive activity finally declined on 14–17 February 2014. The total erupted volume was estimated to be 0.25–0.50 km^3 (bulk deposit volume, 0.14–0.28 km^3 in dense rock equivalent), and the mass eruption rate was 6.5 ± 2.8 x 10^7 kg/s (Maeno et al., 2019). The impacts of tephra fallout were widespread with over 76,000 people evacuated, forty regional flights cancelled and rerouted, and more than 26,000 buildings destroyed or damaged (Global Volcanism Program, 2014; Williams et al., 2020; IFRC, 2014).

A documentation of the eruption sequence by Maeno et al. (2019) and numerical simulations by Tanaka et al. (2016) highlighted that the dispersal process and tephra accumulation were affected by the local winds. At high altitudes of ~17km above sea level, the umbrella cloud was affected by strong winds from the east. Low altitudes of ~5 km above sea level were affected by winds from the southwest, transporting tephra to the northeast and causing a bilobate tephra deposit. Published isopachs of accumulated tephra for this eruption (Figure 2.2) show a subtle bilobate feature that is attributed to the dynamics and evolution of the eruption and the local winds around the volcano (Maeno et al., 2019).

2.4.2 Tephra fall data

The study utilises two sets of tephra fall data, each derived from field surveys by different teams at various times after the eruption. The analysis takes the data in terms of load. When only thickness measurements are available, they are converted to loads based on a deposit bulk density of 1400 kg/m^3 measured by Maeno et al. (2019). The first dataset, here called *Dataset 1*, is the tephra load data obtained from a field study of thickness by Universitas Gadjah Mada (UGM) (Anggorowati and Harijoko, 2015) and later used in inversion modelling by Williams et al. (2020). The measurements were taken 2-3 days post-eruption at 81 locations within 2 to 60 km of the vent (Williams et al., 2020). The other data set, here called *Dataset 2*, consists of tephra load data converted from thickness measurements from a geological survey by Maeno et al. (2019) conducted a month after the eruption. Dataset 2 provides load information at 50 locations, including

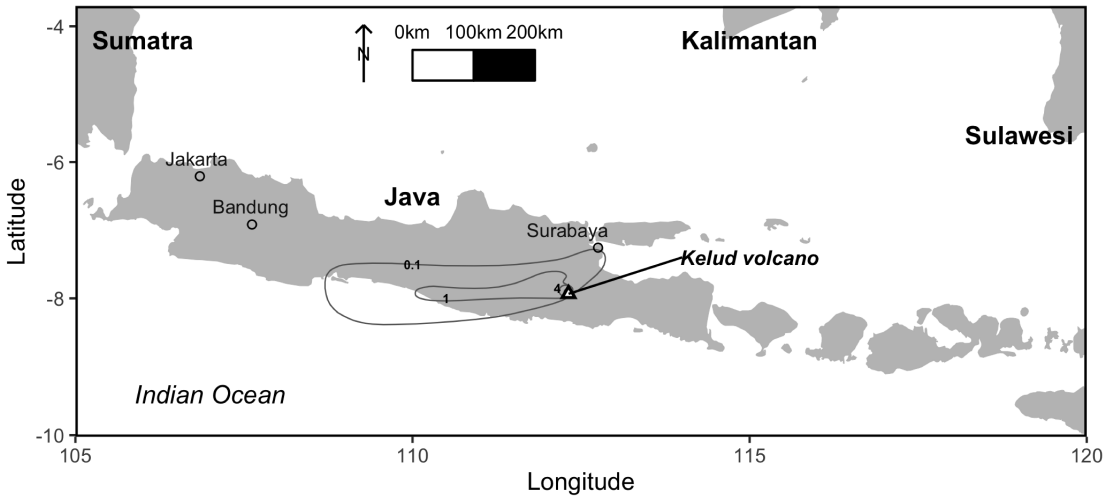

Figure 2.2: Location map of Kelud volcano in Indonesia. The contours represent tephra thicknesses of 0.1, 1, and 4 cm adopted from Maeno et al. (2019)'s study of the 2014 Kelud eruption fallout deposit.

areas up to 75km north of the vent that Dataset 1 doesn't cover. For this study, we exclude the six eyewitness reports also presented by Maeno et al. (2019).

Four outliers were removed from the raw datasets as they were an order of magnitude different than nearby data, potentially related to issues of data collection or significant deposit reworking. Being outside the range of the other observations, these were deemed to have a disproportionately strong influence over the model fits. After removing these outliers, the dataset used in our analyses consists of 127 points. We present a map of the datasets in Figure 2.3.

2.4.3 Previous inversion study

The value of using inversion and forward estimation with process-based models for Kelud volcano has been presented in recent literature. Williams et al. (2020) applied inversion as one of the methods to support remote assessment of tephra fall building damage and vulnerability assessment of buildings around Kelud volcano. In Williams et al. (2020)'s study, thickness measurements were inverted to estimate the best-fit source parameters, which were later used to map a continuous deposit. Such application is important to enhance our knowledge of risk to tephra hazards on the the scale of buildings or regions, especially when there is a high likelihood of future damaging eruptions from Kelud (Maeno et al., 2019).

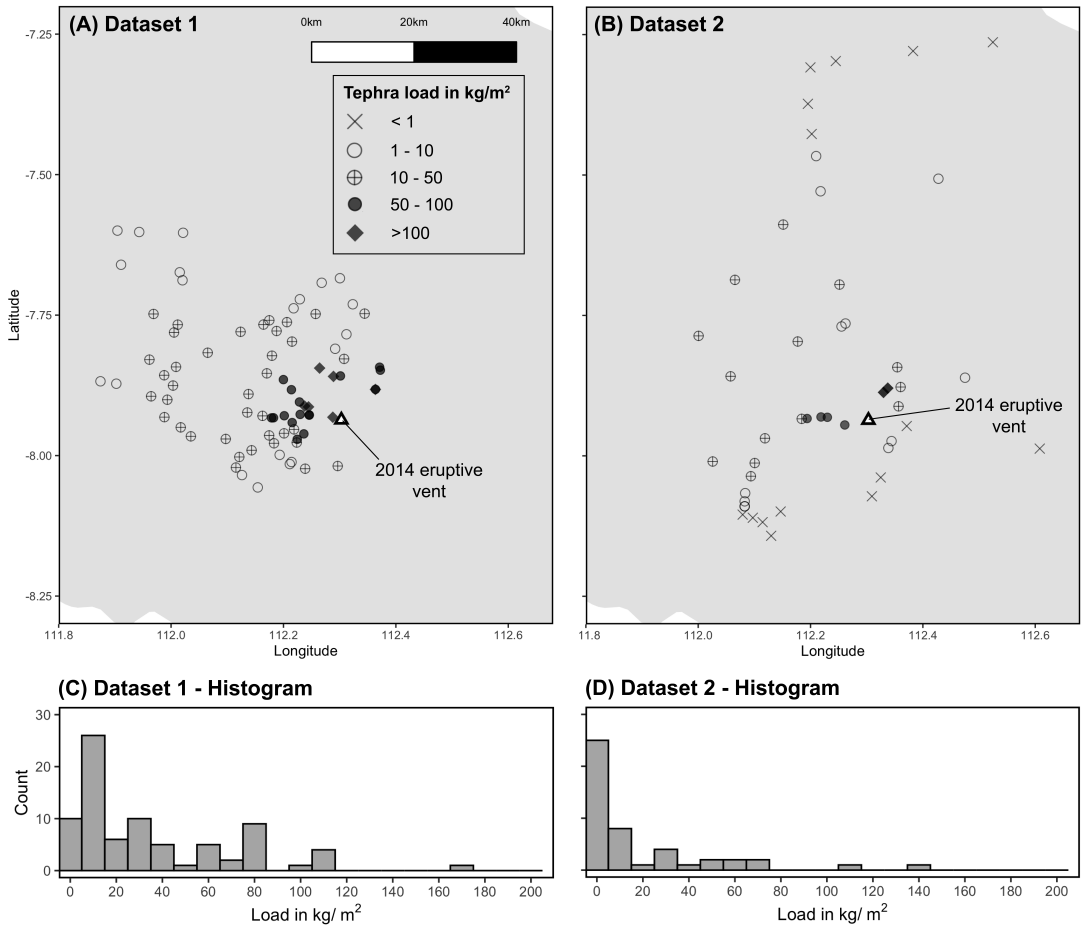

Figure 2.3: Map and histogram of datasets used in the study. The location of Kelud volcano's vent from the 2014 eruption is based on Goode et al. (2019)'s study of the eruption.

Table 2.1: The inversion in this study uses the range of initial values presented in this table. The initial values are selected based on information from: [a] Kristiansen et al. (2015), [b] Maeno et al. (2019), [c] Goode et al. (2019); Maeno et al. (2019), [d] Goode et al. (2019); Maeno et al. (2019), and [e] Williams et al. (2020).

Inverted parameters	Values from literature	Initial values for the inversion
Plume height (km above sea level)	18 to 26 [a]	15 to 23
Erupted mass 10^{10} kg	38 to 66 [b]	10 to 100
Median grain size (ϕ)	-3 to 1 [c]	-3 to 2.5
Phi standard deviation	1 to 3 [d]	0.5 to 3
Fall-time threshold (s)	0.001 - 10,000 [e]	0 to 15,000
Diffusion coefficient ($m\,s^{-2}$)	0.0001 - 10,000 [e]	0 to 15,000
Plume profile (α)	3 [e]	3
Plume profile (β)	0.001 - 3 [e]	0.001 to 3.5

2.5 Methods

2.5.1 Model setup for *Tephra2* inversion

The parameter bounds used in the inversion algorithm are shown in Table 2.1. The ranges of values are selected based on studies in the literature of the 2014 Kelud eruption and a recent inversion for the same eruption in Williams et al. (2020). For this study, some of the ranges of values are widened relative to Williams et al. (2020)'s to ensure that the inversion solution converges within the limits set. We use the default optimisation routine from Connor and Connor (2006)'s inversion algorithm, the Nelder-Mead simplex method. The inversion used a fixed wind profile based on the wind dataset from the European Centre for Medium-Range Weather Forecasts (ECMWF) Era-Interim Reanalysis for the midnight of 13 February 2014 (Dee et al., 2011).

2.5.2 Evaluation of cost function

This paper examines five cost functions, including those currently in the *Tephra2* code (mean square error, chi-square error) and three additional functions.

$$Mean\ absolute\ error\ (MAE) = \frac{1}{n}\sum_{i=1}^{n}|y_i - x_i| \tag{2.4}$$

$$Mean\ absolute\ percentage\ error\ (MAPE) = \frac{100}{n}\sum_{i=1}^{n}\left|\frac{y_i - x_i}{x_i}\right| \tag{2.5}$$

$$Mean\ square\ log\ error\ (MSLE) = \frac{1}{n}\sum_{i=1}^{n}\left(log\frac{(y_i+1)}{(x_i+1)}\right)^2 \tag{2.6}$$

where y_i refers to the model estimate, x_i is the observation, and n is the total number of data points.

Instead of Tokyo log error (Equation 2.3), this study uses MSLE (Equation 2.6), a more well-known cost function in statistics and machine learning. In cases where the observed and predicted values are strictly positive, as in the case of tephra load data, the Tokyo log function is essentially the same as MSLE. In MSLE's formula, the '+1's attached to the observed value x_i and predicted value y_i ensure mathematical stability since log(0) is undefined and both y and x can be 0.

We propose a two-step approach to evaluate the choice of cost function for the *Tephra2* inversion. First, the choice should be guided by the properties of the cost function summarised in Table 2.2 and discussed in Section 2.5.2. The second step is to run test inversions using the shortlisted cost functions and analyse the resulting residuals using goodness-of-fit tests as described in Section 4.2.2.

Selection based on cost functions' properties

The foundation of any cost function is the model residual, defined as $\varepsilon = y - x$, where x refers to the observed value and y is the predicted value of the model. Cost functions almost always include a transformation of the observed value, predicted value or the residual. This transformation influences the model estimates according to these properties: (1) order-dependence, (2) sensitivity to outliers, and (3) symmetry. The equations for the transformed residuals associated to the cost functions are shown in Table 2.2.

Order-dependence describes how the function covers orders of magnitude for the residual. For instance, an order-dependent cost function may utilise the relative error ε/x (e.g. in the chi-square cost function) or the log-transform of the observed and predicted values (e.g. in mean square log error, MSLE). On the other hand, a cost function that's not order-dependent, also known as scale-dependent functions, keep the residual ε as is in the function to retain the units/scale of the observed and modelled values (Walther and Moore, 2005).

If the modeller wishes to balance the treatment of distal and proximal deposits, order-dependent cost functions may be desirable. Since order-dependent cost functions are scaled to the magnitude of the measured value, observations made in thin parts of the deposit are equally important as observations made in the thicker parts of the deposit. This aspect is important due to a few reasons. Tephra deposits thin exponentially with distance from the vent, and outcrops mapped across a single deposit may span orders of

magnitude (Pyle, 1989). Distal measurement of tephra accumulations are important to inform the extrapolation of the thinning rate beyond the outermost isopach. Examples of common order-dependent cost functions include chi-square, MSLE and MAPE.

Some cost functions are more sensitive to outliers than others. Cost functions with squared residuals, for instance, penalise large residuals more heavily than small residuals. Common examples are MSE and root-mean-square-error (RMSE), both of which minimise to the same solution. If we prefer to constrain penalty on large errors and make the function more resistant to outliers, the absolute residual $|\varepsilon|$ can be used instead of ε^2, for instance, with the mean absolute error (MAE). MAE may be more appropriate for instances when the residuals are not normally distributed, when large model residuals don't have to be weighted heavily, and when the presence of outliers is a significant issue.

Lastly, the symmetry of the cost function relates to the treatment of underestimation versus overestimation. MSE, MAE, and chi-square treat residuals symmetrically. MSLE applies more penalty for underestimation than overestimation. Mean absolute percentage error (MAPE) penalises overestimation more than underestimation.

Selection based on cost functions' assumption on residuals

The choice of cost function implies a distribution of residuals. So in addition to their theoretical properties, we can examine the validity of the cost functions by investigating the distribution of resulting residuals using statistical tests such as the Kolmogorov-Smirnov (K-S), the Cramér-von-Mises (CvM) and the Anderson-Darling (A-D) as well as the Shapiro-Wilk (S-W) (Ramachandran and Tsokos, 2015; Stephens, 1986). These tests use different metrics or test statistics to measure how similar the empirical distribution of the residuals is to its assumed one. For example, the K-S test statistic is:

$$D = \max(|F_0(\epsilon) - F_n(\epsilon)|), \tag{2.7}$$

where $F_0(\epsilon)$ is the assumed cumulative distribution function and $F_n(\epsilon)$ is the empirical cumulative distribution of the residuals. The larger D is, the more unlikely the residuals to have been generated from the assumed distribution. Goodness-of-fit can also be assessed graphically using quantile-quantile (Q-Q) plots which compare the empirical quantiles from the model fit to the theoretical quantiles from their assumed distributions. While both statistical tests and Q-Q plots are useful indicators of goodness-of-fit, they both assume that the residuals are themselves independent and identically distributed.

Table 2.2: Cost functions with their formulae, residual transformation and assumed error distributions. In the formulae, x refers to the observation, y the model estimate, n the number of data points and $\varepsilon = y - x$ the residual. For the Gaussian distributions, $\hat{\sigma}$ denotes the estimated standard deviation, while for the Laplace distributions, b denotes the estimated scale. Characteristics of the cost functions are provided with a recommendation of when these are useful for tephra load inversion. The checkmarks indicate if the cost function satisfies a specific characteristic.

	Cost function				
	MSE	MAE	Chi-square	MSLE	MAPE
Formula	$\frac{1}{n}\sum_{i=1}^{n}\varepsilon_i^2$	$\frac{1}{n}\sum_{i=1}^{n}\lvert\varepsilon_i\rvert$	$\frac{1}{n}\sum_{i=1}^{n}(\varepsilon_i^2/x)$	$\frac{1}{n}\sum_{i=1}^{n}\left(log\frac{(y_i+1)}{(x_i+1)}\right)^2$	$\frac{100}{n}\sum_{i=1}^{n}\left\lvert\frac{\varepsilon_i}{x_i}\right\rvert$
Transformed residual $Z(s_i)$	$Predicted - Actual$	$Predicted - Actual$	$\frac{Predicted-Actual}{\sqrt{Actual}}$	$\log_{10}\left(\frac{Predicted+1}{Actual+1}\right)$	$\frac{Predicted-Actual}{Actual}$
Assumed distribution	$\frac{Z(s_i)}{\hat{\sigma}} \sim N(0,1)$	$\frac{Z(s_i)}{\hat{b}} \sim Laplace(0,1)$	$\frac{Z(s_i)}{\hat{\sigma}} \sim N(0,1)$	$\frac{Z(s_i)}{\hat{\sigma}} \sim N(0,1)$	$\frac{Z(s_i)}{\hat{b}} \sim Laplace(0,1)$
Scale-dependent	The units of the observed and predicted values are retained. Useful for interpretability .				
	✓	✓			
Order-dependent	Thinner deposits are as important as thicker deposits. Useful when spanning orders of magnitude.				
			✓	✓	✓
Sensitive to outliers	Estimates fit large values closely. Useful when these are the most reliable and informative.				
	✓		✓		✓
Robust against outliers	Reduced penalty on large residuals. Useful when there are many outliers in the data.				
		✓		✓	
Symmetric	Treats overestimation and underestimation equally. Useful to avoid anomalous skewness in errors.				
	✓	✓	✓		
Asymmetric	Treats overestimation and underestimation unequally. Useful for avoiding either scenario.				
				✓*	✓**

*Larger penalty for underestimation. **Much larger penalty for overestimation.

2.5.3 Weighting the data in the cost function

In order to account for different levels of uncertainty inherent in our datasets, we propose to weigh each data point based on its uncertainty relative to a reference dataset. In this way, less reliable data have correspondingly less influence on the inversion. The reference dataset may be an individual measurement or a group of measurements having the least measurement uncertainty. In this work, we use the prior information that Dataset 2 has a relatively larger uncertainty than Dataset 1 because of the delay in field data acquisition between the two sets of data. Thus, Dataset 1 is set as the reference dataset. In the inversion algorithm, points in this reference dataset are assigned a weight of 1. Other datasets are then assigned weights relative to the uncertainty of the reference data. For example, the points from a dataset assumed to be twice as uncertain as the reference dataset may be assigned a weight, w, of 0.5.

Using weights based on relative uncertainty leads to a weighted cost function, where each data point is weighted relative to the reference dataset. With our proposed weighting scheme, the weighted MSE cost function, for instance, can be written as:

$$\frac{1}{n}\sum_{i=1}^{n} w_i(y_i - x_i)^2 \tag{2.8}$$

where w_i indicates the uncertainty weight assigned to the data point i. For our application, we set Dataset 2's weight to 0.5.

We evaluate the effectiveness of the weighted cost function based on the accuracy of the forward estimates on unseen (out-of-sample) data. The test set consists of a random subset (20%) of Dataset 1, while the training set consists of the rest of the Dataset 1 points and all of Dataset 2 (Figure 2.4). A test set should ideally consist of data that closely resembles the true deposit, so a stratified test set was selected to represent thin and thick deposits in relatively equal proportion as the true deposit. We conducted inversion using the training points, the parameter ranges in Table 2.1, and the weighted form of the cost function. For all the inversions, we generate forward estimates of tephra load on the locations of the test points. To assess predictive performance, we compare the test errors between the unweighted inversion and weighted inversion. The test errors are calculated following the formula of the cost function used in the inversion.

2.5.4 Combining model estimates and data

To estimate the spatial distribution of tephra load across the entire area, we propose to combine both forward model estimates as well as the data. The process consists of three general steps: (1) conduct an inversion-forward estimation to model the distribution

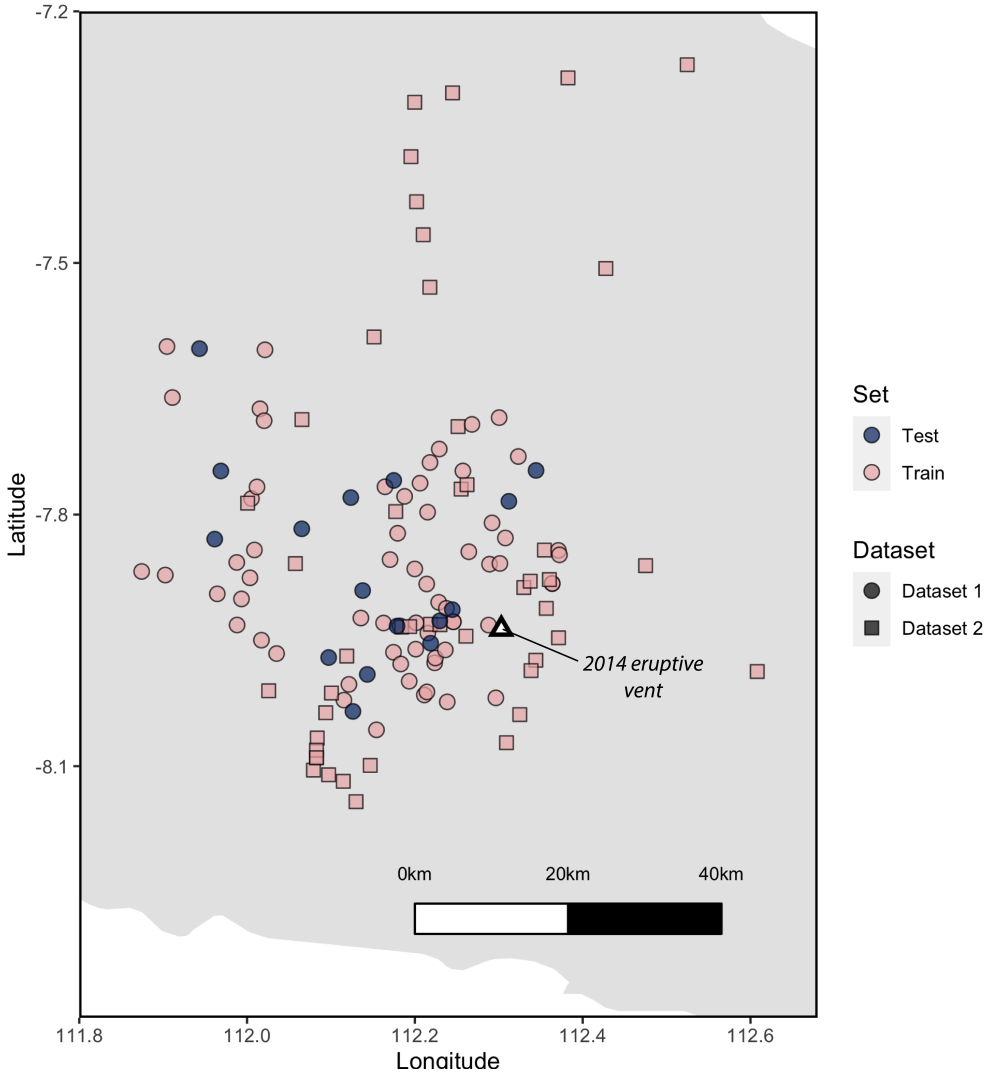

Figure 2.4: The effectiveness of the weighted cost function was evaluated using a train-test split process. Shown is a map of the training and test points used for the methods in Section 2.5.3.

of tephra fallout (2) interpolate the residuals using spatial statistics techniques, and (3) combine the interpolated residuals with the forward model. We test and present two different spatial statistics techniques for the interpolation step. The result is an improved estimate of tephra load that combines the information of the model and data.

Our methods use kriging, one of many interpolation techniques that estimate values at unobserved locations using a limited set of known spatial data. In kriging, the interpolation accounts for the spatial arrangement of the data in such a way that points nearby the site of interest are given more weight than those farther away. This approach differs from another popular method, inverse distance weighted interpolation, in that we do not assume a spatial distribution model beforehand but estimate it from data. Another advantage of kriging is that we can estimate the uncertainty associated with the interpolated value.

Unweighted model-data fusion

We describe the procedure for an *unweighted* model-data fusion approach using kriging. In this approach, there is no consideration of differential uncertainty between individual or groups of data. We employ simple kriging in the following methods, assuming that the difference between model and data across the study area has a mean of zero and follows a multivariate normal distribution (Wackernagel, 2003). The kriging process involves selecting a variogram model that describes the spatial relationship between each pair of data points, quantifying the degree of variation in the sampled values based on their spatial distance. Often, the parameters of the variogram model are user-defined or estimated using statistical software through approaches like maximum likelihood and least-squares estimation. We typically assume stationarity and isotropy, implying that the variogram and the distribution of residuals do not vary with location or direction.

1. Inversion and forward modelling:

    (a) Run *Tephra2* inversion following the model setup in Section 2.5.1 to find the best-fit parameters. Use the most appropriate cost function identified using the steps in Section 2.5.2.

    (b) Estimate the load of tephra fallout at all sites (sampled and unsampled) using the best-fit parameters from the *Tephra2* inversion.

2. Kriging:

    (a) Predict the residuals at all sites (sampled and unsampled sites) using simple kriging interpolation. Note that in the model-data fusion, we predict

residuals at the sampled sites to incorporate the short-range uncertainty at the observation locations. The residual at any prediction location s_o can be calculated as:

$$\hat{Z}(s_o) = \sum_{i=1}^{N} \lambda_i Z(s_i) \tag{2.9}$$

where $Z(s_i)$ is the residual at an observed location, which is calculated using the equation in Table 2.2 that corresponds to the cost function used in Step 1a. N is the number of observed sites. λ_i is the kriging weight applied to the value at the observed location. The kriging weights λ_i are calculated from a variogram model and a covariance matrix Σ, which describes the spatial relationships among the values at the observed sites and the prediction location. The Supplementary Information (Section A.5) provides a step-by-step procedure for simple kriging interpolation that includes formulas for λ_i and the covariance matrix Σ.

3. Fusion:

   (a) Back-transform the kriging predictions $\hat{Z}(s_o)$ to produce residuals with the same units as the data (See the Supplementary Material Section A.3 for sample formulas to use when back-transforming the kriging predictions).

   (b) Add the tephra load estimates from Step1b to the back-transformed residuals from Step 3a. This produces an updated map of tephra fallout that accounts for both the model and the observations.

Weighted model-data fusion

In practice, we could have different amounts of uncertainty associated with different datasets collected, as we do in our case study due to different survey teams measuring tephra load at different time points after the eruption. To account for varying data uncertainty in the interpolation procedure presented in Section 2.5.4, we can use an extension of simple kriging introduced by Worden et al. (2018), which they use in the context of earthquake ground motion intensity estimation. The method starts by identifying a *reference dataset* - a subset of the data with least uncertainty. Then, we define the additional uncertainty associated with other datasets relative to this reference dataset.

For the Kelud test case, we set Dataset 1 as the reference dataset because it was acquired the earliest after the eruption. We can set an uncertainty weight of $w_{k=1} = 1$ for Dataset 1 and $w_{k=2} = 0.5$ for Dataset 2. More generally, for datasets other than

the reference dataset (Dataset $k > 1$), we will always have $w_k < 1$. Based on these uncertainty weights, we can define an adjustment factor that relates the variance of the reference dataset to other datasets (Dataset $k > 1$) as $a_k = \sqrt{w_k}$.

The procedure follows the same steps as in Section 2.5.4 except for Step 2b. With an adjustment factor, the equation for the residual at any prediction location (originally Equation 2.9) would become:

$$\hat{Z}(s_o) = \sum_{i=1}^{N} \lambda_i^{'} a_k Z(s_{i,k}) \tag{2.10}$$

where $Z(s_{i,k})$ is the residual at observation site i associated with dataset k while $\lambda_i^{'}$ is the adjusted kriging weight calculated from an adjusted covariance matrix Σ'. The adjusted covariance matrix can be written as:

$$\Sigma' = \Omega \odot \Sigma \tag{2.11}$$

where $\Omega = \mathbf{a}\mathbf{a}^T$, $\mathbf{a}$ is the vector of adjustment factors corresponding to the observation sites $s_1, \ldots s_N$, and $\odot$ denotes the element-wise multiplication. Note that the covariance matrix and variogram model parameters were estimated using the reference dataset only.

Similar to the simple kriging approach in Section 2.5.4, we can estimate the uncertainty associated with the interpolated values. Also following Steps 3a and 3b in Section 2.5.4, we can add the interpolated residuals to the optimised model estimates. The result is an updated map of the tephra load that accounts for the model estimates, the observations, and the varying uncertainty between different sets of data.

Comparison of the kriging methods

We assess the performance of the kriging methods in Section 2.5.4 and 2.5.4 using leave-one-out cross-validation (LOOCV). Cross-validation is a widely used technique for comparing the test performance of different models. LOOCV, specifically, involves holding out a single observation for testing in each iteration, maximising the total number of points used for testing. This approach allows us to estimate the out-of-sample performance of the model (Shao, 1993). Detailed steps for the LOOCV procedure are provided in the Supplementary Information, Section A.6.

We can also check if the kriging interpolation overfits the training points. To confirm this, we compare the LOOCV errors to pre-kriging training errors calculated using the same performance metrics (root mean square error, chi-square, and mean square log error) from the process-based model fit. Since in LOOCV we are conducting out-of-sample estimation, LOOCV errors which are higher than the training errors from the

Tephra2 fit would suggest that kriging overfits the data.

2.6 Results and Discussion

The study shows that there is a significant influence on the inversion results and forward spatial estimates due to (1) the choice of the cost function in inversion, (2) the treatment and accounting of differential uncertainty of the data, and (3) the treatment and accounting of the spatial characteristics of the data. In the following subsections, we detail these in turn.

2.6.1 Use of a suitable cost function

In order to identify the characteristics of cost functions most applicable to the test case, we assessed the distribution of data values and the presence of outliers. The data cover a wide range of values (near zero to 168 kg/m^2, see Figures 2.3C and 2.3D) so we select an order-dependent cost function for a balanced treatment of data across different orders of magnitude. We also decided to use a cost function that is not sensitive to outliers because of the presence of relatively few large values located close to the vent. Using Table 2.2 as a guide, the cost functions that satisfy such characteristics are MSLE and chi-square.

Although MAPE is also order-dependent, and most interpretable among all the cost functions in Table 2.2 (because the errors it produces are in terms of percentages), we identify it as inappropriate for the test case for reasons beyond its sensitivity to outliers. The Statistics literature has provided evidence of its numerous weaknesses as a cost function. MAPE results to consistently low estimated values when used for optimisation (Tofallis, 2015). Small actual values (less than one) result to extremely large MAPEs, while zero actual values yields infinite errors (Kim and Kim, 2016). Numerous small data are observed in the test case, which is a common occurrence in tephra fallout data. We also provide a short summary of issues associated with MAPE in the Supplementary Information A.2.

Between MSLE and chi-square, we identify MSLE as the more suitable cost function because the residuals associated to the inversion with MSLE best adhered to the cost function's statistical assumption. This was demonstrated with MSLE giving the largest p-values across all the goodness-of-fit tests in Table 2.3. The Q-Q plots in Figure 2.5 also support the conclusion because the matched theoretical and empirical quantiles lie along the diagonal line for MSLE. The Q-Q plots for the cost functions with underlying Laplace distributions (MAE and MAPE) are given in the Supplementary Information, Section A.1.

Table 2.3: Goodness-of-fit tests for different cost functions. The null hypotheses for the Kolmogorov-Smirnov (K-S), the Cramér-von-Mises (CvM), the Anderson-Darling (A-D) and the Shapiro-Wilk (S-W) tests are that the residuals follow the assumed distributions. So, large p-values indicate better adherence to the assumptions. For our tephra case study, the residuals from the MSLE model fit seem to fit its assumed distribution the best. The Shapiro-Wilk test is only applicable for Gaussian distributions, thus, inapplicable for cost functions with underlying Laplace distributions, such as MAE and MAPE.

Cost function	K-S statistic (p-value)	CvM statistic (p-value)	AD statistic (p-value)	S-W statistic (p-value)
MSE	0.155 (0.082)	0.285 (0.149)	1.684 (0.138)	0.937 (0.003)
chi-square	0.216 (0.004)	0.966 (0.003)	4.728 (0.004)	0.948 (0.009)
MSLE	0.060 **(0.967)**	0.039 **(0.938)**	0.327 **(0.916)**	0.916 **(0.205)**
MAE	0.156 (0.079)	0.243 (0.198)	1.520 (0.172)	not applicable
MAPE	0.245 (0.001)	1.264 (0.001)	6.003 (0.001)	not applicable

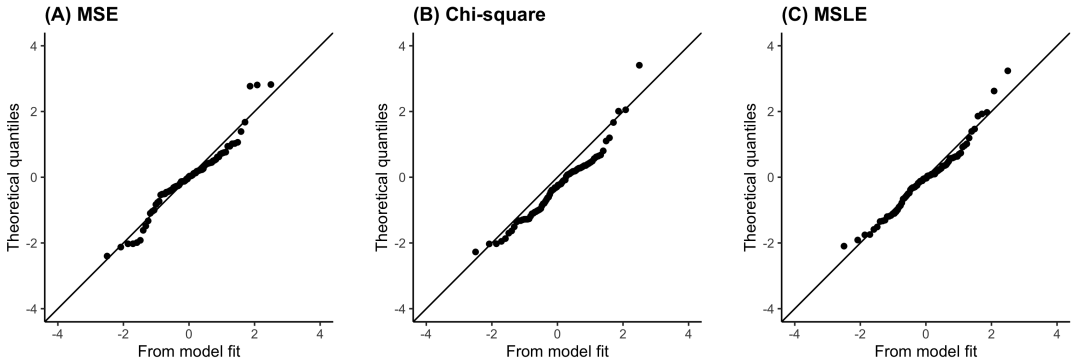

Figure 2.5: Quantile-quantile (Q-Q) plots illustrating goodness-of-fit for the models fitted using different cost functions: MSE, chi-square loss and MSLE. The fit is evaluated by how well the empirical quantiles from the transformed model residuals line up with the theoretical quantiles from the assumed distributions along the diagonal line.

In summary, our analyses emphasise that the selection of cost function needs to be a conscious choice in the inversion of source parameters, an aspect often overlooked. Each cost function comes with assumptions regarding how the model would fit the data. Our results, illustrated in Figure 2.5, reveal that different cost functions can significantly impact the residuals of the best-fit modelled output. More importantly, residual analysis can be used to draw conclusions on the appropriateness of the selected cost function. Through our presented methods, we found that MSLE performs well and has characteristics well-suited for the case study.

2.6.2 Weighting the cost function based on varying uncertainty

The purpose of adding uncertainty-based weights to the cost function in the inversion is to fit the model to the more reliable data, while still considering the information provided by other less reliable data. In the test case, Dataset 2 is the less reliable dataset compared to Dataset 1; nevertheless, Dataset 2 is important to consider as it provides information in the deposit that might not be captured by Dataset 1. For instance, only Dataset 2 consists of load data that are less than 1 kg/m^2. These relatively small measurements are located in areas north and south of the vent where Dataset 1 does not cover (Figure 2.3).

The improved fit to the more reliable data can be visualised by looking at how the distribution of residuals change when using a weighted inversion versus those of an unweighted inversion. For the test case's weighted inversion, the residuals at the locations of the reference dataset (Dataset 1) became more concentrated around zero compared to those of the unweighted inversion (Figure 2.6A). This difference in the distributions in Figure 2.6A indicate that the weighted inversion was successful in terms of fitting better to the reference dataset. As expected, the distribution of residuals for Dataset 2 from the weighted inversion does not indicate an improved fit (Figure 2.6B). The residual distribution for Dataset 2 only show a subtle increase in positive residuals when the inversion was weighted.

We assessed how uncertainty-based weights in the cost function impact the best-fit modelled output of an inversion-forward estimation analysis for tephra fallout. Following the method in Section 2.5.3, we conducted the inversion using MSLE, the cost function that worked best based on the results in Section 2.6.1. Since the selected cost function was MSLE, the test errors were calculated using the MSLE formula (Equation 2.6). When no weights were applied to the training points, the test error is 0.05, whereas, with weights applied, the test error is 0.03 (Table 2.4). Using weights in the inversion resulted in a lower test error, which implies that using weights resulted in

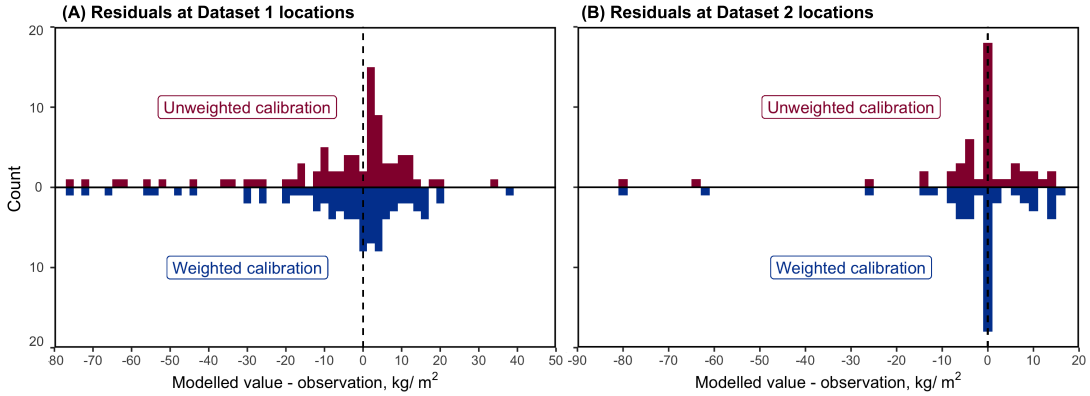

Figure 2.6: A visualisation of improving the fit to the more reliable dataset (Dataset 1) through a weighted inversion. Shown are histograms of residuals for inversions that make use of an unweighted and weighted MSLE cost function. Shown in (A) are residuals at locations of Dataset 1, whereas (B) shows the residuals at Dataset 2 locations.

a better predictive performance at out-of-sample locations. We checked whether using different cost functions would result in the same behaviour. Thus, we repeated the inversions using the same train-test split, uncertainty weights, and initial parameter ranges but using cost functions other than MSLE. The resulting test errors, shown in Table 2.4, indicate that using weights in the inversion consistently reduces test errors, and thus improves the prediction capability of the inversion-forward estimation analysis.

Table 2.4: Multiple inversions were conducted using the same training points (see train-test split in Figure 2.4) and initial parameter ranges (Table 2.1), but using different cost functions. The first set of inversions was run with no uncertainty-based weights applied to the training points. Shown in column (a) are the resulting errors at the test points calculated in the units of the corresponding cost function used in the calibration. Column (b), on the other hand, has weights applied to the training points in the inversion. The test errors show that applying weights results in a consistent decrease in the test errors leading to better predictive performance.

Cost function used in the calibration	Test errors	
	(a) No weights applied to training points	(b) Weights applied to training points
MSE	123.4	109.6
MAE	8.77	8.75
Chi-square	106.1	97.5
MSLE	0.05	0.03
MAPE	68.5	67.1

2.6.3 Influence on the source parameters

Thus far, the presented methodological contributions on the inversion (use of appropriate cost functions, and applying weights to the cost function) were investigated in terms of their impacts on the best-fit modelled outputs and the associated residuals. Acknowledging that the primary focus of an inversion is to optimise for the best-fit source parameters, we summarise the best-fit parameter values from inversions using different cost functions in Table 2.5 and for different weighting schemes in Table 2.6. The purpose of the paper is to not make claims about the true source parameters for the test case, instead we highlight that the source parameters are sensitive to the cost function and weighting in the inversion.

In Section 2.6.1, we discuss how the order-dependence and outlier-sensitivity properties of cost functions may influence the model fit to large (often proximal to the vent) and small values (often distal). In Section 2.6.2, the weighted approach allows a better fit to the more reliable data, no matter the data's magnitude. The relationship of the source parameters to these characteristics, such as the estimation of thicker deposits near the vent or thinner distal deposits, is connected to the physics of tephra transport. For instance, a larger plume height may lead to more tephra deposition at distal sites due to tephra being dispersed farther downwind, while a lower plume height may lead to thicker proximal deposit because of less wind advection. The relationship of observations made in distal and proximal sites to source parameters such as the erupted mass and plume height parameters have been studied by Suzuki et al. (1983), Bonadonna et al. (2005), and Yang et al. (2021).

A full understanding of the sensitivity of the proposed methods to each source parameter would require more extensive sensitivity analyses and preferably a test case with a bigger dataset. Parameter sampling algorithms, such as Markov Chain Monte Carlo algorithms, are popular for evaluating the benefits of new inversion methods (e.g. White et al. (2017); Yang et al. (2021)). Such methods may run the inversion thousands of times using different starting seeds to produce a range of fitted parameter values. The algorithms can extract confidence intervals for the source parameters, which can represent the impact of the new methods on the optimised parameters. While such sensitivity analysis is out of scope of this paper, our analysis highlights the importance of cost function selection and weighted inversion when varying data uncertainties are present when such studies are implemented. In this way, our work can contribute towards improving our understanding of relationships between data uncertainty and source parameters in the inversion.

Table 2.5: Best-fit parameter values from inversions using different cost functions. All inversions used unweighted cost functions, Dataset 1 for training, and the range of parameter values in Table 2.1 (asl = above sea level).

Cost function (no weights applied to training points)	Inverted parameters' best-fit value							
	Column height (km asl)	Erupted mass (10^{10} kg)	Grain size Median (ϕ)	Grain size standard deviation (ϕ)	Fall time threshold (s)	Diffusion coefficient (m s^{-2})	Plume profile, α	Plume profile, β
MSE	23.3	87.7	1.24	1.37	6356	10221	3	3.38
MAE	22.3	66.5	0.79	0.58	14380	10288	3	3.38
Chi-square	23.6	89.9	1.87	2.15	1406	12116	3	2.92
MSLE	17.4	67.7	0.85	1.06	2070	14748	3	1.30
MAPE	24.0	57.8	1.03	1.27	4937	5389	3	2.98

Table 2.6: Best-fit parameter values from inversions using different cost functions. All inversions make use of Dataset 1 and 2 for training. The range of parameter values in Table 2.1 were used to initiate the inversions. The weighted cost functions follow the procedure in Section 2.5.3. (asl = above sea level)

Cost function and associated weighting scheme	Inverted parameters' best-fit value							
	Column height (km asl)	Erupted mass (10^{10} kg)	Grain size Median (ϕ)	Grain size standard deviation (ϕ)	Fall time threshold (s)	Diffusion coefficient (m s^{-2})	Plume profile, α	Plume profile, β
MSE								
Unweighted	23.0	104.4	1.96	1.81	1639	7596	3	2.82
Weighted	23.4	85.3	1.43	1.78	1810	10936	3	3.15
MAE								
Unweighted	24.0	64.7	0.98	1.04	5647	5490	3	3.35
Weighted	23.3	91.9	1.62	1.50	4939	5129	3	3.13
Chi-square								
Unweighted	23.7	47.5	0.56	0.83	14507	3456	3	2.94
Weighted	23.4	49.0	0.63	0.90	13490	3612	3	2.85
MSLE								
Unweighted	19.5	100	1.97	1.87	4846	9019	3	1.39
Weighted	16.6	76.2	1.31	1.55	13993	10657	3	0.96
MAPE								
Unweighted	17.2	16.0	0.25	1.26	14476	2835	**3**	0.37
Weighted	23.5	44.6	0.46	0.64	14852	1971	**3**	2.72

2.6.4 Model-data fusion

We provided a methodology in Section 2.5.4 to combine observations and model estimates in such a way that the relative uncertainties between data are accounted for. The methodology increases the value of the information from the data by using them to examine the spatial structure in the model residuals which can be used together with the information from the model to fill gaps at unsampled locations. Here, we present an analysis of the new estimates of tephra load and associated residuals produced by fusion methods. One advantage of using kriging in the fusion methods is the ability to produce not only the kriging estimates, but also the uncertainties associated to the new estimates. We provide a map of uncertainties related to the new estimates of tephra load in this section in the Supplementary Information, Section A.9.

The manually-contoured isopachs for the 2014 Kelud event by Maeno et al. (2019) (Figure 2.2) show a bilobate shape as influenced by the wind conditions during the tephra dispersion. However, this two-lobe pattern was not captured by *Tephra2* without the additional spatial estimation using its residuals (Figure 2.7). Shown in Figure 2.7 are tephra deposit maps prior and after implementing an unweighted fusion approach described in Section 2.5.4 when MSLE was chosen as the cost function. We see that the model-data fusion approach results in tephra load contours with a two-lobed feature, in line with the manually-contoured isopachs, and the wind shear that occurred across the eruption column,.

The maps in Figure 2.7 also illustrate how the measurements influence the resulting tephra deposit after the fusion. The fusion approach (Figure 2.7B) accounted for Dataset 2's small measurements southeast of the vent (load values ranging from less than 1 to 10 kg/m^2 in Figure 2.3) resulting in lower values of load in this area compared to those in Figure 2.7A. Due to the influence of thick deposit measurements near the vent, the fusion approach produced higher peak load values (~140 kg/m^2) compared to those in the best-fit modelled output (~100 kg/m^2), possibly reflecting sedimentation from the column's edge. Implementing a weighted fusion approach (Section 2.5.4) to combine the model in Figure 2.7A and data results to the tephra deposit map in Figure 2.9B.

While it is difficult to compare the results from the unweighted and weighted fusion based on the contour maps, we can look at the LOOCV to compare their spatial estimation performance. To compare the two approaches fairly, we evaluate estimation performance using metrics corresponding to the cost function assumed. The results in Table 2.7 show that both weighted and unweighted model-data fusion approaches lead to smaller LOOCV errors, and they are smallest for the weighted fusion approach. The same result is seen when other correlation structures such as exponential and Gaussian functions are used instead of the Matérn variogram (see Supplementary Information,

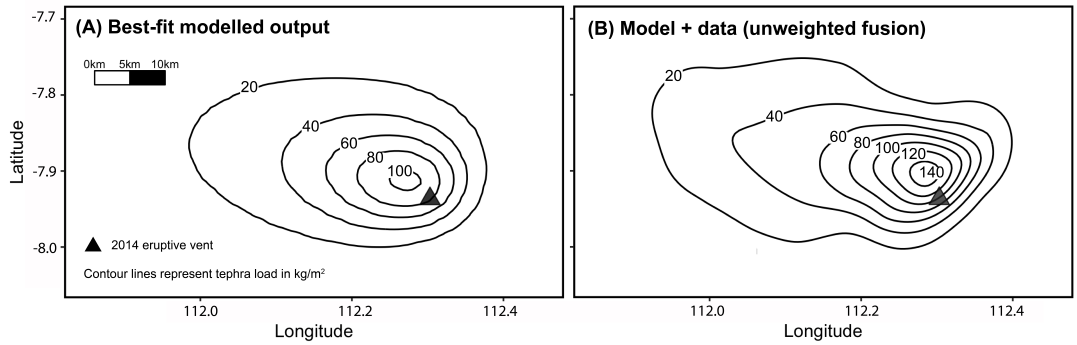

Figure 2.7: The map in A shows the best-fit modelled tephra deposit from an inversion with MSLE as the cost function and with weights applied based on the approach in Section 2.5.3. Shown in B is the result of implementing an unweighted fusion (Section 2.5.4) of the model in A and data. The fusion approach makes use of both Datasets 1 and 2, of which some are located beyond the bounds of the maps shown.

Section A.8). This highlights the advantage of making use of data in the spatial estimation, and the importance of accounting for data uncertainties for generating spatial estimates. Comparing the LOOCV errors to pre-kriging training errors also confirms that the approach is not overfitting.

We conduct a further examination of the residuals following weighted and unweighted fusion. Figure 2.8 presents histograms of these residuals separately for the locations of Datasets 1 and 2 when utilising MSLE for inversion and fusion. We observe that using the weighted fusion approach reduces the spread/variability of the residuals of Dataset 1 points, indicating an improved fit. This is expected since the weighted approach prioritises the fit to the more reliable dataset. On the other hand, the weighted fusion results to a wider spread in the residuals of Dataset 2, which shows the influence of applying less weight.

The importance placed on the fitted process-based model and the data can be balanced by the *nugget parameter* in the variogram model of the kriging procedures. The nugget determines the spatial variability of the modelled quantities in short distances and hence, affects the smoothness of the predicted residual surface: the larger the nugget, the smoother the surface. We demonstrate this variation in smoothness in relation to the nugget value in Figure 2.9 through the use of different spatial models of varying nuggets for the MSLE case. Indeed, the nugget can be a fitted parameter using maximum likelihood estimation for example. However, when the fitted nugget value becomes too low, the predictions are forced to perfectly fit the data. This may be an issue for the context of tephra modelling because the data is inherently uncertain and sparse. In addition, there is often little data at close pairwise distances to get reliable estimates of the nugget. This may create constraints that are

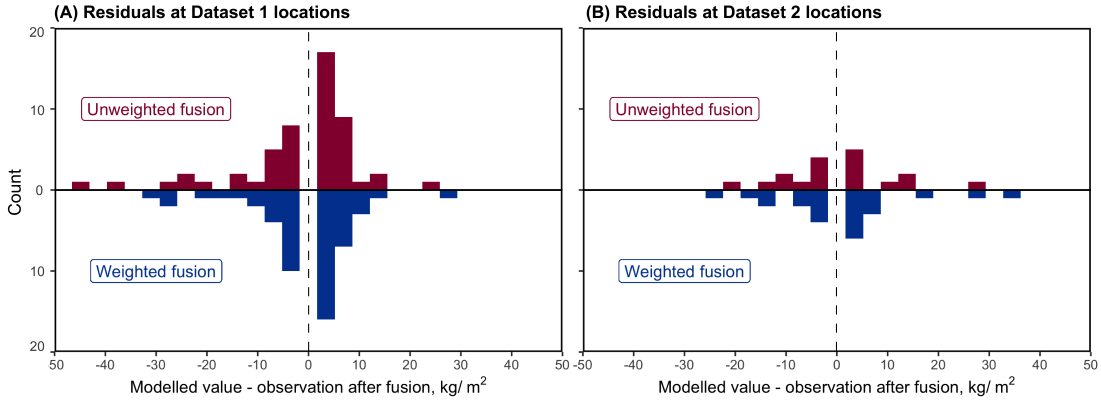

Figure 2.8: Histograms of residuals at locations of Dataset 1 and 2 after implementing the unweighted and weighted fusion approach. The results show the influence of the weighted fusion on the range/variability of the residuals for the two datasets.

Table 2.7: Measures of performance of the unweighted and weighted kriging-based fusion methods in terms of LOOCV errors. For each cost function choice, the errors were calculated using the corresponding performance metric: root mean squared errors for the MSE cost function, chi-square errors for chi-square cost function and mean square log error for MSLE. The training errors before applying the fusion methods are consistently higher than the LOOCV errors, which indicates no overfitting in the kriging method. The Matérn variogram model was used to define the spatial correlation structure. For the formulas shown, x refers to the observed value, y is the model estimation, and n is the number of data points.

Cost function	Performance metric	Formula	Pre-kriging training error	LOOCV error after unweighted fusion	LOOCV error after weighted kriging
MSE	Root-mean-square	$\sqrt{\frac{1}{n}\sum_{i=1}^{n}\varepsilon_i^2}$	16.166	15.470	15.064
Chi-square	Chi-square	$\frac{1}{n}\sum_{i=1}^{n}(\varepsilon_i^2/x_i)$	8.051	5.362	5.300
MSLE	Mean square log	$\frac{1}{n}\sum_{i=1}^{n}\left(log\frac{(y_i+1)}{(x_i+1)}\right)^2$	0.0570	0.040	0.033

physically unrealistic and don't account for the uncertainty in the data. Therefore, it is often better to treat the nugget as a tuning parameter, which is selected as a modelling choice based on expert knowledge. We select the spatial model in Figure 2.9A for the model-data fusion in this paper.

The fusion methods use and build upon simple kriging, which comes with an assumption that the mean of the residuals is zero. Alternatively, if the spatial factors underlying the residuals are known, regression kriging may be used instead of simple kriging. In addition to the variogram that describes the stochastic spatial relationship between residuals, we could use spatial covariates such as topography or distance from the vent to model their mean surface (trend model).

In our analysis, we checked that the assumption of isotropy was not violated (Supplementary Information, Section A.7). We also confirmed the strength of the spatial correlation, which can tell us if kriging would be suitable as an interpolator and if the form of residual is appropriate. Note that extensions towards non-stationary and anisotropic distributions can be made but are out of scope for this paper.

The results show how the model-data fusion approach improves the modelled output of Tephra2 through the use of data. Model-data fusion with Tephra2 may not necessarily yield results similar to those obtained from a more complex model that captures the physical processes of the eruption event better than Tephra2. The influence of accounting for the spatial structure and uncertainty in the data is independent from the effect of utilising improved assumptions for eruption and atmospheric dynamics. Tephra2, however, can be substituted with any other model in the model-data fusion to better capture the physical processes of the eruption and atmospheric condition. The use of data in the fusion approach can improve the irreducible errors that even complex models cannot capture due to model approximations and unaccounted processes inherent in any model.

2.7 Conclusions

We demonstrate several methodological improvements in the inversion and forward estimation modelling processes when using limited, uncertain and spatial data. We test these using a case study of the eruption of the Kelud volcano in 2014. Using data on tephra thickness collected from two field surveys, we conduct a model inversion to estimate the eruption source parameters and use these in a forward model to estimate the spatial distribution of tephra in locations where no data was collected. We make no specific conclusions about the eruption itself or the true distribution of tephra, but instead, use the test case to demonstrate important considerations and approaches to

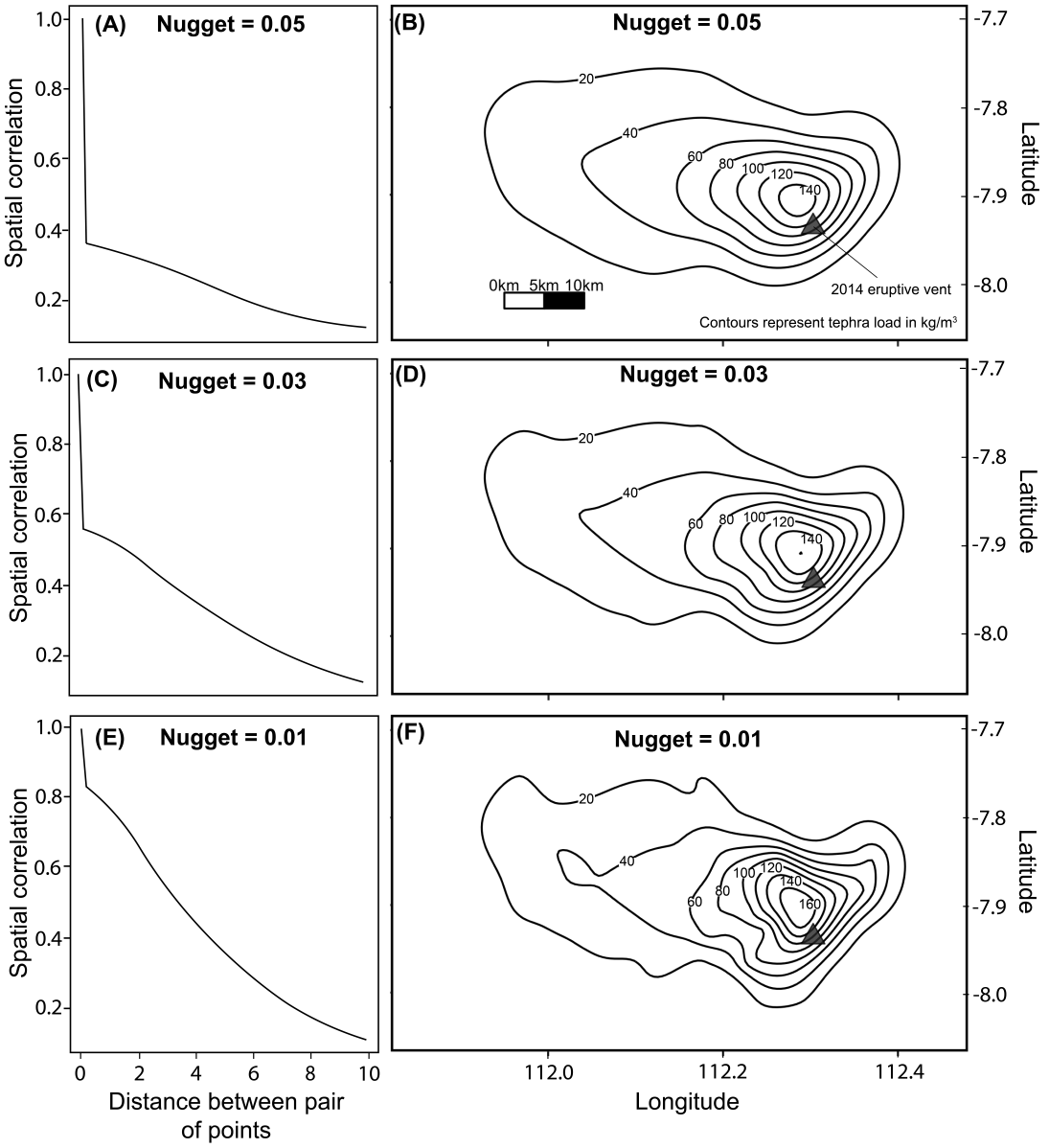

Figure 2.9: A demonstration of how the nugget is treated as a tuning parameter to balance the importance placed on the fitted process-based model and the data. The selection of the nugget is a modelling choice based on expert knowledge. The maps on the right (B, D, and F) show the tephra deposit generated from a weighted fusion of the model output in Figure 2.7A and data. The plots on the left (A, C, and E) are the corresponding spatial model used for the fusion. Figure E shows the spatial model for a nugget value that is fitted using MLE. By tuning the fitted nugget value (resulting in Plots A and C), we can address unrealistic physical constraints often created by a very small nugget. Note that for the spatial models shown, spatial correlation is calculated by dividing the spatial covariance by the sum of the spatially correlated variation and the nugget. In this study, we select the spatial model in Plot A (Nugget = 0.05) for the model-data fusion.

treating data in inversion-forward estimation problems. Our methodological contributions come in three components: (1) the selection of appropriate cost functions accounting for their behaviour and their associated implied distribution of residuals, (2) the treatment of differential uncertainty when combining multiple data sets, and (3) the leveraging of both forward model and data when estimating the spatial distribution of output.

In the inversion setting, this study places attention on the choice of the cost function to define the best fit between modelled output and observations. This modelling choice receives little attention but has a significant impact on the results as seen in Figure 2.5. We demonstrated how the characteristics of cost functions and their inherent assumptions on the distribution of model residuals can be used to inform the selection of appropriate cost functions. We also demonstrate the use of data-weighting in the inversion process to account for the differential uncertainty in data. Varying levels of uncertainties associated with different measurements are taken into account by weighting each observation's contribution to the cost function accordingly.

In the forward estimation, we propose to combine the forward modelled output with measured data using spatial statistics techniques. The output is an updated map of tephra fallout that accounts for both the model and the observations. Both the uncertainty in tephra measurements and their spatial correlation are accounted for in the fusion approach. The importance placed in the model and data can be balanced by the choice of the spatial model and its parameters.

One of the strengths of the weighting approach in both inversion and forward model settings is that, where multiple datasets are available, the approach enables making use of all data, even if some are highly uncertain, while accounting for this uncertainty. With the increasing availability of high volume, low reliability information (e.g. crowd-sourced data from social media), these can nonetheless be used to improve the modelling.

This work serves applications where the inversion and forward prediction workflows are conducted sequentially, and applications where they are done separately. While the test case is focused on *Tephra2*, the methods are applicable to other models that reconstruct the process of tephra fallout such as ASHFALL and FALL3D (Hurst and Turner, 1999; Folch et al., 2009). Beyond applications related to tephra fallout, the guidance could be relevant to those conducting any inversion or calibration modelling using spatial data in earth, environment, and hazards analysis.

2.8 Code and data availability

We have modified the Tephra2 source code described below to accommodate different cost function types and weighted cost functions. For the kriging presented in the study (to combine model estimates and data), we developed scripts written in the R Programming language (R 4.0.2, R Core Team (2020b)). The modified Tephra2 source code, R script for kriging, and processed data are available and organized in Github: https://github.com/ntu-dasl-sg/tephra-spatial-public. I created this repository in 2022.

I conducted inversion calculations using the Komodo computing cluster managed by the Asian School of the Environment (Contact: Edwin Tan; edwintan@ntu.edu.sg) and Nanyang Technological University's High Performance Computing Center; (hpcsupport@ntu.edu.sg). Remote access to this computing cluster is possible with PC/Mac/Linux.

- Software name: tephra2
- Lead developers: Laura J. Connor <lconnor@usf.edu>; Costanza Bonadonna <costanza@cas.usf.edu>; see Bonadonna et al. (2005) and Connor and Connor (2006)
- Year first available: 2013
- Version used in the study: 2.0, Updated 01-27-2018
- Program language: C
- License: GNU General Public License v3.0
- Availability: https://github.com/geoscience-community-codes/tephra2
- Program size: 963 KB
- Hardware requirements: The inversion model requires MPI (Message Passing Interface) libraries and should be run on a computing cluster with multiple compute nodes. The forward model can be compiled without MPI installed.

2.9 Acknowledgments

This work was funded by the Earth Observatory of Singapore (EOS) and is EOS Contribution Number 529. This research is supported by the National Research Foundation Singapore and the Singapore Ministry of Education under the

NRF-NRFF2018-06 award. We are grateful to Edwin Tan for his support in the use of the High-Performance Computing Cluster, Komodo, in the Earth Observatory of Singapore. We thank George Williams for his support and insights related to the tephra load datasets.

Chapter 3

Regional scale risk analysis accounting for time-dependent vulnerability

---

This chapter is a published (peer-reviewed) conference paper.

Rabonza, M.L. and Lallemant, D. (2019). Accounting for time and state-dependent vulnerability of structural systems. *In Proceedings of the 13th International Conference on Applications of Statistics and Probability in Civil Engineering (ICASP13) Sep 2019.* pp. 2298-2305. https://doi.org/10.22725/ICASP13.465

In addition, this chapter cites the following first-author conference paper, which is included in Appendix B.1. The paper demonstrates an additional case study, which is an application of the flexible community-scale analysis shown in this chapter. The application focuses on data derived from New Zealand's seismic retrofit implementation records.

Rabonza, M.L. and Lallemant, D. (2018). A time-dependent model for seismic risk reduction policy analysis. Accepted in the *17th U.S.-Japan-New Zealand Workshop on the Improvement of Structural Engineering and Resilience Nov 2018. https://hdl.handle.net/10356/164235*

Chapter highlights

- *I present a flexible framework to account for time-dependent physical vulnerability in seismic risk analysis.*
- *I model processes that increase vulnerability (deterioration) and policies that mitigate increase in vulnerability (retrofits, maintenance).*
- *I build on the fundamental probabilistic performance based framework by adding a time-varying model for vulnerability.*
- *I provide a tool to study the consequences of seismic mitigation on future seismic risk.*

3.1 Abstract

The typical process of engineering risk analysis assumes a static state of vulnerability through the lifespan of the structure. However, many civil engineering systems change states over time causing significant impact on their vulnerability. Such dynamic changes may involve an increase in vulnerability driven by deterioration processes (e.g. corrosion, fatigue, creep, hazard-induced damage, etc.), or a decrease in vulnerability driven by strengthening interventions (e.g. retrofitting, maintenance, building replacement, etc.). Accounting for these dynamics is critical to properly understand hazard-related risk of civil engineering systems over their lifespan. This paper presents a stochastic framework for accounting for time and state dependent vulnerability in risk analysis of civil engineering systems. Time-homogeneous Markov chains are used to model various state change processes, and integrated within the risk analysis framework in closed-form expressions. Several applications are demonstrated: (1) quantifying risk of structurally deteriorating buildings and the risk reduction impact of maintenance, (2) urban-scale seismic retrofitting policies based on various retrofit rates, and (3) impact of varying rates of building replacement to higher design grade. These demonstrate the importance of accounting for time dependent state change as a significant factor in the life-span vulnerability of the built environment. The study further provides a framework to study and compare various risk reduction policies.

3.2 Introduction

Developing well-informed and proactive strategies for seismic risk reduction requires the ability to predict risk in constantly changing urban environments, and understand how risk reduction policies affect future seismic risk. However, current seismic risk assessment methods focus on understanding risk to infrastructure in only their present state.

In this paper, we present a flexible framework accounting for time and state dependent vulnerability in seismic risk analysis. This allows for the modelling of processes that can increase vulnerability (e.g. deterioration, building expansions, cumulative damage), those policies that mitigate increase in vulnerability (e.g. better maintenance schedule, higher durability construction) and those policies that improve resilience (e.g. seismic retrofits and building replacement to higher standards).

The framework is applied to hypothetical case studies to demonstrate the effects of time and state dependent vulnerability on a single deteriorating building and to a

neighborhood with buildings experiencing deterioration, retrofitting, and building replacements over time. While it is expected that retrofit policies and building replacements lead to decreased seismic risk, and deterioration leads to increased seismic risk over time, this paper demonstrates how risk evolves with time linked to various seismic reduction policies. This methodology is an extension of a time-dependent framework applied to investigate incremental building expansion as the significant driver for increasing risk and vulnerability (Lallemant et al., 2017).

The key contribution of this paper is to provide a tool for stakeholders to investigate the consequences of various seismic mitigation decisions to future seismic risk. The case study presents a proof of concept and a demonstration rather than actual risk prediction. The framework can be utilized to study a more realistic case once information for transition rates, vulnerability and building stock distribution are available.

3.3 Methodology

3.3.1 Proposed framework accounting for time dependent vulnerability in seismic risk analysis

The Performance-Based Earthquake Engineering (PBEE) methodology proposes a systematic methodology to calculate the seismic risk of structures through the probabilistic integration of (1) seismic hazard, (2) seismic demand, (3) damage capacity, combined into a single impact assessment (Krawinkler and Miranda, 2004). Each of these components are described in Table 3.1.

Each step in the probabilistic risk analysis framework comes with inherent uncertainty/variability, thus each associated variable is expressed in the form of conditional probability of exceedance (Figure 3.1. With the basic PBEE framework, the final expression for the decision variable, λ_{DV},is obtained by combining the conditional probabilities using the total probability theorem. The decision variable then serves as a guide for infrastructure managers to create appropriate risk management and mitigation strategies based on a performance target or risk metric.

$$\begin{aligned}\lambda_{DV} = \int_{im}\int_{edp}\int_{dm} & G_{DV|DM}(dv/dm) \\ & \times |dG_{DM|EDP}(dm|edp)| \\ & \times |dG_{EDP|IM}(edp|im)|\nu_{IM}\end{aligned} \tag{3.1}$$

Table 3.1: Four components and associated variables of the Performance-Based Earthquake Engineering framework. Descriptions based on explanations by Krawinkler and Miranda (2004); Deierlein (2004); Moehle and Deierlein (2004)

Framework component	Variable name	Description of variable
Hazard analysis	Intensity measure (IM)	Earthquake induced shaking at study site
Demand analysis	Engineering demand parameter (EDP)	Response of structure to earthquake loading
Damage capacity modelling	Component damage measure (DM)	Seismic-induced damage sustained by structure
Impact assessment	Decision variable(DV)	Performance-related variables for decision making

The basic PBEE framework is not capable of dealing with time-dependence of each of the variables, and does not incorporate other potential time-dependent drivers of vulnerability that could affect future seismic risk. Using the PBEE framework as a starting point, the proposed framework incorporates a new module to account for potential time dependent drivers of vulnerability. A similar performance-based framework which accounts for time varying effects of deterioration for bridges was proposed by Rao et al. (2017). Building on the PBEE methodology and Rao et al. (2017)'s framework, we propose a flexible framework accounting for time and state dependent seismic vulnerability, incorporating drivers such as structural deterioration, maintenance schedule, seismic retrofit policies, building replacement rates and other drivers of vulnerability. The key component in this proposed framework is the analysis of the 'time varying vulnerability state' with associated variable VS and probability $f_{vs}(vs,t)$ of being in a vulnerability state vs at time t. This is the mathematical representation of the selected time and state dependent vulnerability driver. An illustration of the proposed framework is shown in Figure 3.1 along with the associated variables, stochastic representations and examples for each component. Finally, the full equation for the probabilistic decision variable of interest is presented which describes the proposed framework in detail. The equation in Figure 3.1 is characterised by treating the variables as continuous. However, the equation can easily be rewritten to handle discrete states by replacing the integration by a summation over the discrete vulnerability states.

3.3.2 Mathematical representation of vulnerability states and corresponding transition scenario

Along with the proposed framework shown in Figure 3.1, we illustrate in Figure 3.2 several potential time-dependent vulnerability drivers for seismic risk.

A certain vulnerability state can be dependent on the building's degree of deterioration, state of expansion, current structural condition, or the developed retrofit standard depending on the significant vulnerability drivers of interest to a certain structure. Given in Figure 3.2 are suggested relative vulnerability states exhibiting increasing seismic vulnerability (for deterioration and building replacement) and decreasing vulnerability/increased resilience states (for seismic retrofitting).

Using Markov Chains is a simple approach to represent the transition of these discrete states over time. Markov chains are used to map the probability of transitioning from one state to another state in a specific time interval. Markov models are "memoryless", such that the new state is solely dependent on the current state; not on the set of events preceding it (Agresti, 2003). The column showing the 'Transition

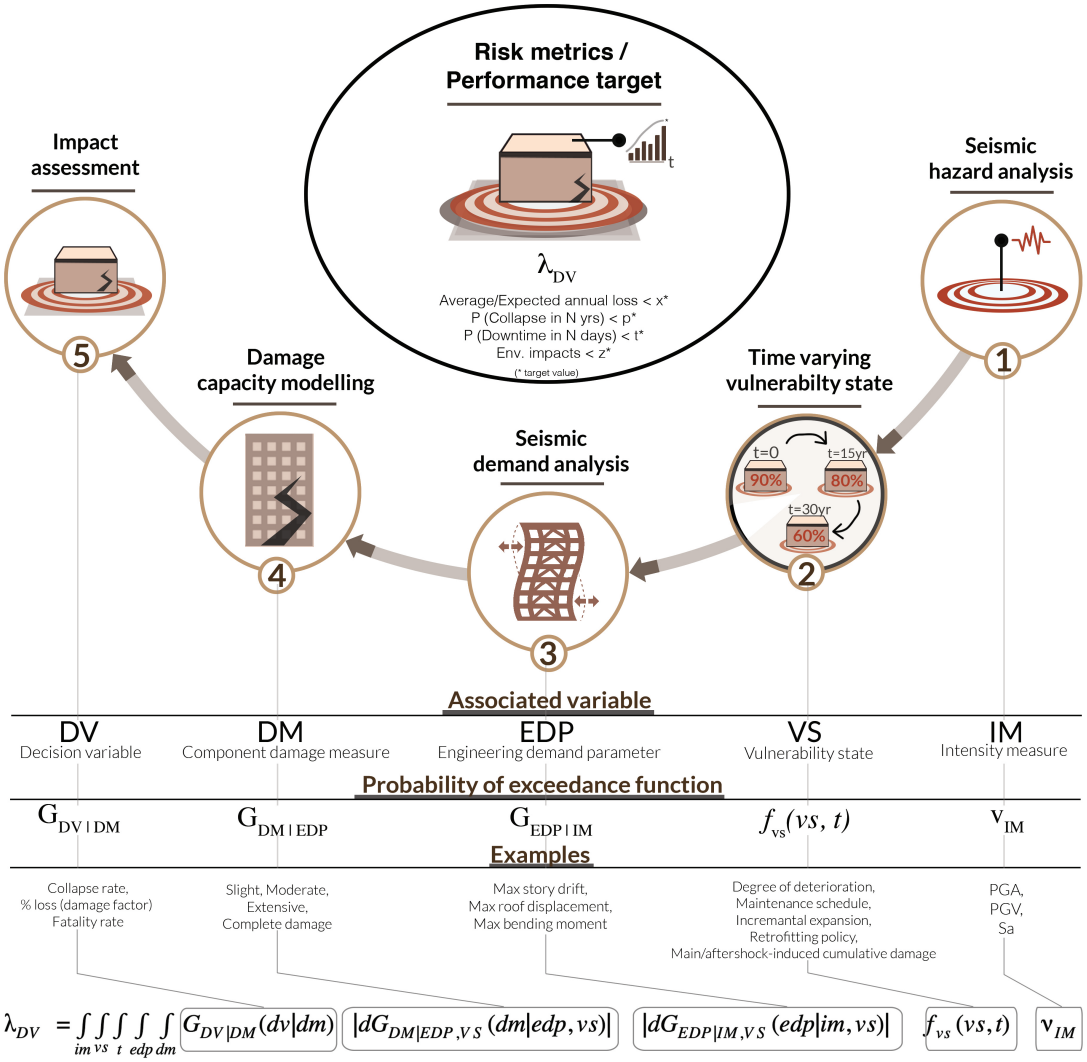

Figure 3.1: Proposed framework accounting for time dependent vulnerability in seismic risk analysis

Potential time-dependent vulnerability drivers for seismic risk	Time-dependent vulnerability states	Transition Scenario *Each circle represents a vulnerability state	Typical transition probability matrix More vulnerability states = larger matrix but same pattern	Factors affecting transition rates, d_{ii}, b_{ii}, and r_{ii}	Factors affecting fragility curve of each vulnerability state
Structural deterioration	Based on degree of deterioration (1) As-new (2) Fairly deteriorated (3) Heavily deteriorated (4) Very heavily deteriorated		$P_d = \begin{bmatrix} d_{1,1} & d_{1,2} & 0 & 0 \\ 0 & d_{2,2} & d_{2,3} & 0 \\ 0 & 0 & d_{3,3} & d_{3,4} \\ 0 & 0 & 0 & d_{4,4} \end{bmatrix}$	• Maintenance schedule • Environmental exposure • Initial building stock quality	• Degree of deterioration
Building replacement	Based on structural condition (1) As-new (2) Fair condition (3) Bad condition (4) Very bad condition	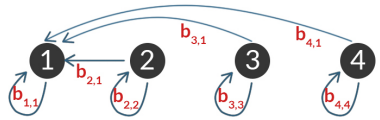	$P_b = \begin{bmatrix} b_{1,1} & 0 & 0 & 0 \\ b_{2,1} & b_{2,2} & 0 & 0 \\ b_{3,1} & 0 & b_{3,3} & 0 \\ b_{4,1} & 0 & 0 & b_{4,4} \end{bmatrix}$	• Bldg replacement policy • Initial building stock quality	• Building condition
Seismic retrofitting	Based on retrofit standard (1) Not retrofitted (2) Low retrofit standard (3) Medium retrofit standard (4) High retrofit standard	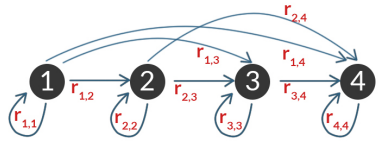	$P_r = \begin{bmatrix} r_{1,1} & r_{1,2} & r_{1,3} & r_{1,4} \\ 0 & r_{2,2} & r_{2,3} & r_{2,4} \\ 0 & 0 & r_{3,3} & r_{3,4} \\ 0 & 0 & 0 & r_{4,4} \end{bmatrix}$ d_{ii}, b_{ii}, r_{ii} are probability rates for which each state transitions to the next state	• Timeframe for mandatory retrofit • Initial building stock quality	• Level of retrofit standard developed,

Figure 3.2: Potential time-dependent vulnerability drivers for seismic risk and associated transition scenario

Scenario' provides a schematic of the types of transition processes linked to each time-dependent vulnerability driver, and can then be mapped into corresponding transition probability matrices.

For instance, a non-retrofitted building can either transition into a retrofitted state with a certain probability within a year, or it can stay in its current state. Similarly, a building can also transition into a more deteriorated state over time with an associated transition probability. A common assumption for analysis incorporating structural deterioration or seismic retrofitting is that once a certain state is reached, it cannot go back to a previous state. For example, we assume that once a building is retrofitted, it is not possible for the building to go back to its unretrofitted state. In the schematic for the transition scenarios (Fig. 3.2) of deterioration and seismic retrofitting, this is shown by having all transition arrows going to the right only. On the contrary, possible transition patterns for building replacements can bring back a building to its original (as-new) state as time goes by as presented by the arrows going to the left in its transition scenario diagram (Figure 3.2). Alternatively, a building could be replaced by another built to higher standards, as is often the case resulting from building code improvements. The same figure also shows a sample transition probability matrix for each vulnerability driver using the given time-dependent vulnerability states. The size of the transition probability matrix depends on the potential vulnerability states considered in the analysis, but they should exhibit similar pattern.

Depending on the transition rates, $d_{i,i}$, $b_{i,i}$, $r_{i,i}$, the transition between the vulnerability states can go either slower or quicker based on different factors. For example, building deterioration rates are usually affected by the level of environmental exposure of the structure, its initial structural quality, or the implemented maintenance schedule which could potentially mitigate the seismic risk over time. It should be noted that the factors affecting transition rates don't necessarily affect the actual fragility curve for each state.

Fragility curves define the state of vulnerability of a building or structure. These curves show the relationship of the earthquake intensity and the probability of exceeding a particular damage level.

Numerous methods exist to derive these curves: (1) analytical (Singhal and Kiremidjian, 1996; Lallemant et al., 2015), (2) empirical (Sanchez-Rodriguez et al., 2005; Noh et al., 2015) or heuristic/ based on expert opinion (Jaiswal et al., 2012).

Given a hazard curve at a study site, the annual collapse rate of a building is

calculated by integrating the fragility curve over the hazard curve in Equation 3.2.

$$\lambda_{Collapse} = \int_{IM_{min}}^{IM_{max}} P(Collapse|IM = im)|d\lambda_{im}(im)| \tag{3.2}$$

where $\lambda_{im}(im)$ is the seismic hazard curve and $|d\lambda_{im}(im)|$ is the absolute value of the derivative of the hazard curve.

For a portfolio of buildings the annual expected number of building collapse at a time t can be calculated using Equation 3.3.

$$\begin{aligned} \lambda_{CollapseTotal}(t) = \sum_{State_1}^{State_n} \int_{IM_{min}}^{IM_{max}} \\ P(Collapse|IM = im)|State = State_i) \\ \times P(State = State_i|D_o = d_o, P = p)(t) \\ \times |d\lambda_{IM}(im)| \end{aligned} \tag{3.3}$$

where $P(Collapse|IM = im)|State = State_i$ is the fragility curve for each building state at collapse, $P(State = State_i|D_o = d_o, P = p)(t)$ is the probability of being in a building state at time t for a given transition probability matrix p and initial state distribution d_o.

It can be shown that the expected vulnerability state distribution D_t at time t is $E(D_t|D_o = d_o) = d_o P^t$ where P is the transition probability matrix of vulnerability states. Therefore 3.3 can be re-written as:

$$\begin{aligned} \lambda_{CollapseTotal}(t) = \sum_{State_1}^{State_n} \int_{IM_{min}}^{IM_{max}} \\ P(Collapse|IM = im)|State = State_i) \\ \times d_o P^t \ |d\lambda_{IM}(im)| \end{aligned} \tag{3.4}$$

3.4 Case studies

3.4.1 Building-level deterioration analysis

We apply the methodology discussed previously to model the changing risk of a hypothetical deteriorating building over time, we focus on three (3) vulnerability states ranging from as-new, heavily deteriorated and very heavily deteriorated for a hypothetical reinforced concrete (RC) building.

A hypothetical vulnerability curve is generated to represent the non-deteriorated state. For simplicity, we only use fragility curves corresponding to "Extensive/ Complete Damage."

Vulnerability curves for the three (3) assumed vulnerability states corresponding to each degree of deterioration,w, are obtained using Equations 3.5 and 3.7 (Rao et al., 2017).

$$m(w) = m_o e^{-\alpha_m w} \tag{3.5}$$

$$\xi(w) = \xi_o(1 - \alpha_\xi w) \tag{3.6}$$

where
$m(w)$, $\xi(w)$= median and dispersion of fragility function at level of deterioration w consecutively ,
m_o, ξ_o = median and dispersion of the fragility function for the column in its non-corroded state consecutively
α_m= exponential decrement function for the median and
α_ξ= coefficient of the linear decrement function for the dispersion of the fragility function.

The coefficients of the decrement function are adopted from estimates by Rao et al. (2017) for a hypothetical RC column built in 1960 to pre-1971 design standards: $m = 1.43$, $\alpha_\xi = -0.18$

Using the framework for this application, we compare the impact of different levels of maintenance on seismic risk over time. Three maintenance schemes are used to demonstrate the diversity of maintenance options for seismic safety: (1) Low, (2) Medium, and (3) High Maintenance. Transition probability matrices are assumed based on a Markovian model developed by Duling (2006) for an RC building constructed with pre-1971 design standards to predict the building service life given three varying levels of maintenance. The percent change in annual collapse risk normalized to baseline risk at t=0 is calculated using Equation 3.2 and presented in Figure 3.3.

The trends shown in the figure highlight the impact of building deterioration on the seismic risk of buildings, and the benefits of maintenance; it demonstrates the importance of accounting for time-dependent vulnerability drivers such as deterioration in studying future seismic risk of a building. This demonstration shows that the proposed framework enables the testing of impact of maintenance or other building mitigation strategies on seismic risk over time. If linked with financial loss information, the framework could be used for cost benefit analysis for mitigation.

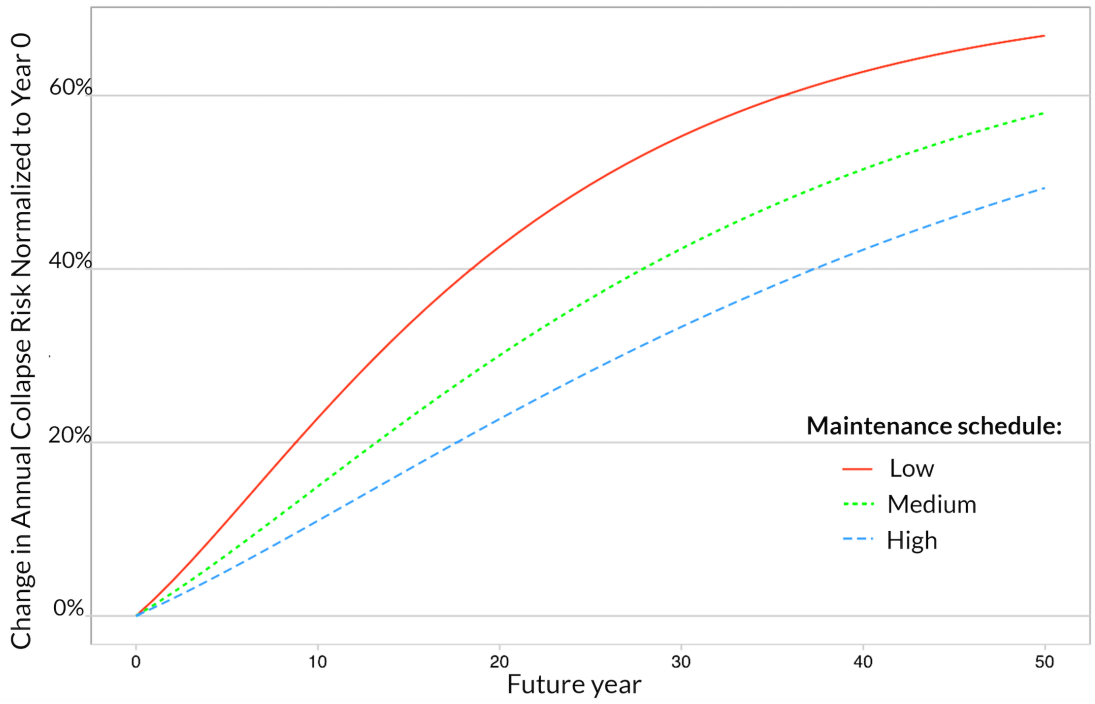

Figure 3.3: Percent change in annual collapse risk normalized to baseline risk at t=0 for a hypothetical building

3.4.2 Policy analysis for community level seismic risk reduction

Using the proposed framework, we can also test the impact of various seismic risk reduction policies at a regional level. A hypothetical urban community was simulated, consisting of four districts each having their own building type distribution and seismic hazard curve. For simplicity of demonstration, the design of buildings are either high grade or low grade, and each can transition to deteriorated states, retrofitted states (for low-grade buildings), or get replaced over time. Hypothetical fragility curves are developed to represent each of these states: (1) Undeteriorated/unretrofitted state (2) Heavily deteriorated state (3) Very heavily deteriorated state (4) Retrofitted state with low standard and (5) Retrofitted state with high standard. The fragility curves for each vulnerability state are shown in figure 3.4.

Hazard curves for each district are synthetically generated as idealized power-law hazard curves of the following form:

$$\lambda_{im}(IM) = k_o IM^{-k} \tag{3.7}$$

Parameters used for the four districts are k0 = 0.0002, 0.0003, 0.00022, 0.00035 and k = 2, 2.1, 2.2, 2.5 for districts 1, 2, 3 and 4 respectively.

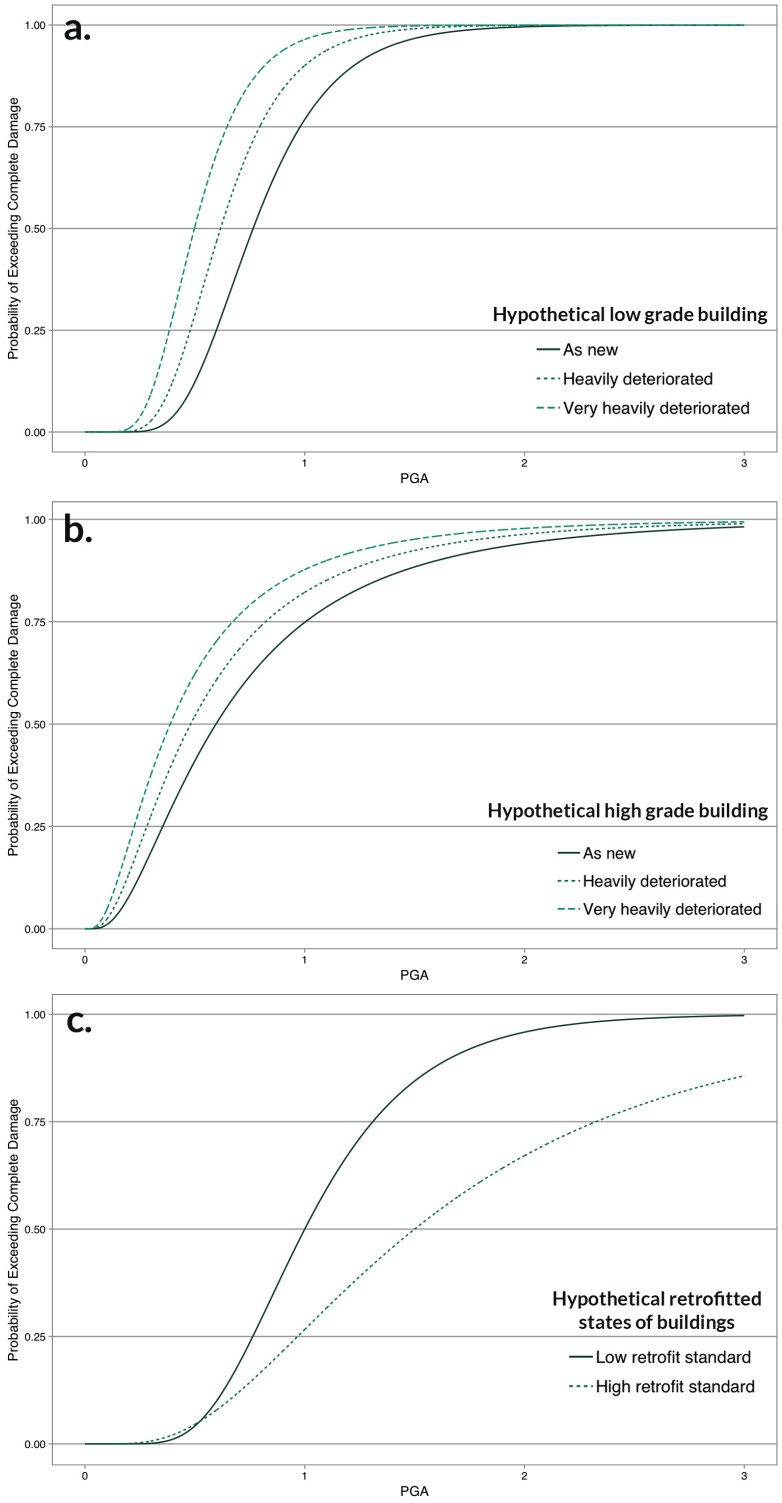

Figure 3.4: Fragility curves for assumed vulnerability states at the hypothetical building stock

Table 3.2: Indices of Transition Probability Matrices. (Abbreviations: HD = Heavily deteriorated, VHD = Very heavily deteriorated, n/a = Unretrofitted building

Index	P1	P2	P3	P4	P5	P6	P7	P8
Building design grade	high	high	high	low	low	low	any	any
Degree of deterioration	as-new	HD	VHD	as-new	HD	VHD	as-new	as-new
Retrofit standard	n/a	n/a	n/a	n/a	n/a	n/a	low	high

$$\begin{Bmatrix} 0.94 & 0.06 & 0 & 0 & 0 & 0 & 0 & 0 \\ 0.0005 & 0.878 & 0.119 & 0 & 0 & 0 & 0.002 & 0.001 \\ 0.0008 & 0 & 0.997 & 0 & 0 & 0 & 0.002 & 0.001 \\ 0 & 0 & 0 & 0.94 & 0.06 & 0 & 0 & 0 \\ 0 & 0 & 0 & 0.0005 & 0.878 & 0.119 & 0.002 & 0.001 \\ 0 & 0 & 0 & 0.0008 & 0 & 0.997 & 0.002 & 0.001 \\ 0 & 0 & 0 & 0 & 0 & 0 & 0.999 & 0.001 \\ 0 & 0 & 0 & 0 & 0 & 0 & 0 & 1 \end{Bmatrix}$$

Figure 3.5: Transition probability matrix calibrated for a low quality seismic risk reduction scheme described in Table 3.3

$$\begin{Bmatrix} 0.97 & 0.03 & 0 & 0 & 0 & 0 & 0 & 0 \\ 0.004 & 0.929 & 0.06 & 0 & 0 & 0 & 0.003 & 0.004 \\ 0.004 & 0 & 0.989 & & 0 & 0 & 0.003 & 0.004 \\ 0 & 0 & 0 & 0.97 & 0.03 & 0 & 0 & 0 \\ 0 & 0 & 0 & 0.004 & 0.929 & 0.06 & 0.003 & 0.004 \\ 0 & 0 & 0 & 0.004 & 0 & 0.989 & 0.003 & 0.004 \\ 0 & 0 & 0 & 0 & 0 & 0 & 0.999 & 0.001 \\ 0 & 0 & 0 & 0 & 0 & 0 & 0 & 1 \end{Bmatrix}$$

Figure 3.6: Transition probability matrix calibrated for a high quality seismic risk reduction scheme described in Table 3.3

The purpose of the framework developed is to compare the impact of various policies on seismic risk over time. The types of decisions in the policy-making space includes the level of retrofit standards used, maintenance schedule and rate of development (building replacement) in each district. All these are being implemented while taking into account deterioration rate. Mathematically, the transition matrix for this type of problem is represented by a combination of the typical transition probability matrices shown in Figure 3.2. Two community-level policies are simulated using the proposed framework as described in Table 3.3. Corresponding transition probability matrices for each policy are shown in Figures 3.5 and 3.6. Each value corresponds to the probability of each state described in Table 3.2 to transition to the next state.

Using Equation 3.3, the change in risk linked to these two policies implemented on the hypothetical building stock is demonstrated in Figure 3.7. As expected, mandatory retrofit schemes with shorter time frames result in early and rapid reduction in seismic risk (Figure 3.7). Also, better maintenance schedules significantly slow down the deterioration of a building portfolio thus reducing seismic risk over time. Demonstrated in the hypothetical building stock case as well is that encouraging development or high building replacement rates to better code standards contributes to seismic risk reduction over time. This demonstration of a policy analysis for community level seismic risk reduction demonstrates the capability of the proposed framework to compare various policy choices related to different standard of improvements such as building codes or time frame for which these policies are enforced/implemented.

Note that the framework can be used to test complex combinations of policies, including encouraging development in lower-hazard districts, different retrofit time-frames, retrofit standards, new building codes, and much more.

3.5 Conclusion

This paper presents a flexible framework accounting for time dependent vulnerability in seismic risk analysis. This enables modelling both of those processes that increase vulnerability (e.g.deterioration, building expansions, cumulative damage), those policies that mitigate increase in vulnerability (e.g. better maintenance schedule, higher durability construction) and those policies that improve resilience (e.g. seismic retrofits and building replacement to higher standards).

We provided multiple applications of the proposed framework for risk analysis that accounts for time-dependent vulnerability. We demonstrated a building-level

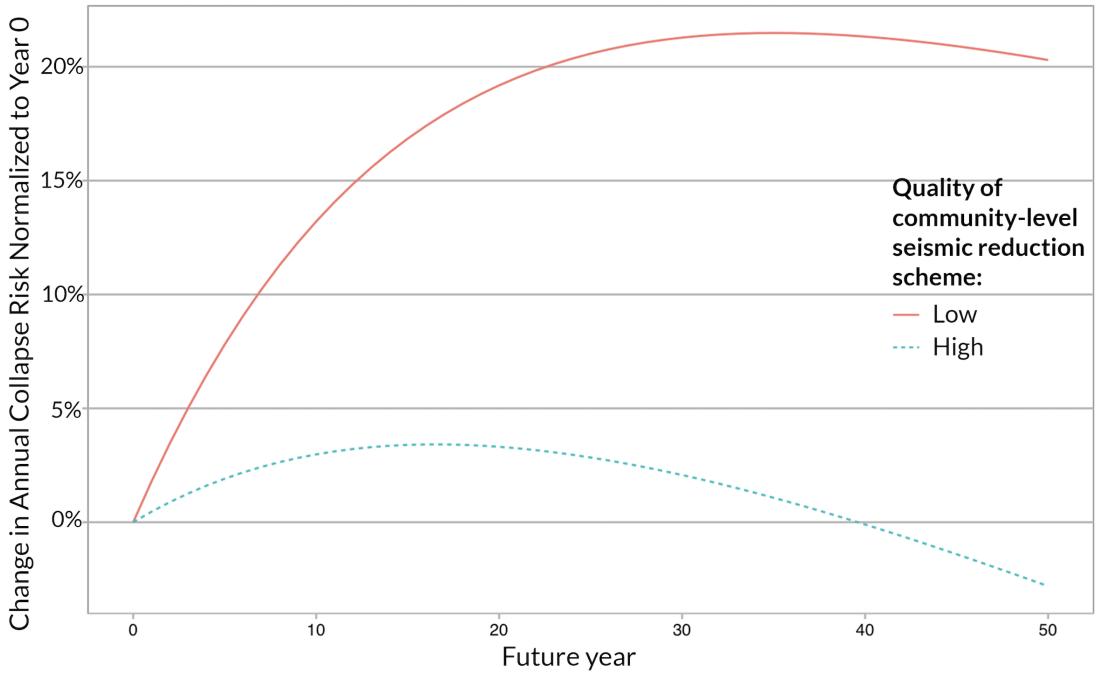

Figure 3.7: Percent change in annual collapse risk normalized to baseline risk at t=0 for a hypothetical building stock. Refer to Table 3.3 for descriptions of each policy

Table 3.3: Features of seismic reduction policies tested on a hypothetical community

Policy feature	Low quality seismic reduction scheme	High quality Seismic reduction scheme
Retrofit policy	Voluntary, long time frame, low standard	Mandatory, short time frame, high standard
Building replacement policy	Low rate of replacement	High rate of replacement
Maintenance schedule	Low level maintenance schedule	High level maintenance schedule

deterioration analysis and a community-level seismic risk reduction policy analysis. The applications vary in terms of the modelled drivers of changing vulnerability and the scale of application (building-level vs. community-scale). In Appendix B.1, I include a short paper that demonstrates a variation of the flexible community-scale analysis shown in this chapter. The application focuses on testing seismic retrofitting programs with varying levels of retrofit standard, time-frame of implementation and whether the program is mandatory or voluntary. The case study in Appendix B.1 uses fragility data and transition probabilities derived from New Zealand's seismic retrofit implementation records. This example further highlights the potential and flexibility of the time-dependent risk framework presented in this chapter to evaluate specific risk interventions.

Overall, the methodology builds on the fundamental probabilistic performance based framework by adding a component for time-varying features which affect vulnerability. The framework allows stakeholders to study the consequences of different mitigation schemes to future seismic risk, and analyse its sensitivity to the initial building stock quality, the structural deterioration rate, maintenance schedule, features of mandatory retrofit policies in terms of their time-frame and standard, building replacement rate, urban development rates and pattern, and other drivers of changing risk.

3.6 Acknowledgments

This research is funded through a National Research Foundation (Singapore) Fellowship grant (NRF–NRFF2018–06), along with an Earth Observatory of Singapore scholarship.

Chapter 4

Learning from successes, not catastrophe: Using counterfactual analysis to highlight successful disaster risk reduction intervention

---

Chapter 4 is a journal article published as follows. Appendix C.1 pertains to the Supplementary Material published with the paper.

Rabonza M.L., Lin Y.C. and Lallemant D. (2022) Learning From Success, Not Catastrophe: Using Counterfactual Analysis to Highlight Successful Disaster Risk Reduction Interventions. *Front. Earth Sci.* 10:847196. doi: 10.3389/feart.2022.847196

In addition, this chapter cites the following first-author paper, which is included in Appendix C.2. The paper presents the concept of four situations in which disaster risk reduction interventions go un-noticed. Two out of the four situations are addressed in Chapter 4's case studies.

Rabonza, M.L., Lallemant, D., Lin, Y. C., Tadepalli, S., Wagenaar, D., Nguyen, M., Choong, J., Liu, C. J. N., Sarica, G. M., Widawati, B. A. M., Balbi, M., Khan, F., Loos, S. & Lim, T. N. (2022). Shedding light on avoided disasters : measuring the invisible benefits of disaster risk management using probabilistic counterfactual analysis. *A contributing paper to the United Nations Office for Disaster Risk Reduction (UNDRR) Global Assessment Report 2022*. https://www.undrr.org/publication/shedding-light-avoided-disasters-measuring-invisible-benefits-disaster-risk-reduction

Chapter highlights

- *I combine probabilistic risk analysis and counterfactual analysis to quantify and highlight the benefits of risk reduction that often go unnoticed.*
- *I estimate the benefits of an intervention in a past earthquake, and for a hazard that has not yet occurred.*
- *I highlight the success of the seismic retrofitting program for schools in Nepal during the 2015 Gorkha earthquake, and the benefits of scaling up the program.*

4.1 Abstract

In the aftermath of a disaster, news and research attention is focused almost entirely on catastrophic narratives and the various drivers that may have led to the disaster. Learning from failure is essential to preventing future disasters. However, hyperfixation on the catastrophe obscures potential successes at the local scale, which could serve as important examples and learning resources in effective risk mitigation. To highlight effective risk mitigation actions that would otherwise remain unnoticed, we propose the use of probabilistic downward counterfactual analysis. This approach uses counterfactual modelling of a past hazard event with consequences made worse (i.e. downward counterfactual) by the absence of the mitigation intervention. The approach follows probabilistic risk analysis procedures where uncertainties in the simulated events and outcomes are accounted for and propagated. We demonstrate the method using a case study of Nepal's School Earthquake Safety Program, implemented before the 2015 M_w 7.8 Gorkha earthquake. Using a school building database for Kathmandu Valley, Nepal, we present two applications: (1) the quantification of lives saved during the Gorkha earthquake as a result of the retrofitting of schools in Kathmandu Valley since 1999, (2) the quantification of the annual expected lives saved if the pilot retrofitting program was extended to all school buildings in Kathmandu Valley based on a probabilistic seismic hazard model. The shift in focus from realised outcome to counterfactual alternative enables the quantification of the benefits of risk reduction programs amidst disaster, or for a hazard that has yet to unfold. Such quantified counterfactual analysis can be used to celebrate successful risk reduction interventions, providing important positive reinforcement to decision-makers with political bravery to commit to the implementation of effective measures.

4.2 Introduction

Success in disaster risk management (DRM) means that natural hazard events do not turn into disasters, and communities continue to function and be resilient to shocks and stresses from hazards. Since the extent of a disaster can be characterised by loss of life and disruptions to the physical, built and social environments, (Mileti, 1999; Smith, 2005; Moore, 1958), the extent of success of risk reduction interventions manifest primarily as reduced impact. As such, success is measured as an *absence* (e.g. no damage, fewer casualties, etc). This poses a challenge for recognising and incentivising important investments in DRM interventions since they are made

invisible by their very nature.

In the aftermath of earthquakes, storms, and floods, narratives of catastrophe dominate the interest of media, political and research communities. However, this hyper-fixation on the catastrophe can obscure important successes amid the broader disaster. Another challenge is to recognize successful interventions if the hazard they were designed for has not yet occurred. This happens when we rely on a disaster occurrence to make mitigation benefits visible. For extreme and rare hazard events, for example, the benefits of risk reduction may manifest only in the distant future. Because of the significant time delay between the interventions and their benefits being manifested, such interventions can be perceived as unsuccessful or squandered until the event occurs. These are two of the challenges described in Rabonza and Lallemant et al. (2022) where successful DRM interventions are made invisible: *invisible success in the midst of broader disaster*, and *invisible success due to yet unrealised benefits* (Full paper included as Supplementary in the Appendix). These *invisible successes* of mitigation interventions are related to a cognitive tendency called *outcome bias* - the tendency to judge the quality of a decision by the outcome alone (Robson, 2019).

To address outcome bias, we propose a *probabilistic downward counterfactual analysis* approach. It relies on comparing the outcome of a realised event in which a risk reduction was implemented, to an alternative branch of history (i.e. *counterfactual*) in which the disaster risk reduction intervention was not implemented. Throughout the paper, we use the term *realised* to refer to events or outcomes that transpired (in juxtaposition to counterfactual), in alignment with prior literature on probability and counterfactual analysis (Roese, 1997). An imagined scenario where an intervention is absent is considered a *downward counterfactual* because the assumed outcome is worse than what was observed in reality (Roese, 1997). This is in contrast with an *upward counterfactual* where the assumed outcome is better. Probabilistic downward counterfactual analysis is *probabilistic* in that it follows probabilistic risk analysis procedures to propagate and account for uncertainties in events and outcomes. In this paper, we present two applications of probabilistic downward counterfactual analysis to highlight the effectiveness of risk reduction in terms of probabilistic lives saved. The first application estimates the benefits of an intervention in a past earthquake through comparison of fatalities modelled without the risk intervention and actual fatalities. The second application estimates the probabilistic benefits of a mitigation for a hazard that has not yet occurred. Instead of an actual past event, a hazard model is used to calculate the intervention's benefits.

The paper's main contribution is in combining the probabilistic risk analysis framework and counterfactual analysis to calculate and highlight lives saved from

successful disaster risk reduction interventions, that otherwise go unnoticed. The significance and novelty of this work is in shifting our perception of the benefits of risk reduction intervention, by using an appropriate counterfactual scenario as the baseline against which to calculate and judge these benefits. Rather than focusing entirely on realised outcomes, the analysis of counterfactual outcomes shines light on the value of a mitigation intervention by demonstrating what would have been without such intervention. Downward counterfactual risk analysis has only so far been used to identify potential worse impacts for the purpose of insurance, preparedness, or future mitigation (e.g. Lin et al., 2020; Aspinall and Woo, 2019; Woo, 2019; Woo and Mignan, 2018; Shepherd et al., 2018; Woo et al., 2017; Oughton et al., 2019; Aspinall and Woo, 2019). This study pioneers a systematic approach to creating incentives for good decision-making on the basis of probabilistic risk. The quantification of probabilistic lives saved by effective risk reduction programs in a major hazard event serves as a powerful indicator of the intervention's success that would otherwise remain unnoticed amidst a disaster. In addition, the calculated probabilistic benefits of an intervention provide important incentive and encouragement to decision-makers committed to implementing effective measures even if the benefits are not materialized yet by the occurrence of a hazard event. Altogether, this work is a new domain of application of counterfactual analysis with much potential across the broad spectrum of hazards.

The proposed framework has significant implications to multiple potential stakeholders. For policymakers, there is currently little political capital gained from investing in resilience if the benefits of such investments are invisible. By having the benefits of these investments visible to their constituents, policymakers will be incentivised for risk-informed decision-making. For donors and funders, this framework would enable them to monitor progress in terms of probabilistic impacts reduced, even if such benefits remain unrealized until a disaster strikes. For disaster risk management practitioners, while it is important to learn from failures, it is equally important to learn from successes, and share them broadly so they can be emulated, scaled, and adapted in other contexts where they are needed. Importantly, it also provides a mechanism to recognise and elevate the important, humble, long-term, and dedicated work conducted by many to keep our communities safe, even when their work is unseen.

The paper is organized as follows. Section 4.3 introduces the proposed framework in the context of probabilistic risk analysis. In Section 4.4, we describe the earthquake risk intervention that will be the focus of our two applications: the school earthquake retrofitting program in Nepal, implemented before the 2015 M_w 7.8 Gorkha

earthquake. In the subsequent sections, we present the methods (Section 4.5) and two applications (Section 4.6) that shed light on the benefits of the retrofitting program. The first application estimates the number of lives saved during the Gorkha earthquake as a result of the retrofitting of schools in Kathmandu Valley since 1997. The second application calculates the annual expected lives saved if the retrofitting program was extended to all school buildings based on a probabilistic seismic hazard model we generated for Kathmandu Valley, Nepal. This is followed by Discussion (Section 4.7) and Conclusion (Section 4.8).

4.3 Counterfactual risk analysis framework

The main idea of counterfactual disaster risk analysis is to explore alternative branches of history to assess past situations where a disaster might have occurred but was averted or failed to materialise (Woo, 2018). Impacts associated with a past event, i.e. a realised event, can be expressed as the function of the (a) Hazard, the likelihood of potentially damaging events, (b) Exposure, the characteristics of assets such as people, buildings and infrastructure and (c) Vulnerability, the susceptibility of the exposed assets to sustain impact for a given hazard intensity (United Nations Office for DRR, 2009). Then, we can write the losses from the realised event as

$$I_{realised} = f\left(\theta_H, \theta_E, \theta_V\right), \tag{4.1}$$

where θ_H, θ_E, and θ_V are the hazard, exposure and vulnerability parameters consecutively. Modifications ($\delta_.$) of one or multiple parameters that define the realised event allow one to define the impact of a counterfactual event:

$$I_{counterfactual} = f\left(\theta_H + \delta_H, \theta_E + \delta_E, \theta_V + \delta_V\right), \tag{4.2}$$

The purpose of the deviations, δ_H, δ_E, and δ_V, to the realised event's parameters is to explore counterfactuals. δ_H helps us explore counterfactuals in the hazard (e.g. what if the earthquake had occurred at a slightly different location, or with opposite directivity of rupture?). δ_E helps us explore counterfactuals in the exposure (e.g. what if the 1906 San Francisco earthquake were to hit today's building stock?). δ_V helps us explore counterfactuals in vulnerability (e.g. what if all unreinforced masonry buildings had been retrofitted?). In this paper, we focus on δ_V, while δ_H and $\delta_E = 0$, to highlight the value of effective vulnerability reduction programs that often go unnoticed.

Modelling the impact of events with either Equation 4.1 or 4.2 relies on probabilistic risk analysis. Traditionally used in engineering reliability assessments

and performance-based design, probabilistic risk analysis has been an established approach to assess the risks from natural hazards to entire regions and cities (Paté-Cornell, 2002; Stergiou and Kiremidjian, 2010). Probabilistic risk analysis systemically quantifies the potential impacts of hazard events on a system and the likelihood that such consequences would occur (Bedford et al., 2001). In the case of Equations 1 and 2, the impacts $I_{realised}$ and $I_{counterfactual}$ and their likelihood are obtained through the joint probability of the risk parameters.

The expected benefits (B) of effective risk mitigation is then calculated as the difference between the expected value (the mean) of impacts of the realised event $E(I_{realised})$ and the counterfactual event $E(I_{counterfactual})$ (see Equation 4.3 and Figure 4.1). Assuming the realised impacts are less than those of the counterfactual, B is expected to be a positive value in Equation 4.3.

$$B = E(I_{counterfactual}) - E(I_{realised}) \tag{4.3}$$

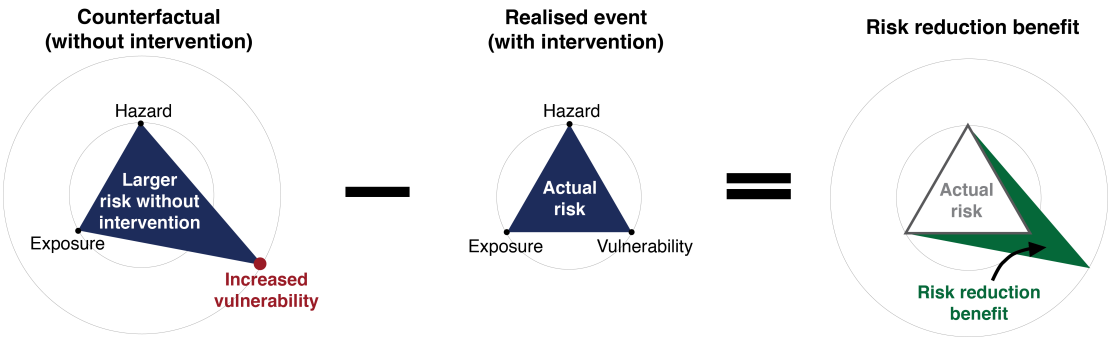

Figure 4.1: The concept of the counterfactual risk analysis framework for quantifying the probabilistic benefits of effective risk reduction. This graphic serves as a demonstration of the framework that is specific for a risk intervention that reduces vulnerability.

4.4 Invisible success of seismically retrofitting schools in Nepal

In this paper, we implement the proposed framework to highlight invisible benefits of effective earthquake risk mitigation. Specifically, we focus on one of the most significant risk interventions in recent years that led to improved construction practices - the seismic retrofitting of school buildings in Nepal. Amid the destruction and tragic loss during the Gorkha earthquake, the life-saving benefit of the school retrofitting was obscured. Likewise if an earthquake event has not yet occurred, retrofitting program may seem like

a waste even though an earthquake may occur at any time. Probabilistic counterfactual risk analysis can be used to shed light on these invisible benefits.

School buildings in Nepal are recognized to be at high risk amidst the region's high seismicity from the convergence of the Indian tectonic plate with the Eurasian plate, and due to informal construction practices done with little engineering guidance (Marasini et al., 2020). Damage to school buildings was extensive from large earthquakes in recent history - the 1988 M_w 6.6 Udayapur earthquake (Gupta, 1988), and the 2011 M_w 6.9 Sikkim/Nepal border earthquake (Rai et al., 2012). The 2015 Gorkha earthquake is a unique example in terms of the impacts on schools because the earthquake happened on a Saturday, whilst the school was not in session. Had the earthquake hit on a school day, over one million students would have been affected (Dixit et al., 2014).

Seismic retrofitting of school buildings started in 1997 through the leadership of the National Society for Earthquake Technology (NSET) as part of Nepal's School Earthquake Safety Program (SESP) (Marasini, 2019). By the time of the Gorkha earthquake in 2015, 300 schools had been retrofitted, 160 of which were in Kathmandu Valley. It was a big achievement that none of the schools retrofitted under SESP collapsed or needed major repairs after the earthquake. Because the buildings were found to be structurally sound, all the retrofitted buildings served as safe shelters and required fewer temporary classrooms (Marasini, 2019). Following the direction of SESP towards safe learning facilities, the Government of Nepal aims to achieve minimum school safety criteria nationwide by 2030 through the Comprehensive School Safety Master Plan developed by Nepal's Ministry of Education, Science and Technology (CEHRDC, 2018) based on the global Comprehensive School Safety Framework (UNISDR and GADRRRES, 2017). Recognizing the need to strengthen more than 60,000 school buildings all over Nepal (Marasini et al., 2020), one of the activities in the Master Plan is to retrofit school buildings in earthquake-affected areas.

4.5 Methods

4.5.1 School building database

The analyses in this paper are carried out on a database of Nepalese school buildings surveyed and georeferenced in 2013 through the partnership of the Open Data for Resilience Initiative (OpenDRI) and the Government of Nepal with support from Kathmandu Living Labs (OpenDRI, 2012). The building database covers Kathmandu Valley and was produced to understand the seismic risk in the education and health infrastructure. Parts in the dataset related to educational infrastructure were tagged as

either *school*, *college*, *university*, or *kindergarten*. The database provides information on the location, number of daytime occupants on a school day, structure type, and whether the school building was retrofitted or not. We chose the OpenDRI dataset for this paper because these building attributes allow us to determine which school buildings were retrofitted under SESP before the 2015 Gorkha earthquake. In addition, the buildings' structure type can be used to identify the buildings' vulnerability, while the number of daytime occupants can be used for fatality calculations.

After screening the raw OpenDRI dataset for missing information or non-school buildings, the final dataset we use for this work consists of 5029 school buildings, of which 70 were retrofitted (see Figure 4.2). We highlight that the OpenDRI dataset we use for this study provides information on only 70 out of the 160 retrofitted school buildings identified by NSET in Kathmandu Valley's affected areas (Marasini, 2019). The database consists of buildings with unreinforced masonry-type (URM-type) and reinforced concrete-type (RC-type) structures. The daytime occupancy for the 70 retrofitted schools go up to 800, with a mean of 134, whereas the occupancy for the 5029 school buildings go up to 2000 with a mean of 120.

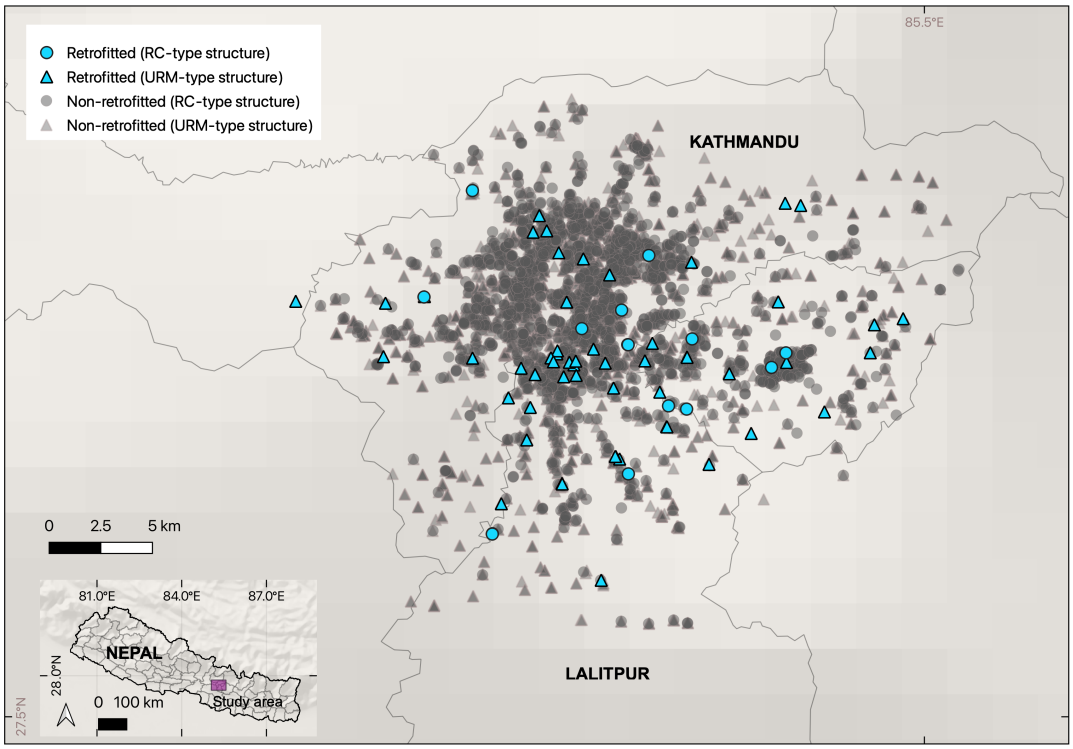

Figure 4.2: A map of the building database used in the analysis showing distribution of schools retrofitted and non-retrofitted as well as structure type.

4.5.2 Building vulnerability modelling

A fundamental step in estimating the benefit of a seismic retrofitting intervention involves obtaining the structure's probability to exceed a certain damage level before and after the intervention. This paper focuses only on the collapse damage level since a vast majority of earthquake fatalities worldwide are due to building collapse (Spence, 2007). Collapse fragility curves are used to represent the probability of collapse for a given earthquake intensity and building class.

In this work, we have adopted collapse fragility curves developed by other authors to represent the probability of collapse of the buildings in their retrofitted and non-retrofitted states. The collapse fragility curves we use for the Nepalese school building stock in this study are presented in Figure 4.3. The median η and lognormal standard deviation β of the fragility curves expressed as PGA lognormal distributions are shown in Table 4.1.

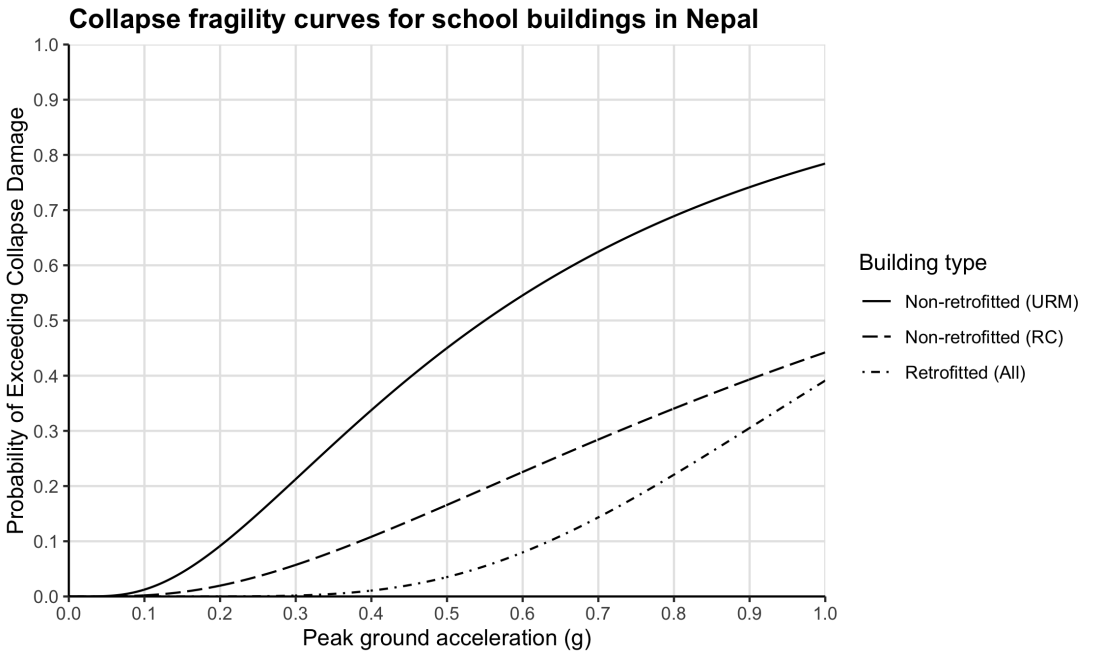

Figure 4.3: Collapse fragility curves adopted in the analysis.

For non-retrofitted buildings, we adopt Giordano et al. (2021a)'s empirical-based fragility curves specifically developed for Nepalese school buildings. The curves were generated using a Bayesian approach to incorporate well-established fragility models such as the HAZUS database (Federal Emergency Management Agency, 2015) and World Bank's Structural Integrity and Damage Assessment database (SIDA) that was conducted under the Global Program for Safer Schools (Worldbank, 2019). The collapse fragility curves from Giordano et al. (2021a) were assigned to the buildings in

Table 4.1: Fragility curve parameters adopted in the analysis for the school buildings in the OpenDRI database. The parameters follow a lognormal model where η (g) is the median PGA and β is the lognormal standard deviation.

Reference	Building class	Structural state of building	Collapse state parameters	
			η	β
(Giordano et al., 2021a)	Non-retrofitted URM - Unreinforced masonry bearing wall, low-rise (pre-code)	Un-retrofitted	0.55	0.76
(Giordano et al., 2021a)	Non-retrofitted RC - Concrete frame buildings with unreinforced masonry infill walls, low-rise (low code)	Un-retrofitted	1.13	0.84
(Giordano et al., 2021b)	Retrofitted stone masonry buildings	Retrofitted	1.133	0.452

the OpenDRI dataset based on their structure type - unreinforced load-bearing wall schools were assigned the URM collapse fragility curve, while reinforced concrete schools were assigned the RC collapse fragility.

For retrofitted buildings, we use the collapse fragility curve developed by Giordano et al. (2021b) for retrofitted stone masonry buildings in Nepal that are considered to have good quality material. The fragility curves in Giordano et al. (2021b) were produced analytically using a non-linear static pushover analysis for stone masonry buildings retrofitted with the 'RC strong-back approach'. It should be noted that the selected fragility curve for retrofitted school buildings does not necessarily represent the variation in the retrofit solutions available in Nepal, as well as the workmanship and original quality of the buildings, rather this is the best information available to the authors at the time of writing.

4.5.3 Expected fatalities from building collapse

A vast majority of earthquake fatalities worldwide are due to building collapse (Spence, 2007). Therefore, this paper focuses on quantifying the fatalities from earthquake-induced building collapse, and the reduced estimated fatalities from retrofitting interventions.

To estimate fatalities due to building collapse, we adopt a semi-empirical casualty model that takes advantage of the availability of detailed building inventory and collapse fragility curves specific to the building types in Nepal. The approach is adopted from the semi-empirical forward model implemented in the USGS Prompt Assessment of Global Earthquakes for Response (PAGER) system (Jaiswal et al., 2011) for determining the extent of earthquake impacts globally. In contrast to USGS PAGER's use of Modified Mercalli shaking intensities, the earthquake intensity for this study is expressed in terms of peak ground accelerations. In this study, we calculate the total estimated fatalities $E[I]$ for a given building portfolio having a total number of m buildings from a single

earthquake event. Each building i in the portfolio has a known structure type k_i. Using the empirical casualty model, we can write $E[I]$ as

$$E[I] = \sum_{i=1}^{m} O_i \cdot FR_i(k_i) \cdot C_i(im_i, k_i) \tag{4.4}$$

where O_i is the total exposed population inside building i at the time of the earthquake, $FR_i(k_i)$ is the fatality rate associated with the collapse of building i based on its structure type k_i, and $C_i(im_i, k_i)$ is the probability of collapse of building i given the earthquake intensity at its location im_i and its structure type k_i.

A fixed fatality rate of $FR_i(k_i) = 20\%$ for all structure types k_i in the dataset is adopted for the study. This fatality rate is based on NSET's recommendation for both RC and masonry building classes, of which all the buildings in the dataset fall into (NSET, 2000). This comes with an assumption that the same level of casualty is expected regardless of the level of school (e.g. primary or higher grades), nature of escape routes, or the occupants' level of preparedness.

By calculating $E[I]$ for a counterfactual and a realised scenario using Equation 4.4, and plugging into Equation 4.3, we can calculate the expected benefits of effective risk mitigation in terms of lives saved. In order to generate the entire probability distribution of fatalities, we conduct Bernoulli simulations (10,000) for collapse given a shaking intensity $C_i(im_i)$ at each building location and for each building class k_i for both the realised and counterfactual scenario. The complete source code is available at https://github.com/ntu-dasl-sg/frontiers2021-PLS.

4.6 Applications

4.6.1 Lives saved during the 2015 Gorkha earthquake due to the school retrofitting in Kathmandu Valley

In order to quantify the reduced fatalities from the school retrofit program in Kathmandu Valley, we estimate the fatalities during the 2015 Gorkha earthquake in the 70 retrofitted school buildings in our database as well as in the counterfactual scenario where these are not retrofitted. By chance, the earthquake occurred during a school holiday, during which occupancy was very low. For both re-analysis scenarios (current retrofit and counterfactual non-retrofit schools), we analyse fatalities for the expected occupancy during the school day. While there were a total of 160 schools retrofitted in Kathmandu Valley at the time of the 2015 Gorkha earthquake (Marasini, 2019), our database contained information on 70. Hence while the focus of our analysis is on the

life-saving benefit of the retrofit of the 70 schools in our data, the true reduction in fatalities due to the earthquake retrofitting program is much greater. A map of the 70 retrofitted school buildings used in this analysis is shown in Figure 4.4.

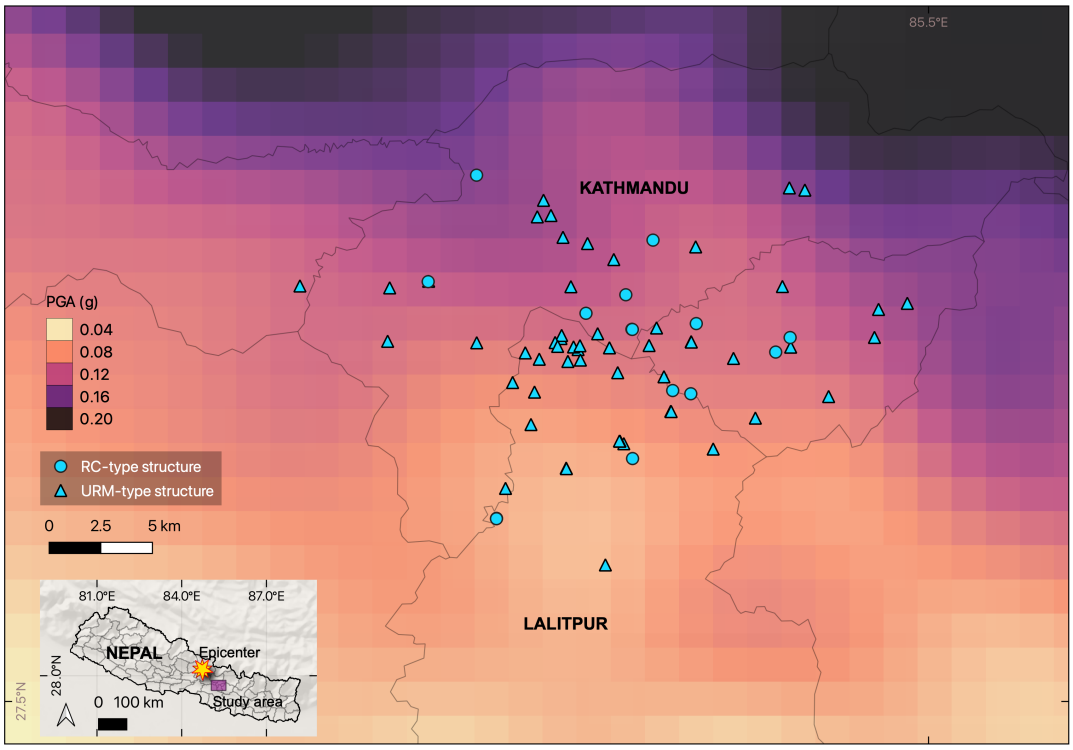

Figure 4.4: A map of the 70 retrofitted schools and their corresponding structure type used in the analysis described in Section 4.6.1. The basemap shows the hazard model developed by Chen and Wei (2019) for the 2015 Gorkha earthquake in terms of peak ground acceleration (in g-units).

The shaking intensity at the school sites during the 2015 Gorkha earthquake is obtained from the broadband ground-motion simulations produced by Chen and Wei (2019) for the earthquake event. This hazard model was selected because the location of sources of the high-frequency energy (strong-motion generation areas) is a critical factor in explaining the relatively low damage phenomenon observed in Kathmandu Valley during the 2015 Gorkha earthquake (Gallovič, 2016; Koketsu et al., 2016), aside from the effects of site conditions and rupture directivity (Dixit et al., 2015; Rajaure et al., 2017; Gallovič, 2016; Koketsu et al., 2016). A map of the PGA values at the location of the retrofitted buildings is shown in Figure 4.4. With this hazard model, PGA values at the location of the retrofitted buildings range from 0.065 to 0.149 g, and come in a resolution of 0.0167 degrees, or around 1.85km. More details about the PGA data are summarised in Chen and Wei (2019) and its companion paper, Wei et al. (2018).

In order to calculate the estimated impacts in a counterfactual scenario, $E[I]_{counterfactual}$, in which the SESP seismic retrofitting program was absent before the Gorkha earthquake, we use Equation 4.4 to estimate the total fatalities for the 70 buildings under this counterfactual scenario. The probability of collapse $C_i(im_i, k_i)$ of any building i is obtained from the fragility curve of the building at its *non-retrofitted state* and the Gorkha earthquake event-specific PGA at the building's location im_i. The collapse fragility curves for the non-retrofitted state are assigned as described in Section 4.5.2, and the PGA values at the building locations are extracted from Chen and Wei (2019)'s hazard model. Using these inputs in Equation 4.4 results to $E[I]_{counterfactual}$ = 25 fatalities.

The expected fatalities from the realised event $E[I]_{realised}$ can be calculated using the same approach, but using the collapse fragility curves corresponding to the *retrofitted state* of the buildings as assigned in Section 4.5.2. This approach results in $E[I]_{realised}$ = 0 fatalities, which is the expected total number of fatalities in the realised scenario for the 70 buildings. By comparing the fatalities from the two scenarios as in Equation 4.3, we estimate that the lives of approximately 25 school occupants were saved in Kathmandu by the retrofit of the 70 schools (see Figure 4.5).

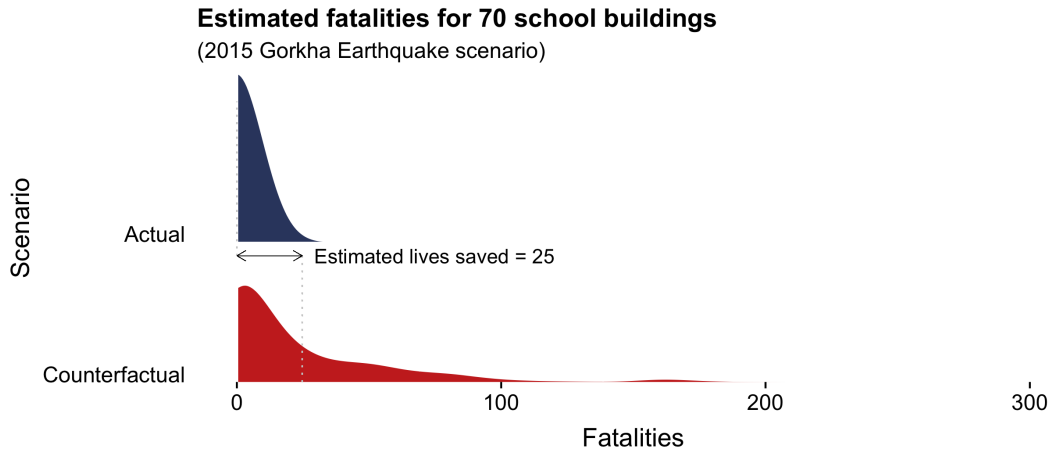

Figure 4.5: Distribution of estimated fatalities from the 2015 M_w 7.8 Gorkha earthquake based on earthquake intensity values from Chen and Wei (2019). Two scenarios are shown: the actual scenario where all 70 school buildings were retrofitted prior to the 2015 Gorkha earthquake, and a counterfactual scenario where the schools were not retrofitted. Our analysis show an estimated 25 lives in the 70 retrofitted schools.

In an attempt to explore the sensitivity of the casualty estimates to different hazard models for the 2015 Gorkha earthquake, we repeated the analysis using a PGA map from the USGS ShakeMap (USGS ShakeMap, 2015; Wald and Allen, 2007). While

using Chen and Wei (2019)'s hazard model results in 25 lives saved, using the USGS ShakeMap hazard model results in 68 lives saved (see Figure C.1 in the Appendix). The analysis using either model highlights the life-saving benefit of the school retrofitting program, but we believe that the fatality analysis using Chen and Wei (2019)'s model is more accurate in terms of representing the shaking during the 2015 Gorkha earthquake. Chen and Wei (2019)'s model better captures the amplification or attenuation of the seismic shaking as it accounts for the location of sources of the high-frequency energy (strong-motion generation areas), rupture directivity, and site conditions critical in understanding the relatively low damage phenomenon observed in Kathmandu Valley during the earthquake.

4.6.2 Annual expected lives saved through scaling the retrofit programs to all schools in Kathmandu Valley

Part of the Comprehensive School Safety Master Plan is the ambition to scale earthquake retrofitting to all vulnerable schools (CEHRDC, 2018). As such, we develop a second case study to better understand the life-saving impact of such a program. We assess expected fatalities if the 5029 schools in Kathmandu Valley were retrofitted, and if they remained in their current state. This analysis is conducted for the entire seismic hazard of Nepal, to better reflect the distribution of potential events to impact Kathmandu Valley.

A probabilistic seismic hazard analysis (PSHA) was developed for the school building sites based on twenty-three independent seismic source zones for Nepal identified by Ram and Wang (2013) and adopted in Chaulagain et al. (2015)'s PSHA model. The ground motion prediction equation by Chiou and Youngs (2014) for active shallow crust regions is used within a logic tree for an event-based probabilistic seismic hazard calculation in the OpenQuake-engine (Silva et al., 2014). To reach statistical convergence, 100,000 stochastic event sets with a 1-year time interval were generated (Silva, 2016). The result of the simulation is a large number of realisations of seismic events and corresponding shaking at the locations of the schools within a year. The resulting hazard curves for some selected schools in the database are shown in Figure 4.6.

For every event generated, the number of fatalities in the building portfolio due to collapse is estimated using Equation 4.4. In the fatality calculation of each event, we incorporate the probability distribution of school building occupancy. In Nepal, schools are open and run 220 days a year, and each school day lasts for 6 hours (Government of Nepal, 2009). This means that out of the 8760 hours in a year, 1320 (15%) are school hours in Nepal. To account for this, we simulate a large number of Bernoulli trials for

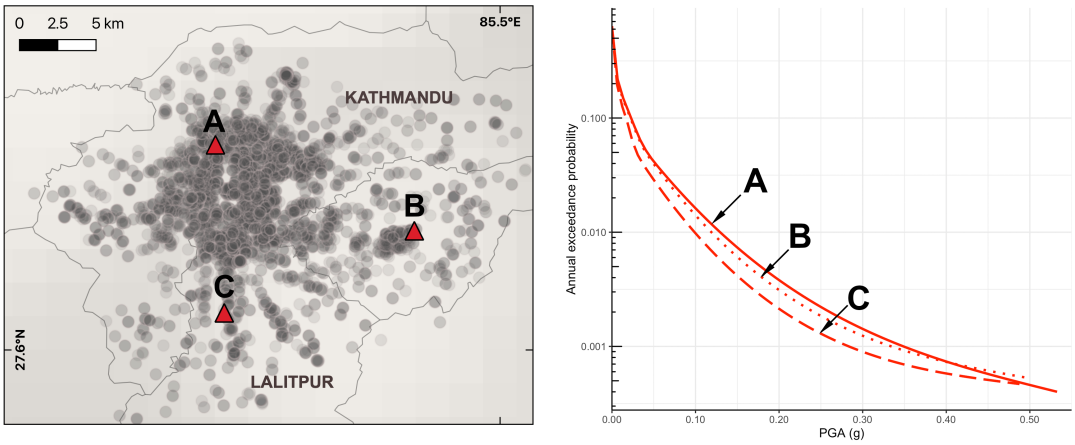

Figure 4.6: Hazard curves for three sample school building locations in the analysis.

each event that takes a 15% probability of occurring during school hours. The resulting annual fatality exceedance probability curves for two different retrofitting scenarios are shown in Figure 4.7. The fatality calculation in this study assumes no uncertainty related to the time of the day during school hours. This means that the building occupancy is constant during school hours, whereas outside school hours, the building occupancy is 0.

The average annual fatalities are obtained by integrating the integrating the annual fatality exceedance probability curve. For the scenario in which none of the 5029 school buildings is retrofitted, we estimate 13 average annual fatalities, whereas when the retrofitting program is extended to all buildings, we estimate an average of 1 annual fatality. In this probabilistic analysis, we calculate an average of 12 annual lives saved from scaling the retrofit program in all of Kathmandu Valley.

4.7 Discussion

4.7.1 A counterfactual analysis approach to celebrate effective risk reduction

In a field focused on long-term resilience to rare (i.e. volatile) hazard events, perceptions of risk are biased by realised outcomes. The perception of *no impacts* when in fact DRM work is successful can result in policymakers and society at large to undervalue the importance of proactive intervention. Shedding light on successes and *what might have been*, not only recognizes the outstanding work of those working to reduce risk, but is also a crucial component of encouraging decision-makers to continue investments

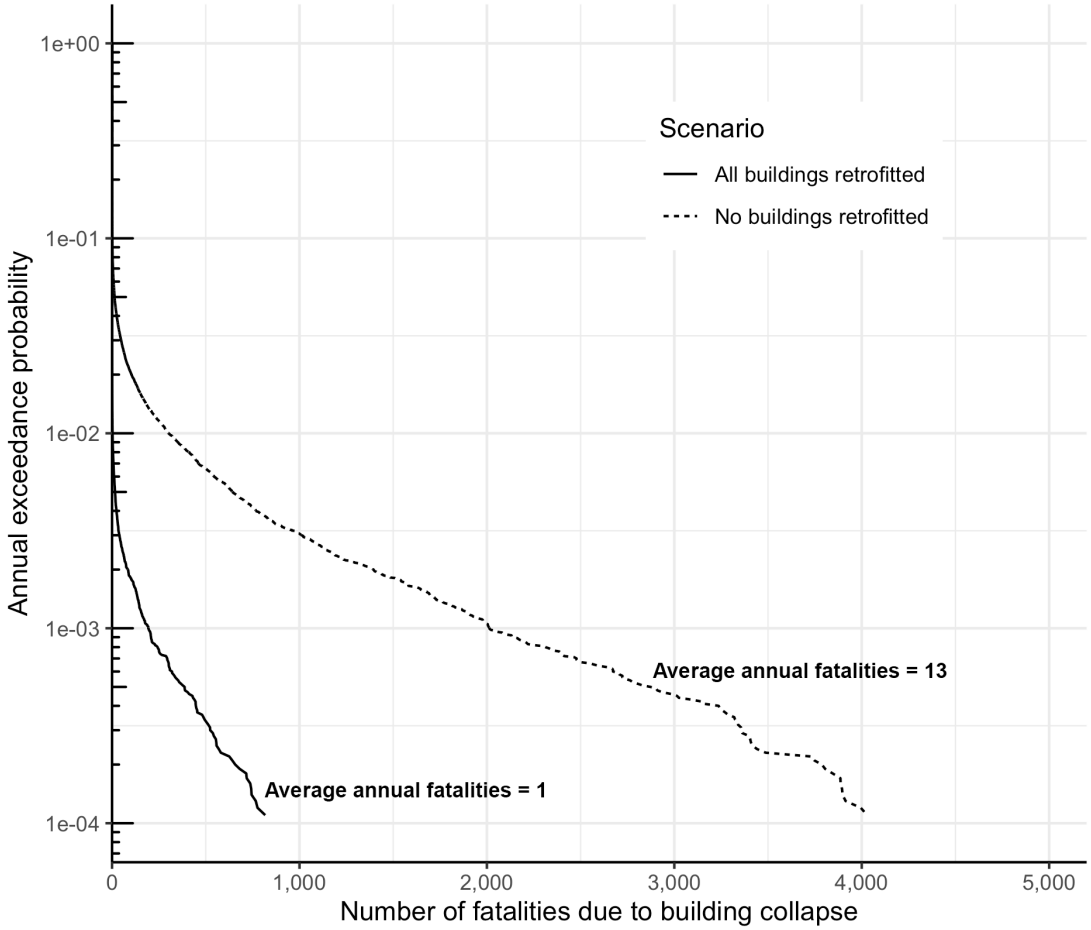

Figure 4.7: Benefits of extending Nepal's school retrofit program to 5029 schools in the database in terms of the shift in the annual fatality exceedance curve.

in measures that keep our communities safe.

We highlight the need to celebrate the often invisible successes of disaster risk reduction interventions, in order to incentivise, better learn and replicate investments in such interventions. We further propose and demonstrate the use of a probabilistic counterfactual risk analysis framework to identify, quantify and highlight these invisible successes. The framework demonstrates that judgement of a risk reduction intervention should be based on a broad exploration of possible outcomes, not only on specific outcomes.

We demonstrated two applications of the probabilistic downward counterfactual risk analysis to (1) celebrate lives saved by a disaster risk reduction intervention (earthquake school retrofitting) amidst a past event (the 2015 Gorkha earthquake in Nepal), and (2) assess expected annual lives saved due to the intervention with the use of a probabilistic hazard model. The two applications show that even in the midst of a tragic disaster,

or if a hazard event has not occurred yet, there are often successes in risk reduction intervention to celebrate. The counterfactual analysis showed that numerous expected fatalities were avoided during the Gorkha earthquake because of the government-led retrofitting of school buildings starting in 1997, and many more could be saved if the retrofit program were scaled to all schools in Kathmandu Valley.

4.7.2 Lives saved as a risk reduction benefit metric

In our demonstrations, the risk benefit of DRM intervention is measured in terms of a reduction in loss of life - the first target metric within the Sendai Framework For Disaster Risk Reduction (UNISDR, 2015b). A risk benefit metric in financial units can also be used, as with a typical cost-benefit analysis. However such analysis tends to highlight interventions that effectively protect high-value areas instead of high-vulnerability areas, which exacerbates inequities (Markhvida et al., 2020; Lallemant et al., 2020).

More alternative risk reduction benefit metrics for this analysis include the number of displaced people, business downtime, damage to buildings and cultural heritage, psychological distress and more. For the Nepal case study, for example, the benefits of retrofitting go well beyond the reduced physical vulnerability of the buildings. Retrofitted schools served as immediate community shelters, field hospitals and relief centres. Classes in the retrofitted buildings were operated without fear, resulting in less demand for temporary classrooms (Marasini et al., 2020). Loss avoidance is not the only invisible benefit of disaster mitigation, and the benefits of DRM interventions go beyond reduction of impact. Certain intervention designs can have co-benefits such as retrofit programs that improve the environmental comfort of classrooms, that serve as training platforms to local constructors who replicate the methods in other building constructions, or that are linked with student and teacher earthquake preparedness programs (Spence and So, 2021).

4.7.3 First order approach

The analyses and estimates of lives saved presented are first order and serve as proof of concept of the counterfactual framework to highlight successes in DRM. Following are limitations that need to be noted for future work:

- The analysis did not account for fatalities from partially collapsed buildings. To account for this, one may use NSET's recommendation to use a 10% fatality rate

for heavily damaged buildings (NSET, 2000)

- The building portfolio dataset we use in the two case studies is only a subset of all the schools within the study area. The dataset used for the first case study (Section 4.6.1) contains only 70 out of the 160 retrofitted schools in Kathmandu Valley. For the second case study (Section 4.6.2), we also did not include school building data that has no information on the occupancy and structure type.
- For the second case study, the assumption that all 5,029 school buildings will be retrofitted seems in line with the plans of the Government of Nepal. However, it is not a forecast of the future, as much uncertainty remains. We hope that our analysis serves to support policy decisions for more resilient schools.

4.7.4 Broader applications with other domains of hazard and interventions

Probabilistic downward counterfactual risk analysis has potential for application to other hazards. A key step of the framework is to identify which risk component the intervention influences. Earthquake risk reduction, for example, influences either the reduction of exposure or vulnerability. Measures such as restricting development in high-hazard zones decrease exposure, whereas better construction standards decrease the structural vulnerability of buildings and infrastructure.

Beyond earthquake risk reduction, the proposed framework can also be used in other domains of hazard. Following are a few selected examples of natural hazards and corresponding interventions that could be celebrated using counterfactual analysis. Enclosed in parenthesis are the risk component/s that the intervention influences.

1. **Earthquake**
    - Reconstruction and seismic retrofit (Vulnerability)
    - Construction inspection (Vulnerability)
    - Preparedness exercises (Exposure, Vulnerability)
2. **Tropical cyclone and Tsunami**
    - Early warning system and timely announcements (Exposure)
    - Evacuation and provision of temporary shelters (Exposure and Vulnerability)
    - Public awareness about the hazard (Exposure and Vulnerability)

3. **Flood**
    - Limiting urban development in flood-prone zones (Exposure, Vulnerability)
    - Enhanced flood management infrastructure (Exposure, Hazard)
    - Timely emergency response (Vulnerability, Exposure)
    - Preservation or restoration of natural ecosystems for flood mitigation (Hazard)
4. **Landslides**
    - Early warning system via geodynamic monitoring (Exposure)
    - Mitigation infrastructure, e.g. drainage systems (Exposure, Hazard)
5. **Wildfires**
    - Early warning system via dynamic weather forecasts (Exposure)

4.8 Conclusion

This study combines the probabilistic risk analysis framework and counterfactual analysis to quantify and highlight the significant benefits of successful disaster risk reduction interventions that often go unnoticed. By using an appropriate counterfactual scenario as a baseline against which to compare realised outcomes, it makes clear that the impact of hazards would be much worse without important investments in risk reduction.

Using this approach, we demonstrate that an estimated 25 lives were saved (probabilistically) during the 2015 Gorkha earthquake from the retrofitting of 70 schools in Kathmandu Valley alone. If such a retrofitting program were scaled to all the approximately 5,029 schools in Kathmandu Valley, we estimate a reduction of 12 annual school children fatalities based on the significant seismic hazard of the region. These are clearly important programs that should be prioritized, celebrated, scaled, and replicated in areas with high seismic risk.

Loss of life reduction is an important metric for risk reduction, not only because the life-safety of children and all people is paramount, but also because doing so centres attention on high-vulnerability areas and buildings, even if the financial losses associated may be small. However loss-avoidance is not the only invisible benefit of disaster mitigation, and the many co-benefits can also be included to further highlight the value of risk reduction interventions.

While this study demonstrates the application of probabilistic counterfactual risk analysis to quantify the life-saving value of a school earthquake retrofitting program in Kathmandu Valley, the methodology can be used in other contexts and hazards. Programs for typhoon and tsunami early warning, hazard informed urban development planning, flood-management through nature-based solution are all examples of important programs whose true benefits could be more accurately valued through the use of probabilistic counterfactual analysis. In so doing, such analysis would provide increased incentives to invest in risk reduction programs, learn from ones with demonstrated success, and serve to encourage those whose humble work is critically important even when often unnoticed.

4.9 Code and data availability

The complete source code for the analysis is written in the R Programming language (R 4.0.2, R Core Team (2020b)). All code and data for the study presented in this chapter is available at at https://github.com/ntu-dasl-sg/frontiers2021-PLS.

4.10 Funding

This project is supported by the National Research Foundation, Prime Minister's Office, Singapore under the NRF-NRFF2018-06 award, the Earth Observatory of Singapore, the National Research Foundation of Singapore, and the Singapore Ministry of Education under the Research Centers of Excellence initiative. MR is supported by a PhD scholarship from the Earth Observatory of Singapore.

4.11 Acknowledgments

We thank Dr. Nama Budhathoki, Kathmandu Living Labs and the GFDRR Open Data for Resilience Initiative for data on school buildings in Nepal. We also thank Dr. Shengji Wei and Dr. Meng Chen for data and information on the broadband simulations in Kathmandu for the 2015 Gorkha earthquake, and Dr. Michele Nguyen for the guidance on the use of the OpenQuake engine.

Chapter 5

Conclusions

The past few decades have seen significant progress and transformation in the field of disaster risk science, with the development of risk modelling frameworks to quantify the impact of natural hazards. These frameworks have been providing core information to risk reduction managers so that they can base their decisions towards a path of resilience. However, current frameworks still under-emphasise key elements important for decision-making, which this research aims to address. Specifically, this research focuses on the need for: (1) considering spatial and uncertainty characteristics in hazard modelling, (2) incorporating time-dependent processes that affect vulnerability, and (3) highlighting the successes and benefits of risk reduction. The goal of this thesis is to develop frameworks that shift the current state-of-the-art analytics in risk and hazard quantification towards more effective tools to support decision-making in reducing risk in dynamic regions. The following research questions from Chapter 1 (Introduction) are answered in the next sections.

1. How can we make the most of limited and uncertain spatial data in inversion and forward estimation with process-based hazard models?
2. How do we account for time-dependent physical vulnerability in regional scale seismic risk analysis?
3. How do we highlight the success of risk reduction programs implemented in the past and the benefits they will provide in the future using risk analytics?

I then discuss the limitations this research and provide recommendations for future research and practice. Finally, I share personal reflections on the implications of the

contributions made on the field of regional scale analytics and support of disaster risk reduction.

5.1 Contributions and relevance

5.1.1 Hazard modelling using limited and uncertain spatial data

How can we make the most of limited and uncertain spatial data in inversion and forward estimation with process-based hazard models?

Process-based models for understanding hazard processes often rely on limited, uncertain, and spatial data. In Chapter 2, I show the importance of effectively utilising uncertainty and spatial information in data when reconstructing past volcanic eruption characteristics and associated tephra fallout from different sets of field observations. The methodological contributions of Chapter 2 include: (1) selecting appropriate cost functions based on their theoretical properties and assumptions on the residual distribution, (2) addressing differential uncertainty when combining multiple data sets, and (3) utilising both forward model and data to estimate the spatial distribution of output. These concepts are illustrated through the study of the tephra fallout of the 2014 eruption of Kelud volcano in Java, Indonesia, and the Tephra2 model. The research can benefit other scientists who aim to their estimates when conducting calibration and forward estimation with spatially-distributed data.

The research provided multiple contributions for the selection of appropriate cost functions in inversion. Chapter 2 is the first study to place attention and investigate the impact of the choice of cost function in tephra fall inversion. The cost function is a key modelling component that defines how the output deviates from observations, and yet little attention is usually given to the choice of cost function in the inversion of source parameters. The analyses highlighted that the selection of cost function needs to be a conscious choice since each has associated assumptions on how the model would fit the data, and the influence on the values of calibrated parameters is significant. Proper cost function selection is an important addition to the suite of techniques in hazard model calibration that make the most of limited and uncertain data (e.g. uncertainty quantification techniques, resampling methods, etc.). Given that the main requirements in proper cost function selection consist of an understanding of the cost functions' theoretical properties and their assumptions, the approach is relatively computationally-cheap and easier to adopt for other applications. The table presented

in Table 2.2, for instance, can be used as a guide by hazard modellers to narrow down potential cost functions for their calibration task, including applications beyond tephra fall hazards.

Chapter 2's main methodological contribution for cost function selection is the two-step approach to evaluate the choice of cost function for inversion/calibration problems using process-based models. For the first step, I demonstrated how to consider the cost functions' theoretical properties most relevant to the data (e.g. sensitivity to outliers, suitability for data spanning orders of magnitude, treatment of under/overestimation) to narrow than suitable cost functions. In the second step, I demonstrated that choosing a cost function implies making an assumption of the type of distribution of the residuals (where residuals are the difference between the modeled output and the observation), and thus should be a consideration for finding an appropriate cost function. I proposed and implemented multiple goodness-of-fit tests (statistical and graphical) to check the suitability of the choice of cost function with the distributional assumption on the residuals. The study added three more alternative cost functions to the developers' version of the Tephra2 code as of writing: mean absolute error (MAE), mean absolute percentage error (MAPE), and mean square log error (MSLE). Based on the cost function properties and distribution of residuals, the research identified MSLE as the cost function that performs best and has characteristics well-suited for the case study. An important takeaway from these methodological contribution is that no metric is inherently better for all applications. Choosing a cost function implies making an assumption on the type of distribution of the residuals. Hence, in its correct application based on the assumed residual distribution, a cost function is optimal.

Another fundamental contribution of this work is how the weighting approach in both inversion and forward model settings allows the use of all data, even if some are highly uncertain, while accounting for this uncertainty. With the increasing availability of high volume, low reliability information (e.g. crowd-sourced data from social media) in disaster risk and hazard modelling, these can nonetheless be used to improve the modelling. In Chapter 2, the Tephra2 inversion algorithm has been extended to account for varying uncertainty across different data points, rather than treating each data point equally in the optimisation. The study proposed the use of uncertainty-based weights to the observations in the cost function. The approach made it possible to consider the varying levels of data uncertainty brought by different field campaigns conducted at significantly different times after the eruption.

In forward estimation, I present another approach to make the most of limited and uncertain spatial data. I developed a model-data fusion methodology that combines

both forward model estimates and the data to generate improved estimates of the spatial distribution of tephra load across an area of interest. The approach utilises a spatial statistics approach called kriging to account for the spatial arrangement of the data in such a way that points nearby the site of interest are given more weight than those farther away. The study demonstrated that the importance placed in the model and data can be balanced by the choice of the spatial model and its parameters.

The strength of the model-data fusion approach is for applications wherein the main goal is to obtain spatial predictions that best agree with observations while accounting for their spatial distribution. While the calibration ensures the best fit to the model in terms of the chosen cost function, the modelled outputs may diverge from observations in a spatially-structured way due to physics-based approximations, unaccounted spatial processes or uncertainties inherent in the model. Often, such model-data disagreements do not pose issues for specific hazard modelling goals such as estimating the total volume/mass of tephra produced by an eruption. However, capturing the spatial complexity of observations is an important consideration for risk assessment activities such as building-level damage assessments (e.g. Williams et al. (2020)'s remote assessment of tephra fall damage from the 2014 Kelud eruption). The model-data fusion approach allow building-level hazard estimates to reflect not only the output of the process-based model at the building site, but also the values and spatial distribution of field data recorded at or nearby the building. It should be noted that since calibration with process-based models have broad applications within and outside hazard modelling, potential applications of the model-data fusion approach go beyond tephra hazard applications.

I also developed an extension of the model-data fusion methodology that accounts not only the spatial arrangement in the data, but also the different levels of uncertainty associated with different datasets collected from the field. The study demonstrated that accounting for varying data uncertainty improves the performance of the model-data fusion based on out-of-sample errors from a cross validation. The strength of both model-data fusion methods is that they are capable of producing not only a map of tephra distribution, but also a map of uncertainties associated to the modelled tephra load in a forward estimation. The approach was able to calculate uncertainties because kriging was used in the development of the model-data fusion approach.

The applications of the work in Chapter 2 go beyond tephra fall modelling. Inversion/calibration and forward prediction workflows are typical in understanding many processes in other natural hazards, which include geophysical (e.g. tsunamis, earthquakes, landslides), shallow (e.g. ground subsidence), atmospheric (e.g. storms), hydrological (e.g., floods, droughts), and biophysical processes (e.g. wildfires). For

instance, in the field of earthquake hazard modelling, the methods can be adopted for better calibration and forward modelling of ground motion prediction equations (GMPEs), which typically rely on spatial and uncertain observations of ground shaking. In fact, the inversion/calibration and forward prediction workflow visualised in Figure 2.1 is typical outside the field of hazard modelling as well. The guidance in Chapter 2 could be relevant to those utilising spatial data to calibrate a model.

5.1.2 Modelling time-dependent vulnerability

How do we account for time-dependent physical vulnerability in regional scale seismic risk analysis?

Increasing regional-scale resilience has gathered traction in recent years in local, national, and global entities, which highlights the importance of risk-informed planning for disaster risk reduction. Simultaneously, however, current methods fall short in characterising the temporal dynamics of urban environments in terms of rapidly changing physical vulnerability. These dynamics may stem from deterioration processes or construction practice that can increase vulnerability, or hazard mitigation activities that can reduce vulnerability. For regional-scale risk analysis, accounting for these dynamics is critical not only to understand the hazard-related risk over time, but also to study the influence of policies on future risk.

In Chapter 3, I developed a regional scale seismic risk analysis that accounts for time-dependent physical vulnerability. To do so, I extended the Performance-Based Earthquake Engineering (PBEE) methodology (Krawinkler and Miranda, 2004) framework (a fundamental engineering approach to assess impact from earthquake damage) to account for time-dependent vulnerability driven by multiple regional scale policies and deterioration. To model state change processes that increase or decrease physical vulnerability from seismic damage, I developed a time-homogeneous Markov chain simulation approach. The Markov chain approach is integrated with the risk analysis framework to model future regional-scale seismic risk driven by time-dependent vulnerability.

Current earthquake risk analysis methods like PBEE are designed for the application of single buildings or infrastructure. In Chapter 3, the case studies span from building-level to regional-scale applications. Specifically, I demonstrate the influence of time-dependent vulnerability for a single deteriorating building, and for a community with buildings experiencing deterioration, retrofitting, and building replacements over time. The impact quantification focuses on physical impact metrics

such as expected building collapse. While it is expected that retrofit policies and building replacements lead to decreased seismic risk, and deterioration leads to increased seismic risk over time, the study demonstrated how risk evolves with time linked to various seismic reduction policies.

The study introduced a proof of concept and a demonstration of a tool for decision-makers to investigate the consequences of various seismic mitigation decisions (that influence physical vulnerability) to future seismic risk. The study demonstrated how the framework allows comparison between single policies or combinations of policies using a hypothetical building portfolio. The framework serves to support global efforts that aim to target risk levels acceptable for society (e.g. the development and setting of specific targets for disaster risk reduction in the Sendai Framework (UNISDR, 2015a)). Ultimately, the work underlines the significance of time-dependent risk models to understand hazard-related risk of urban environments over the lifespan of its infrastructures. A better understanding of feedback loops between dynamic vulnerability and disaster impacts can support proactive policy decisions in risk reduction.

5.1.3 A framework to incentivise, celebrate, and learn from effective risk reduction

How do we highlight the success of risk reduction programs implemented in the past and the benefits they will provide in the future using risk analytics?

The field of disaster risk management faces the challenge of its failures being catastrophic while its successes go unnoticed. This makes it difficult to identify, celebrate, and spread positive lessons learned that could be emulated elsewhere, or to incentivise proactive decision-making on the basis of recognised successes. I have previously identified four types of situations where successful disaster risk management interventions are made invisible in a policy report (Rabonza and Lallemant et al., 2022): (i) success made invisible in the midst of broader disaster, (ii) success made invisible by nature of the success, (iii) success made invisible due to yet unrealised benefits, (iv) success made invisible due to randomness of specific outcome. Chapter 4 presented analytics of how we can shed light on (i) and (iii), but the framework is applicable for all four types of invisibilities.

I propose and demonstrate the use of probabilistic downward counterfactual analysis to shed light on these otherwise invisible successes. Downward counterfactual analysis rely on the understanding of how a realised event could have been worse, as a

way to highlight the benefits of an intervention. I further use the risk analysis framework to ascribe estimated probabilities to the simulated counterfactuals. The estimated probabilities constrain the counterfactual exploration to realistic scenarios. By using an appropriate counterfactual scenario as a baseline against which to compare realised outcomes, the framework makes clear that the impact of hazards would be much worse without important investments in risk reduction.

Probabilistic counterfactual analysis addresses the challenge of incentivising effective decisions, and highlighting their realised or future benefits when evaluating disaster risk measures. By accounting for alternative scenarios with their associated probabilities and explicitly identifying how a mitigation measure decreases the impact on society, it counters the natural cognitive perceptions which hinder the way people process risk and hence measure and evaluate mitigation successes. Since the framework can also be applied to measures for which success has not been realised to consider all possible future scenarios, it can quantify the long-term benefits of disaster risk reduction decisions. The study demonstrated a new domain of application of counterfactual risk that goes beyond pointing out worse potential outcomes for the purpose of insurance, preparedness, future mitigation and learnings from failures in risk management.

I applied probabilistic downward counterfactual risk analysis to (1) recognise lives saved by an earthquake-resistant building intervention in the aftermath of a specific event (the 2015 Gorkha earthquake in Nepal) and (2) predict the annual lives that could be saved in the future if the same intervention were implemented using a probabilistic hazard model. Both examples illustrate that risk reduction efforts can lead to positive outcomes, even in the face of a tragic disaster or in anticipation of one. The analysis revealed that a significant number of deaths were prevented during the Gorkha earthquake due to the government-led retrofitting of schools beginning in 1997. Additionally, many more lives could be saved if the retrofitting program were extended to all schools in the Kathmandu Valley.

The innumerable successful DRM interventions implemented in communities worldwide represent a critical data-set to learn from, adapt, share and implement such activities where they are further needed. This is only possible if these successes are identified, analysed and celebrated. I propose the use of probabilistic downward counterfactual analysis to highlight and quantify the benefits of DRM interventions that otherwise remain invisible. This can serve to lift up the iterative, long-term, humble, dedicated and politically courageous actions required for long-term resilience building.

5.2 General limitations and future work

5.2.1 Framework flexibility

The frameworks proposed in the dissertation are intentionally flexible. Chapter 2 demonstrates a framework that can be used for both applications where the inversion and forward prediction workflows are performed sequentially and applications where they are performed separately. While the test case focuses on the Tephra2 model, the methods are applicable to other process-based models that reconstruct the tephra fallout process. Beyond tephra fallout applications, the guidance are useful for other types of hazard modelling (e.g. calibration of GMPEs) and anyone conducting inversion or calibration modeling with spatially-distributed data beyond hazard analysis.

The time-dependent urban risk framework presented in Chapter 3 is intentionally flexible, wherein the three fundamental components - hazard, vulnerability, and exposure - are considered as plug and play pieces. The case studies in Chapter 3 are limited and focused to modelling the vulnerability component's time-dependence, but the hazard and exposure inputs can be changed to be dynamic as well. Similarly, the specific hazard models and fragility models can be interchanged.

There is future work in the use of dynamic risk frameworks to further study the feedback loops between changing exposure and hazard. This is most relevant for flooding applications, since urban growth is a driver of increasing hazard due to the increase in impervious surface. For such an analysis, the exposure model can be interchanged with urban growth models that can account for historical land-use, transportation networks and slope (e.g. SLEUTH by Clarke et al. (1997)), or models that consider socio-economic characteristics (e.g. Java Spatial Model by Zondag et al. (2009); ADB (2016); Sjarief et al. (2003)).

Finally, the counterfactual risk analysis framework for celebrating benefits of risk reduction is also developed to be flexible (Chapter 4). The key step in the framework is identifying the risk component that the intervention influences. For instance, seismic retrofitting influence physical vulnerability, while evacuation efforts influence exposure in a risk analysis. In Section 4.7.4, I provide multiple examples of interventions with the associated risk components that they aim to influence. The list can be used to identify future potential applications of counterfactual risk analysis framework for highlighting successes in interventions.

The counterfactual risk analysis can be extended to highlight the expected progress and benefits of policy implementation for *each succeeding year in the future*. The second

case study in Chapter 4 is limited to the assessment of the number of lives saved – (1) the present time where only some schools are retrofitted, and (2) a certain time in the future where all vulnerable schools are retrofitted. By using a time-dependent vulnerability model (such as introduced in Chapter 3) and appropriate transition rates of retrofitting every year, the future benefits of the retrofitting intervention can be estimated at incremental points in time.

5.2.2 Methodological lens

The results of the dissertation aim to provide methodological contributions that address the research questions in Chapter 1, rather than demonstrate a more accurate re-analysis of the impacts of the hazard events in the case studies (i.e. the 2014 Kelud eruption in Chapter 2 and the 2015 Nepal earthquake in Chapter 4). Chapter 2's results do not make any claim or conclusions about the characteristics and true source parameters of the 2014 Kelud eruption. Similarly, Chapter 4 does not aim to assess the accuracy of the hazard model used for the 2015 Nepal earthquake.

In Chapter 4, the framework only provide *estimates* of fatalities, which are affected by the choice of the hazard model and the fatality model at an extent that was not extensively explored. As in any model, these estimates serve as useful indicators of risk, but are not necessarily accurate predictions. For such methods, transparency on the underlying methods is key. In Chapter 4, I present the fatality results with their wide distributions to indicate their uncertainty (Figure 4.5).

5.2.3 Metrics of loss and vulnerability

Considering that Chapter 3's scope only considers *physical* vulnerability, the case studies utilised normalised building collapse risk as the metric for seismic risk. The results can be extended to calculate financial losses by using fragility curves for partial damage states and the corresponding loss. Beyond asset-based losses, there is much potential in extending time-dependent risk framework to account for non-asset based losses. Instead of using fragility curves for building damage the vulnerability component, relationships that relate hazard intensity with the non-asset based loss metric can be utilised.

Chapter 4 focused on loss of life reduction. Other metrics of successful risk management interventions include reducing injuries, number of affected or displaced people, building damage, business interruption, livelihood losses, damage to cultural heritage, psychological distress and much more. Counterfactual analysis can be applied equally for these alternative metrics. Furthermore, it is becoming increasingly

recognised that the benefits of risk management activities can go beyond impact reduction and loss-avoidance, and in fact should be designed as such (Lallemant et al., 2021). For instance, the reduction of background risk encourages positive risk taking (e.g., investment in productive assets, entrepreneurial activities), enables long term financial planning (e.g., to build up savings), and potentially increases the value of protected lands (Tanner et al., 2015). Investments in multi-purpose disaster risk reduction measures can also yield benefits that are unrelated to the reduction of background risks. These co-benefits can be economic (e.g., increased agriculture productivity with improved irrigation for drought management), political (e.g., improved governance through strengthening the disaster risk management capacity of civil society), social (e.g. increased parks and green leisure areas), and/or environmental (e.g., carbon sequestration, sediment and nutrient retention from protection or afforestation of wetlands). The nature and level of these co-benefits depend on the design of the disaster risk reduction measure (Tanner et al., 2015).

5.2.4 Hazards accounted for in the models

It is worth noting that the models presented in Chapters 3 and 4 only consider risk in terms of ground shaking. Secondary seismic hazards (sometimes more destructive) such as liquefaction, landslides, and tsunamis are not considered. Topography and basin effects are not included as shaking amplification factors. All of these considerations are linked to geography, which urban growth patterns are sensitive to. By not accounting for these factors, the frameworks may underestimate the increase in seismic risk.

5.3 Chapter-specific limitations and future work

5.3.1 Chapter 2: Other cost functions

Research on selecting the most appropriate cost function shed light on specific cost functions that are often used in research and practice, and yet have many weaknesses. A popular example of such a cost function with many shortcomings is MAPE (described in detail in Appendix A). It should be noted that the literature have proposed multiple alternatives to MAPE to address its shortcomings, which are not included in Chapter 2 but worth investigating for future work (e.g. symmetric MAPE, and scaled versions of mean absolute error and mean square error (Hyndman and Koehler, 2006)).

5.3.2 Chapter 2: Approaches to weighting based on uncertainty

I highlight that uncertainty in measured tephra data is rarely quantified, or even reported in field studies in literature. Currently, there is no standard approach to quantify such data related uncertainty (Engwell et al., 2015). The quantification of differential uncertainty in Chapter 2's datasets is therefore simplified for the purpose of the study.

In Chapter 2, the difference in uncertainty between the two datasets in the test case was inferred based on the time delay in measurement since the time of the eruption and consultation with experts. It was assumed that measurements that are most reliable and contain the least uncertainty are those taken from a well-preserved deposit, i.e. those taken soon after an eruption had little deposit reworking. For future research, the uncertainty-based weights can account for other factors: (a) observational errors across different people measuring the same deposit, (b) systematic bias due to erosion or wind patterns, (c) preferential sampling due to ease of access, and (d) spatial clustering of data. There is future work in calculating weights based on spatial clustering, in which techniques in spatial statistics can be utilised: (1) Voronoi-Dirichlet tesselations (Bavaud, 1998), (2) Gaussian kernel/density approaches to weighting (Cronie and Van Lieshout, 2018; Scott, 1992; Loader, 2012), and entropy or dispersion-based weighting (Zhu et al., 2020).

5.3.3 Chapter 3: Data limitations

The time-dependent risk framework in Chapter 3 relies on critical reliable data that may not often be available for certain geographical contexts or intervention database. The study used a hypothetical building portfolio due to limitations in data. Other limitations of the demonstration include the limited number of building typology, and the simplified hazard model that is represented as a single hazard curve for each district.

Thus, an important future work is to test the framework to an actual building portfolio. The main inputs required for such an application are the hazard model, building fragility database and transition probability matrices. Currently, developing the transition probability matrices pose the most challenge as they are rarely known in practice. In Chapter 3, I showed that the matrices can be estimated through a maximum likelihood estimation approach based on the historical data of the intervention's progress. However, such information is not always available in some regions and applications, thus I believe there should be more work and research done to calculate transition probability matrices. Similarly, the framework relies on the

quality of the fragility curves used in the study. The research project serves to promote the development of better data like fragility curves.

Amidst data limitations for real-life applications, the next easier application is to use published virtual urban areas such as Ellingwood et al. (2016)'s Centerville Virtual Community or Cremen et al. (2022)'s Futureville. These are models of physical-social infrastructure systems developed to test long-term policies for resilience with defined building inventory, supporting public infrastructure systems, and socio-demographics.

5.3.4 Chapter 4: Setting appropriate counterfactuals

As in all risk analyses, the process of counterfactual analysis requires scrutiny and transparency in the assumptions, data and analysis conducted. Doing so aims to avoid both misuse of the counterfactual framework and misrepresentation of the benefits of disaster risk management. An example of misuse would be inflating the benefits of a risk intervention by cherry-picking 'ideal' counterfactuals - e.g. a hazard scenario too extreme and unrepresentative of the current knowledge of the hazard that the calculated lives saved would inflate.

5.3.5 Chapter 4: Analytics for other types of invisibilities in successful risk management

Chapter 4 does not cover case studies that address the following situations where successful risk interventions may go unnoticed (derived from Rabonza and Lallemant et al. (2022), and seen in Appendix C.2):

1. **Success made invisible by nature of the success.** A hazard becomes a disaster on account of the impacts it has on society. If mitigation efforts are so successful that there are no perceivable impacts, both the potential disaster and the successful mitigation are made invisible.

2. **Success made invisible by the randomness of the specific outcome.** Hazards are stochastic processes, hence any single occurrence is only one of several possibilities that could have occurred. Recognising that the parameters of the event that actually occurred could easily have been different, successes can be made invisible if the hazard randomly does not strain mitigation measures, e.g. a near-miss.

A great example of #1 – an intervention so successful that there are no perceivable impacts – is an effective evacuation effort before a potentially destructive hazard event

hits a community. Future research that aim to analyse the benefits of an evacuation program can be done by referring to the schematic of the proposed framework for highlighting successes in Figure 4.1. Since an evacuation effort influences the exposure component, the reduction in exposure is considered rather than the reduced vulnerability shown in Figure 4.1. Similar with the case studies presented in Chapter 4, a hazard model and representation of vulnerability is required.

Analysis that address #2 (success made invisible by the randomness of the specific outcome) involve the use of a probabilistic hazard model. This model is produced through the simulation of a large number of realisations of hazard events and corresponding impact to the exposure. A probabilistic seismic hazard model was utilised in Chapter 4 to study the future life-saving impact of the schools retrofitting program, but the probabilistic hazard model can also be used to highlight that the 2015 Nepal earthquake is only one of several possible events that could have occurred.

5.4 Final remarks

This final section conveys my broader reflections on the applications and contributions of the dissertation. I also include a description of the *Averted Disaster Award*, which is a recently-launched global recognition that was developed directly from the ideas presented in Chapter 4 and another paper I lead (Rabonza and Lallemant et al., 2022).

5.4.1 Towards integration across disciplines

The research I have conducted in NTU was motivated by the many personal interests and skills I wanted to explore and learn in the field of hazards and disaster research. The outcome is a convergence of the earthquake modelling skills from my civil engineering background, my experience in probabilistic hazards modelling, my recent introduction to volcano hazards in the Asian School of the Environment, my new-found interest in spatial statistics, and my passion to understand social perceptions in risk. My dissertation presented concepts from multiple disciplines spanning from physics-based methods to insights rooted from social psychology.

Indeed, the field of hazards and disaster research has an established history of inclusive forms of multidisciplinary research (Kendra and Nigg, 2014) to produce new insights for risk communication, recovery, and decision-making (Mileti, 1999; Olson et al., 2020; Birkland, 2006). It is my belief that increasing our knowledge about natural processes of hazards alone is not sufficient to lead our communities towards a more safe and resilient path. To illustrate, a specific technical intervention, which may seem to be brilliant solution for one issue has the potential to create a completely new

challenge (Peek et al., 2020). For instance, in Portland Oregon, efforts to save lives by the seismic retrofit of unreinforced masonry homes and churches threatened to displace African American communities with a long history of dispossession (Njus, 2019). Therefore, risk analytics should be complemented with specific actions that aim to reduce inequalities, injustices, historical and socio-technical issues that turn natural hazards into disasters. These are important factors in which the dissertation's case studies have not accounted for, but instead proposed for future work.

My research advocates and hopefully contributes tools for integrating multiple techniques and perspectives in analytics to improve our understanding of hazards and to promote resilience. It is my conviction that there is great value in incorporating advancements in hazard quantification (e.g. Chapter 2), modelling time-dependent processes in risk (e.g. Chapter 3), and incentivising good efforts in risk reduction (e.g. Chapter 4) when they also account for social, political, and economic processes that put people and assets in harm's way.

5.4.2 Towards decision-making on the basis of probabilistic risk

An important concept that emerges from this study is that the value of a risk reduction intervention should not be judged on the basis of specific outcomes, but also on the basis of a broader exploration of potential outcomes. The same *good decision* may seem like overkill against a specific outcome, or may seem completely insufficient judged against another. Especially in a field focused on long-term resilience and often rare (therefore volatile) events, *realised outcomes* bias our perceptions and judgements.

This is also relevant to the monitoring of risk reduction targets, including those of the Sendai Framework for the years 2015-2030 (UNISDR, 2015b). Mortality on any given year, or specific place, may not reflect adequate or inadequate disaster planning, but rather chance outcomes. To illustrate in the case of earthquakes, even countries with high seismic hazard can experience no destructive earthquakes in the span of 15 years. An example of this is Haiti, where from 1900 to 2009, earthquakes killed less than 10 people. However,in 2010, a strong earthquake killed more than 200,000 people. The mean earthquake fatality rate in Haiti between 1900 and 2000 was less than 0.1 fatalities per year. After 2010, this mean fatality rate became more than 1,800 fatalities per year. Therefore, using observed disaster loss data for a short snapshot of time could result to complacency in those countries spared by disasters. In other words, some countries will think they are doing so well because they have fewer casualties for decades, whereas some countries will think they did really badly. But in fact, neither of those countries will actually know what the true risk situation is by using just a few decades of data.

Therefore, to be able to achieve targets in risk reduction, decisions should be made on the basis of probabilistic risk. Encouraging long-term resilience, which may not 'pay-off' for decades (e.g. for climate-adaptation), will therefore require a shift in focus from realised outcome to unrealised risk reduction.

5.4.3 Towards systematic celebration of averted disasters

Multiple times in my PhD, I had the opportunity to ask the following set of questions in front of expert audience and plenaries in the field of disaster risk (i.e. academics, industry experts, politicians, military personnel, etc.):

> Can I ask a show of hands – who has heard about **Hurricane Katrina**?

Typically, almost all of them raises their hands.

> How about **Typhoon Haiyan?**

Again, most of them raises their hands.

> Now, what about **Cyclone Fani?**

Every single time, almost no one raises their hands for Cyclone Fani.

Fani, was the largest cyclone to make landfall in India in the past two decades, but the reason no one knows about it is that there was a successful evacuation program that resulted to nearly zero fatalities in this event. The impact was so little compared to the 10,000 fatalities from the 1999 Odisha Cyclone - a cyclone that hit the same area and has the same intensity as Fani. Because the evacuation was so successful, it did not really make much news. This is one of the situations that my work has identified where successful disaster risk reduction interventions go unnoticed or invisible, wherein the perception is that nothing happened, and there's a need to highlight that nothing happening is extraordinary.

In Chapter 4, I present other situations where successful risk reduction may go un-noticed such as amid a catastrophe. The 2015 earthquake in Nepal caused widespread destruction and numerous tragic fatalities, and yet amid this disaster there were important successes that deserve highlighting. Because of the earthquake retrofit program implemented by the government of Nepal, none of the retrofitted schools collapsed during the 2015 earthquake. In this situation, people focus only on the catastrophe, but even within the catastrophe, there are important interventions that we should celebrate. Chapter 4 demonstrated the use of probabilistic counterfactual analysis to analyse these often unnoticed benefits of risk reduction measures.

This is what underpins the *Averted Disaster Award*, a premier global recognition that was launched since 2021 from the support of the World Bank Group, Understanding Risk Community, and the Global Facility for Disaster Reduction and Recovery (GFDRR). The award is based on the concepts presented in Chapter 4 and the paper I lead for the United Nations Global Assessment Report 2022 (Rabonza and Lallemant et al., 2022). The idea of the award is to identify, highlight, and share the hard work that people are doing around the world to reduce the impact of climate and disaster risk. The applicants were also guided in the use of the counterfactual analysis. The award has been an impactful (non-academic) achievement that was produced from the scientific ideas from this dissertation.

Submissions for the Averted Disaster Award have covered amazing programs such as using nature-based solutions for flood risk reduction, early warning systems, socially-inclusive approaches to disaster risk management, climate policy, coastal protections against rising seas and storms, risk financing programs, strengthening of buildings and homes, and technology for better monitoring of hazards and risk. The award aims to highlight these efforts through the Averted Disaster Award so that they can be shared, replicated, adapted, and scaled up in the places that need them. For more information and complete list of partner organisations, see our official website:

- The Averted Disaster Award
- https://averteddisasteraward.org
- Supported by the Understanding Risk Community, Global Facility for Disaster Reduction and Recovery (GFDRR), The World Bank Group, Earth Observatory of Singapore, Anticipation Hub

Bibliography

ADB, . *River Basin Management Planning in Indonesia: Policy and Practice*. Asian Development Bank, 2016. ISBN 978-92-9257-388-1. OCLC: 957700275.

Agresti, Alan. *Categorical data analysis*, volume 482. John Wiley & Sons, 2003.

Aljawhari, Karim; Gentile, Roberto; Freddi, Fabio, and Galasso, Carmine. Effects of ground-motion sequences on fragility and vulnerability of case-study reinforced concrete frames. *Bulletin of Earthquake Engineering*, 19(15):6329–6359, 2021.

Amaya-Gómez, Rafael; Sánchez-Silva, Mauricio; Bastidas-Arteaga, Emilio; Schoefs, Franck, and Munoz, Felipe. Reliability assessments of corroded pipelines based on internal pressure–a review. *Engineering Failure Analysis*, 98:190–214, 2019.

Amoako, Clifford and Frimpong Boamah, Emmanuel. Build as you earn and learn: informal urbanism and incremental housing financing in Kumasi, Ghana. *Journal of Housing and the Built Environment*, 32(3):429–448, 2017.

Anggorowati, A and Harijoko, A. Distribusi area, volume, serta karakteristikmineralogi dan geokimia endapan tefra jatuhan dari erupsi Gunung Keludtahun 2014. In *Seminar Nasional Kebumian KE-8: Academia-Industry Linkage*, page 778–789. 2015. URL `https://repository.ugm.ac.id/135520/`.

Armienti, Pietro; Macedonio, G, and Pareschi, MT. A numerical model for simulation of tephra transport and deposition: Applications to may 18, 1980, mount st. helens eruption. *Journal of Geophysical Research: Solid Earth*, 93(B6):6463–6476, 1988.

Armstrong, J Scott and Fildes, Robert. Correspondence on the selection of error measures for comparisons among forecasting methods. *Journal of Forecasting*, 14 (1):67–71, 1995.

Arnalds, Olafur; Thorarinsdottir, Elin Fjola; Thorsson, Johann; Waldhauserova, Pavla Dagsson, and Agustsdottir, Anna Maria. An extreme wind erosion event of the fresh Eyjafjallajökull 2010 volcanic ash. *Scientific reports*, 3(1):1–7, 2013.

Aspinall, Willy and Woo, Gordon. Counterfactual analysis of runaway volcanic explosions. *Frontiers in Earth Science*, 7:222, 2019.

Ayris, Paul Martin and Delmelle, Pierre. The immediate environmental effects of tephra emission. *Bulletin of volcanology*, 74(9):1905–1936, 2012.

Bastidas-Arteaga, Emilio and Stewart, Mark G. Damage risks and economic assessment of climate adaptation strategies for design of new concrete structures subject to chloride-induced corrosion. *Structural Safety*, 52:40–53, 2015.

Bastidas-Arteaga, Emilio and Stewart, Mark G. Economic assessment of climate adaptation strategies for existing reinforced concrete structures subjected to chloride-induced corrosion. *Structure and Infrastructure Engineering*, 12(4):432–449, 2016.

Bavaud, Francois. Models for spatial weights: a systematic look. *Geographical analysis*, 30(2):153–171, 1998.

Bear-Crozier, Adele; Pouget, Solène; Bursik, Marcus; Jansons, Emile; Denman, Jarrad; Tupper, Andrew, and Rustowicz, Rose. Automated detection and measurement of volcanic cloud growth: towards a robust estimate of mass flux, mass loading and eruption duration. *Natural Hazards*, 101(1):1–38, 2020.

Bedford, Tim; Cooke, Roger, and others, . *Probabilistic risk analysis: foundations and methods*. Cambridge University Press, 2001.

Biass, S; Todde, A; Cioni, R; Pistolesi, M; Geshi, N, and Bonadonna, Costanza. Potential impacts of tephra fallout from a large-scale explosive eruption at Sakurajima volcano, Japan. *Bulletin of Volcanology*, 79(10):1–24, 2017.

Biegler, Lorenz; Biros, George; Ghattas, Omar; Heinkenschloss, Matthias; Keyes, David; Mallick, Bani; Marzouk, Youssef; Tenorio, Luis; van Bloemen Waanders, Bart, and Willcox, Karen. Large-scale inverse problems and quantification of uncertainty. 2011.

Birkland, Thomas A. *Lessons of disaster: Policy change after catastrophic events*. Georgetown University Press, 2006.

Blix, Ines; Kanten, Alf Børre; Birkeland, Marianne Skogbrott; Solberg, Øivind; Nissen, Alexander, and Heir, Trond. Thinking about what might have happened:

Counterfactual thinking and post-traumatic stress in individuals directly and indirectly exposed to the 2011 Oslo bombing. *Applied cognitive psychology*, 30 (6):983–991, 2016. ISSN 0888-4080. doi: 10.1002/acp.3289. Publisher: Wiley Subscription Services, Inc.

Blond, N; Bel, Liliane, and Vautard, Robert. Three-dimensional ozone data analysis with an air quality model over the paris area. *Journal of Geophysical Research: Atmospheres*, 108(D23), 2003.

Blong, Russell; Enright, Neal, and Grasso, Paul. Preservation of thin tephra. *Journal of Applied Volcanology*, 6(1):10, 2017.

Bonadonna, Costanza and Costa, Antonio. Modeling of tephra sedimentation from volcanic plumes. *Modeling volcanic processes: The physics and mathematics of volcanism*, pages 173–202, 2013.

Bonadonna, Costanza; Connor, Charles B; Houghton, BF; Connor, Laura; Byrne, M; Laing, A, and Hincks, TK. Probabilistic modeling of tephra dispersal: Hazard assessment of a multiphase rhyolitic eruption at Tarawera, New Zealand. *Journal of Geophysical Research: Solid Earth*, 110(B3), 2005.

Bonadonna, Costanza; Biass, Sébastien, and Costa, Antonio. Physical characterization of explosive volcanic eruptions based on tephra deposits: propagation of uncertainties and sensitivity analysis. *Journal of Volcanology and Geothermal Research*, 296:80–100, 2015.

Cabaneros, Sheen Mclean and Hughes, Ben. Methods used for handling and quantifying model uncertainty of artificial neural network models for air pollution forecasting. *Environmental Modelling & Software*, page 105529, 2022.

Calderón, Alejandro and Silva, Vitor. Exposure forecasting for seismic risk estimation: Application to Costa Rica. *Earthquake Spectra*, 37(3):1806–1826, 2021.

Carey, Steven and Sparks, RSJ. Quantitative models of the fallout and dispersal of tephra from volcanic eruption columns. *Bulletin of volcanology*, 48(2):109–125, 1986.

Caudron, Corentin; Taisne, Benoît; Garcés, Milton; Alexis, Le Pichon, and Mialle, Pierrick. On the use of remote infrasound and seismic stations to constrain the eruptive sequence and intensity for the 2014 Kelud eruption. *Geophysical Research Letters*, 42(16):6614–6621, 2015. doi: https://doi.org/10.1002/2015GL064885. URL `https://agupubs.onlinelibrary.wiley.com/doi/abs/10.1002/2015GL064885`.

CEHRDC, . Comprehensive School Safety Minimum Package: Volume 1 – Report. Sano Thimi, Bhaktapur, Nepal: Centre For Education and Human Resource Development. 2018. Accessed 2021-12-20. https://www.preventionweb.net/publication/nepal-comprehensive-school-safety-minimum-package.

Chaulagain, Hemchandra; Rodrigues, Hugo; Silva, Vitor; Spacone, Enrico, and Varum, Humberto. Seismic risk assessment and hazard mapping in Nepal. *Natural Hazards*, 78(1):583–602, 2015.

Chen, Chao; Twycross, Jamie, and Garibaldi, Jonathan M. A new accuracy measure based on bounded relative error for time series forecasting. *PloS one*, 12(3):e0174202, 2017.

Chen, Meng and Wei, Shengji. The 2015 Gorkha, Nepal, earthquake sequence: II. broadband simulation of ground motion in Kathmandu. *Bulletin of the Seismological Society of America*, 109(2):672–687, 2019.

Chiou, Brian S-J and Youngs, Robert R. Update of the Chiou and Youngs NGA model for the average horizontal component of peak ground motion and response spectra. *Earthquake Spectra*, 30(3):1117–1153, 2014.

Clarke, K C; Hoppen, S, and Gaydos, L. A self-modifying cellular automaton model of historical urbanization in the san francisco bay area. (24):247–261, 1997.

Connor, Charles B; Connor, Laura J; Bonadonna, Costanza; Luhr, J; Savov, I, and Navarro-Ochoa, C. Modelling tephra thickness and particle size distribution of the 1913 eruption of Volcán de Colima, Mexico. In *Volcán de Colima*, pages 81–110. Springer, 2019.

Connor, L. J. and Connor, C. B. Inversion is the key to dispersion: understanding eruption dynamics by inverting tephra fallout. In *Statistics in Volcanology*. Geological Society of London, 01 2006. ISBN 9781862392083.

Connor, Laura; Connor, Chuck, and Saballos, Armando. Tephra2 users manual. *University of South Florida, Tampa, FL, accessed Sept*, 24:2017, 2011.

Constantinescu, Robert; Hopulele-Gligor, Aurelian; Connor, Charles B; Bonadonna, Costanza; Connor, Laura J; Lindsay, Jan M; Charbonnier, Sylvain, and Volentik, Alain CM. The radius of the umbrella cloud helps characterize large explosive volcanic eruptions. *Communications Earth & Environment*, 2(1):1–8, 2021.

Costa, Antonio; Folch, A; Macedonio, G; Giaccio, B; Isaia, R, and Smith, VC. Quantifying volcanic ash dispersal and impact of the campanian ignimbrite super-eruption. *Geophysical Research Letters*, 39(10), 2012.

Cremen, Gemma; Galasso, Carmine, and McCloskey, John. Modelling and quantifying tomorrow's risks from natural hazards. *Science of the Total Environment*, page 152552, 2021.

Cremen, Gemma; Galasso, Carmine, and McCloskey, John. A simulation-based framework for earthquake risk-informed and people-centered decision making on future urban planning. *Earth's Future*, 10(1):e2021EF002388, 2022.

Cronie, Ottmar and Van Lieshout, Maria Nicolette Margaretha. A non-model-based approach to bandwidth selection for kernel estimators of spatial intensity functions. *Biometrika*, 105(2):455–462, 2018.

Dee, Dick P; Uppala, S M; Simmons, Adrian J; Berrisford, Paul; Poli, Paul; Kobayashi, Shinya; Andrae, U; Balmaseda, MA; Balsamo, G; Bauer, d P, and others, . The era-interim reanalysis: Configuration and performance of the data assimilation system. *Quarterly Journal of the royal meteorological society*, 137(656):553–597, 2011.

Deierlein, Gregory G. Overview of a comprehensive framework for earthquake performance assessment. In *Performance-Based Seismic Design Concepts and Implementation, Proceedings of an International Workshop*, pages 15–26, 2004.

Deierlein, Gregory G and Zsarnóczay, Adam. State of the art in computational simulation for natural hazards engineering. 2021.

Denby, Bruce; Schaap, Martijn; Segers, Arjo; Builtjes, Peter, and Horálek, Jan. Comparison of two data assimilation methods for assessing pm10 exceedances on the european scale. *Atmospheric Environment*, 42(30):7122–7134, 2008.

Diggle, Peter J. and Jr, Paulo J. Ribeiro. *Model Based Geostatistics*. Springer, New York, 2007.

Dixit, Amod Mani; Yatabe, Ryuichi; Dahal, Ranjan Kumar, and Bhandary, Netra Prakash. Public school earthquake safety program in Nepal. *Geomatics, Natural Hazards and Risk*, 5(4):293–319, 2014.

Dixit, Amod Mani; Ringler, Adam T; Sumy, Danielle F; Cochran, Elizabeth S; Hough, Susan E; Martin, Stacey S; Gibbons, Steven; Luetgert, James H; Galetzka, John; Shrestha, Surya Narayan, and others, . Strong-motion observations of the M 7.8

Gorkha, Nepal, earthquake sequence and development of the N-SHAKE strong-motion network. *Seismological Research Letters*, 86(6):1533–1539, 2015.

Dominguez, Lucia; Bonadonna, Costanza; Forte, Pablo; Jarvis, Paul Antony; Cioni, Raffaello; Mingari, Leonardo; Bran, Donaldo, and Panebianco, Juan Esteban. Aeolian remobilisation of the 2011-Cordón Caulle Tephra-Fallout Deposit: example of an important process in the life cycle of Volcanic Ash. *Frontiers in Earth Science*, 7:343, 2020.

Dong, You and Frangopol, Dan M. Adaptation optimization of residential buildings under hurricane threat considering climate change in a lifecycle context. *Journal of Performance of Constructed Facilities*, 31(6):04017099, 2017.

El Hassan, Jinane; Bressolette, Philippe; Chateauneuf, Alaa, and El Tawil, Khaled. Reliability-based assessment of the effect of climatic conditions on the corrosion of rc structures subject to chloride ingress. *Engineering Structures*, 32(10):3279–3287, 2010.

Ellingwood, Bruce R; Cutler, Harvey; Gardoni, Paolo; Peacock, Walter Gillis; van de Lindt, John W, and Wang, Naiyu. The centerville virtual community: A fully integrated decision model of interacting physical and social infrastructure systems. *Sustainable and Resilient Infrastructure*, 1(3-4):95–107, 2016.

Engle, Robert F. On the limitations of comaring mean square forecast errors: Comment. *Journal of Forecasting*, 12(8):642–644, 1993.

Engwell, SL; Sparks, RSJ, and Aspinall, WP. Quantifying uncertainties in the measurement of tephra fall thickness. *Journal of Applied Volcanology*, 2(1):1–12, 2013.

Engwell, SL; Aspinall, WP, and Sparks, RSJ. An objective method for the production of isopach maps and implications for the estimation of tephra deposit volumes and their uncertainties. *Bulletin of volcanology*, 77(7):1–18, 2015.

Federal Emergency Management Agency, . 2.1 earthquake model technical manual. *Federal Emergency Management Agency, Washington, DC*, 2015.

Ferguson, Bruce and Smets, Peer. Finance for incremental housing; current status and prospects for expansion. *Habitat International*, 34(3):288–298, 2010.

Folch, Arnau; Costa, Antonio, and Macedonio, Giovanni. Fall3d: A computational model for transport and deposition of volcanic ash. *Computers & Geosciences*, 35 (6):1334–1342, 2009.

Fontijn, Karen; Williamson, David; Mbede, Evelyne, and Ernst, Gerald GJ. The Rungwe volcanic province, Tanzania–a volcanological review. *Journal of African Earth Sciences*, 63:12–31, 2012.

Gaillard, Jean-Christophe. Disaster studies inside out. *Disasters*, 43:S7–S17, 2019.

Galasso, Carmine; McCloskey, John; Pelling, Mark; Hope, Max; Bean, Chris; Cremen, Gemma; Guragain, Ramesh; Hancilar, Ufuk; Menoscal, Jonathan; Mwelu, Keziah, and others, . Risk-based, pro-poor urban design and planning for tomorrow's cities. 2021.

Gallovič, František. Modeling velocity recordings of the M w 6.0 South Napa, California, earthquake: Unilateral event with weak high-frequency directivity. *Seismological Research Letters*, 87(1):2–14, 2016.

Gentile, Roberto and Galasso, Carmine. Hysteretic energy-based state-dependent fragility for ground-motion sequences. *Earthquake Engineering & Structural Dynamics*, 50(4):1187–1203, 2021.

Georgoudas, Ioakeim G; Sirakoulis, G Ch; Scordilis, Emmanuel M, and Andreadis, Ioannis. A cellular automaton simulation tool for modelling seismicity in the region of Xanthi. *Environmental Modelling & Software*, 22(10):1455–1464, 2007.

Giordano, Nicola; De Luca, Flavia; Sextos, Anastasios; Ramirez Cortes, Fernando; Fonseca Ferreira, Carina, and Wu, Jingzhe. Empirical seismic fragility models for Nepalese school buildings. *Natural Hazards*, 105(1):339–362, 2021a.

Giordano, Nicola; Norris, Alastair; Manandhar, Vibek; Shrestha, Liva; Paudel, Dev R; Quinn, Natalie; Rees, Elizabeth; Shrestha, Hima; Marasini, Narayan P; Prajapati, Rajani, and others, . Financial assessment of incremental seismic retrofitting of nepali stone-masonry buildings. *International Journal of Disaster Risk Reduction*, 60:102297, 2021b.

Global Volcanism Program, . Report on Kelut (Indonesia). *Bulletin of the Global Volcanism Network*, 39(2), 2014. doi: https://doi.org/10.5479/si.GVP.BGVN201402-263280.

Gómez-Romero, Mariela; Lindig-Cisneros, Roberto, and Galindo-Vallejo, Sebastiana. Effect of tephra depth on vegetation development in areas affected by volcanism. *Plant Ecology*, 183(2):207–213, 2006.

Goode, Louise R; Handley, Heather K; Cronin, Shane J, and Abdurrachman, Mirzam. Insights into eruption dynamics from the 2014 pyroclastic deposits of Kelut volcano, Java, Indonesia, and implications for future hazards. *Journal of Volcanology and Geothermal Research*, 382:6–23, 2019.

Government of Nepal, . School sector reform plan 2009-2015. 2009. Accessed 2022-03-28. https://www.moe.gov.np/assets/uploads/files/SSRP_English.pdf.

Grillakis, Manolis G; Koutroulis, Aristeidis G, and Tsanis, Ioannis K. Multisegment statistical bias correction of daily GCM precipitation output. *Journal of Geophysical Research: Atmospheres*, 118(8):3150–3162, 2013.

Guo, Shuaicheng; Si, Ruizhe; Dai, Qingli; You, Zhanping; Ma, Yunxiang, and Wang, Jiaqing. A critical review of corrosion development and rust removal techniques on the structural/environmental performance of corroded steel bridges. *Journal of cleaner production*, 233:126–146, 2019.

Gupta, Satyendra P. *Report on eastern Nepal earthquake 21 August 1988: Damages and recommendations for repairs and reconstruction*. Asian Disaster Preparedness Center, Asian Institute of Technology, 1988.

Haer, Toon; Husby, Trond G; Botzen, WJ Wouter, and Aerts, Jeroen CJH. The safe development paradox: An agent-based model for flood risk under climate change in the European Union. *Global Environmental Change*, 60:102009, 2020.

Hargie, Kirstin A.; Van Eaton, Alexa R.; Mastin, Larry G.; Holzworth, Robert H.; Ewert, John W., and Pavolonis, Michael. Globally detected volcanic lightning and umbrella dynamics during the 2014 eruption of Kelud, Indonesia. *Journal of Volcanology and Geothermal Research*, 382:81–91, 2019. ISSN 0377-0273. doi: https://doi.org/10.1016/j.jvolgeores.2018.10.016. URL `https://www.sciencedirect.com/science/article/pii/S0377027318304591`. Lessons learned from the recent eruptions of Sinabung and Kelud Volcanoes, Indonesia.

Hayes, Josh L.; Calderón B, Rodrigo; Deligne, Natalia I.; Jenkins, Susanna F.; Leonard, Graham S.; McSporran, Ame M.; Williams, George T., and Wilson, Thomas M. Timber-framed building damage from tephra fall and lahar: 2015 Calbuco eruption, Chile. *Journal of Volcanology and Geothermal Research*, 374:142–159, 2019. ISSN 0377-0273. doi: https://doi.org/10.1016/j.jvolgeores.2019.02.017. URL `https://www.sciencedirect.com/science/article/pii/S0377027318303718`.

Hayes, Shannon K; Montgomery, David R, and Newhall, Christopher G. Fluvial sediment transport and deposition following the 1991 eruption of mount pinatubo. *Geomorphology*, 45(3-4):211–224, 2002.

Hemmati, Mona; Ellingwood, Bruce R, and Mahmoud, Hussam N. The role of urban growth in resilience of communities under flood risk. *Earth's future*, 8(3): e2019EF001382, 2020.

Hemmati, Mona; Mahmoud, Hussam N; Ellingwood, Bruce R, and Crooks, Andrew T. Shaping urbanization to achieve communities resilient to floods. *Environmental Research Letters*, 16(9):094033, 2021.

Hodson, Timothy O. Root mean square error (RMSE) or mean absolute error (MAE): when to use them or not. *Geoscientific Model Development Discussions*, pages 1–10, 2022.

Hollós, R; Fodor, N; Merganičová, K; Hidy, D; Árendás, T; Grünwald, T, and Barcza, Z. Conditional interval reduction method: A possible new direction for the optimization of process based models. *Environmental Modelling & Software*, 158:105556, 2022.

Horalek, Jan; Kurfurst, Pavel; Denby, P; de Smet, Peter; de Leeuw, Frank; Brabec, Marek, and Fiala, Jaroslav. Interpolation and assimilation methods for european scale air quality assessment and mapping. *Part II: Development and testing new methodologies, ETCACC Technical paper*, 8:2005, 2005.

Horálek, Jan; Denby, Bruce; de Smet, Peter; de Leeuw, FAAM; Kurfürst, Pavel; Swart, RJ, and van Noije, Twan. Spatial mapping of air quality for european scale assessment. Technical report, ETCACC, 2006.

Hurst, AW and Turner, Richard. Performance of the program ASHFALL for forecasting ashfall during the 1995 and 1996 eruptions of Ruapehu volcano. *New Zealand Journal of Geology and Geophysics*, 42(4):615–622, 1999.

Hyndman, Rob J and Koehler, Anne B. Another look at measures of forecast accuracy. *International journal of forecasting*, 22(4):679–688, 2006.

IFRC, . Emergency plan of action (EPoA) Indonesia Volcanic eruption-Mt Kelud. In *Situation Report by the International Federation of Red Cross And Red Crescent Societies*. 2014. URL `https://reliefweb.int/report/indonesia/indonesia-volcanic-eruption-mt-kelud-emergency-plan-action-epoa-operation-n`.

IPCC, . *Climate Change 2022: Impacts, Adaptation and Vulnerability*. Summary for Policymakers. Cambridge University Press, Cambridge, UK and New York, USA, 2022. ISBN 9781009325844.

Isaac, Tobin; Petra, Noemi; Stadler, Georg, and Ghattas, Omar. Scalable and efficient algorithms for the propagation of uncertainty from data through inference to prediction for large-scale problems, with application to flow of the antarctic ice sheet. *Journal of Computational Physics*, 296:348–368, 2015. ISSN 0021-9991. doi: https://doi.org/10.1016/j.jcp.2015.04.047. URL `https://www.sciencedirect.com/science/article/pii/S0021999115003046`.

Jaiswal, KS; Wald, David J; Earle, Paul S; Porter, Keith A, and Hearne, Mike. Earthquake casualty models within the USGS Prompt Assessment of Global Earthquakes for Response (PAGER) system. In *Human casualties in earthquakes*, pages 83–94. Springer, 2011.

Jaiswal, KS; Aspinall, W; Perkins, D; Wald, D, and Porter, KA. Use of expert judgment elicitation to estimate seismic vulnerability of selected building types. In *Proc. 15th World Conference on Earthquake Engineering, Lisbon, Portugal, 24-28 Sep 2012*, 2012.

Johnston, Kevin; Ver Hoef, Jay M; Krivoruchko, Konstantin, and Lucas, Neil. *Using ArcGIS geostatistical analyst*, volume 380. Esri Redlands, 2001.

Kashani, Mohammad M; Maddocks, Jake, and Dizaj, Ebrahim Afsar. Residual capacity of corroded reinforced concrete bridge components: State-of-the-art review. *Journal of Bridge Engineering*, 24(7):03119001, 2019.

Kassteele, J van de; Koelemeijer, RBA; Dekkers, ALM; Schaap, M; Homan, CD, and Stein, A. Statistical mapping of pm10 concentrations over western europe using secondary information from dispersion modeling and modis satellite observations. *Stochastic environmental research and risk assessment*, 21:183–194, 2006.

Kendra, James and Nigg, Joanne. Engineering and the social sciences: Historical evolution of interdisciplinary approaches to hazard and disaster. *Engineering Studies*, 6(3):134–158, 2014.

Kim, Sungil and Kim, Heeyoung. A new metric of absolute percentage error for intermittent demand forecasts. *International Journal of Forecasting*, 32(3):669–679, 2016.

Koketsu, Kazuki; Miyake, Hiroe; Guo, Yujia; Kobayashi, Hiroaki; Masuda, Tetsu; Davuluri, Srinagesh; Bhattarai, Mukunda; Adhikari, Lok Bijaya, and Sapkota, Soma Nath. Widespread ground motion distribution caused by rupture directivity during the 2015 Gorkha, Nepal earthquake. *Scientific reports*, 6(1):1–9, 2016.

Krawinkler, Helmut and Miranda, Eduardo. Performance-based earthquake engineering, 2004.

Kristiansen, Nina Iren; Prata, AJ; Stohl, Andreas, and Carn, Simon A. Stratospheric volcanic ash emissions from the 13 February 2014 Kelut eruption. *Geophysical Research Letters*, 42(2):588–596, 2015.

Lallemant, David. *Modeling the future disaster risk of cities to envision paths towards their future resilience*. Stanford University, 2015.

Lallemant, David; Kiremidjian, Anne, and Burton, Henry. Statistical procedures for developing earthquake damage fragility curves. *Earthquake Engineering & Structural Dynamics*, 44(9):1373–1389, 2015.

Lallemant, David; Burton, Henry; Ceferino, Luis; Bullock, Zach, and Kiremidjian, Anne. A framework and case study for earthquake vulnerability assessment of incrementally expanding buildings. *Earthquake Spectra*, 33(4):1369–1384, 2017.

Lallemant, David; Loos, Sabine; McCaughey, Jamie W; Budhathoki, Nama, and Khan, Feroz. Informatics for equitable recovery: Supporting equitable disaster recovery through mapping and integration of social vulnerability into post-disaster impact assessments. Technical report, 2020.

Lallemant, David; Hamel, Perrine; Balbi, Mariano; Lim, Tian Ning; Schmitt, Rafael, and Win, Shelly. Nature-based solutions for flood risk reduction: A probabilistic modeling framework. *One Earth*, 4(9):1310–1321, 2021.

Le Pennec, Jean-Luc; Ruiz, Gorki A; Ramón, Patricio; Palacios, Enrique; Mothes, Patricia, and Yepes, Hugo. Impact of tephra falls on Andean communities: The influences of eruption size and weather conditions during the 1999–2001 activity of Tungurahua volcano, Ecuador. *Journal of Volcanology and Geothermal Research*, 217:91–103, 2012.

Leach, Melissa; Rockström, Johan; Raskin, Paul; Scoones, Ian; Stirling, Andy C; Smith, Adrian; Thompson, John; Millstone, Erik; Ely, Adrian; Arond, Elisa, and others, . Transforming innovation for sustainability. *Ecology and Society*, 17(2), 2012.

Li, Yue and Stewart, Mark G. Cyclone damage risks caused by enhanced greenhouse conditions and economic viability of strengthened residential construction. *Natural Hazards Review*, 12(1):9–18, 2011.

Li, Zhouyayan; Duque, Felipe Quintero; Grout, Trevor; Bates, Bradford, and Demir, Ibrahim. Comparative analysis of performance and mechanisms of flood inundation map generation using height above nearest drainage. 2022.

Liel, Abbie B. *Assessing the collapse risk of California's existing reinforced concrete frame structures: Metrics for seismic safety decisions*. Stanford University, 2008.

Liel, Abbie B and Deierlein, Gregory G. Using collapse risk assessments to inform seismic safety policy for older concrete buildings. *Earthquake spectra*, 28(4):1495–1521, 2012.

Liel, Abbie B; Haselton, Curt B, and Deierlein, Gregory G. The effectiveness of seismic building code provisions on reducing the collapse risk of reinforced concrete moment frame buildings. 2006.

Liel, Abbie B; Haselton, Curt B; Deierlein, Gregory G, and Baker, Jack W. Incorporating modeling uncertainties in the assessment of seismic collapse risk of buildings. *Structural safety*, 31(2):197–211, 2009.

Lin, Yolanda C; Jenkins, Susanna F; Chow, Jun Rui; Biass, Sebastien; Woo, Gordon, and Lallemant, David. Modeling downward counterfactual events: Unrealized disasters and why they matter. *Frontiers in Earth Science*, page 443, 2020.

Loader, Catherine. Smoothing: local regression techniques. In *Handbook of computational statistics*, pages 571–596. Springer, 2012.

Loos, Sabine; Lallemant, David; Baker, Jack; McCaughey, Jamie; Yun, Sang-Ho; Budhathoki, Nama; Khan, Feroz, and Singh, Ritika. G-dif: A geospatial data integration framework to rapidly estimate post-earthquake damage. *Earthquake Spectra*, 36(4):1695–1718, 2020.

Madankan, Reza; Pouget, S; Singla, Puneet; Bursik, Marcus; Dehn, Jon; Jones, M; Patra, A; Pavolonis, Michael; Pitman, E Bruce; Singh, Tarunraj, and others, . Computation of probabilistic hazard maps and source parameter estimation for volcanic ash transport and dispersion. *Journal of Computational Physics*, 271:39–59, 2014.

Maeno, Fukashi; Nakada, Setsuya; Yoshimoto, Mitsuhiro; Shimano, Taketo; Hokanishi, Natsumi; Zaennudin, Akhmad, and Iguchi, Masato. A sequence of a plinian eruption preceded by dome destruction at kelud volcano, indonesia, on february 13, 2014, revealed from tephra fallout and pyroclastic density current deposits. *Journal of Volcanology and Geothermal Research*, 382:24 – 41, 2019. ISSN 0377-0273. doi: https://doi.org/10.1016/j.jvolgeores.2017.03.002. URL `http://www.sciencedirect.com/science/article/pii/S0377027317301385`. Lessons learned from the recent eruptions of Sinabung and Kelud Volcanoes, Indonesia.

Magill, Christina; Wilson, Thomas, and Okada, Tetsuya. Observations of tephra fall impacts from the 2011 Shinmoedake eruption, Japan. *Earth, Planets and Space*, 65 (6):677–698, 2013.

Makridakis, Spyros. Accuracy measures: theoretical and practical concerns. *International journal of forecasting*, 9(4):527–529, 1993.

Mannen, Kazutaka. Particle segregation of an eruption plume as revealed by a comprehensive analysis of tephra dispersal: theory and application. *Journal of volcanology and geothermal research*, 284:61–78, 2014.

Marasini, N. NSET Experiences on Safer Schools Initiative. In *Asian Conference on Disaster Reduction, Ankara, Republic of Turkey*. ACM, November 2019. Accessed 20 Nov 2021. https://bit.ly/32P4pjC.

Marasini, N.P.; Shrestha, S.N.; Guragain, R.; Shrestha, H.; Prajapati, R, and Khatiwada, P. Enhancing earthquake safety of schools: Lessons learned from Nepal. In *Proceedings of the 17th World Conference on Earthquake Engineering*, pages Article No. 3g–0023, Sendai, Japan, September 2020.

Markhvida, Maryia; Walsh, Brian; Hallegatte, Stephane, and Baker, Jack. Quantification of disaster impacts through household well-being losses. *Nature Sustainability*, 3(7):538–547, July 2020. ISSN 2398-9629. doi: 10.1038/s41893-020-0508-7. Number: 7 Publisher: Nature Publishing Group.

Mastin, Larry G; Guffanti, M; Servranckx, R; Webley, P; Barsotti, S; Dean, K; Durant, A; Ewert, John W; Neri, A; Rose, William I, and others, . A multidisciplinary effort to assign realistic source parameters to models of volcanic ash-cloud transport and dispersion during eruptions. *Journal of Volcanology and Geothermal Research*, 186 (1-2):10–21, 2009.

McGranahan, Gordon; Balk, Deborah, and Anderson, Bridget. The rising tide: assessing the risks of climate change and human settlements in low elevation coastal zones. *Environment and urbanization*, 19(1):17–37, 2007.

Medvec, Victoria Husted; Madey, Scott F., and Gilovich, Thomas. When less is more: Counterfactual thinking and satisfaction among Olympic medalists. *Journal of Personality and Social Psychology*, 69(4), 1995. ISSN 1939-1315(Electronic),0022-3514(Print). doi: 10.1037/0022-3514.69.4.603.

Mesta, Carlos; Cremen, Gemma, and Galasso, Carmine. Urban growth modelling and social vulnerability assessment for a hazardous Kathmandu Valley. *Scientific reports*, 12(1):1–16, 2022.

Mileti, Dennis. *Disasters by design: A reassessment of natural hazards in the United States*. Joseph Henry Press, 1999.

Moehle, Jack and Deierlein, Gregory G. A framework methodology for performance-based earthquake engineering. In *13th world conference on earthquake engineering*, volume 679, 2004.

Moore, Harry Estil. Tornadoes over Texas: A study of Waco and San Angelo in disaster. 1958.

Morley, Steven Karl; Brito, Thiago Vasconcelos, and Welling, Daniel T. Measures of model performance based on the log accuracy ratio. *Space Weather*, 16(1):69–88, 2018.

Newhall, Christopher G and Self, Stephen. The volcanic explosivity index (VEI) an estimate of explosive magnitude for historical volcanism. *Journal of Geophysical Research: Oceans*, 87(C2):1231–1238, 1982.

Newman, Jeffrey Peter; Maier, Holger Robert; Riddell, Graeme Angus; Zecchin, Aaron Carlo; Daniell, James Edward; Schaefer, Andreas Maximilian; van Delden, Hedwig; Khazai, Bijan; O'Flaherty, Michael John, and Newland, Charles Peter. Review of literature on decision support systems for natural hazard risk reduction: Current status and future research directions. *Environmental Modelling & Software*, 96:378–409, 2017.

Njus, Elliot. Portland naacp joins fight over city's earthquake warning placards, linking them to legacy of white supremacy. *The Oregonian*, Jan 2019. URL `https://www.oregonlive.com/business/2019/01/portland-naacp-joins-`

fight-over-citys-earthquake-warning-placards-linking-them-to-legacy-of-white-supremacy.html.

Noh, Hae Young; Lallemant, David, and Kiremidjian, Anne S. Development of empirical and analytical fragility functions using kernel smoothing methods. *Earthquake Engineering & Structural Dynamics*, 44(8):1163–1180, 2015.

NSET, . Seismic vulnerability of the public-school buildings of Kathmandu Valley and methods for reducing it. Technical report, 2000. https://nset.org.np/nset2012/images/publicationfile/20130724114208.pdf.

Oden, Tinsley; Moser, Robert, and Ghattas, Omar. Computer predictions with quantified uncertainty, part i. *SIAM News*, 43(9):1–3, 2010.

Oishi, Masayuki; Nishiki, Kuniaki; Geshi, Nobuo; Furukawa, Ryuta; Ishizuka, Yoshihiro; Oikawa, Teruki; Yamamoto, Takahiro; Nanayama, Futoshi; Tanaka, Akiko; Hirota, Akinari, and others, . Distribution and mass of tephra-fall deposits from volcanic eruptions of Sakurajima Volcano based on posteruption surveys. *Bulletin of Volcanology*, 80(4):1–16, 2018.

Olson, Richard S; Emel Ganapati, N; Gawronski, Vincent T; Olson, Robert A; Salna, Erik, and Pablo Sarmiento, Juan. From disaster risk reduction to policy studies: Bridging research communities. *Natural hazards review*, 21(2):04020014, 2020.

OpenDRI, . Understanding Nepal's Risks" Open Data for Resilience Initiative Project. Technical report, Open Data for Resilience Initiative Project, 2012. https://opendri.org/project/nepal/.

Osores, Soledad; Ruiz, Juan; Folch, Arnau, and Collini, Estela. Volcanic ash forecast using ensemble-based data assimilation: an ensemble transform kalman filter coupled with the fall3d-7.2 model (etkf–fall3d version 1.0). *Geoscientific Model Development*, 13(1):1–22, 2020.

Oughton, Edward J; Ralph, Daniel; Pant, Raghav; Leverett, Eireann; Copic, Jennifer; Thacker, Scott; Dada, Rabia; Ruffle, Simon; Tuveson, Michelle, and Hall, Jim W. Stochastic counterfactual risk analysis for the vulnerability assessment of cyber-physical attacks on electricity distribution infrastructure networks. *Risk Analysis*, 39(9):2012–2031, 2019.

Papadopoulos, Athanasios N; Bazzurro, Paolo, and Marzocchi, Warner. Exploring probabilistic seismic risk assessment accounting for seismicity clustering and damage accumulation: Part i. hazard analysis. *Earthquake Spectra*, 37(2):803–826, 2021.

Pardini, Federica; Corradini, Stefano; Costa, Antonio; Esposti Ongaro, Tomaso; Merucci, Luca; Neri, Augusto; Stelitano, Dario, and de'Michieli Vitturi, Mattia. Ensemble-based data assimilation of volcanic ash clouds from satellite observations: application to the 24 december 2018 mt. etna explosive eruption. *Atmosphere*, 11(4): 359, 2020.

Paté-Cornell, Elisabeth. Risk and uncertainty analysis in government safety decisions. *Risk analysis*, 22(3):633–646, 2002.

Peek, Lori and Guikema, Seth. Interdisciplinary theory, methods, and approaches for hazards and disaster research: An introduction to the special issue. *Risk Analysis*, 41 (7):1047–1058, 2021.

Peek, Lori; Tobin, Jennifer; Adams, Rachel M; Wu, Haorui, and Mathews, Mason Clay. A framework for convergence research in the hazards and disaster field: The natural hazards engineering research infrastructure converge facility. *Frontiers in Built Environment*, 6:110, 2020.

Pieri, David C and Baloga, Stephen M. Eruption rate, area, and length relationships for some Hawaiian lava flows. *Journal of volcanology and geothermal research*, 30(1-2): 29–45, 1986.

Pouget, Solène; Bursik, Marcus; Webley, Peter; Dehn, Jon, and Pavolonis, Michael. Estimation of eruption source parameters from umbrella cloud or downwind plume growth rate. *Journal of volcanology and geothermal research*, 258:100–112, 2013.

Pyle, David M. The thickness, volume and grainsize of tephra fall deposits. *Bulletin of Volcanology*, 51(1):1–15, 1989.

Pyle, D.M. Chapter 1 - field observations of tephra fallout deposits. In Mackie, Shona; Cashman, Katharine; Ricketts, Hugo; Rust, Alison, and Watson, Matt, editors, *Volcanic Ash*, pages 25–37. Elsevier, 2016. ISBN 978-0-08-100405-0. doi: https://doi.org/10.1016/B978-0-08-100405-0.00004-5. URL `https://www.sciencedirect.com/science/article/pii/B9780081004050000045`.

Qin, Hao and Stewart, Mark G. Risk-based cost-benefit analysis of climate adaptation measures for australian contemporary houses under extreme winds. *Journal of Infrastructure Preservation and Resilience*, 1(1):1–19, 2020.

R Core Team, . *R: A Language and Environment for Statistical Computing*. R Foundation for Statistical Computing, Vienna, Austria, 2020a. URL `https://www.R-project.org/`.

R Core Team, . *R: A Language and Environment for Statistical Computing*. R Foundation for Statistical Computing, Vienna, Austria, 2020b. URL https://www.R-project.org/.

Rabonza and Lallemant, ; Lin, Yolanda; Tadepalli, Sanjana; Wagenaar, Dennis; Michele, Nguyen; Choong, Jeanette; Liu, Celine J.N.; Sarica, Gizem Mestav; Widawati, Bernadeti Ausie Miranda; Balbi, Mariano; Khan, Feroz; Loos, Sabine, and Lim, Tian Ning. Shedding light on avoided disasters: Measuring the invisible benefits of disaster risk management using probabilistic counterfactual analysis. *Global Assessment Report on Disaster Risk Reduction 2022*, 2022. https://hdl.handle.net/10356/153502.

Raghunandan, Meera; Liel, Abbie B, and Luco, Nicolas. Aftershock collapse vulnerability assessment of reinforced concrete frame structures. *Earthquake Engineering & Structural Dynamics*, 44(3):419–439, 2015.

Rai, Durgesh C; Mondal, Goutam; Singhal, Vaibhav; Parool, Neha; Pradhan, Tripti, and Mitra, Keya. Reconnaissance report of the M6. 9 Sikkim (India–Nepal border) earthquake of 18 September 2011. *Geomatics, Natural Hazards and Risk*, 3(2):99–111, 2012.

Rajaure, S; Asimaki, Domniki; Thompson, Eric M; Hough, S; Martin, Stacey; Ampuero, JP; Dhital, MR; Inbal, A; Takai, N; Shigefuji, M, and others, . Characterizing the Kathmandu Valley sediment response through strong motion recordings of the 2015 Gorkha earthquake sequence. *Tectonophysics*, 714:146–157, 2017.

Ram, Thapa Dilli and Wang, Guoxin. Probabilistic seismic hazard analysis in Nepal. *Earthquake Engineering and Engineering Vibration*, 12(4):577–586, 2013.

Ramachandran, Kandethody M. and Tsokos, Chris P. Chapter 7 - goodness-of-fit tests applications. In Ramachandran, Kandethody M. and Tsokos, Chris P., editors, *Mathematical Statistics with Applications in R*, pages 371–408. Academic Press, Boston, 2nd edition, 2015. ISBN 978-0-12-417113-8. doi: https://doi.org/10.1016/B978-0-12-417113-8.00007-2. URL https://www.sciencedirect.com/science/article/pii/B9780124171138000072.

Rao, Anirudh S; Lepech, Michael D, and Kiremidjian, Anne. Development of time-dependent fragility functions for deteriorating reinforced concrete bridge piers. *Structure and Infrastructure Engineering*, 13(1):67–83, 2017.

Ribeiro Jr, Paulo J.; Diggle, Peter J.; Schlather, Martin; Bivand, Roger, and Ripley, Brian. *geoR: Analysis of Geostatistical Data*, 2020. URL `https://CRAN.R-project.org/package=geoR`. R package version 1.8-1.

Robson, David. The bias that can cause catastrophe. *BBC*, Oct 2019. URL `https://www.bbc.com/worklife/article/20191001-the-bias-behind-the-worlds-greatest-catastrophes`.

Roese, Neal J. Counterfactual thinking. *Psychological bulletin*, 121(1):133, 1997.

Roese, Neal J. and Olson, James M. *What Might Have Been: The Social Psychology of Counterfactual Thinking*. Psychology Press, New York, January 2014. ISBN 978-1-317-78047-2.

Sanchez-Rodriguez, Roberto; Seto, Karen C; Solecki, William D; Kraas, Frauke, and Laumann, Gregor. Science plan: urbanization and global environmental change. In *Science plan: urbanization and global environmental change*. 2005.

Sanderson, Dylan R; Cox, Daniel T; Amini, Mehrshad, and Barbosa, Andre R. Coupled urban change and natural hazard consequence model for community resilience planning. *Earth's Future*, page e2022EF003059, 2022.

Sarica, Gizem Mestav; Zhu, Tinger, and Pan, Tso-Chien. Spatio-temporal dynamics in seismic exposure of asian megacities: Past, present and future. *Environmental Research Letters*, 15(9):094092, 2020.

Scarpati, Claudio; Cole, Paul, and Perrotta, Annamaria. The Neapolitan Yellow Tuff—a large volume multiphase eruption from Campi Flegrei, southern Italy. *Bulletin of Volcanology*, 55(5):343–356, 1993.

Scollo, S; Folch, A, and Costa, A. A parametric and comparative study of different tephra fallout models. *Journal of Volcanology and Geothermal Research*, 176(2): 199–211, 2008.

Scott, David W. Multivariate density estimation: Theory, practice and visualisation. john willey and sons. *Inc., New York*, 1992.

Scott, James C. *Seeing like a state: How certain schemes to improve the human condition have failed*. Yale University Press, 1998.

Sevieri, Giacomo and Galasso, Carmine. Typhoon risk and climate-change impact assessment for cultural heritage asset roofs. *Structural Safety*, 91:102065, 2021.

Shao, Jun. Linear model selection by cross-validation. *Journal of the American statistical Association*, 88(422):486–494, 1993.

Shepherd, Theodore G; Boyd, Emily; Calel, Raphael A; Chapman, Sandra C; Dessai, Suraje; Dima-West, Ioana M; Fowler, Hayley J; James, Rachel; Maraun, Douglas; Martius, Olivia, and others, . Storylines: an alternative approach to representing uncertainty in physical aspects of climate change. *Climatic change*, 151(3-4):555–571, 2018.

Silva, Vitor. Critical issues in earthquake scenario loss modeling. *Journal of Earthquake Engineering*, 20(8):1322–1341, 2016.

Silva, Vitor; Crowley, Helen; Pagani, Marco; Monelli, Damiano, and Pinho, Rui. Development of the OpenQuake engine, the Global Earthquake Model's open-source software for seismic risk assessment. *Natural Hazards*, 72(3):1409–1427, 2014.

Singhal, Ajay and Kiremidjian, Anne S. Method for probabilistic evaluation of seismic structural damage. *Journal of Structural Engineering*, 122(12):1459–1467, 1996.

Sjarief, Roestam; Verhaeghe, Robert, and Grasoff, Poul. Integration of conservation in regional planning: the jabotabek case. In *Regional Development in a Decentralized Era: Natural Resources Management*, page 18, 2003.

Small, Christopher and Nicholls, Robert J. A global analysis of human settlement in coastal zones. *Journal of coastal research*, pages 584–599, 2003.

Smith, Denis. *Through a glass darkly-a response to Stallings'" Disaster, Crisis, Collective Stress, and Mass Deprivation"*, volume 2. Xlibris Press, 2005.

Spence, R. J. S.; Kelman, I.; Baxter, P. J.; Zuccaro, G., and Petrazzuoli, S. Residential building and occupant vulnerability to tephra fall. *Natural Hazards and Earth System Sciences*, 5(4):477–494, 2005. doi: 10.5194/nhess-5-477-2005. URL `https://nhess.copernicus.org/articles/5/477/2005/`.

Spence, Robin. Saving lives in earthquakes: successes and failures in seismic protection since 1960. *Bulletin of Earthquake Engineering*, 5(2):139–251, 2007.

Spence, Robin and So, Emily. *Why Do Buildings Collapse in Earthquakes?: Building for Safety in Seismic Areas*. John Wiley & Sons, 2021.

Stephens, MA. Tests Based on EDF Statistics, Chapter 4. In D'Agostino, RB and Stephens, MA, editors, *Goodness-of-Fit Techniques*, pages 97–104. Taylor & Francis Group, Boca Raton, 1st edition, 1986.

Stergiou, Evangelos C and Kiremidjian, Anne S. Risk assessment of transportation systems with network functionality losses. *Structure and Infrastructure Engineering*, 6(1-2):111–125, 2010.

Stewart, Mark G. and Deng, Xiaoli. Climate impact risks and climate adaptation engineering for built infrastructure. *ASCE-ASME Journal of Risk and Uncertainty in Engineering Systems, Part A: Civil Engineering*, 1(1):04014001, 2015. doi: 10.1061/AJRUA6.0000809. URL https://ascelibrary.org/doi/abs/10.1061/AJRUA6.0000809.

Stewart, Mark G; Wang, Xiaoming, and Nguyen, Minh N. Climate change adaptation for corrosion control of concrete infrastructure. *Structural Safety*, 35:29–39, 2012.

Stewart, Mark G; Val, Dimitri V; Bastidas-Arteaga, Emilio; O'Connor, Alan, and Wang, Xiaoming. Climate adaptation engineering and risk-based design and management of infrastructure. *Maintenance and safety of aging infrastructure*, pages 641–684, 2014.

Stohl, Andreas; Prata, AJ; Eckhardt, Sabine; Clarisse, Lieven; Durant, Adam; Henne, S; Kristiansen, Nina Iren; Minikin, Andreas; Schumann, Ulrich; Seibert, P, and others, . Determination of time-and height-resolved volcanic ash emissions and their use for quantitative ash dispersion modeling: the 2010 Eyjafjallajökull eruption. *Atmospheric Chemistry and Physics*, 11(9):4333–4351, 2011.

Suzuki, Takeo and others, . A theoretical model for dispersion of tephra. *Arc volcanism: physics and tectonics*, 95:113, 1983.

Suzuki, Y.J. and Iguchi, M. Determination of the mass eruption rate for the 2014 mount kelud eruption using three-dimensional numerical simulations of volcanic plumes. *Journal of Volcanology and Geothermal Research*, 382:42–49, 2019. ISSN 0377-0273. doi: https://doi.org/10.1016/j.jvolgeores.2017.06.011. URL https://www.sciencedirect.com/science/article/pii/S0377027317303657. Lessons learned from the recent eruptions of Sinabung and Kelud Volcanoes, Indonesia.

Tanaka, Hiroshi L; Iguchi, Masato, and Nakada, Setsuya. Numerical simulations of volcanic ash plume dispersal from Kelud volcano in Indonesia on February 13, 2014. *Journal of Disaster Research*, 11(1):31–42, 2016.

Tanner, T.; Surminski, S.; Wilkinson, E., and Reid, R. The Triple Dividend of Resilience: Realising development goals through the multiple benefits of disaster risk management. Technical report, Global Facility for Disaster Risk Reduction and

Recovery (GFDRR) at the World Bank and Overseas Development Institute (ODI), 2015.

Thompson, EM; Wald, David J, and Worden, CB. A vs30 map for california with geologic and topographic constraintsa vs30 map for california with geologic and topographic constraints. *Bulletin of the Seismological Society of America*, 104(5): 2313–2321, 2014.

Thompson, Mary Anne; Lindsay, Jan M; Wilson, Thomas M; Biass, Sebastien, and Sandri, Laura. Quantifying risk to agriculture from volcanic ashfall: a case study from the Bay of Plenty, New Zealand. *Natural Hazards*, 86(1):31–56, 2017.

Tofallis, Chris. A better measure of relative prediction accuracy for model selection and model estimation. *Journal of the Operational Research Society*, 66(8):1352–1362, 2015.

Tralli, David M; Blom, Ronald G; Zlotnicki, Victor; Donnellan, Andrea, and Evans, Diane L. Satellite remote sensing of earthquake, volcano, flood, landslide and coastal inundation hazards. *ISPRS Journal of Photogrammetry and Remote Sensing*, 59(4): 185–198, 2005.

Uhlenbrook, Stefan; Roser, Stefan, and Tilch, Nils. Hydrological process representation at the meso-scale: the potential of a distributed, conceptual catchment model. *Journal of Hydrology*, 291(3-4):278–296, 2004.

UN Environment, . *Global Status Report 2017, Towards a zero-emmision, efficient and resilient buildings and construction sector*. United Nations Environment Programme, London, UK, 2017.

UNISDR, . *Sendai Framework for Disaster Risk Reduction 2015-2030*. UNISDR (United Nations International Strategy for Disaster Reduction), 2015a. URL `https://www.undrr.org/publication/sendai-framework-disaster-risk-reduction-2015-2030`.

UNISDR, . Sendai framework for disaster risk reduction 2015-2030. In *Third United Nations World Conference on Disaster Risk Reduction (WCDRR)—Resilient People. Resilient Planet.*, 2015b.

UNISDR, and GADRRRES, . Comprehensive school safety. united nations international strategy for disaster reduction and global alliance for disaster risk reduction resilience in the education sector. 2017. Accessed 2021-12-20. http://gadrrres.net/uploads/files/resources/CSS- Framework-2017.pdf.

United Nations, . World Populations Dashboard. Available at https://www.unfpa.org/data/world-population-dashboard (2022/23/12), 2022.

United Nations General Assembly, . Report of the open-ended intergovernmental expert working group on indicators and terminology relating to disaster risk reduction. *United Nations General Assembly: New York, NY, USA*, 41, 2016.

United Nations Office for DRR, . United Nations Office for Disaster Risk Reduction, UNISDR Terminology and Disaster Risk Reduction. Technical report, United Nations International Strategy for Disaster Reduction, Geneva, Switzerland, 2009.

USGS ShakeMap, . PGA Map for the M 7.8 - 67 km NNE of Bharatpur, Nepal earthquake event. *USGS ShakeMap Earthquake Hazards Program*, 2015. Accessed 12 01 2021. https://earthquake.usgs.gov/earthquakes/eventpage/us20002926/shakemap/pga.

Vermeesch, Pieter. *geostats: An Introduction to Statistics for Geoscientists*, 2022. URL https://CRAN.R-project.org/package=geostats. R package version 1.5.

Volentik, Alain CM; Bonadonna, Costanza; Connor, Charles B; Connor, Laura J, and Rosi, Mauro. Modeling tephra dispersal in absence of wind: Insights from the climactic phase of the 2450 BP Plinian eruption of Pululagua volcano (Ecuador). *Journal of Volcanology and Geothermal Research*, 193(1-2):117–136, 2010.

Wackernagel, Hans. *Linear Regression and Simple Kriging*, pages 15–26. Springer Berlin Heidelberg, Berlin, Heidelberg, 2003. ISBN 978-3-662-05294-5. doi: 10.1007/978-3-662-05294-5_3. URL https://doi.org/10.1007/978-3-662-05294-5_3.

Wald, David J and Allen, Trevor I. Topographic slope as a proxy for seismic site conditions and amplification. *Bulletin of the Seismological Society of America*, 97 (5):1379–1395, 2007.

Walker, GPL and Croasdale, R. Characteristics of some basaltic pyroclastics. *Bulletin volcanologique*, 35(2):303–317, 1971.

Walther, Bruno A and Moore, Joslin L. The concepts of bias, precision and accuracy, and their use in testing the performance of species richness estimators, with a literature review of estimator performance. *Ecography*, 28(6):815–829, 2005.

Wang, Tianjia; Shen, Yonggang; Xie, Xu, and Chai, Jing. Ground-motion simulation using stochastic finite-fault method combined with a parameter calibration process based on historical seismic data. *Natural Hazards*, pages 1–20, 2022.

Wang, Xiaoming; Stewart, Mark G, and Nguyen, Minh. Impact of climate change on corrosion and damage to concrete infrastructure in australia. *Climatic change*, 110 (3):941–957, 2012.

Ward, Philip J; Jongman, Brenden; Aerts, Jeroen CJH; Bates, Paul D; Botzen, Wouter JW; Diaz Loaiza, Andres; Hallegatte, Stephane; Kind, Jarl M; Kwadijk, Jaap; Scussolini, Paolo, and others, . A global framework for future costs and benefits of river-flood protection in urban areas. *Nature climate change*, 7(9):642–646, 2017.

Wardman, JB; Wilson, TM; Bodger, PS; Cole, JW, and Stewart, C. Potential impacts from tephra fall to electric power systems: a review and mitigation strategies. *Bulletin of volcanology*, 74(10):2221–2241, 2012.

Weber, Elke U. Experience-based and description-based perceptions of long-term Risk: Why global warming does not scare us (Yet). *Climatic Change*, 77(1):103–120, July 2006. ISSN 1573-1480. doi: 10.1007/s10584-006-9060-3.

Wei, Shengji; Chen, Meng; Wang, Xin; Graves, Robert; Lindsey, Eric; Wang, Teng; Karakaş, Çağıl, and Helmberger, Don. The 2015 Gorkha (Nepal) earthquake sequence: I. Source modeling and deterministic 3D ground shaking. *Tectonophysics*, 722:447–461, 2018.

White, JT; Connor, Charles B; Connor, L, and Hasenaka, T. Efficient inversion and uncertainty quantification of a tephra fallout model. *Journal of Geophysical Research: Solid Earth*, 122(1):281–294, 2017.

Willcox, Karen E; Ghattas, Omar, and Heimbach, Patrick. The imperative of physics-based modeling and inverse theory in computational science. *Nature Computational Science*, 1(3):166–168, 2021.

Williams, Caroline J; Davidson, Rachel A; Nozick, Linda K; Trainor, Joseph E; Millea, Meghan, and Kruse, Jamie L. Regional county-level housing inventory predictions and the effects on hurricane risk. *Natural Hazards and Earth System Sciences*, 22(3): 1055–1072, 2022.

Williams, George T; Jenkins, Susanna F; Biass, Sébastien; Wibowo, Haryo Edi, and Harijoko, Agung. Remotely assessing tephra fall building damage and vulnerability: Kelud Volcano, Indonesia. *Journal of Applied Volcanology*, 9(1):1–18, 2020.

Wilson, TM; Cole, JW; Stewart, C; Cronin, SJ, and Johnston, DM. Ash storms: impacts of wind-remobilised volcanic ash on rural communities and agriculture following the

1991 Hudson eruption, southern Patagonia, Chile. *Bulletin of Volcanology*, 73(3): 223–239, 2011.

Woo, Gordon. Counterfactual disaster risk analysis. *Variance*, 10:279–291, 2018.

Woo, Gordon. Downward counterfactual search for extreme events. *Frontiers in Earth Science*, 7:340, 2019.

Woo, Gordon and Mignan, Arnaud. Counterfactual analysis of runaway earthquakes. *Seismological Research Letters*, 89(6):2266–2273, 2018.

Woo, Gordon; Maynard, T, and Seria, J. Reimagining history: counterfactual risk analysis. *Lloyd's emerging risk report, London*, 2017.

Worden, C Bruce; Thompson, Eric M; Baker, Jack W; Bradley, Brendon A; Luco, Nicolas, and Wald, David J. Spatial and spectral interpolation of ground-motion intensity measure observations. *Bulletin of the Seismological Society of America*, 108(2):866–875, 2018.

Worden, CB; Wald, DJ; Allen, TI; Lin, K; Garcia, Daniel, and Cua, Georgia. A revised ground-motion and intensity interpolation scheme for ShakeMap. *Bulletin of the Seismological Society of America*, 100(6):3083–3096, 2010.

Worldbank, . Global library of school infrastructure. *Global Program for Safer Schools*, 2019. https://gpss.worldbank.org/en/glosi/about-glosi.

Yang, David Y and Frangopol, Dan M. Societal risk assessment of transportation networks under uncertainties due to climate change and population growth. *Structural Safety*, 78:33–47, 2019.

Yang, David Y. and Frangopol, Dan M. Risk-based portfolio management of civil infrastructure assets under deep uncertainties associated with climate change: a robust optimisation approach. *Structure and Infrastructure Engineering*, 16(4): 531–546, 2020. doi: 10.1080/15732479.2019.1639776. URL `https://doi.org/10.1080/15732479.2019.1639776`.

Yang, Qingyuan; Pitman, E Bruce; Bursik, Marcus, and Jenkins, Susanna F. Tephra deposit inversion by coupling Tephra2 with the Metropolis-Hastings algorithm: algorithm introduction and demonstration with synthetic datasets. *Journal of Applied Volcanology*, 10(1):1–24, 2021.

Yun, Sang-Ho; Hudnut, Kenneth; Owen, Susan; Webb, Frank; Simons, Mark; Sacco, Patrizia; Gurrola, Eric; Manipon, Gerald; Liang, Cunren; Fielding, Eric, and others,

. Rapid damage mapping for the 2015 m w 7.8 gorkha earthquake using synthetic aperture radar data from cosmo–skymed and alos-2 satellites. *Seismological Research Letters*, 86(6):1549–1556, 2015.

Zamanian, Soroush; Hur, Jieun, and Shafieezadeh, Abdollah. A high-fidelity computational investigation of buried concrete sewer pipes exposed to truckloads and corrosion deterioration. *Engineering Structures*, 221:111043, 2020.

Zanini, Mariano Angelo; Toska, Klajdi; Faleschini, Flora, and Pellegrino, Carlo. Seismic reliability of reinforced concrete bridges subject to environmental deterioration and strengthened with frcm composites. *Soil Dynamics and Earthquake Engineering*, 136:106224, 2020.

Zhelavskaya, IS; Spasojevic, Maria; Shprits, YY, and Kurth, WS. Automated determination of electron density from electric field measurements on the van allen probes spacecraft. *Journal of Geophysical Research: Space Physics*, 121(5):4611–4625, 2016.

Zheng, Youtong and Rosenfeld, Daniel. Linear relation between convective cloud base height and updrafts and application to satellite retrievals. *Geophysical Research Letters*, 42(15):6485–6491, 2015.

Zhu, Yuxin; Tian, Dazuo, and Yan, Feng. Effectiveness of entropy weight method in decision-making. *Mathematical Problems in Engineering*, 2020, 2020.

Zondag, B; Grashoff, P S, and Verhaeghe, R J. Use of the java spatial model in policy making. In *International Seminar on "Climate Change Impacts on Water Resources and Coastal Management in Developing Countries"*., pages 1–13, 2009.

Appendices

Appendix A

Supplementary for Chapter 2

A.1 Q-Q plots for MAE and MAPE

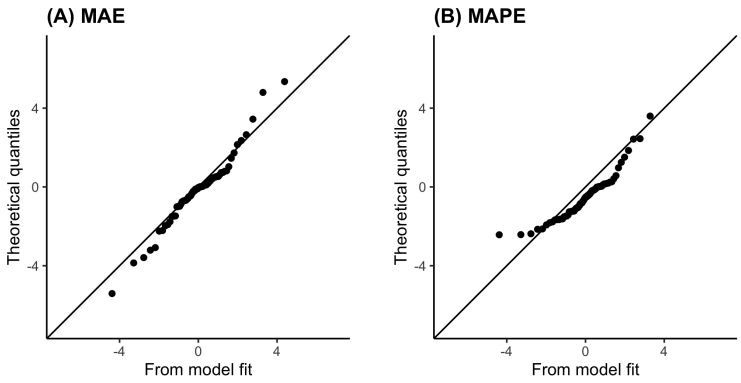

Figure A.1: Quantile-quantile (Q-Q) plots illustrating goodness-of-fit for the different models fitted using different cost functions: mean absolute error (MAE) and mean absolute percentage error (MAPE). The fit is evaluated by how well the empirical quantiles from the transformed model residuals line up with the theoretical quantiles from the assumed distributions along the diagonal line.

A.2 MSLE vs. MAPE

A widely-used order-dependent cost function is the mean absolute percentage error (MAPE), which is obtained by aggregating the relative errors using the mean and then

converting to a percentage:

$$\frac{100}{n}\sum_{i=1}^{n}\left|\frac{\varepsilon_i}{x_i}\right| \tag{A.1}$$

MAPE is used in different areas of research such as atmospheric science and space science (e.g. Grillakis et al., 2013; Zheng and Rosenfeld, 2015; Zhelavskaya et al., 2016). Despite being easy to interpret due to its usage of the percentage, MAPE has been proven to have problems when used in model calibration:

1. MAPE is asymmetric with respect to overestimation and underestimation (Hyndman & Koehler, 2006; Makridakis, 1993; Tofallis, 2015).

2. MAPE is constrained to be positive, so its distribution is generally positively skewed (Hyndman & Koehler, 2006; Swanson et al., 2000).

3. MAPE becomes undefined when the true value is zero (Hyndman & Koehler, 2006).

4. MAPE is not resistant to outliers (Swanson et al., 2000; Tofallis, 2015).

To elaborate on the first point, a prediction of 100 where the observed value is 50 gives a different magnitude of error (100%) than a prediction of 50 where the observed value is 100 (50%). Underprediction is therefore less heavily penalized than overprediction, even if the order of the error is the same. The third point also means that MAPE is not an appropriate metric where the quantity being predicted is likely to be zero (e.g. Tofallis, 2015).

A.3 Back transformation

If MSE was used as the cost function in the inversion, the final prediction map can be written as $\widehat{Y} = \mu + \hat{\epsilon}$ where μ denotes the forward model prediction. The associated spatial prediction uncertainty $Var[\widehat{Y}(\mathbf{x})]$ is equivalent to $Var\left[\epsilon(\mathbf{x})|\epsilon(\mathbf{x}_1), \ldots, \epsilon(\mathbf{x}_N)\right]$.

For the other cost functions related to Gaussian distributions, namely the chi-square error and MSLE, we can transform the residuals as outlined in Table 3 before applying simple kriging. We would then need to back-transform the predicted residuals and their prediction errors to obtain the final prediction maps.
For chi-square loss:

$$\widehat{Y} = \mu + \sqrt{\mu}\hat{\epsilon} \text{ and } Var[\widehat{Y}] = \mu Var[\hat{\epsilon}]. \tag{A.2}$$

For MSLE:

$$\widehat{Y} = \exp\left(\frac{\log_{10}(\mu+1) - \hat{\epsilon}}{\log_{10} e} + \frac{[\epsilon(\mathbf{x})|\epsilon(\mathbf{x}_1),\ldots,\epsilon(\mathbf{x}_N)]}{2(\log_{10} e)^2}\right) - 1 \tag{A.3}$$

$$\text{and } Var[\widehat{Y}] = \left[\exp\left(\frac{[\epsilon(\mathbf{x})|\epsilon(\mathbf{x}_1),\ldots,\epsilon(\mathbf{x}_N)]}{(\log_{10} e)^2}\right) - 1\right]\exp\left(2\frac{\log_{10}(\mu+1) - \hat{\epsilon}}{\log_{10} e} + \frac{[\epsilon(\mathbf{x})|\epsilon(\mathbf{x}_1),\ldots,\epsilon(\mathbf{x}_N)]}{(\log_{10} e)^2}\right) \tag{A.4}$$

A derivation of the prediction formulae for MSLE is given in Section A.4 of this Supplementary Material.

A.4 Derivation of the MSLE prediction formulae

When we use mean squared logarithmic error (MSLE) as a loss function to calibrate our forward model, we are implicitly assuming a Gaussian distribution on its transformed residual $Z(s_i) = \log_{10}\left(\frac{Predicted+1}{Actual+1}\right)$ where $Predicted = \mu$ is the forward model prediction and *Actual* is the observed tephra load (see Table 2 in the Main Paper). Hence, to model spatial deviations from the forward model, we conduct simple kriging or the method in Worden et al. (2018) on the transformed residuals.
Let $\hat{\epsilon} = \mathbb{E}[\epsilon(\mathbf{x})|\epsilon(\mathbf{x}_1),\ldots,\epsilon(\mathbf{x}_N)]$ denote the kriging prediction and $[\epsilon(\mathbf{x})|\epsilon(\mathbf{x}_1),\ldots,\epsilon(\mathbf{x}_N)]$ the prediction variance. Then:

$$\log_{10}(Actual+1) \sim N(\log_{10}(Predicted+1) - \hat{\epsilon}, [\epsilon(\mathbf{x})|\epsilon(\mathbf{x}_1),\ldots,\epsilon(\mathbf{x}_N)]), \tag{A.5}$$

since $\log_{10}(Actual+1) = \log_{10}(Predicted+1) - \log_{10}\left(\frac{Predicted+1}{Actual+1}\right)$.
Change bases from 10 to e, we have:

$$\log_e(Actual+1) = \frac{\log_{10}(Actual+1)}{\log_{10}(e)} \sim N\left(\frac{\log_{10}(Predicted+1) - \hat{\epsilon}}{\log_{10}(e)}, \frac{[\epsilon(\mathbf{x})|\epsilon(\mathbf{x}_1),\ldots,\epsilon(\mathbf{x}_N)]}{(\log_{10}(e))^2}\right), \tag{A.6}$$

This means that $Actual + 1 \sim logNormal\left(\frac{\log_{10}(Predicted+1)-\hat{\epsilon}}{\log_{10}(e)}, \frac{[\epsilon(\mathbf{x})|\epsilon(\mathbf{x}_1),\ldots,\epsilon(\mathbf{x}_N)]}{(\log_{10}(e))^2}\right)$. Using the formulae for the mean and the variance of a logNormal random variable, and writing *Predicted* as μ, the estimated tephra load and its prediction variance are:

$$\widehat{Y} = \exp\left(\frac{\log_{10}(\mu+1) - \hat{\epsilon}}{\log_{10} e} + \frac{[\epsilon(\mathbf{x})|\epsilon(\mathbf{x}_1),\ldots,\epsilon(\mathbf{x}_N)]}{2(\log_{10} e)^2}\right) - 1 \tag{A.7}$$

$$\text{and } [\widehat{Y}] = \left[\exp\left(\frac{[\epsilon(\mathbf{x})|\epsilon(\mathbf{x}_1),\ldots,\epsilon(\mathbf{x}_N)]}{(\log_{10} e)^2}\right) - 1\right]\exp\left(2\frac{\log_{10}(\mu+1) - \hat{\epsilon}}{\log_{10} e} + \frac{[\epsilon(\mathbf{x})|\epsilon(\mathbf{x}_1),\ldots,\epsilon(\mathbf{x}_N)]}{(\log_{10} e)^2}\right). \tag{A.8}$$

A.5 Simple kriging interpolation

The procedure for simple kriging interpolation is as follows:

1. For each pair of residuals at the sampled sites, calculate the variogram value γ as half of the mean-squared difference between their values.

2. Define a model of spatial variation (i.e. variogram model) that best relates the variogram values from Step 1, and the corresponding separation distances (h) for each pair of locations. The variogram model's parameters may be user-defined or estimated using a maximum likelihood estimation approach. In defining the variogram model, we adopt the Matérn function, and use the geostats and geoR packages in R programming environment for fitting (Diggle and Jr, 2007; Ribeiro Jr et al., 2020; Vermeesch, 2022; R Core Team, 2020a).

3. Estimate the elements of the covariance matrix, Σ, which describes the spatial relationships among the values at the observed sites and the prediction location. The covariance matrix has a size of $N \times N$, and its $i - j$th element is defined as

$$c(s_i, s_j) = \sigma^2 \gamma(h) + \tau^2, \tag{A.9}$$

   where σ^2 is the amount of spatially correlated variation, $\gamma(h)$ is the variogram model from Step 2, τ^2 is the variogram value at zero separation distance, and h is the distance between the two observation sites s_i and s_j. The parameters σ^2 and τ^2 are derived from the variogram model. The variable τ^2 is more commonly known as the *nugget* in the geostatistics literature, and it represents the variability in the interpolated at very short separation distances.

4. Calculate kriging weights λ_i as:

$$\begin{pmatrix} \lambda_1 \\ \vdots \\ \lambda_N \end{pmatrix} = \begin{pmatrix} c(s_1, s_1) & \cdots & c(s_1, s_N) \\ \vdots & \ddots & \vdots \\ c(s_N, s_1) & \cdots & c(s_N, s_N) \end{pmatrix}^{-1} \begin{pmatrix} c(s_1, s_0) \\ \vdots \\ c(s_N, s_0) \end{pmatrix} \tag{A.10}$$

5. Calculate the residual for all sites in the study area. The residual at any prediction location s_o can be written as:

$$\hat{Z}(s_o) = \sum_{i=1}^{N} \lambda_i Z(s_i) \tag{A.11}$$

where $Z(s_i)$ is the residual at an observed location s_i calculated using the equations for $Z(s_i)$ in Table 2 in the main text, λ_i is the weight applied to the value at the observed location, and N is the number of observed sites.

6. The associated kriging error can be calculated as:

$$Var(\hat{Z}(s_o) - Z(s_o)) = c(s_0, s_0) - \begin{pmatrix} c(s_1, s_0) \\ \vdots \\ c(s_N, s_0) \end{pmatrix}' \begin{pmatrix} c(s_1, s_1) & \cdots & c(s_1, s_N) \\ \vdots & \ddots & \vdots \\ c(s_N, s_1) & \cdots & c(s_N, s_N) \end{pmatrix}^{-1} \begin{pmatrix} c(s_1, s_0) \\ \vdots \\ c(s_N, s_0) \end{pmatrix} \tag{A.12}$$

A.6 LOOCV procedure

LOOCV computes the test performance for all reference data points. The following steps are conducted for both the simple kriging in Section 4.4.1 of the main text, and its extension in Section 4.4.2 which accounts for varying data uncertainty:

1. We make use of the transformed residuals at the observation sites ($Z(s_i)$) calculated for Section 4.4.1 Step 2a. For brevity, we refer to the transformed residual at an observation site as *observation point* in the steps that follow.

2. We set aside one observation point as a test point, while the other observation points form the training set. Note that we only use observation points from the reference dataset (i.e. Dataset 1) as test set. The idea is to evaluate the performance of the interpolation approach on the most reliable data.

3. Using only the training points, kriging interpolation is conducted for the test point.

4. This interpolated value of transformed residual is combined to the optimised model estimate for the test location following Section 4.4.1's Steps 3a and 3b. The result is an updated value of tephra load at test site.

5. The above steps are repeated until all points from Dataset 1 are evaluated as a test point. For all iterations, the interpolated load estimates are compared against the observed tephra load values based on a performance metric (e.g. root mean square error, chi-square, and mean square log error). The result is the LOOCV error associated with the kriging interpolation approach used in Step 3.

A.7 Checks for isotropy and residual form

We investigate the strength of the spatial correlation when the residuals are transformed in different forms, with the aim of finding which residual form is best for the kriging methods. We hypothesize that the log-residual is more suitable for use in kriging, since in Section 5.1, we identified that MSLE is the most suitable cost function for the case study.

In Figure A.2, we show the empirical and fitted variograms for the different forms of residuals. Annotated in the figures are the variograms' *range*, which vary across the variogram models shown. For instance, the range up to which log residuals can be interpolated (around 22km) was around three times larger than for the actual residuals (around 7km). This indicates that the log residuals are more appropriate to interpolate the residuals. Because of this evidence, we proceed with using log residuals for the spatial interpolation of the model deviations.

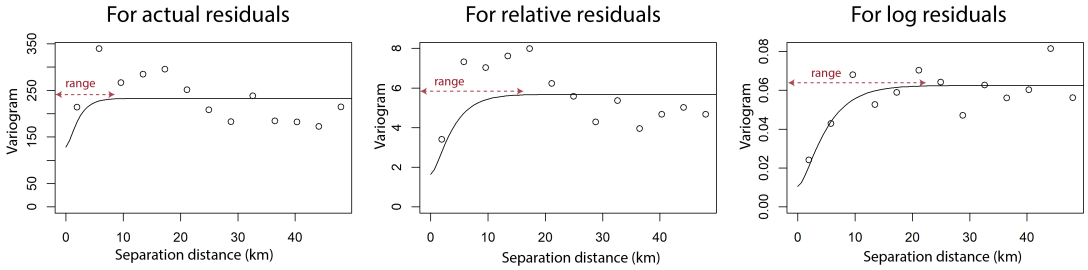

Figure A.2: Empirical and fitted Matérn variogram for actual and log residuals. Note that the widely different range of semivariance values in the y-axis is due to the scale of which the residuals are transformed. The range of the variograms (indicated with a dotted line) indicate the lag distances where data is spatially correlated. Beyond the range, interpolation does not occur.

We also confirmed the validity of assuming an isotropic field when modelling the spatial correlation, for which we use directional variograms. This step serves as a statistical check of the assumptions made in the kriging methodology since exterior factors (i.e. related to the physics of tephra deposition) may affect the spatial structure of the dataset and the model deviations. To generate the directional variograms, the variance for pairs of data were calculated for specific directions within a certain tolerance. Since the correlation structure appears similar for all the directional variograms in Figure A.3, there's no evidence of anisotropy. Hence, the assumption of an isotropic field is acceptable.

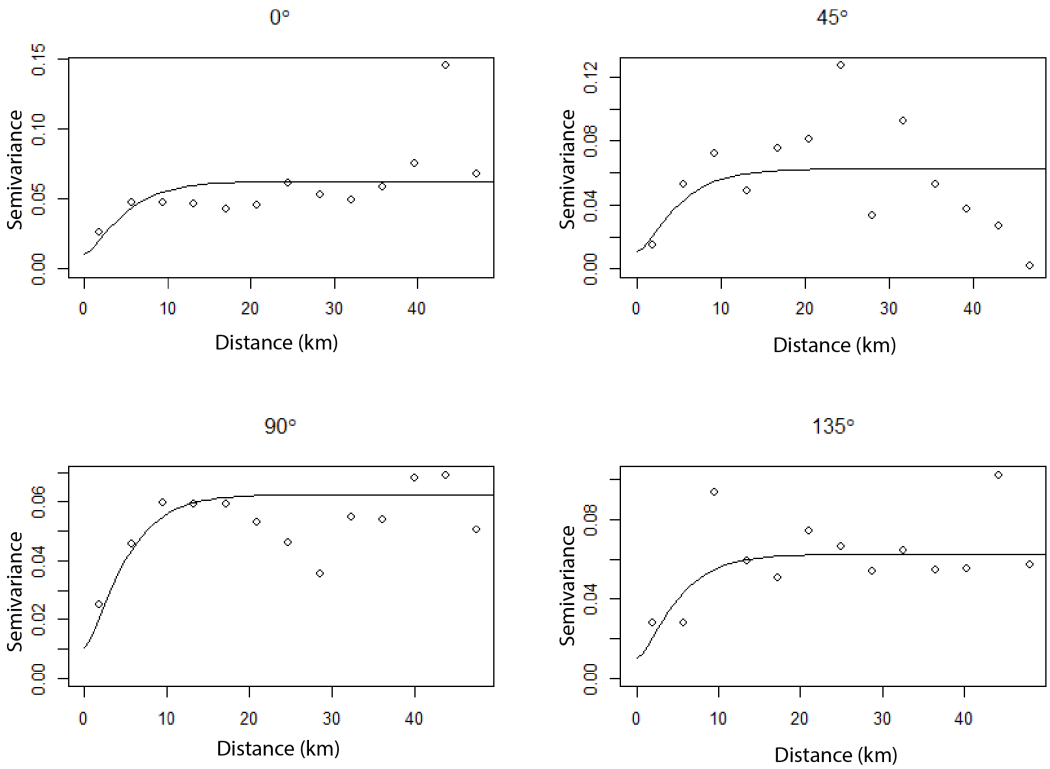

Figure A.3: The fitted omnidirectional Matérn model (shown in solid line) and empirical directional variograms (points) for the directions N0E, N45E, N90E, and N135E. An angular tolerance of 22.5 is set for generating the directional variograms.

Table A.1: Measures of performance of the unweighted and weighted kriging-based fusion methods in terms of LOOCV errors for different variogram models. The errors were calculated using three different metrics with formulas indicated in the table: root mean squared errors, chi-square errors and mean square log error. The training errors before applying the fusion methods are consistently higher than the LOOCV errors, which indicates no overfitting in the kriging method.

Cost function	Performance metric	Variogram model	Pre-kriging training error	LOOCV error after unweighted fusion	LOOCV erro weighted kr
MSE	Root-mean-square	Matérn	16.166	15.470	15.064
		Exponential		15.307	14.984
		Gaussian		15.924	15.717
Chi-square	Chi-square	Matérn	8.051	5.362	5.300
		Exponential		5.404	5.359
		Gaussian		5.494	5.533
MSLE	Mean square log	Matérn	0.0570	0.040	0.033
		Exponential		0.0395	0.034
		Gaussian		0.040	0.034

A.8 Leave-one-out cross-validation errors from fusion with different variogram models

Table A.1 shows the leave-one-out cross-validation (LOOCV) errors after weighted and unweighted fusion. For all cost functions and variogram models considered except the case of the Gaussian model for the chi-square cost function, the errors are lower for weighted fusion as compared to those from the unweighted fusion. In addition, the LOOCV errors are lower than the pre-kriging training error, indicating that there was no overfitting due to kriging.

A.9 Standard deviation of the tephra load estimates from model fusion

In Figure A.4, we show the maps of standard deviations associated with the tephra load estimates from the weighted and unweighted fusion. Note that the standard deviations are higher for larger estimated loads because the kriging was performed on a relative, logarithmic scale.

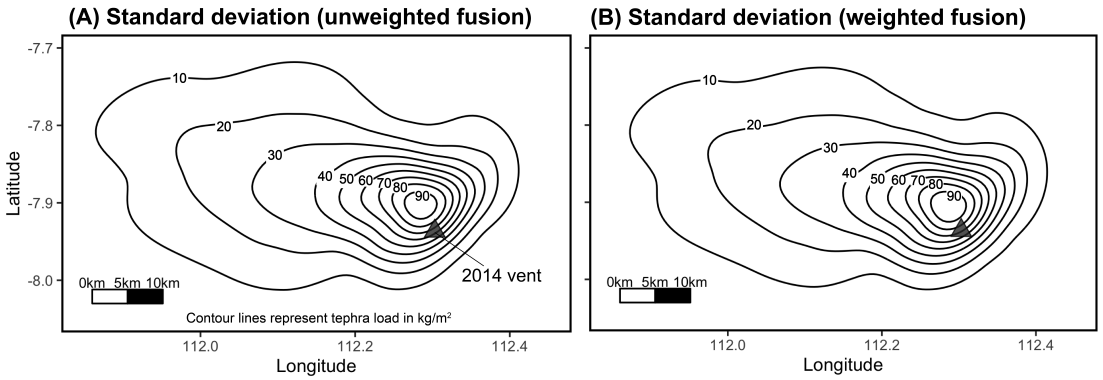

Figure A.4: Map of standard deviations associated with the estimates of tephra load from the fusion of the best-fit modelled output (using MSLE as cost function) shown in Figure 7A in the main text. The map in A corresponds to the unweighted fusion estimates in Figure 7B while B is associated with the weighted fusion estimates in Figure 9B.

Appendix B

Supplementary for Chapter 3

B.1 Relevant first-author publication for Chapter 3

Cited in Chapter 3 is a peer-reviewed conference paper:

Rabonza, M.L. and Lallemant, D. (2018). A time-dependent model for seismic risk reduction policy analysis. Accepted in the *17th U.S.-Japan-New Zealand Workshop on the Improvement of Structural Engineering and Resilience Nov 2018*

A TIME-DEPENDENT MODEL FOR SEISMIC RISK REDUCTION POLICY ANALYSIS

Maricar L. Rabonza, David Lallemant
Nanyang Technological University
Singapore

Abstract
The seismic risk of cities is constantly changing as cities themselves evolve in time. Key to making informed policy decisions to promote resilient cities is the ability to futurecast the risk of cities based on such potential policy decisions. This work demonstrates a flexible stochastic framework for analysing the potential seismic risk trajectories of cities. The model can be used to better understand how various retrofit policy standard and implementation time-frames affect seismic risk over time. Each policy or combination of policies can be compared with each other, and with the baseline case of "doing nothing." The model therefore serves as a seismic risk reduction policy analysis tool, and also as an advocacy tool, demonstrating that "the risk of doing nothing" is itself a policy decision, usually with the worst of possible consequences. The framework is demonstrated with a hypothetical case-study, which can serve as template for the analysis of real cities.

Introduction
Current earthquake risk assessment methods focus on understanding risk to existing infrastructure in its current state. Yet our ability to make informed and proactive policy decisions to reduce seismic risk depends on our ability to predict risk in dynamic urban development environments, and more importantly the impact of various risk reduction policies on future seismic risk.

In this paper, we propose a flexible stochastic framework for testing and comparing various seismic risk reduction policies, and their sensitivity to various factors including the level of retrofit standard, the time-frame of implementation, the pre-existing quality of building stock, the natural urban development rates and more.

The framework is then applied to a hypothetical case study to demonstrate the broader risk impact as neighborhoods implement seismic retrofits over time amidst varying rates and patterns of urban development. Multiple retrofit policies are compared, both in terms of the level of retrofit standards and the mandatory time frame to retrofit. While it is obvious that retrofit policies lead to decreased seismic risk, this study shows the time-evolution of risk linked to each of the potential retrofit strategies. This methodology is adopted from a framework used to investigate incremental building expansion as the significant driver for increasing vulnerability and risk (Lallemant, 2017).

The main contribution of the paper is to provide a flexible stochastic method to analyze future seismic risk driven by various dynamic processes. The case study serves as a proof of concept rather than prediction of actual risk. Certain simplifying assumptions are made and significant drivers of changing risk are not accounted for such as natural replacement rates of buildings, and structural deterioration over time. The case study can be refined and expanded so it becomes more realistic once actual data for transition rates, vulnerability, and building stock distribution are available.

Methodology
Seismic retrofits occur as discrete processes over time. Such processes can be modeled mathematically using Markov chains. These map the probability of transitioning from one state to another in a given time interval. For instance, in any given year, a vulnerable building can transition into a retrofitted one with a certain probability. This probability of transition therefore represents the annual retrofit rate for this

building type, and is influenced by the retrofit policy (e.g. mandated vs volunteer, etc). Markov models are "memoryless" meaning that any transition to a new state is not dependent on the sequence of events preceding it; thus, it is dependent only on the current state (Agresti, 2003). In the case of numerous building types and retrofit options, all transition probabilities form a transition probability matrix, such as described in Equation 1, which is used to simulate to probability that a building state transitions to another in a given time period. For the purposes of this study, we focus on 5 common building typologies shown in Table 1 as indices (P2 to P6), along with their retrofitted states for a low standard (P7 to P9) and high standard (P10 to P12). Indice P1 is used to represent urban growth, as the probability of an empty site transitioning into a new building. Therefore P1,2 would represent the probability of a green-field site being developed to construct a Concrete Frame Building, while P6,9 represents the probability of transitioning from a vulnerable URM (Unreinforced masonry) building to a URM retrofitted to minimum standards, and so forth.

$$P = \begin{pmatrix} p_{1,1} & p_{1,2} & p_{1,3} & \cdots & p_{1,12} \\ p_{2,1} & p_{2,2} & p_{2,3} & \cdots & p_{2,12} \\ p_{3,1} & p_{3,2} & p_{3,3} & \cdots & p_{3,12} \\ \vdots & \vdots & \vdots & \ddots & \vdots \\ p_{12,1} & p_{12,2} & p_{12,3} & \cdots & p_{12,12} \end{pmatrix} \quad (1)$$

Where each index is described in Table 1 below.

Table 1. Indices of Transition Probability Matrices

Index	P1	P2	P3	P4	P5	P6	P7	P8	P9	P10	P11	P12
Building type	Empty Site	CF	CF- I	CW	TIM	URM	CF	CF-I	URM	CF	CF-I	URM
Level of retrofit	None	None	None	None	None	None	Low	Low	Low	High	High	High

Abbreviations: CF = Concrete Frame; I = Infilled; CW = Concrete Wall; TIM = Timber Framed.

The transition matrices assume that retrofitted buildings do not transition to lower states (from retrofitted to non-retrofitted), and some states are "absorbing states" which are states that cannot be left once entered. The absorbing states represent our simplifying assumption that once buildings are retrofitted, no further modifications are further done. Transition probability rates can either be derived from statistics of building state distribution over time or assumed from reasonable outcomes of building state distribution.

Also, for a building stock with a initial distribution of typologies described by a normalized vector d_o, and a transition probability matrix P, the expected distribution D_t after *t steps* can be calculated as:

$$E\,(D_t \mid D_o = d_o) \;=\; d_o \;\; P^t \quad (2)$$

The vulnerability of each of the building is defined by fragility curves. These curves relate the earthquake intensity and the probability of exceeding or experiencing a certain level of damage. They can be derived analytically (Singhal and Kiremidjian 1996, Lallemant et al. 2015), empirically (Laumann 2005, Noh et al 2014) or heuristically based on expert opinion (Jaiswal et al. 2012).

The annual collapse rate of each building is obtained by integrating the fragility curve over the hazard curve as described in equation 3.

$$\lambda_{Collapse} = \int_{IM_{min}}^{IM_{max}} P(Collapse \mid IM = im) \mid d\lambda_{IM}(im)\mid \quad (3)$$

Where $\lambda_{IM}(im)$is the ground motion hazard curve and $|d\lambda_{IM}(im)|$is the absolute value of the derivative of the hazard curve.

Since buildings can be in one of several states over time, then collapse rate given an unknown state at time *t* is therefore:

$$\lambda_{Collapse}(t) = \sum_{State\ 1}^{State\ n} \int_{IM_{min}}^{IM_{max}} P(Collapse \mid IM = im \mid State = State_i)\, P(State = State_i \mid Do = d_0, P = p)\,(t) \mid d\lambda_{IM}(im)\mid \quad (4)$$

Where $P(Collapse \mid IM = im \mid State = State_i)$is the collapse fragility curve for each building type/state, $P(State = State_i \mid Do = d_0, P = p)\,(t)$ is the probability of being in each building state at time *t* given a starting state distribution $d_0$and transition probability matrix *p*.

Equations 3 and 4 can be combined as:

$$\lambda_{Collapse}(t) = \sum_{State\ 1}^{State\ n} \int_{IM_{min}}^{IM_{max}} P(Collapse \mid IM = im \mid State = State_i)\, d_0 P^t \mid d\lambda_{IM}(im)\mid \quad (5)$$

Finally, for a portfolio of buildings described by a vector $d_0 N$ where N is the total number of buildings and $d_0$their initial distribution (% of each building types/states), the annual expected number of buildings collapse at time *t* is described as:

$$\lambda_{Collapse\ Total}(t) = \Lambda_{collapse}\, N d_0 P^t \mid d\lambda_{IM}(im)\mid \quad (6)$$

Hypothetical Case-Study

Using the methodology described previously, we can test the impact of various policies on regional seismic risk over time. A hypothetical region is used to demonstrate the framework. The region contains four districts. For simplicity, each of the four districts in the region has its own building type distribution and seismic hazard curve, described in Figure 1 and 2 respectively.

Hazard Curves. Four hypothetical hazard curves are developed as idealized power-law hazard curves of the following form:

$$\lambda_{IM}(IM) = k_o\ IM^{-k} \quad (7)$$

Parameters used for the four districts are k0 = 0.0002, 0.0003, 0.00022, 0.00035 and k = 2, 2.1, 2.2, 2.5 for districts 1, 2, 3 and 4 respectively. The resulting fragility curves are shown in Figure 2.

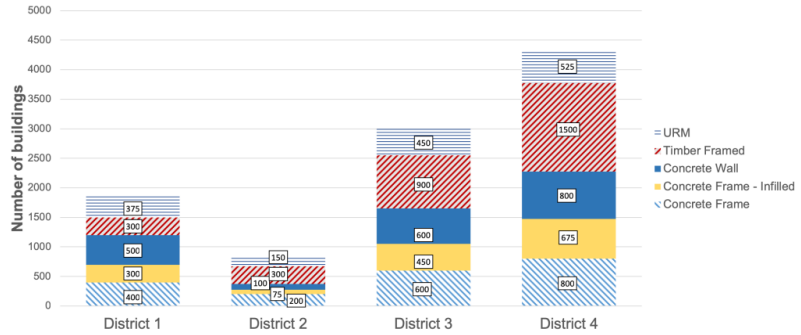

Figure 1. Distribution of building typologies for 4 hypothetical districts

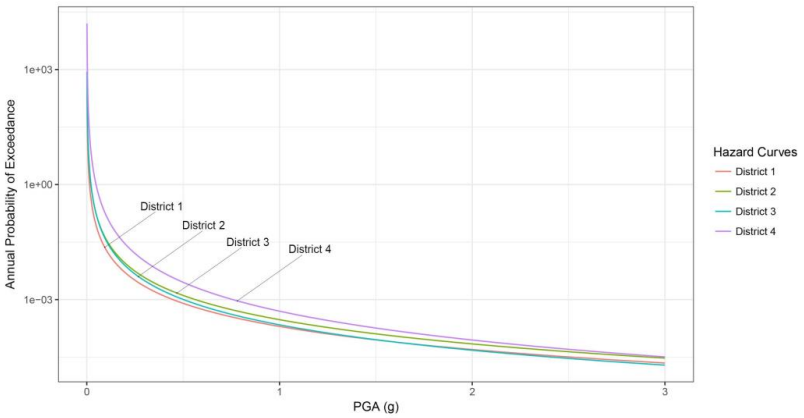

Figure 2. Hypothetical hazard curves for the four districts in the region. Parameters k0 = 0.0002, 0.0003, 0.00022, 0.00035 and k = 2, 2.1, 2.2, 2.5 are used to create these idealized power-law curves from equation 7.

Building Vulnerability Curves. The building vulnerability curves used are the empirical vulnerability curves obtained from damage surveys following the 2010-2011 Canterbury earthquake sequence (Blackbourn & Davey, 2017). For simplicity, we only use fragility curves corresponding to "Extensive / Complete Damage." In addition, hypothetical curves are developed representing Low Retrofit and High Retrofit Standards. While the actual curves do not directly correspond to the 33% and 67% National Building Standard (NBS) for retrofits of earthquake-prone buildings, these are meant to represent such "low" and high" retrofit standard policies.

Seismic Risk Reduction Policies. The purpose of the framework developed is to compare the impact of various policies (or absence of policies) on seismic risk over time. The types of decisions in the policy-making space includes the level of retrofit standards used, the time-frame for their implementation, the urban development rates (e.g. limits in development to particular regions) and more. Seven policy scenarios are used to demonstrate the diversity of policy options for seismic safety. These are described in Table 2.

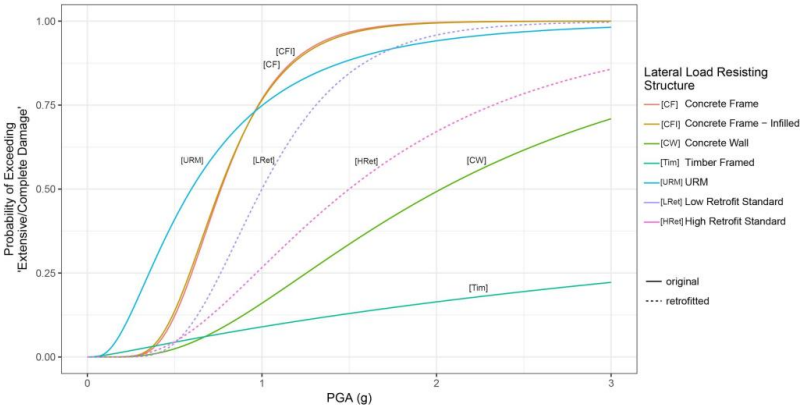

Figure 3. Vulnerability curves for several lateral load resisting structures obtained from empirical damage surveys following the 2010-2011 Canterbury earthquake sequence (Blackbourn & Davey, 2017) and hypothetical low and high retrofit standards.

Table 2. Seismic risk reduction policy scenarios

Policy Scenario	*Type of implementation*	*Retrofit quality*	*Time frame*	*Assumptions*
Policy 1	No retrofits	Not applicable	Not applicable	Natural urban growth drives the construction of new buildings. New buildings are assumed to be either concrete wall or timber framed buildings, both of which have low vulnerability.
Policy 2	Voluntary retrofits	Based on building owner discretion	Long (35 years)	The management of risk is left to the to the discretion of the building owners and tenants, and thus owners are principally responsible for building safety. Information dissemination and promoting voluntary retrofits helps the public make informed decision about earthquake risk. Adapted from previous studies, it is assumed that 59% percent of owners of earthquake-prone buildings have retrofitted their building within 35 years, of which 73% have opted for the minimum retrofit standard and 27% have opted for higher retrofit standards (Egbelakin et al., 2013).
Policy 3	Mandatory	Low standard	Short (15 years)	95% of owners adhere to this policy, of which 95% opted for minimum retrofit standards and 5% opted for higher standards.
Policy 4	Mandatory	Low standard	Long (35 years)	95% of owners adhere to this policy, of which 95% opt for minimum retrofit standards and 5% opt for higher standards.
Policy 5	Mandatory	High standard	Short (15 years)	95% of owners conduct of retrofit, of which 95% adhere to higher retrofit standards while 5% nonetheless opt for minimum retrofit standards.
Policy 6	Mandatory	High standard	Long (35 years)	95% of owners conduct of retrofit, of which 95% adhere to higher retrofit standards while 5% nonetheless opt for minimum retrofit standards.

Policy 7	Mandatory	High standard	Short (15 years)	Same as Policy 5 + limited urban development in District 4 95% of owners conduct of retrofit, of which 95% adhere to higher retrofit standards while 5% nonetheless opt for minimum retrofit standards. In addition, no further urban development is allowed in District 4 due to higher seismic hazard. All urban development is concentrated in the three other districts.

Mathematical Representations of Retrofit Policies. Each of the seven policies described above can be converted to transition probability matrices and included in a Markov Chain simulation used in equation 6. Transition probability matrices are mathematical representation of the probability of transition from one state to another for the entire building stock of the region in a given time-step. Indeed, urban growth can be represented as the probability of transitioning from an empty lot to a building in a 1 year period. Retrofit rates can be represented as the probability of transitioning from an earthquake-prone building to a retrofitted building in a 1 year period.

For each policy, a transition probability matrix is calibrated based on retrofit outcomes after 15 or 35 years described previous. We show below an example of the transition probability matrix calibrated for Policy 6 (High-retrofit standard, long frame for implementation).

$$P = \begin{pmatrix} 0.985 & 0 & 0 & 0.0075 & 0.0075 & 0 & 0 & 0 & 0 & 0 & 0 & 0 \\ 0 & 0.819 & 0 & 0.0075 & 0 & 0 & 0.009 & 0 & 0 & 0.172 & 0 & \\ 0 & 0 & 0.819 & 0 & 0 & 0 & 0 & 0 & 0 & 0 & 0 & 0 \\ 0 & 0 & 0 & 1 & 0 & 0 & 0 & 0 & 0 & 0 & 0 & 0 \\ 0 & 0 & 0 & 0 & 1 & 0 & 0 & 0 & 0 & 0 & 0 & 0 \\ 0 & 0 & 0 & 0 & 0 & 0.819 & 0 & 0 & 0.009 & 0 & 0 & 0.172 \\ 0 & 0 & 0 & 0 & 0 & 0 & 1 & 0 & 0 & 0 & 0 & 0 \\ 0 & 0 & 0 & 0 & 0 & 0 & 0 & 1 & 0 & 0 & 0 & 0 \\ 0 & 0 & 0 & 0 & 0 & 0 & 0 & 0 & 1 & 0 & 0 & 0 \\ 0 & 0 & 0 & 0 & 0 & 0 & 0 & 0 & 0 & 1 & 0 & 0 \\ 0 & 0 & 0 & 0 & 0 & 0 & 0 & 0 & 0 & 0 & 1 & 0 \\ 0 & 0 & 0 & 0 & 0 & 0 & 0 & 0 & 0 & 0 & 0 & 1 \end{pmatrix} \quad (8)$$

Results - Effect of Policy on Regional Seismic Risk

Using Equation 6, we can test the impact of various policies on regional seismic risk over time. Figures 4 and 5 show how the choices described by the 7 policies presented in this study affect the level of seismic risk in our region and scenario. These choices affect not only the level of risk reached, but also how risk changes in time. Mandatory retrofit schemes result in rapid reduction in seismic risk. Since seismic collapse risk is also a factor of the total exposure, Figure 4 shows an eventual increase in risk for all policies, due to natural urban growth.

Conclusion

This study provides a simplified demonstrations for a time-dependent seismic risk analysis framework which enables the investigation of various seismic risk mitigation policies and their impacts over time. Overall, the framework enables stakeholders to analyze future seismic risk and its sensitive to the initial building stock quality, the level of retrofit standard developed, the time-frame for mandatory retrofit, the rate and pattern of urban development and other drivers of changing risk.

The current demonstration has several limitations. Numerous drivers of changing risk are not accounted for, including the natural replacement rate of buildings, and structural deterioration of buildings over time. Other limitations of this demonstration include the simplified hazard model represented as a single

hazard curve for each district, the limited number of building types, and the testing of only two retrofit standards. While normalized collapse risk is used as the sole metric for seismic risk, the analysis could easily be extended to expected financial loss, by incorporating the non-collapse damage-state fragility curves and their corresponding loss distributions.

This type of time-dependent analysis can be effectively used to develop and compare novel seismic risk mitigation policies, and be integrated within cost-benefit policy analysis. The Markov chain transition probability matrices can be used to represent numerous discrete or continuous state-change processes affecting seismic risk. As such, the current study provides a flexible framework for further study into drivers of seismic risk, accounting for those drivers of increasing risk along with policies for its reduction.

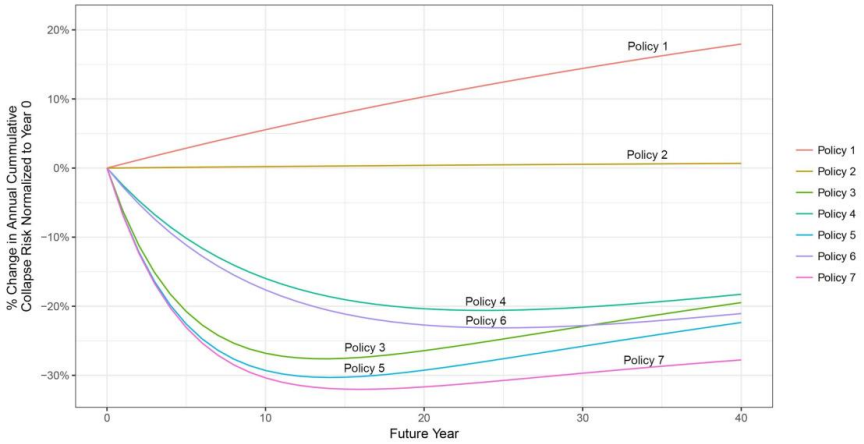

Figure 4. Percent change in annual collapse risk normalized to baseline risk at t=0, for each of the 7 policies and assuming an urban growth rate of 1.5% per year.

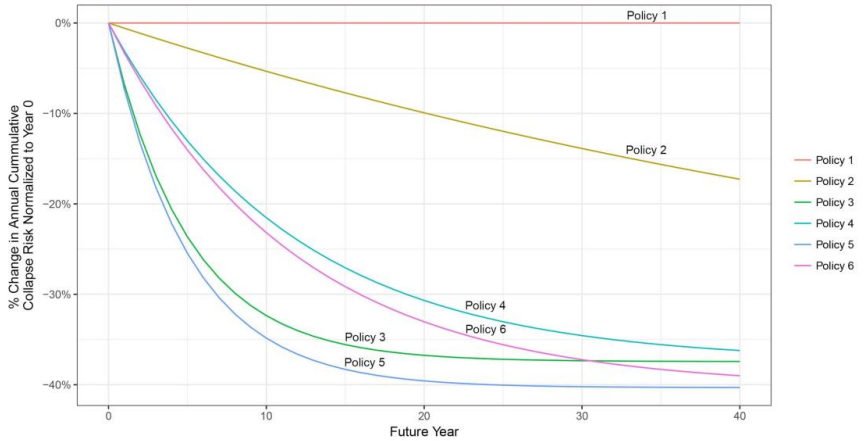

Figure 5. Percent change in annual collapse risk normalized to baseline risk at t=0, for each of the 6 policies and assuming no urban growth (hence policy 7 is not included).

Acknowledgements

This research is funded through a National Research Foundation (Singapore) Fellowship grant (NRF–NRFF2018–06), along with an Earth Observatory of Singapore scholarship.

References

Agresti, A., 2003, *Categorical data analysis* (Vol. 482), John Wiley & Sons.

Blackbourn T, Davey R, 2014, "Seismic Fragility Assessment of Canterbury Buildings", presented at *2017 NZSEE Conference, New Zealand, 2017*, PDF available at <http://db.nzsee.org.nz/2017/O5B.3_Blackbourn.pdf>. Accessed October 2018.

Egbelakin, T. 2013, "Assessing Regulatory Framework Efficacy for Seismic Retrofit Implementation in New Zealand". In *In Proceedings of CIB World Building Congress: Construction and Society* (pp. 5-9).

Jaiswal, K. S., Aspinall, W., Perkins, D., Wald, D., & Porter, K. A., 2012, "Use of expert judgment elicitation to estimate seismic vulnerability of selected building types", In *Proc. 15th World Conference on Earthquake Engineering, Lisbon, Portugal, 24-28 Sep 2012*.

Lallemant, D., Kiremidjian, A., & Burton, H., 2015,. "Statistical procedures for developing earthquake damage fragility curves", *Earthquake Engineering & Structural Dynamics, 44*(9), 1373-1389.

Lallemant, D., Burton, H., Ceferino, L., Bullock, Z., & Kiremidjian, A., 2017, "A framework and case study for earthquake vulnerability assessment of incrementally expanding buildings", *Earthquake Spectra, 33*(4), 1369-1384.

Laumann, G., 2005, "Science Plan: urbanization and global environmental change", *Bonn, Germany, International Human Dimensions Programme on Global Environmental Change*, 61.

Noh, H. Y., Lallemant, D., & Kiremidjian, A. S., 2015, "Development of empirical and analytical fragility functions using kernel smoothing methods", *Earthquake Engineering & Structural Dynamics, 44*(8), 1163-1180.

Singhal, A., & Kiremidjian, A. S., 1996, "Method for probabilistic evaluation of seismic structural damage", *Journal of Structural Engineering, 122*(12), 1459-1467.

Appendix C

Supplementary for Chapter 4

C.1 Re-analysis of lives saved during the 2015 Gorkha Earthquake

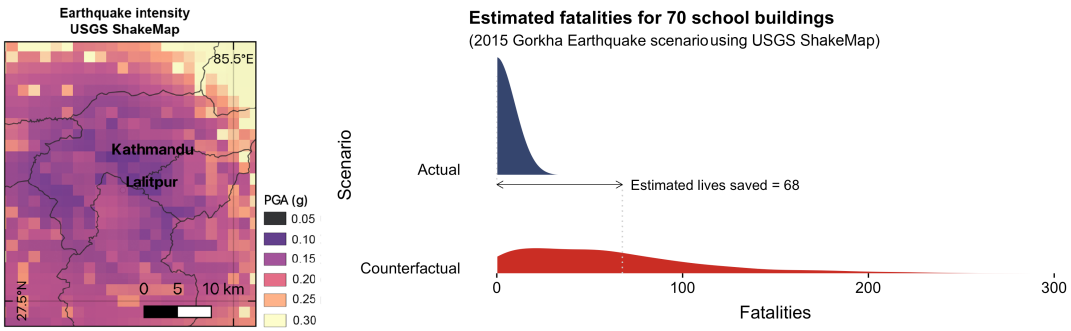

Figure C.1: A re-analysis of the case study described in Section 5.1 is performed using the peak ground acceleration map for the 2015 M_w 7.8 Gorkha earthquake obtained from USGS ShakeMap (2015) (shown on the left). Using this hazard model, our analysis show an estimated of 68 lives saved in the 70 retrofitted schools.

C.2 Relevant first-author publication for Chapter 4

Cited in Chapter 4 is a paper published as a Contributing Paper to the Global Assessment Report (GAR) on Disaster Risk Reduction 2022 by the United Nations

Office for Disaster Risk Reduction (UNDRR)

Rabonza, M.L., Lallemant, D., Lin, Y. C., Tadepalli, S., Wagenaar, D., Nguyen, M., Choong, J., Liu, C. J. N., Sarica, G. M., Widawati, B. A. M., Balbi, M., Khan, F., Loos, S. & Lim, T. N. (2022). Shedding light on avoided disasters : measuring the invisible benefits of disaster risk management using probabilistic counterfactual analysis. *A contributing paper to the United Nations Office for Disaster Risk Reduction (UNDRR) Global Assessment Report 2022*. https://www.undrr.org/publication/shedding-light-avoided-disasters-measuring-invisible-benefits-disaster-risk-reduction

United Nations Office for Disaster Risk Reduction

GAR

Global Assessment Report on Disaster Risk Reduction

2022

CONTRIBUTING PAPER

Shedding light on avoided disasters: Measuring the invisible benefits of disaster risk management using probabilistic counterfactual analysis

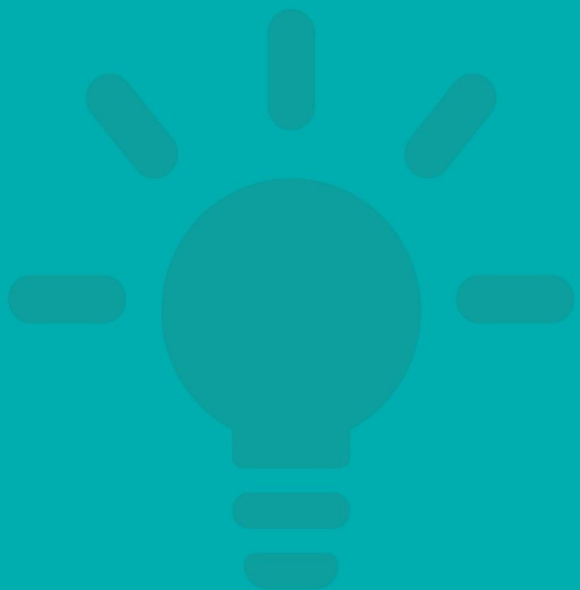

Maricar Rabonza
David Lallemant
Yolanda C. Lin
Sanjana Tadepalli
Dennis Wagenaar
Michele Nguyen
Jeanette Choong
Celine J.N. Liu
Gizem Mestav Sarica
Bernadeti Ausie Miranda Widawati
Mariano Balbi
Feroz Khan
Sabine Loos
Lim Tian Ning

Disclaimer:

The designations employed and the presentation of the material in this publication do not imply the expression of any opinion whatsoever on the part of the Secretariat of the United Nations concerning the legal status of any country or territory or of its authorities or concerning the delimitations of its frontiers or boundaries. The designations of country groups in the text and the tables are intended solely for statistical or analytical convenience and do not necessarily express a judgment about the stage reached by a particular country or area in the development process. Mention of the names of firms and commercial products does not imply the endorsement of the United Nations.

Note: The designations employed and the presentation of maps in this report do not imply the expression of any opinion whatsoever on the part of the Secretariat of the United Nations concerning the legal status of any country, territory, city or area or of its authorities or concerning the delimitation of its frontiers or boundaries.

Citation: UNDRR (YYYY), *Insert full name of publication*, United Nations Office for Disaster Risk Reduction (UNDRR).

For additional information, please contact:

United Nations Office for Disaster Risk Reduction (UNDRR)
9-11 Rue de Varembé, 1202 Geneva, Switzerland, Tel: +41 22 917 89 08

Shedding light on avoided disasters: Measuring the invisible benefits of disaster risk reduction using probabilistic counterfactual analysis

Authors

Maricar Rabonza, David Lallemant, Yolanda C. Lin, Sanjana Tadepalli, Dennis Wagenaar, Michele Nguyen, Jeanette Choong, Celine J.N. Liu, Gizem Mestav Sarica, Bernadeti Ausie Miranda Widawati, Mariano Balbi, Feroz Khan, Sabine Loos, Lim Tian Ning

Abstract

The goal of Disaster Risk Management (DRM) is to ensure that society continues to function, thrive, and recover quickly despite shocks arising from natural or human actions; to ensure, in short, that natural hazards do not become disasters. Success in the world of DRM means 'nothing happens,' but this poses a dilemma towards recognising and incentivising successful DRM interventions since they are made invisible by the very nature of their success. How then do we highlight and learn from successes if we do not see them? Likewise, how do we incentivise policymakers to make better risk-informed decisions when they are not credited for pro-active actions nor accountable for the consequences of doing nothing? This study discusses four types of situations where successful DRM interventions are made invisible: (i) success made invisible in the midst of broader disaster, (ii) success made invisible by nature of the success, (iii) success made invisible due to yet unrealised benefits, (iv) success made invisible due to the randomness of the specific outcome. We propose the use of probabilistic counterfactual analysis to calculate and highlight the 'probabilistic lives saved' from disaster risk management interventions, that would otherwise remain unnoticed. Two case-studies are provided, a school seismic retrofit program in Nepal and a cyclone evacuation effort in India. An important conclusion that emerges from these studies is that the value of risk reduction interventions should not be judged on the basis of specific outcomes, but on the basis of a broader exploration of potential outcomes. The shift in focus from realised outcome to counterfactual alternative provides a framework to identify and learn from successes in DRM, and reward individuals and institutions who have displayed political bravery in committing to the implementation of DRM measures despite invisible benefits.

Keywords: Probabilistic analysis; Counterfactual risk assessment; Risk communication; Risk perception

Contents

Introduction & Motivation

The goal of Disaster Risk Management (DRM) is to ensure that society continues to function, thrive, and recover quickly despite shocks arising from natural or human actions; to ensure, in short, that natural hazards do not become disasters. Disasters are "social in nature" — they stem not solely from the hazard, but from the interactions of the physical, built and social environments (Mileti, 1999). The extent of a disaster can be characterized by loss of life (Moore, 1958), as well as considerable damage and social, political and economic disruptions (Smith, 2005). DRM efforts try to ensure that such disaster elements are avoided (i.e. 'nothing happens'), but this poses a dilemma for recognising and incentivising successful DRM interventions since they are made invisible by the very nature of their success. In addition, if the benefits of DRM actions manifest primarily as reduced impact when a hazard event occurs, these benefits may only be realised far in the future — particularly for rare and extreme events. Hence relying on the realisation of a disaster to evaluate mitigation efforts ignores the significant time delay between the investment in DRM and the hazard. When a large hazard event which 'tests' mitigation actions does occur, both news and research tend to focus on losses caused by the catastrophe, and very rarely is a past mitigation intervention revisited for analysis.

How then do we incentivise policymakers to make better risk-informed decisions when they are not credited for pro-active actions nor accountable for the consequences of doing nothing? There is a pressing need to develop better frameworks to judge the successes of DRM interventions, both to recognise and celebrate good decisions as well as to create incentives for further investment in mitigation. Literature suggests that celebration of past successes can benefit disaster risk reduction. For instance, inspirational visions can be key components of transformations to sustainability or resilience by helping communities articulate their values and desired futures (Wiek and Iwaniec, 2014). This can even help shape the very reality they forecast or explain. Focusing attention on these successes offers a novel way forward because it can help sustain and amplify efforts that already exist, and enable learning from positive examples rather than hyperfixation on the many negative ones which dominate the news and research literature (e.g. Leach et al., 2012). Shedding light on otherwise invisible benefits of successful DRM interventions is crucial to the achievement of large-scale transformations (Scott, 1998).

In this paper, we focus on four types of situations where successful DRM interventions are made invisible:

1) **Success made invisible in the midst of broader disaster.** Successful mitigation may result in fewer losses after a disaster, but this success is obscured amid the catastrophe and losses that were still incurred.
2) **Success made invisible by nature of the success.** A hazard becomes a disaster on account of the impacts it has on society. If mitigation efforts are so successful that there are no perceivable impacts, both the potential disaster and the successful mitigation are made invisible.
3) **Success made invisible due to yet unrealised benefits.** On account of the large time delay between the mitigation intervention and its benefits being realised, mitigation efforts could be seen as unsuccessful or unnecessary until a hazard event occurs.

4) **Success made invisible by the randomness of the specific outcome.** Hazards are stochastic processes, hence any single occurrence is only one of several possibilities that could have occurred. Recognising that the parameters of the event that actually occurred could easily have been different, successes can be made invisible if the hazard randomly does not strain mitigation measures, e.g. a near-miss.

To address these invisibilities, we develop and demonstrate a novel application of probabilistic counterfactual risk analysis to highlight and celebrate successful DRM interventions based on *counterfactual outcomes* rather than realised past outcomes or unrealised future outcomes. The systematic implementation of such analysis would enable us to (i) build a collection of case studies of past interventions that feature well-articulated, specific, implemented, and measured successes towards a safer, more resilient future, (ii) give a quantitative measure that focuses on celebrating benefits of intervention, independent of the specific occurrence of the hazard event against which the intervention was implemented, (iii) provide a means for crediting policymakers for sound decisions, even if the benefits of these decisions are not felt till much after decisions were taken, (iv) monitor progress in disaster risk reduction independent of the realised outcome of such interventions.

The potential stakeholders for this framework are multiple. Policy-makers (central and local governments) can be incentivized to invest more in risk reduction, by making visible to their constituents the benefits of such investments, even if these benefits are not realized. The framework would also enable disaster risk management practitioners to learn from positive lessons (rather than negative ones), which can be emulated in similar contexts. It can also serve donors as a means to evaluate projects and monitor progress, even if no tangible benefits are seen until a disaster strikes.

The paper is organised as follows. In Section 2, we draw on research on risk perception and social psychology, as well as the political aspects of disaster policy to highlight some of the challenges faced in evaluating disaster risk measures. This motivates our proposed framework of probabilistic counterfactual analysis. In Section 3, we introduce the framework in the context of DRM. Two case studies are used to illustrate the framework in Section 4: a school earthquake retrofitting program in Nepal and the evacuation of coastal communities in India prior to the landfall of a major cyclone. These showcase the different types of situations where successful DRM interventions are made invisible and the applicability of the method for different hazards. To provide further examples of where the method can be applied, we also provide a list of sample DRR measures. These include instances where successes are made invisible due to yet unrealised benefits, and cover different hazards as well as geographical regions. In Section 5, we discuss our results from our case studies as well as possible extensions and limitations. Finally, we conclude in Section 6 by summarising the work and its implications.

Risk perception and the invisibility of DRM

Even though effective mitigation of extreme events is both possible and already happening, there are many challenges faced in recognising and evaluating them.

If disaster risk management interventions are successful in their goal to eliminate or reduce the impacts of hazards on society, fewer people will experience the impacts of disasters. Research on risk perception has shown that people significantly underweigh low-probability events they do not have experience with (Tversky and Kahneman, 1973; Hertwig et al., 2004; Newell et al., 2016). This results in a strange paradox: the more mitigation efforts help successfully avoid disasters, the more we might underweight the risks posed by hazards and extreme events. This invisibility of mitigation successes is further exacerbated by the perception of disasters as the result of hazards that overwhelm societies - rare events, or "acts of god" for which it is impossible to prepare (Gaillard, 2019).

The field of social psychology provides further insight into why DRM evaluation is often so challenging. Research has shown that people's emotional responses to events are influenced by their perception of "what might have been" (Medvec et al., 1995; Roese and Olson, 2014). A disaster event is a break from normalcy that triggers imaginations of alternative realities or *counterfactuals*: What if the disaster had never happened? What if it had hit a neighbouring town instead? In the aftermath of negative experiences, these counterfactuals are usually in an "upward" direction, where one imagines a better outcome than the realised outcome (Blix et al., 2016), e.g. thinking about the ways in which one could have avoided a car accident. Perceiving the benefits of mitigation, however, often requires comparing reality to a worse outcome or "downward counterfactual", which is not a natural cognitive process, e.g. imagining a car accident happening on a routine trip to work. Further, counterfactuals are typically triggered by shock or surprise (Epstude and Roese, 2008; Kahneman, 1995). When a disaster has not happened yet or has been so successfully avoided that the hazard event is not perceived as a disaster, this "trigger" is missing.

Another challenge faced in recognising successful mitigation measures is that good DRM decisions are made invisible by the fact that they are evaluated only against the outcome that occurs instead of all possible events that could have occurred. The extreme case occurs when success has not been realised because the hazard has not occurred. As with many actions to mitigate climate change, DRM interventions require immediate sacrifice for seemingly uncertain benefits at a much later time (Weber, 2006). This time delay means that mitigation successes are rendered invisible until the eventual realisation of a hazard; excepting situations when mitigation measures also introduce co-benefits, which are a crucial part of effective DRM and which we discuss further in our conclusion.

Probabilistic counterfactual analysis addresses the aforementioned challenges faced in evaluating disaster risk measures. By accounting for alternative scenarios with their associated probabilities and explicitly identifying how a mitigation measure decreases the impact on society, it counters the natural cognitive perceptions which hinder the way people process risk and hence measure and evaluate mitigation successes. Since the framework can also be applied to measures for which success has not been realised to consider all possible future scenarios, it can quantify the long-term benefits of DRM decisions. It is essential that we invest in disaster mitigation, especially given the increasing frequency of disasters in the context of climate change (Jha et al., 2011). However, doing so in the light of the time delay between the intervention and its benefits combined with the invisibility of successful risk

reduction means that decisions to invest in mitigation require remarkable political bravery. If these decisions are not recognised and rewarded, the interventions may be seen as ineffective or unnecessary with potentially disastrous consequences. Probabilistic counterfactual analysis provides a framework to rightly assess these difficult decisions.

Highlighting success in disaster risk management through counterfactual analysis

Counterfactual Analysis and DRM

The concept of counterfactual analysis is an old one. It is indeed closely linked to the analysis of causality theory in philosophy (Todorova, 2015), and often associated with 20th century theorising on "possible worlds" used in formal logic, philosophy, linguistics and more (Lewis, 2005). Counterfactual analysis typically starts with the creation of "what if..." scenarios, around which alternative branches of history can be explored. Combining counterfactual analysis with probabilistic methods, we can further constrain the scope of potential alternative branches of history by accounting for their relative probabilities based on best available data.

The idea that realised history is but one among many alternative "worlds" is a useful concept that supports our application of counterfactual analysis to shed light on invisible benefits of disaster risk management. Through this lens, in cases A and B of Figure 1 we shed light on *successes made invisible in the midst of broader disaster* and *successes made invisible by nature of their success* by comparing a past disaster (realised history) to an alternative world in which a particular DRM intervention was not implemented. In case C of Figure 1, we shed light on *successes made invisible due to yet unrealised benefits* by comparing a past with no hazard event (realised history) to alternative worlds where hazard events occurred according to their probability-magnitude characteristics (obtained from probabilistic hazard analysis). In case D of Figure 1, we shed light on *successes made invisible due to the randomness of specific outcomes* by comparing a past hazard event that had relatively small consequences (realised history) to alternative worlds representing the full spectrum of potential realisations of that hazard event. Each of these cases are examples of downward counterfactual analysis, where the alternative realisation is worse, to demonstrate the value of DRM interventions.

The use of counterfactual analysis has received growing attention in the disaster risk management field, though mostly to highlight failings in DRM rather than successes. Counterfactual analysis has been used to provide a way to capture the range of outcomes due to highly uncertain and random variables in a small but growing variety of applications including earthquakes (Woo and Mignan, 2018; Lin et al., 2020), climate change (Shepherd et al., 2018), terrorism and cyber security (Woo et al., 2017; Oughton et al., 2019), and volcanic eruptions (Aspinall and Woo, 2019). In previous applications, counterfactual exploration of alternative hazard events at different times of day, locations, or magnitude/intensity have shown that randomness plays a large role in the specific consequences of hazard events (Woo, 2019; Lin et al., 2020). Downward counterfactual risk analysis has been used primarily to point out worse potential outcomes for the purpose of insurance, preparedness, or future mitigation (e.g. Woo, 2019; Lin et al., 2020; Aspinall and Woo, 2019). We propose the use of downward counterfactual analysis to quantify improvements in resilience or celebrate past successes in DRM: this marks a fundamental shift in the application of counterfactuals in risk analysis. By focusing on celebration of past successes, this work presents a novel domain of application of counterfactual disaster risk analysis beyond highlighting potential worse outcomes and failures in DRM.

Figure 1. A schematic of invisibilities in mitigation successes using stilt houses as the mitigation and flooding as the hazard.

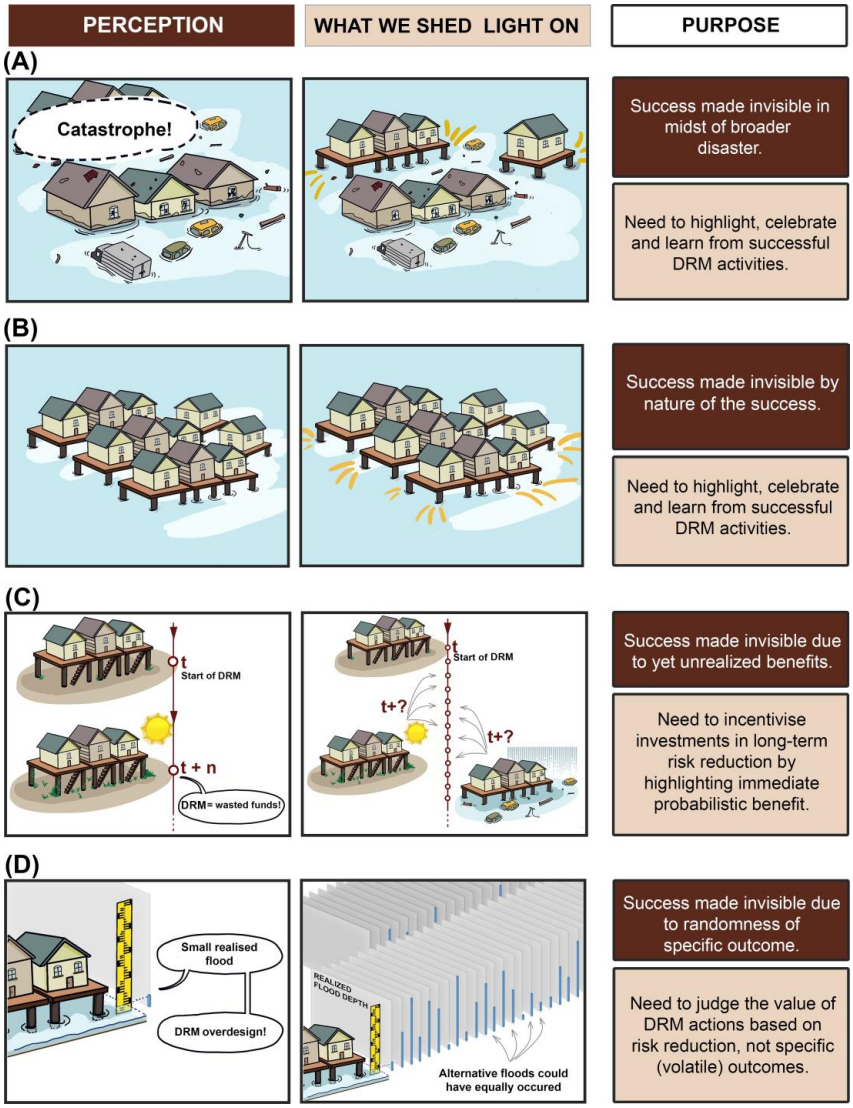

Counterfactual Analysis and Risk Analysis

Risk can be broadly defined as the likelihood of future undesired consequences produced from potentially damaging events such as natural hazards. The most common framework to quantify risk expresses it as a function of three distinct but interrelated

components (UNISDR, 2009): (A) Hazard, which refers to the likelihood of potential damaging events, (B) Exposure, which refers to the location and attributes of community assets such as people, buildings and infrastructure and (C) Vulnerability, which refers to the susceptibility of the exposure to sustain impact or harm for a given hazard intensity. Thus, risk can be seen as a function of a set of parameters that characterise each of the three components.

In the counterfactual analysis framework, the first step is to characterise the factual, realised event, around which counterfactuals can be defined and analysed (e.g. Lin et al., 2020). The impact resulting from the realised event should be characterised in terms of its relevant risk parameters:

$$Irealised = f(\theta_H, \theta_E, \theta_V), (1)$$

where θ_H are the hazard parameters (e.g. magnitude of the event, its location, time etc.), θ_E are the exposure parameters (e.g. location of buildings and the number of people exposed), and θ_V are the vulnerability parameters (e.g. structural building characteristics, social vulnerability characteristics, etc.).

This then sets the basis for exploring alternatives where a single or multiple of the risk parameters are modified in order to define a new, *counterfactual* event:

$$I_{counterfactual} = f(\theta_H + \delta_H, \theta_E + \delta_E, \theta_V + \delta_V), (2)$$

where $\delta_{\cdot}$ are the variations over one or many of the parameters that defined the original past event.

In most situations, we will treat the factual realised event as deterministic, where all parameters $\theta_H, \theta_E, \theta_V$ are known and fixed. Alternatively, we may want to treat some parameters as fixed and some as unknown. However, it is often useful to explore a broad range of counterfactual events, accounting for their relative probabilities. This is then an application of the risk analysis framework to counterfactual analysis. In this setting, some of the parameters in equation 2 are unknown, but with known probability distributions (e.g. frequency-magnitude curves of earthquake occurrence). The probability of each counterfactual alternative is then associated with the joint-probability of unknown parameters. In practice this rarely has an analytical formulation, and is calculated by means of simulation (e.g. Monte-Carlo simulation).

Comparing the realised event (fixed or probabilistic) to the distribution of counterfactual events enables us to quantify the benefits (*B*) of positive actions towards risk mitigation (see equation 3 and Figure 2).

$$B = I - I_{counterfactual} \quad (3)$$

Figure 2: Conceptual diagram of the counterfactual risk analysis framework.

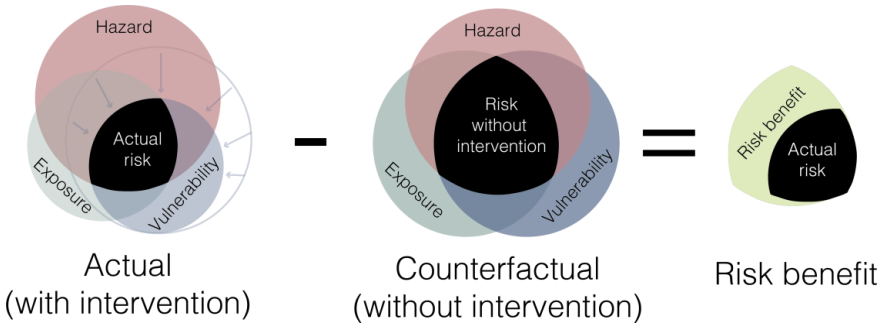

In our demonstration, we measure the benefits of DRM intervention in terms of *probabilistic lives saved*. Indeed, the reduction of mortality is the first target indicator within the Sendai Framework For Disaster Risk Reduction (UNISDR, 2015), reflecting the primary goal of global DRM practice to save lives. We also note that our approach is similar to the measure of 'years of life saved' by medical interventions that is calculated systematically in the field of public health (Tengs et al., 1995). Similar analysis could be conducted for measuring reduced losses in financial terms, as is often the case in cost-benefit analysis, though these analyses have the tendency to highlight "successful" DRM interventions as those that protect high-value areas rather than high-vulnerability areas, often exacerbating inequities (Markhvida et al., 2020; Lallemant et al.,2020).

Case studies – Celebrating success

We illustrate the use of probabilistic counterfactual analysis to highlight invisible benefits of DRM, and also to demonstrate its capability to adapt to a wide range of hazards and DRM interventions. The two case studies in this section were chosen as they exemplify three of the invisibilities highlighted in the paper, cover two major hazards, and two very different types of DRM interventions (structural upgrading and early-warning respectively). The first case study focuses on a school earthquake retrofitting program in Nepal. It illustrates Case A of Figure 1, where a very successful risk reduction program was made invisible amid the tragedy of a broader catastrophe. The second case study focuses on the evacuation of coastal communities in India prior to a major cyclone making landfall. It illustrates Case B and D of Figure 1, where the benefits of the massive evacuation is made invisible by nature of it having been so successful (i.e. news focuses on perceivable losses thus rarely highlights avoided disaster), and partially obscured by the lesser severity of the actualised hazard compared to that expected at the time. Finally, we finish this section by presenting a list of DRM interventions that fit Case C in Figure 1 - interventions with invisible successes due to yet unrealized benefits. This illustrates the diversity, creativity and broad geographic coverage of important DRM interventions which deserve to be highlighted, analysed and learned from.

Seismic retrofit of schools in Nepal

Event description

On Saturday, April 25, 2015 at 11:56am local time, a Mw 7.8 earthquake occurred about 80 km northwest of Kathmandu, the capital of Nepal (Hayes et al., 2017). It was followed by numerous aftershocks (Goda et al., 2015; Prakash et al., 2016). According to the Post-Disaster Needs Assessment, the Nepal earthquake resulted in 8,790 casualties, 22,300 injuries, and over 8 million impacted persons (about one-third of the population of Nepal) in 31 districts, resulting in an estimated 7 billion U.S. dollars of direct economic losses (Nepal NPC, 2015). In the education sector, 8,242 public schools were affected, including 25,134 fully destroyed classrooms and 22,097 partially damaged (Nepal NPC, 2015).

Before the event, the risk of such a large earthquake in the region is well known. It has been hypothesised that the recurrence interval of a “great Himalayan earthquake” (Mw > 8.0) is between 750 ± 140 and 870 ± 350 years on average in the east Nepal region (Bollinger et al., 2014). At the location of the 2015 earthquake, the last major earthquake was in 1344. And since the last destructive Nepal earthquake in 1934, studies have hinted strain buildup towards Kathmandu (Goda et al., 2015; Prakash et al., 2016).

DRM intervention

Amidst Nepal’s high seismic hazard and predominance of vulnerable non-engineered building construction (BCPR, 2004; Rodrigues et al., 2018), Government of Nepal recognized the need for earthquake-safe construction to reduce school vulnerability. In this work, we highlight the number of lives saved by the timely intervention of the School Earthquake Safety Program (SESP), a school retrofit program initiated in 1997 by the National Society for Earthquake Technology (NSET) and continued through the Nepal Safer Schools Projects (NSSP) by the Department of Education (Marasini, 2019). Prior to the earthquake, NSET reported that a majority of public schools were built via construction techniques using unsafe materials such as non-reinforced adobe, stone rubble in mud mortar, and brick in mud mortar (NSET, 2000). The safety of Nepal’s public school buildings is particularly important, as they serve as emergency shelters, housing tents and sites for medical services (Dixit et al., 2014). Furthermore, the collapse of a school building can cause intense psychological impacts to community members and especially children, and the return to school for students provides a sense of normalcy after a disaster (Dixit et al., 2014).

The primary aim of the School Earthquake Safety Program was to raise earthquake safety awareness in Nepal through outreach and capacity building amongst teachers, students, and parents, and to strengthen school buildings through seismic retrofitting by local masons (NSET, 2012). The first seismically retrofitted school was completed in 1999. By the time of the Nepal earthquake in April 2015, 300 schools were retrofitted, 160 of which were in the most affected districts. Among the 160 retrofit schools in the affected districts, 125 reported no damage, with 35 only reporting hairline cracks on plaster. Notably, none of the retrofitted schools collapsed or needed major repairs (Marasini, 2019). Our dataset shown in Figure 4 contained information on 70 of the 300 retrofitted schools (OpenDRI, 2012).

Figure 3. For each of the 70 retrofitted school buildings shown as circles on the map, PGA (in %g) are extracted as hazard input, and the daytime occupancy (represented by the size of the circles) are used to estimate the probabilistic fatalities. The dataset also contains physical characteristics that indicate potential for collapse (e.g. construction typology, number of stories, fragility curves).

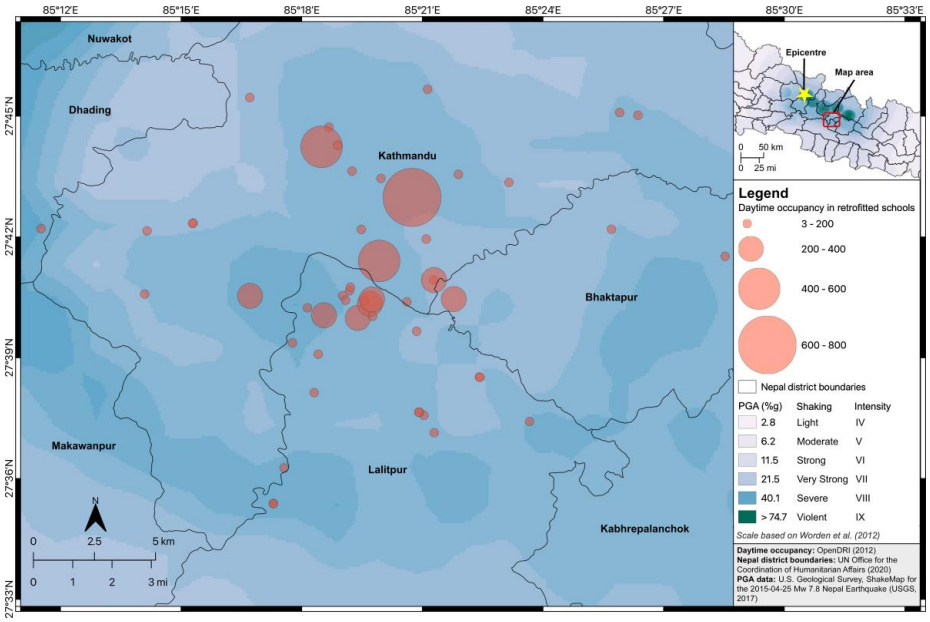

Probabilistic counterfactual analysis

The downward counterfactual analysis is applied through a probabilistic approach to estimate building collapse for two scenarios: (1) the realised case where all 70 school buildings of interest were retrofitted, and (2) a counterfactual case where the school buildings are not retrofitted. For each school, we estimate the probability of exceeding a collapse damage state based on the following modelling parameters:

1) Earthquake hazard in terms of peak ground accelerations (PGA) generated using the USGS Global ShakeMap system (Wald and Allen, 2007),
2) School building characteristics including location, daytime occupancy, number of stories, and construction typology (OpenDRI, 2012)
3) Fragility curves describing the probability of collapse given the earthquake shaking intensity and construction typology. For the unretrofitted schools,collapse fragility curves were adopted from a study on earthquake mitigation in Kathmandu Valley before the Nepal Earthquake (JICA and MOHA, 2002). For retrofitted schools, we assumed a collapse fragility curve for a specially designed RC building from the same JICA and MOHA (2002) study. For the complete values of the fragility curves as two-parameter lognormal distribution functions, for all 70 schools in the analysis, see Rabonza et al. (2020).

We then implemented a Monte Carlo simulation, generating 30,000 realisations of Bernoulli trials of collapse based on the estimated collapse exceedance probabilities (probability of collapse for each building at the ground motion intensity estimated from the 2015 earthquake). To obtain a distribution of probabilistic fatalities, we obtained school building occupancy data (OpenDRI, 2012) and assumed a 20% fatality rate consistent with NSET's calculations for masonry and reinforced concrete buildings (Coburn and Spence, 2002; NSET, 2000). For the first scenario, the realised case, we use fragility curves to estimate collapse probability exceedance corresponding to a retrofitted building, whereas for the second scenario, we assume that the whole building stock consists of unretrofitted buildings and use unretrofitted fragility curves. For a complete description of the modelling parameters, see (Rabonza et al., 2020).

Results

The results of the counterfactual analysis show that the retrofit program saved hundreds of lives. In the realised scenario of retrofitted buildings, 7 out of the 70 school buildings on average were predicted to collapse (10% collapse rate), whereas for the counterfactual case, 33 out of the 70 school buildings were predicted to collapse on average (47% collapse rate). Figure 4 shows the distribution of fatalities due to collapsed school buildings in both scenarios.

Based on the analysis of the counterfactual Nepal earthquake without the risk reduction intervention, we estimate that the lives of approximately 1014 students and teachers were saved in Kathmandu by the retrofit of just these 70 schools in this single event. This was obtained by comparing the estimated mean casualties (n = 289) for the realised retrofitted case, shown in yellow, and the much higher mean casualties (n = 1303) for the counterfactual unretrofitted case, shown in green. We note that the actual reported number of casualties in the 70 retrofitted schools is unknown, and likely much lower still than our prediction, since no retrofitted schools collapsed. This is likely due to better performance of school buildings than modelled according to their fragility curves. Hence the number of lives saved may be conservative.

This case study highlights the invisible success of the SESP program amidst the 2015 Nepal earthquake,and illustrates how the counterfactual probabilistic analysis can be applied to celebrate previously invisible benefits in the context of a past disaster.

Figure 4: Relative number of lives saved due to the school retrofit policy implemented in Nepal before the 2015 earthquake. Estimated fatalities for the realised retrofitted case and the counterfactual, unretrofitted case, where 70 school buildings were not retrofitted prior to the 2015 earthquake. Fatality estimates are based on 30,000 simulations and show an average of 1014 lives saved, calculated as the difference in the average number of fatalities for both cases.

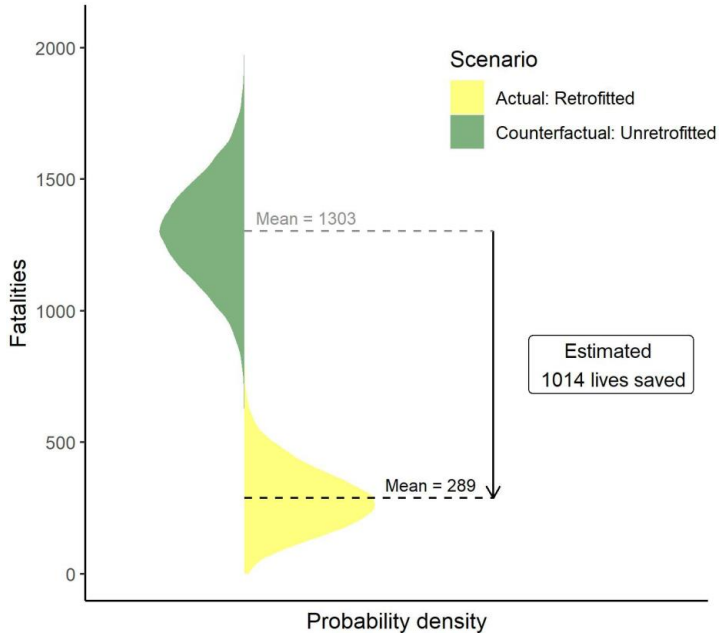

Cyclone evacuation in India

Event description

'Extremely Severe Cyclonic Storm' Fani hit the East Indian coast of Odisha on May 3rd 2019. With a maximum sustained surface wind speed of 204km/h, (RSMC New Delhi, 2019), it was the strongest tropical cyclone to strike the region since the 1999 Odisha super cyclone (WMO, 2019).

Cyclone Fani left an official count of 89 fatalities in India and Bangladesh, 64 of them in the East Indian state of Odisha. Of the 64 deaths, 51 are extreme wind-related fatalities (i.e. crushed by uprooted trees, collapsed walls and roof) (News18 India, 2019; UNICEF, 2019). The state bore the brunt of the human and economic impact of the cyclone, with approximately 16.5 million people in over 18,388 villages affected and approximately 362,000 houses experiencing catastrophic damage. Total damage and losses in the state was estimated to be 3.5 billion U.S. dollars (Government of Odisha, 2019; Mishra and Ojha, 2020).

DRM intervention

Despite the considerable impact on human lives and property, the damagecaused by Cyclone Fani was small in comparison to the Odisha super cyclone of 1999, which resulted in approximately 10,000 fatalities and 4.5 billion U.S. dollars of damage (Kalsi, 2006). The reduced human and economic losses was partly a result of the fact that the observed peak storm surge height of 1.5m (RSMC New Delhi, 2019), was much below the 4m peak predicted (ECHO, 2019), as well as the 6.7m peak of the 1999 cyclone (Kalsi, 2006). At the same time, loss of life was also much reduced as a result of large-scale evacuation efforts taken by the government of Odisha, who evacuated approximately 1.55 million people towards 9,177 shelters before the cyclone's landfall. In contrast, at the time of the 1999 super cyclone, Odisha state only had 23 cyclone shelters for evacuation (IFRC, 2001).

Probabilistic counterfactual analysis

We calculate probabilistic lives saved as a result of the evacuation during Cyclone Fani through two counterfactual scenarios. We modelled the outcome of the *realised flood event without the realised evacuation efforts*, in comparison to the realised evacuation scenario. This is an example of Case B from Figure 1, where we highlight the success of the evacuation which otherwise went unnoticed by nature of its success. We also modelled the counterfactual realisations of Cyclone Fani with higher storm surge as originally predicted before the cyclone's landfall, also without evacuation efforts. This represents the family of *expected* cyclone surges given what was known at the time, and against which the mass evacuation decision was made. This then is an example of Case D from Figure 1, where we highlight the success of the evacuation made invisible by the randomness of the hazard.

Counterfactual realisations of storm surge were used to generate flood maps using the bathtub flood method (Yunus et al., 2016), and accounting for local tides, surge heights (GDACS, 2019) and elevation (Yamazaki et al., 2017). We used a tide level of 1.5m which corresponds to the average monthly high tide in Puri (Meteo365, 2021). Exposed population was derived from gridded population density data (WorldPop, 2021), downscaled with higher resolution World Settlement Footprint map (Marconcini et al., 2020). The result is a detailed 10m resolution population density map for the area. A flood fatality model was used to estimate fatality rate as a function of water depth, as per the cumulative lognormal distribution model by Jonkman (Jonkman, 2007):

$$F_D(h) = \Phi\left(\frac{(\ln h) - 7.6}{2.75}\right)$$

Figure 5. Modelled flood depths for the predicted and realised cyclone flood event with the population exposure per hectare. The predicted event uses a 3.6m storm surge.

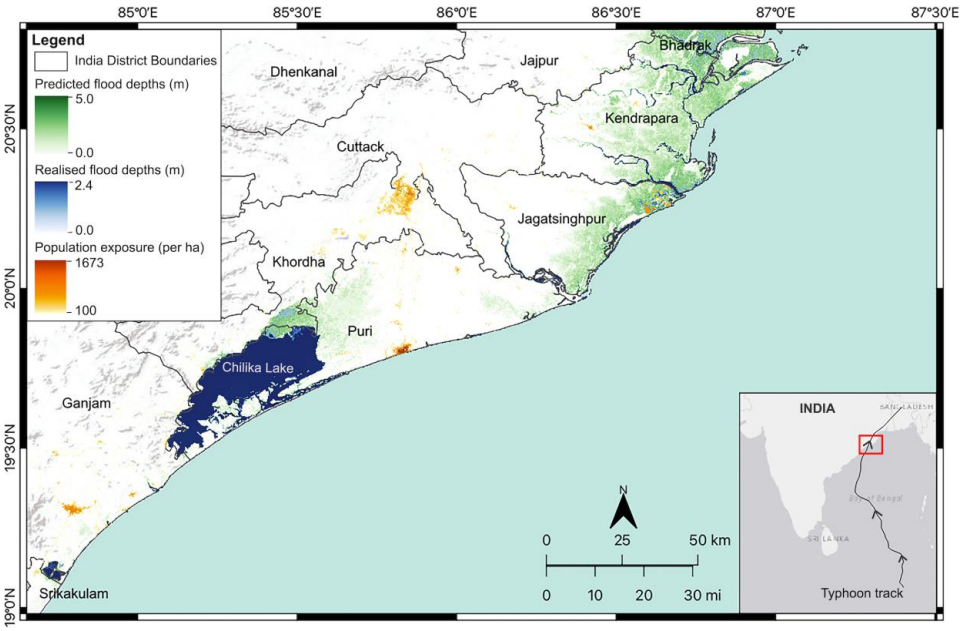

A limitation of the approach is the high uncertainty in both the fatality model and the initial storm surge height. To take these uncertainties into account, Monte Carlo analysis was performed to simulate different storm surge heights and different parameters of the fatality function. The storm surge height was sampled from a normal distribution with a mean of 3.6m and standard deviation of 1.1m, matching the range of estimates before the cyclone made landfall (Mohanty, 2019; ECHO, 2019). The mean parameter of the fatality model was likewise treated as uncertain and normally distributed with standard deviation of 1m. Figure 5 shows the modelled flood depths and population exposure per hectare with both the realised and predicted storm surge heights.

We make note that the model only accounts for fatalities resulting from flooding, and therefore excludes those caused by winds. This is because the majority of cyclone fatalities in high-fatality cyclonic events are a result of floods, as was the case in the 1999 super cyclone (Kalsi, 2006). However, it should be noted that this limitation would lead to an underestimation of fatalities in our models.

We note that the storm surge level of 1.5 meters is in the same order of magnitude as the vertical uncertainty in the DEM. This is a common limitation for flood modelling with global data and the Multi-Error-Removed Improved-Terrain DEM we applied was specifically made to reduce this issue (Yamazaki et al., 2017). The results remain uncertain, and are therefore to be used for illustrative purposes. Higher resolution DEM, tidal, exposure and fatality models would improve the counterfactual predictions.

Results

In reality, Cyclone Fani caused 63 fatalities. The first counterfactual scenario, using the realised surge height but counterfactual absence of evacuation, would have led to an estimated 767 fatalities (mean = 767, Interquartile range = 240 - 970). The second counterfactual scenario, using the counterfactual storm surge that was expected prior to landfall and absence of evacuation, would have led to an estimated 10380 fatalities (mean = 10380, Interquartile range = 2750 - 13200). Figure 6 shows the distribution of fatalities as a result of flooding in both scenarios.

The first counterfactual scenario highlights the benefits of life-saving interventions in a realised hazard event in this case, the evacuation efforts during Cyclone Fani. The second counterfactual scenario highlights the fact that the full benefits of the evacuation efforts may have been partially obscured by the lesser severity of the realised hazard.

Figure 6. Estimated fatalities for actual and counterfactual cases. The counterfactual cases correspond to the realised storm surge with no evacuation, as well as the expected storm surge (against which the evacuation plan was made) with no evacuation. The estimates are based on 250 and 1,350 simulations respectively.

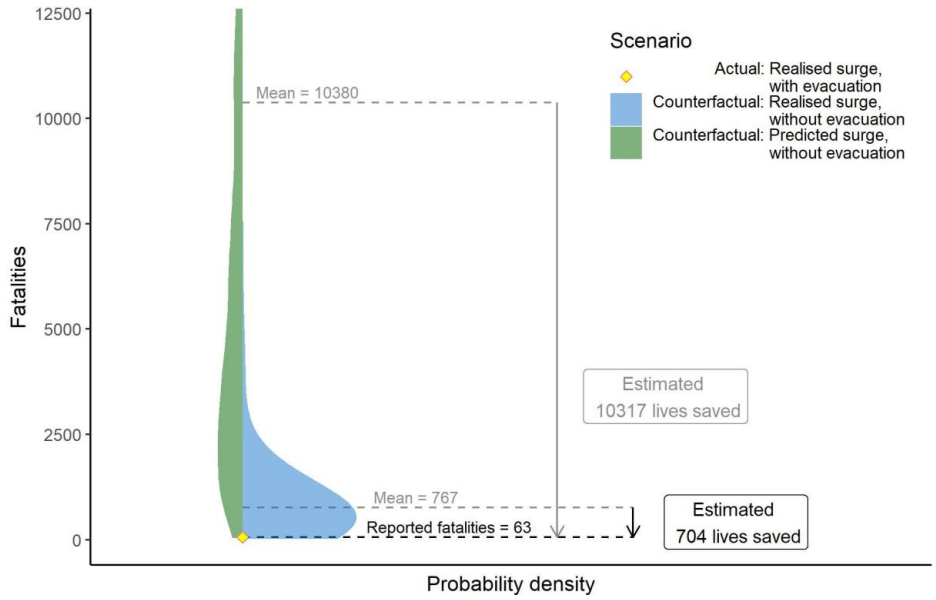

Through this lens, it can be seen that the effective evacuation of coastal communities preceding Cyclone Fani is associated with an estimated 704 lives saved in the realised storm surge event, and 10317 lives saved in the predicted storm surge event.

This scenario thus highlights the usefulness of our model in drawing attention to potential 'invisible' benefits of risk reduction interventions, some of which may otherwise not be fully realised or acknowledged after a hazard event with a lower-than-expected severity. In doing so, it further highlights how our models may allow us to better monitor progress in disaster risk reduction independent of the realised outcome of such interventions.

Success made invisible due to yet unrealised benefits

The two case studies illustrate the use of counterfactual probabilistic risk analysis to highlight the lives saved by DRM measures. While these are in the context of earthquakes and floods, the methodology can be adapted for a wide range of hazards and measures. In Table 1, we present a list of DRM interventions implemented in various regions of the world. This is a small reflection of the diversity of measures which should be analysed, celebrated and shared even if their benefits have yet to be realised. Each intervention targets one or more risk components, which can help define the counterfactual scenarios required for evaluation.

Measuring probabilistic lives saved as a result of an intervention should become standard practice in the DRM field. The shift in focus from specific outcome to *probabilistic lives saved* offers a framework to reward individuals and institutions who have displayed political bravery in committing to the implementation of DRM measures despite time delay in the realisation of its benefits, lack of follow up risk auditing and other challenges. This simple gesture can motivate further good work.

Table 1. Table of example disaster risk reduction measures (DRR) for which counterfactual risk analysis can be applied for evaluation. The risk components affected are coded as H for hazard, E for exposure and V for vulnerability.

DRR Measure	Risk Component	Example
Earthquake		
Reconstruction and retrofit	V	In San Francisco, a mandatory retrofit program for older, wood-framed multi-family buildings with soft-story conditions was created in 2013 (SFDBI, 2021).
Construction inspection	V	In Turkey, the 2001 Construction Inspection Law led to better building quality control (Gunes, 2015).
Public awareness	E, V	In Kyrgyzstan, the safe evacuation of 32 children from summer camp after the 2011 M6.1 earthquake was attributed to preparedness exercises (ECHO, 2013).
Flood		
Urban planning	V	In China, the 'Sponge City' concept was established in 2014 to promote filtration and storage of stormwater in highly urbanized areas (Chan et al., 2018).
Flood management infrastructure	E	In the Philippines, a polder wall for protecting the Valenzuela-Obando-Meycauayan (VOM) area was constructe in 2014 (JICA, 2018).
	H	In Netherlands, the Delta Works programme was implemented between 1954 and 1997 to construct dams and other flood protection infrastructure (Kind, 2014).
Emergency response	V	In Gambia, integration of DRR interventions in emergency response proved its worth during the 2012 floods (ECHO, 2013).
Typhoon/Tropical Storm		
Public awareness	E, V	In the Philippines, explanations from barangay officials on the deadliness of storm surges led to a successful preemptive evacuation on Manicani Island implemented two days before Typhoon Haiyan hit. As a result, only one out of more than 3000 residents died (Canoy, 2013; Lagmay et al., 2015).
Early warning system	E	In Bangladesh, a Doppler Radar system, which gave timely warning, was partly credited for the lower than expected casualty count of 190 during Cyclone Aila in 2009 (Izumi et al., 2019).

Storm risk management	E, V	In Myanmar, cyclone shelters provided refuge during Cyclone Mahasen in 2013, their year of completion (JICS, 2013).
Landslide/Avalanche		
Early warning system	E	In Bolivia, no victims were reported after the 2011 mega landslide due to the evacuation effort informed by a geodynamic hazard monitoring system (ECHO, 2013).
Mitigation infrastructure	E, V	In Tajikistan, a 120m long mudflow channel was rehabilitated to protect a village of 1760 inhabitants (UNDRR, 2006).
Tsunami		
Public awareness	E, V	In Indonesia, disaster risk education was provided in schools around Ciletuh-Palabuhanratu UNESCO Globa Geopark (Muslim et al., 2019)
Fire/Drought		
Early warning system	E	In Lebanon, a wildfire forecast system using dynamic weather forecasts was launched in 2016 (Mitri et al., 2017).
Irrigation	H, E, V	In Malaysia, irrigation recycling which begun in 1970 saved more than 3000ha of crop in the 2015-16 drought (JICA, 2018).

Discussion

The Nepal 2015 earthquake case shows that even in the midst of a tragic disaster, there are often successes to celebrate that prevented many more lives from being lost. Our counterfactual analysis demonstrated that the successful earthquake retrofit of 300 school buildings as part of the government-led School Earthquake Safety Program saved hundreds of probabilistic lives. The benefits of the retrofitting program were even further obscured since the earthquake occurred on a Saturday while school sessions were off (luckily!).

The 2019 Cyclone Fani made landfall on the Indian coast without leading to the major disaster feared. This was the result of the evacuation of 1.55 million people, and the fact that the predicted extreme storm surge didn't occur. The result was that 'only' 64 fatalities occurred in the case study area (UNICEF, 2019), the majority of them wind fatalities (News18 India, 2019). This is relatively few compared to similarly severe cyclones in the region. We applied our probabilistic counterfactual analysis to look at what would have happened without evacuation and what would have happened if the predicted storm surge had occurred. We found that the evacuation probably saved hundreds of lives and if the predicted storm surge had occurred the lives saved could have reached in the thousands to even ten thousands. This counterfactual analysis shows that the evacuation was necessary, successful, and presents important lessons for other regions and countries impacted by tropical storm hazards.

The case studies utilise first order risk analyses and contain numerous modelling uncertainties. The studies are therefore intended to serve as demonstration of the probabilistic downward counterfactual analysis approach, but the specific results and estimated lives saved have significant uncertainty, as demonstrated by the wide distributions of simulations shown in Figure 4 and Figure 6.

The case studies focus only on loss of life reduction. Other metrics of successful DRM interventions include reducing injuries, number of affected or displaced people, building damage, business interruption, livelihood losses, damage to cultural heritage, psychological distress and much more. Probabilistic downward counterfactual analysis can be applied equally for these alternative metrics.

Furthermore, it is becoming increasingly recognised that the benefits of DRM activities can go beyond impact reduction and loss-avoidance, and in fact should be designed as such. For instance, the reduction of background risk encourages positive risk taking (e.g., investment in productive assets, entrepreneurial activities), enables long term financial planning (e.g., to build up savings), and potentially increases the value of protected lands (Tanner et al., 2015). Investments in multi-purpose disaster risk reduction measures can also yield benefits that are unrelated to the reduction of background risks. These co-benefits can be economic (e.g., increased agriculture productivity with improved irrigation for drought management), political (e.g., improved governance through strengthening the disaster risk management capacity of civil society), social (e.g. increased parks and green leisure areas), and/or environmental (e.g., carbon sequestration, sediment and nutrient retention from protection or afforestation of wetlands). The nature and level of these co-benefits depend on the design of the disaster risk reduction measure (Tanner et al., 2015).

Conclusions

The field of disaster risk management faces the challenge of its failures being catastrophic while its successes go unnoticed. This makes it difficult to identify, celebrate, and spread positive lessons learned that could be emulated elsewhere, or to incentivise proactive decision-making on the basis of recognised successes. We have identified four types of situations where successful DRM interventions are made invisible: (i) success made invisible in the midst of broader disaster, (ii) success made invisible by nature of the success, (iii) success made invisible due to yet unrealised benefits, (iv) success made invisible due to randomness of specific outcome.

We propose and demonstrate the use of probabilistic downward counterfactual analysis to shed light on these otherwise invisible successes. Downward counterfactual analysis is the counter-intuitive process of understanding how a realised event could have been worse, as a way to highlight the benefits of an intervention. This application goes beyond the existing uses of counterfactual risk analysis that focus on pointing out worse potential outcomes for the purpose of insurance, preparedness, future mitigation and learnings from failures in DRM.

We further use the risk analysis framework to ascribe estimated probabilities to the simulated counterfactuals. The estimated probabilities constrain the counterfactual exploration to realistic scenarios. As in all risk analyses, the process requires scrutiny and transparency in the assumptions, data and analysis conducted. Doing so aims to avoid both misuse of the counterfactual framework and misrepresentation of the benefits of DRM. An example of misuse would be inflating the benefits of a DRM intervention by cherry-picking 'ideal' counterfactuals e.g. a hazard scenario too extreme and unrepresentative of the current knowledge of the hazard that the calculated lives saved would inflate.

An important concept that emerges from this study is that the value of a risk reduction intervention should not be judged on the basis of specific outcomes, but also on the basis of a broader exploration of potential outcomes. The same *good decision* may seem like overkill against a specific outcome, or may seem completely insufficient judged against another. Especially in a field focused on long-term resilience and often rare (therefore volatile) events, *realised outcomes* bias our perceptions and judgements. This is also relevant to the monitoring of risk reduction targets, including those of the Sendai Framework (UNISDR, 2015). Mortality on any given year, or specific place, may not reflect adequate or inadequate disaster planning, but rather chance outcomes. Encouraging long-term resilience, which may not 'pay-off' for decades (e.g. for climate-adaptation), will therefore require a shift in focus from realised outcome to unrealised risk reduction.

The innumerable successful DRM interventions implemented in communities worldwide (e.g. in Table 1) represent a critical data-set to learn from, adapt, share and implement such activities where they are further needed. This is only possible if these successes are identified, analysed and celebrated. We propose the use of probabilistic downward counterfactual analysis to highlight and quantify the benefits of DRM interventions that otherwise remain invisible. This can serve to lift up the iterative, long-term, humble, dedicated and politically courageous actions required for long-term resilience building.

Acknowledgements

We thank Dr. Nama Budhathoki, Kathmandu Living Labs and the GFDRR Open Data for Resilience Initiative for data on retrofitted schools in Nepal. This project is supported by the National Research Foundation, Prime Minister's Office, Singapore under the NRF-NRFF2018-06 award, the Earth Observatory of Singapore (EOS), the National Research Foundation of Singapore, and the Singapore Ministry of Education under the Research Centers of Excellence initiative.

References

W. Aspinall and G. Woo. Counterfactual analysis of runaway volcanic explosions. *Frontiers in Earth Science*, 7:222, 2019.

BCPR. Reducing Disaster Risk : A Challenge for Development. Technical report, United Nations Development Programme Bureau for Crisis Prevention and Recovery, New York, NY, 2004.

I. Blix, A. B. Kanten, M. S. Birkeland, Solberg, A. Nissen, and T. Heir. Thinking About What Might Have Happened: Counterfactual Thinking and Post-traumatic Stress in Individuals Directly and Indirectly Exposed to the 2011 Oslo Bombing. *Applied cognitive psychology*, 30(6):983–991, 2016. ISSN 0888-4080. doi: 10.1002/acp.3289. Publisher: Wiley Subscription Services, Inc.

L. Bollinger, S. N. Sapkota, P. Tapponnier, Y. Klinger, M. Rizza, J. Van der Woerd, D. Tiwari, R. Pandey, A. Bitri, and S. Bes de Berc. Estimating the return times of great Himalayan earthquakes in eastern Nepal: Evidence from the Patu and Bardibas strands of the Main Frontal Thrust. *Journal of Geophysical Research: Solid Earth*, 119(9):7123–7163, 2014.

J. Canoy. Evacuation saves Guiuan islanders' lives. ABS-CBN News, Available at https://news.abs-cbn.com/nation/regions/11/18/13/ evacuation-saves-guiuan-islanders-lives (2013/11/19), 2013.

F. K. S. Chan, J. A. Griffiths, D. Higgitt, S. Xu, F. Zhu, Y.-T. Tang, Y. Xu, and C. R. Thorne. "Sponge City" in China—A breakthrough of planning and flood risk management in the urban context. *Land use policy*, 76:772–778, 2018.

A. Coburn and R. Spence. *Earthquake protection*. John Wiley & Sons, Chichester, England, 2002.

A. M. Dixit, R. Yatabe, R. K. Dahal, and N. P. Bhandary. Public school earthquake safety program in nepal. *Geomatics, Natural Hazards and Risk*, 5(4):293–319, 2014.

ECHO. Disaster Risk Reduction: Increasing resilience by reducing disaster risk in humanitarian action. *DG ECHO thematic policy document*, (5), 2013.

ECHO. India - Tropical Cyclone Fani update (DG ECHO, GDACS, IMD, media) (ECHO Daily Flash of 01 May 2019), may 2019.

K. Epstude and N. J. Roese. The Functional Theory of Counterfactual Thinking. *Pers Soc Psychol Rev*, 12(2):168–192, May 2008. ISSN 1088-8683. doi: 10.1177/1088868308316091. Publisher: SAGE Publications Inc.

J.-C. Gaillard. Disaster studies inside out. *Disasters*, 43:S7–S17, 2019.

GDACS. Overall Red alert Tropical Cyclone for FANI-19. https://www.gdacs.org/Cyclones/report.aspx?eventid=1000561&episodeid=27&eventtype=TC, 2019.

K. Goda, T. Kiyota, R. M. Pokhrel, G. Chiaro, T. Katagiri, K. Sharma, and S. Wilkinson. The 2015 Gorkha Nepal earthquake: Insights from earthquake damage survey. *Frontiers in Built Environment*, 1:8, 2015.

Government of Odisha. Cyclone Fani: Damage, loss and needs assessment. Technical report, Government of Odisha, Odisha, 2019.

O. Gunes. Turkey's grand challenge: Disaster-proof building inventory within 20 years. *Case Studies in Construction Materials*, 2:18–34, 2015.

G. P. Hayes, E. K. Meyers, J. W. Dewey, R. W. Briggs, P. S. Earle, H. M. Benz, G. M. Smoczyk, H. E. Flamme, W. D. Barnhart, R. D. Gold, et al. Tectonic summaries of magnitude 7 and greater earthquakes from 2000 to 2015. Technical report, US Geological Survey, 2017.

R. Hertwig, G. Barron, E. U. Weber, and I. Erev. Decisions from Experience and the Effect of Rare Events in Risky Choice. *Psychol Sci*, 15(8):534–539, Aug. 2004. ISSN 0956-7976. doi: 10.1111/j.0956-7976.2004.00715.x.

IFRC. World Disasters Report 2001: Focus on Recovery. Technical Report 5, International Federation of Red Cross And Red Crescent Societies, 2001.

T. Izumi, R. Shaw, M. Ishiwatari, R. Djalante, and T. Komino. 30 Innovations for Disaster Risk Reduction by IRIDeS, Keio University, the University of Tokyo, UNU-IAS, CWS Japan, Japan. Technical report, 2019.

A. Jha, J. Lamond, R. Bloch, N. Bhattacharya, A. Lopez, N. Papachristodoulou, A. Bird, D. Proverbs, J. Davies, and R. Barker. *Five Feet High and Rising: Cities and Flooding in the 21st Century*. The World Bank, 2011. doi: 10.1596/1813-9450-5648.

JICA. Project for Strengthening Institutional and Policy Framework on Disaster Risk Reduction (DRR) and Climate Change Adaptation (CCA) Integration [ASEAN] Final Report. Technical report,

2018.

JICA and MOHA. The study on earthquake disaster mitigation in the Kathmandu Valley, Kingdom of Nepal. Technical report, 2002.

JICS. Myanmar Thirteen Primary School-cum-Cyclone Shelters completed for the development of education in Myanmar and secure the lives of Myanmar people. https://www.jics.or.jp/jics_html-e/activities/grant/disaster/ myanmar201312.html, 2013. Accessed: 2021-02-16.

S. N. Jonkman. *Loss of life estimation in flood risk assessment: Theory and applications*. PhD thesis, Delft University of Technology, 2007.

D. Kahneman. Varieties of counterfactual thinking. In *What might have been: The social psychology of counterfactual thinking*, pages 375–396. Lawrence Erlbaum Associates, Inc, Hillsdale, NJ, US, 1995. ISBN 978-0-8058-1613-6 978-0-8058-1614-3.

S. R. Kalsi. Orissa super cyclone – A Synopsis. *Mausam*, 57(1):1–20, 2006.

J. M. Kind. Economically efficient flood protection standards for the Netherlands. *Journal of Flood Risk Management*, 7(2):103–117, 2014.

A. M. F. Lagmay, R. P. Agaton, M. A. C. Bahala, J. B. L. T. Briones, K. M. C. Cabacaba, C. V. C. Caro, L. L. Dasallas, L. A. L. Gonzalo, C. N. Ladiero, J. P. Lapidez, M. T. F. Mungcal, J. V. R. Puno, M. M. A. C. Ramos, J. Santiago, J. K. Suarez, and J. P. Tablazon. Devastating storm surges of Typhoon Haiyan. *International Journal of Disaster Risk Reduction*, 11:1–12, 2015. ISSN 2212-4209. doi: https://doi.org/10. 1016/j.ijdrr.2014.10.006.

D. Lallemant, S. Loos, J. W. McCaughey, N. Budhathoki, and F. Khan. Informatics for equitable recovery: Supporting equitable disaster recovery through mapping and integration of social vulnerability into post-disaster impact assessments. Technical report, 2020.

M. Leach, J. Rockström, P. Raskin, I. Scoones, A. C. Stirling, A. Smith, J. Thompson, E. Millstone, A. Ely, E. Arond, et al. Transforming innovation for sustainability. *Ecology and Society*, 17(2), 2012.

D. Lewis. On the Plurality of Worlds. *Central Works of Philosophy, Volume 5: The Twentieth Century: Quine and After*, 5:246, 2005.

Y. Lin, S. Jenkins, J. Chow, S. Biass, G. Woo, and D. Lallemant. Modeling Downward Counterfactual Events: Unrealized Disasters and why they Matter. *Frontiers in Earth Science*, 8:575048, 2020.

N. Marasini. NSET Experiences on Safer Schools Initiative. https://www.adrc.asia/ acdr/2019/documents/S3-05_NSET_Nepal.pdf, Nov 2019.

M. Marconcini, A. Metz-Marconcini, S. Üreyen, D. Palacios-Lopez, W. Hanke, F. Bachofer, J. Zeidler, T. Esch, N. Gorelick, A. Kakarla, M. Paganini, and E. Strano. Outlining where humans live, the World Settlement Footprint 2015. *Scientific Data*, 7(1): 1–14, 2020. ISSN 20524463. doi: 10.1038/s41597-020-00580-5.

M. Markhvida, B. Walsh, S. Hallegatte, and J. Baker. Quantification of disaster impacts through household well-being losses. *Nature Sustainability*, 3(7):538–547, July 2020. ISSN 2398-9629. doi: 10.1038/s41893-020-0508-7. Number: 7 Publisher: Nature Publishing Group.

V. H. Medvec, S. F. Madey, and T. Gilovich. When less is more: Counterfactual thinking and satisfaction among Olympic medalists. *Journal of Personality and Social Psychology*, 69(4):603–610, 1995. ISSN 1939-1315(Electronic),0022-3514(Print). doi: 10.1037/0022-3514.69.4.603.

Meteo365. Tide Times and Tide Chart for Puri. https://www.tide-forecast.com/ locations/Puri/tides/latest, 2021.

D. Mileti. *Disasters by design: A reassessment of natural hazards in the United States*. Joseph Henry Press, 1999.

S. P. Mishra and A. Ojha. Fani, an Outlier among pre-monsoon intra-seasonal cyclones over Bay of Bengal. *International Journal on Emerging Technologies*, 11(2):271–282, 2020.

G. Mitri, S. Saba, M. Nader, and D. McWethy. Developing Lebanon's fire danger forecast. *International Journal of Disaster Risk Reduction*, 24:332–339, 2017.

D. Mohanty. Odisha orders evacuation of a million people before Cyclone Fani's landfall, May 2019.

H. E. Moore. Tornadoes over Texas: A study of Waco and San Angelo in disaster. 1958.

D. Muslim, E. Haerani, F. Muslim, and G. Muslim. Toward the safe live-able built environment around Ciletuh-Palabuhanratu Geopark Area in Sukabumi Regency, Indonesia. In *IOP Conference Series: Earth and Environmental Science*, volume 248, page 012036. IOP Publishing, 2019.

Nepal NPC. Nepal earthquake 2015: Post disaster needs assessment, Vol. B: Sector Reports. Technical report, Kathmandu, Nepal: National Planning Commission (NPC), 2015.

B. R. Newell, T. Rakow, E. Yechiam, and M. Sambur. Rare disaster information can increase risk-taking. *Nature Climate Change*, 6(2):158–161, Feb. 2016. ISSN 1758-6798. doi: 10.1038/nclimate2822.

News18 India. Death Toll from Cyclone Fani Rises to 64 after Odisha Confirms Fresh Casualties, may 2019. URL https://www.news18.com/news/india/death-toll-from-cyclone-fani-rises-to-64-as-odisha-confirms-fresh-casualties-21384 html.

NSET. Seismic vulnerability of the public-school buildings of Kathmandu Valley and methods for reducing it. Technical report, National Society for Earthquake Technology, 2000.

NSET. School Earthquake Safety Program (SESP). Earthquake Safe Communities in Nepal. http://www.nset.org.np/nset2012/index.php/successstory/ successstoryview/successstoryid-4, 2012.

OpenDRI. Understanding Nepal's Risks" Open Data for Resilience Initiative Project. https://opendri.org/project/nepal/, 2012.

E. J. Oughton, D. Ralph, R. Pant, E. Leverett, J. Copic, S. Thacker, R. Dada, S. Ruffle, M. Tuveson, and J. W. Hall. Stochastic Counterfactual Risk Analysis for the Vulnerability Assessment of Cyber-Physical Attacks on Electricity Distribution Infrastructure Networks. *Risk Analysis*, 39(9):2012–2031, 2019.

R. Prakash, R. K. Singh, and H. Srivastava. Nepal earthquake 25 april 2015: source parameters, precursory pattern and hazard assessment. *Geomatics, Natural Hazards and Risk*, 7(6):1769–1784, 2016.

M. L. Rabonza, Y. Lin, and D. Lallemant. Celebrating successful earthquake risk reduction through counterfactual probabilistic analysis. In *Proceedings of the 17th World Conference on Earthquake Engineering*, pages Article No. 8c–0059, Sendai, Japan, September 2020.

H. Rodrigues, A. Furtado, N. Vila-Pouca, H. Varum, and A. R. Barbosa. Seismic assessment of a school building in Nepal and analysis of retrofitting solutions. *International Journal of Civil Engineering*, 16(11):1573–1589, 2018.

N. J. Roese and J. M. Olson. *What Might Have Been: The Social Psychology of Counterfactual Thinking*. Psychology Press, New York, Jan. 2014. ISBN 978-1-317-78047-2.

I. M. D. RSMC New Delhi. Extremely Severe Cyclonic Storm "FANI" over eastcentral equatorial Indian Ocean and adjoining southeast Bay of Bengal (26 April – 04 May, 2019): Summary. Technical report, Regional Specialised Meteorological Centre Tropical Cyclones, New Delhi, India Meteorological Department, New Delhi, 2019.

J. C. Scott. *Seeing like a state: How certain schemes to improve the human condition have failed*. Yale University Press, New Haven and London, 1998.

SFDBI. Mandatory soft story program. https://sfdbi.org/softstory, 2021. Accessed: 2021-02-15.

T. G. Shepherd, E. Boyd, R. A. Calel, S. C. Chapman, S. Dessai, I. M. Dima-West, H. J. Fowler, R. James, D. Maraun, O. Martius, et al. Storylines: an alternative approach to representing uncertainty in physical aspects of climate change. *Climatic change*, 151(3-4):555–571, 2018.

D. Smith. *Through a glass darkly-a response to Stallings'" Disaster, Crisis, Collective Stress, and Mass Deprivation"*, volume 2. Xlibris Press, 2005.

T. Tanner, S. Surminski, E. Wilkinson, and R. Reid. The Triple Dividend of Resilience: Realising development goals through the multiple benefits of disaster risk management. Technical report, Global Facility for Disaster Risk Reduction and Recovery (GFDRR) at the World Bank and Overseas Development Institute (ODI), 2015.

T. O. Tengs, M. E. Adams, J. S. Pliskin, D. G. Safran, J. E. Siegel, M. C. Weinstein, and J. D. Graham. Five-hundred life-saving interventions and their cost-effectiveness. *Risk analysis*, 15(3):369–390, 1995.

M. Todorova. Counterfactual construction of the future: Building a new methodology for forecasting. *World Futures Review*, 7(1):30–38, 2015. doi: 10.1177/ 1946756715587004.

A. Tversky and D. Kahneman. Availability: A heuristic for judging frequency and probability. *Cognitive Psychology*, 5(2):207–232, Sept. 1973. ISSN 0010-0285. doi: 10.1016/0010-0285(73)90033-9.

UNDRR. Disaster Risk Reduction: 20 Examples from Good Practice from Central Asia. Technical report, Dushanbe: United Nations International Strategy for Disaster Reduction (UN/ISDR) Central Asia, 2006.

UNICEF. UNICEF India Cyclone Fani Situation Report 2 (national). Available at https://reliefweb.int/report/india/ unicef-india-cyclone-fani-situation-report-2-national (2019/05/12), 2019.

UNISDR. United Nations Office for Disaster Risk Reduction, UNISDR Terminology and Disaster Risk Reduction. Technical report, United Nations International Strategy for Disaster Reduction, Geneva, Switzerland, 2009.

UNISDR. Sendai framework for disaster risk reduction 2015-2030. In *Third United Nations World Conference on Disaster Risk Reduction (WCDRR)—Resilient People. Resilient Planet.*, 2015.

USGS. Shakemap — Earthquake ground motion and shaking intensity maps. *US Geol. Surv.*, 2017. doi: https://doi.org/10.5066/F7W957B2.

D. J. Wald and T. I. Allen. Topographic slope as a proxy for seismic site conditions and amplification. *Bulletin of the Seismological Society of America*, 97(5):1379–1395, 2007.

D. U. Weber. Experience-Based and Description-Based Perceptions of Long-Term Risk: Why Global Warming does not Scare us (Yet). *Climatic Change*, 77(1):103– 120, July 2006. ISSN 1573-1480. doi: 10.1007/s10584-006-9060-3.

A. Wiek and D. Iwaniec. Quality criteria for visions and visioning in sustainability science. *Sustainability Science*, 9(4):497–512, 2014.

WMO. World Meteorological Organization Technical Document : Tropical cyclone operational plan for the Bay of Bengal and the Arabian Sea. Technical Report Tropical Cyclone Programme Report No. TCP-21, Secretariat of the World Meteorological Organization, Geneva, 2019.

G. Woo. Downward counterfactual search for extreme events. *Frontiers in Earth Science*, 7:340, 2019.

G. Woo and A. Mignan. Counterfactual analysis of runaway earthquakes. *Seismological Research Letters*, 89(6):2266–2273, 2018.

G. Woo, T. Maynard, and J. Seria. Reimagining history: counterfactual risk analysis. *Lloyd's emerging risk report, London*, 2017.

C. Worden, M. Gerstenberger, D. Rhoades, and D. Wald. Probabilistic relationships between ground-motion parameters and modified Mercalli intensity in California. *Bulletin of the Seismological Society of America*, 102(1):204–221, 2012.

WorldPop. Open Spatial Demographic Data and Research. https://www.worldpop. org/, 2021. Accessed: 15 February 2021.

D. Yamazaki, D. Ikeshima, R. Tawatari, T. Yamaguchi, F. O'Loughlin, J. C. Neal, C. C. Sampson, S. Kanae, and P. D. Bates. A high-accuracy map of global terrain elevations. *Geophysical Research Letters*, 44(11):5844–5853, 2017. ISSN 19448007. doi: 10.1002/2017GL072874.

A. P. Yunus, R. Avtar, S. Kraines, M. Yamamuro, F. Lindberg, and C. S. Grimmond. Uncertainties in tidally adjusted estimates of sea level rise flooding (bathtub model) for the Greater London. *Remote Sensing*, 8(5), 2016. ISSN 20724292. doi: 10.3390/ rs8050366.